



COST is supported by the EU RTD Framework Programme and ESF provides the COST Office through an EC contract.

Benchmark studies

Experimental validation of numerical models in fire engineering

January 2014

COST- the acronym for European **CO**operation in the field of **Scientific** and **Technical** Research- is the oldest and widest European intergovernmental network for cooperation in research. Established by the Ministerial Conference in November 1971, COST is presently used by the scientific communities of 35 European countries to cooperate in common research projects supported by national funds.

The funds provided by COST - less than 1% of the total value of the projects - support the COST cooperation networks, COST Actions, through which, with only around € 20 million per year, more than 30.000 European scientists are involved in research having a total value which exceeds € 2 billion per year. This is the financial worth of the European added value which COST achieves.

A bottom up approach (the initiative of launching a COST Action comes from the European scientists themselves), à la carte participation (only countries interested in the Action participate), equality of access (participation is open also to the scientific communities of countries not belonging to the European Union) and flexible structure (easy implementation and light management of the research initiatives) are the main characteristics of COST.

As precursor of advanced multidisciplinary research COST has a very important role for the realisation of the European Research Area (ERA) anticipating and complementing the activities of the Framework Programmes, constituting a ridge towards the scientific communities of emerging countries, increasing the mobility of researchers across Europe and fostering the establishment of Networks of Excellence in many key scientific domains such as: Biomedicine and Molecular Biosciences; Food and Agriculture; Forests, their Products and Services; Materials, Physics and Nanosciences; Chemistry and Molecular Sciences and Technologies; Earth System Science and Environmental Management; Information and Communication Technologies; Transport and Urban Development; Individuals, Society, Culture and Health. It covers basic and more applied research and also addresses issues of pre-normative nature or of societal importance.

Web: <http://www.cost.eu>



COST Action TU0904
Integrated Fire Engineering and Response
fire.fsv.cvut.cz/ifer

Benchmark studies

Experimental validation of numerical models in fire engineering

Ed. Wald F., Burgess I., Kwasniewski L., Horová K., Caldová E.

The production of this publication is supported by COST.

ISBN – 978-80-01-05443-7

CTU Publishing House, Czech Technical University in Prague

January 2014

200 copies, 198 pages

© COST Office, 2014

No permission to reproduce or utilise the contents of this book by any means is necessary, other than in the case of images, diagrammes or other material from other copyright holders. In such cases, permission of the copyright holders is required. This book may be cited as: COST Action TU0904 – Benchmark studies, Experimental validation of numerical models in fire engineering.

LIST OF CONTENTS

| | |
|-------------------------------------------------------------------------------------------------------------------------------------------------------|-----|
| PREFACE | 5 |
| FUNDAMENTAL BENCHMARK CASES | |
| 1 Benchmark studies for partially heated steel beams | 9 |
| 2 Lateral torsional-buckling of class 4 steel plate girders under fire conditions: experimental and numerical comparison | 21 |
| 3 Local buckling of class 4 sections at elevated temperature | 34 |
| 4 Numerical and experimental analysis of RC beams exposed to different fire models | 48 |
| 5 Numerical behaviour of steel columns under localized fire loading | 60 |
| 6 Baseline study on the behaviour of cold-formed steel elements subjected to fire | 73 |
| 7 Benchmark modelling for concrete filled structural hollow sections | 86 |
| 8 Numerical and experimental analysis of RC columns exposed to fire | 98 |
| 9 Temperature distribution in R/C cross-section subjected to heating and then freely cooled down by air | 107 |
| 10 Numerical behaviour of T-stub joint component at ambient and elevated temperatures | 123 |
| COMPLEX BENCHMARK CASES | |
| 11 Model benchmarking and the Growth Phase of Dalmarnock Fire Test One | 134 |
| 12 FDS-CFD analysis of temperature development in an enclosure from a fire with a defined heat release rate | 147 |
| 13 The comparison of the results of a full scale evacuation test to the calculation method of Hungarian regulations and to the Pathfinder software | 157 |
| 14 Charring of timber | 173 |
| 15 Old masonry vulnerability against fire action | 180 |
| INDEX OF AUTHORS | 195 |
| ACTION MEMBERS | 196 |

PREFACE

The process of verification and validation of engineering models and their results has been an integral part of advanced structural design practice and research for some years. Both of these are strongly supported by information technologies at all levels, from conceptual design, pre-design, calculations, drawings, fabrication and on the construction site – as well as integration with building services and architectural finishes through Building Information Modelling (BIM) systems. The transfer of data on all of these aspects of planned and existing structures is the domain of object-orientated databases, which can be used during the life of the structure for refurbishment, and will in future also be used for demolition. For the purposes of fire safety and structural fire engineering design both purpose-designed and general software tools are used. Reliable means of verification of numerical models, both simple and advanced, is an essential part of the analytical design process. For advanced design using commercial software a range of worked examples (benchmark studies) are necessary to check that a software tool is being applied correctly to particular problems, including validation examples to check the physical correctness of results. In the structural Eurocodes for fire engineering design (for example EN1991-1-2 [1]) general principles are summarised for the application of advanced models.

This publication is divided into two volumes; ‘Verification of numerical models in fire engineering’ and ‘Experimental validation of numerical models in fire engineering’. They are intended to help European researchers, educators and design engineers with their application of advanced numerical modelling for fire engineering. To complement the textual presentation of the examples the input and output data are included in MS Excel tables so that the studies can be reproduced in detail by the users of the volume. These can be downloaded from the web page fire.fsv.cvut.cz/ifer/benchmark.

Issues concerning safety, including Fire safety, are nationally managed in the European Union, and legal requirements are determined by the specific experiences of each country. While the political motivation for this approach is obvious, and local circumstances vary between countries, this can easily lead to similar processes having to be re-researched and re-invented country-by-country. In the context of the European Union as a whole, fire safety requirements are based on EU Regulation No 305/2011 [2]. This document of The European Parliament and Council lays down harmonised conditions for the marketing of construction products as an essential requirement for construction works. In Annex I of this Directive, the essential requirements for structural resistance and stability, and for fire safety, are summarised. The construction works must be designed and built in such a way that, in the event of the outbreak of fire:

- The load-bearing capacity of the construction can be assumed for a specific period of time – although this is based on the assumption of a standardised fire time-temperature curve which clearly does not represent the real conditions in any naturally occurring fire;

- The generation and spread of fire and smoke within the building are limited;
- The spread of the fire to neighbouring properties is limited;
- Occupants can leave the buildings or be rescued by other means;
- The safety of rescue teams is taken into consideration.

The load-bearing capacity of a structure may be modelled on the basis of the principles summarised in the various parts of the structural Eurocodes which deal with fire. With the introduction of common standards in areas related to fire safety, it seems obvious that in such an important area the sharing of experience and research should be facilitated, and hence that networks such as COST TU0904 are necessary. However, the need for integration has a further dimension. Fire engineering researchers tend to specialise in areas such as fire dynamics, structural fire engineering, active/passive fire protection, environmental protection or human response. Since the background sciences of these disciplines differ there is little interaction between them. Practitioners, including fire engineers, building/fire control authorities, and fire-fighters tend to consider fire safety as a whole, but lack in-depth awareness of recent advances in research and are outside the academic research networks. By encouraging exchange of information on different aspects of fire engineering and response between researchers in different countries, this network intends to create an awareness of the current state of the art, and to avoid repetition of research. The benefit to the non-research community derives from its exposure to advanced research findings, discussion with researchers, and the sharing of best practice. The input from this community makes researchers aware of real-world constraints, and reveals where new research and standards are needed.

The Action has divided its membership loosely into three themed Working Groups, although clearly its overall mission of promoting integration means that these groups have interacted on many key activities. The Working Groups are:

- WG1 Fire Behaviour and Life Safety focuses on the behaviour and effects of fire in buildings, combining this research-based knowledge with the most effective means of protecting human life against the occurrence of fire in the built environment. This includes active measures in fire-fighting with the effects of building form on the inherent risk to inhabitants.
- WG2 Structural safety covers the response of different building types to fires and the rapidly developing research field of structural fire engineering, including new materials and technologies and passive protection measures. Crucial problems of structural fire engineering concern change of use of buildings and the current imperatives of sustainability, energy saving and protection of the environment after fire.
- WG3 Integrated Design brings together design, practice and research across the disciplines of fire in the built environment. In structural design this includes integration of fire resistance with

all the other functional requirements of a building, from concept onwards, rather than simply adding fire protection after all other processes are complete. Active input from practitioners, regulators and fire-fighters through this group is vital to the success of the Action.

The Action started in March 2010, and now has 22 nations of the EU participating, as well as researchers from New Zealand. Its first deliverable, the State of the Art Report [3] attempted to bring together the current state of research, mainly in the participating countries but set into the context of knowledge world-wide. The second deliverable, emanating from the Action Conference in Prague in 29 April 2011, allowed all experts in the Action, as well as international researchers in general, to present current research findings in two Conference Proceedings [4]. The third deliverable, a compilation of Case Studies [5] presented current advanced design practice and accumulated knowledge in fire engineering. These included, within the fire engineering applications presented, explanations of the decision processes, the scientific assumptions and the practical constraints, as well as integration of the different aspects of fire engineering. The fourth deliverable, on Fire Brigade Reports and Investigations [6], consists of a set of contributions from members of the Action relating to: the organisation of national fire and rescue provision in different EU countries; available statistical data; recommendations for questions to be included in standardised fire fighters' reports in order to improve the comparability of national statistics; and lessons to be learned from specific disasters.

František Wald and Ian Burgess

21 Feb 2013

References

- [1] EN 1991-1-2, Eurocode 1: *Actions on structures - Part 1-2: General actions - Actions on structures exposed to fire*, CEN Brussels, 2002, 59 pp.
- [2] *Regulation (EU) No 305/2011 of the European Parliament and Council, Harmonised conditions for the marketing of construction*, 9 March 2011, URL: eur-lex.europa.eu.
- [3] *Integrated Fire Engineering and Response - State of the Art Report*, CTU – Publishing House, Czech Technical University in Prague, 2011, 239 pp., ISBN 978-80-01-04598-5, for download at fire.fsv.cvut.cz/ifer/WP1.
- [4] *Applications of Structural Fire Engineering*, Czech Technical University in Prague, Česká technika, 2011 and 2013, for download at fire.fsv.cvut.cz/ASFE11 and fire.fsv.cvut.cz/ASFE13
- [5] *Integrated Fire Engineering and Response – Case Studies*, CTU – Publishing House, Czech Technical University in Prague, 2012, 374 pp., ISBN 978-80-01-05004-0, for download at fire.fsv.cvut.cz/ifer/WP2.
- [6] *Integrated Fire Engineering and Response – Fire Brigade Reports and Investigations*, CTU – Publishing House, Czech Technical University in Prague, 2013, 168 pp., ISBN 978-80-01-05200-6, for download at fire.fsv.cvut.cz/ifer/WP3.

Neno Toric, nenno.toric@gradst.hr

WG2 - Ian Burgess, ian.burgess@sheffield.ac.uk

1 BENCHMARK STUDIES FOR PARTIALLY HEATED STEEL BEAMS

Summary

This article presents benchmark studies which can be used for testing numerical models dealing with 3D analysis and geometrically/materially nonlinear structural analyses of structures affected by fire. The proposed benchmarks are based on four fire tests conducted on simply supported and partially heated steel members. Structural analyses of four different fire tests were carried out using the commercial version of the Vulcan software. Two of the benchmark studies include partially heated simply supported steel beams loaded with a vertical force, and the other two include partially heated simply supported beams loaded with a vertical and a compressive force. Temperatures used in the numerical modelling were based on those measured during the fire tests.

Tab. 1.1 List of benchmark studies

| TEMPERATURE CURVE | REF | CONTENTS |
|-------------------|------|------------------------------------------------------------------------|
| Nonlinear | BMS1 | Simply supported steel beam, vertical force=200 kN |
| | BMS2 | Simply supported steel beam, vertical force=275 kN |
| | BMS3 | Simply supported steel beam, vertical force=200 kN, axial force=400 kN |
| | BMS4 | Simply supported steel beam, vertical force=250 kN, axial force=400 kN |

Table 1.2 Main parameters of benchmark studies

| REF | CONTENTS |
|----------|------------------------------------------------------------------------------------------------------------------------------------------------------------------------------------------------------------------------------------------------------------------------------------------------------------------------------------------------------------------------------------------------------------------|
| BMS1,2&3 | Midspan deflection, axial force at midspan and different types of heating curves for each of the finite elements of: BMS1 - Simply supported steel beam, vertical force=200 kN BMS2 - Simply supported steel beam, vertical force=275 kN BMS3 - Simply supported steel beam, vertical force=200 kN, axial force=400 kN BMS4 - Simply supported steel beam, vertical force=250 kN, axial force=400 kN |

1.1 INTRODUCTION

1.1.1 Background of the study

The benchmarks were created at the University of Sheffield during a COST short term scientific mission titled “Numerical modelling of steel structures exposed to fire” in February, 2013. The studies were created on the basis of several fire experiments previously carried out by the University of Split. Four fire tests conducted on partially heated simply supported steel beams were used to create benchmarks. Different load level and heating rate was used for each of the tests, thus making each of the benchmarks unique. A mechanical analysis was conducted in Vulcan software with the direct application of the recorded fire temperatures of the steel members.

1.1.2 Description of the fire tests

Details regarding the experiments conducted can be found in literature (Boko et al., 2012; Torić et al., 2013a; Torić et al., 2013b), and only a brief description will be given in this report. The experimental programme (Fig. 1.1) included heating of steel beams with a span of 2,5 m by applying transient heating, and subsequently loading them in different ways (flexure and flexure combined with axial compression). Lateral support was ensured during the loading at mid-span in order to prevent lateral-torsional buckling.

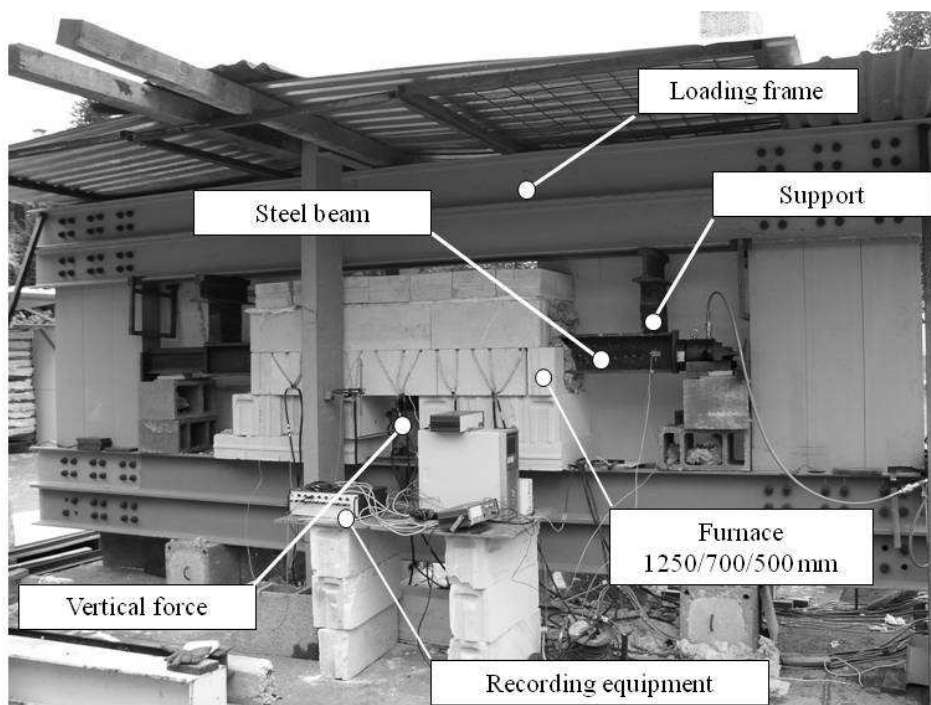


Fig. 1.1 Steel members test setup

Fig. 1.2 shows the locations of discrete temperature measuring points at which the temperature development was observed over time, as well as the structural model used for numerical modelling. Table 1.3 presents the measured temperatures from all four furnace tests, which were used by others to conduct full heat transfer analysis. Vertical force V at midspan and the axial force H at the end of the beam were inserted with the help of hydraulic plates. Temperature increase in the furnace was governed by one flame burner. Table 1.4 presents a summary of the testing parameters for the tests conducted. Steel grade of the beams was classified as S355J2G3 according to Eurocode 3 classification. Mechanical properties of the steel S355 were determined experimentally with the following values: $f_{y,20} = 362.4$ MPa and $E_{y,20} = 209000.0$ MPa, where $f_{y,20}$ – yield strength at 20°C and $E_{y,20}$ – modulus of elasticity at 20°C.

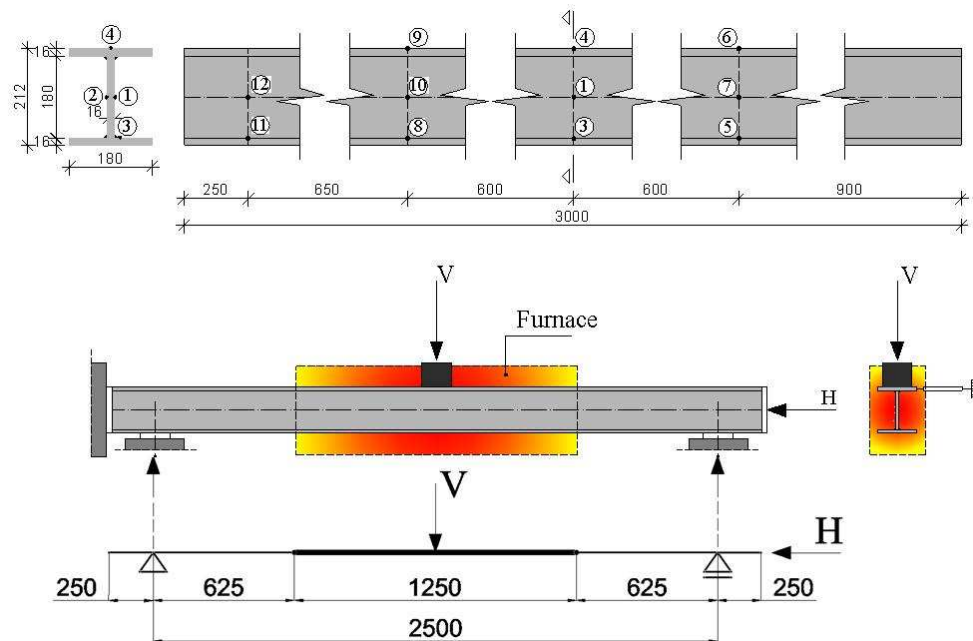


Fig. 1.2 Temperature measuring points and structural model

1.2 MECHANICAL ANALYSIS

1.2.1 Short description of Vulcan software

Numerical analysis was carried out using the structural fire analysis software Vulcan (Huang et al., 1999; Cai et al., 2003; Huang et al., 2009; Dong et al., 2013). The software has been being developed by the Fire research group at the University of Sheffield for over 20 years. Vulcan is a software capable of conducting three-dimensional analysis in fire conditions of steel and composite frames.

Tab. 1.3 Measured temperature in the furnace

| Time (min) | Test 1 (°C) | Test 2 (°C) | Test 3 (°C) | Test 4 (°C) |
|------------|----------------|----------------|----------------|----------------|
| 0 | 17,3 | 13,7 | 12,8 | 8,5 |
| 10 | 225,3 | 144,2 | 79,9 | 100,6 |
| 20 | 349,7 | 239,1 | 114,9 | 137,6 |
| 30 | 425,0 | 389,4 | 148,2 | 185,7 |
| 40 | 460,0 | 485,6 | 181,9 | 239,1 |
| 50 | 452,8 | 551,6 | 214,3 | 285,4 |
| 60 | 450,0 | - | 246,3 | 338,6 |
| 70 | 462,0 | - | 274,2 | 383,6 |
| 80 | 476,2 | - | 306,9 | 436,6 |
| 90 | 499,1 | - | 333,2 | 477,4 |
| 100 | 527,2 | - | 367,6 | 516,3 |
| 110 | 552,7 | - | 398,2 | - |
| 120 | 563,4 | - | 425,6 | - |
| 130 | - | - | 453,2 | - |
| 140 | - | - | 479,7 | - |
| 150 | - | - | 492,0 | - |
| 160 | - | - | 506,1 | - |
| 170 | - | - | 520,9 | - |
| 180 | - | - | 537,6 | - |
| 190 | - | - | 550,2 | - |

Tab. 1.4 Testing parameters for steel beams

| Testing method | | Transient | | | |
|---------------------|----------|-----------|--------|-----------------------|--------|
| Load type | | Flexure | | Flexure + axial force | |
| Member (Steel S355) | | Test 1 | Test 2 | Test 3 | Test 4 |
| Test time (min) | | 115 | 45 | 190 | 100 |
| Force (kN) | Axial | - | - | 400 | 400 |
| | Vertical | 200 | 275 | 200 | 250 |

There is a number of finite elements in the software for modelling purpose, including a three-noded beam-column element, a nine-noded slab element, shear connector and spring elements. The main assumption used if combining two or more different types of finite elements is that they are all defined in a common reference plane which coincides with the mid-surface of the slab element (Huang et al., 1999). Beam-column elements are represented as three-noded line elements with six degrees of freedom per node (Cai et al., 2003, Huang, 2009). Figure 1.3 presents the three-noded line element incorporated in Vulcan.

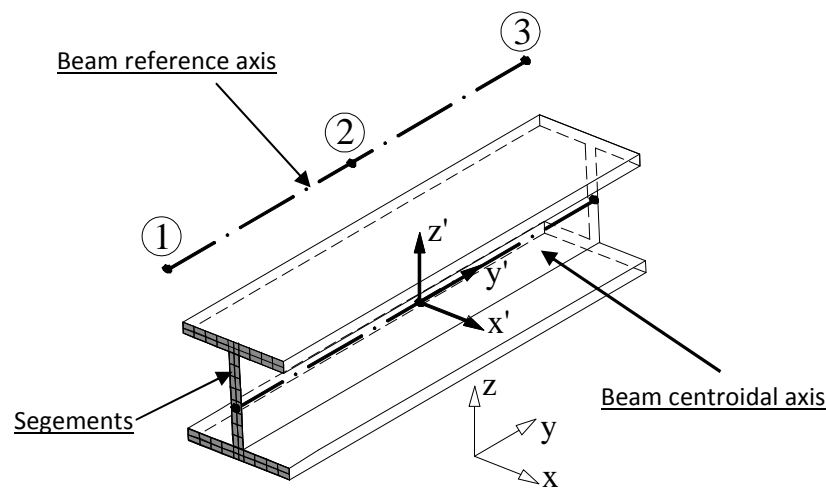


Fig. 1.3 Three-noded line element

The main assumptions for the three-noded line elements and stress-strain calculation in the cross-section are as follows: elements are straight and prismatic; plane cross-sections remain plane under flexural deformations (Bernouli's hypothesis) and there is no slip between different types of material.

Material and geometrically nonlinear analyses are incorporated in the program. Geometrically nonlinear analysis is based on the Total Lagrangian description, with the displacements of any point within the element specified in relation to its initial position. Materially nonlinear analysis is taken into account by dividing the cross-section into a number of segments which can be exposed to different level of stress and temperature. Different types of temperature profiles (temperature patterns) can be used to take into account temperature variation across the cross-section. Vulcan software is capable of conducting classic nonlinear static analysis.

1.2.2 Numerical analysis

Material constitutive behaviour model that was used in the benchmarks was based on the Eurocode 3 stress-strain temperature curves (EN 1993-1-2, 2005) including the corresponding thermal strain model.

Reduction factors for yield strength, modulus of elasticity and the proportionality limit were also taken from Eurocode 3. Fig 1.4 presents the stress-strain curves and Fig 1.5 presents the reduction factors for yield strength and modulus of elasticity from Eurocode 3.

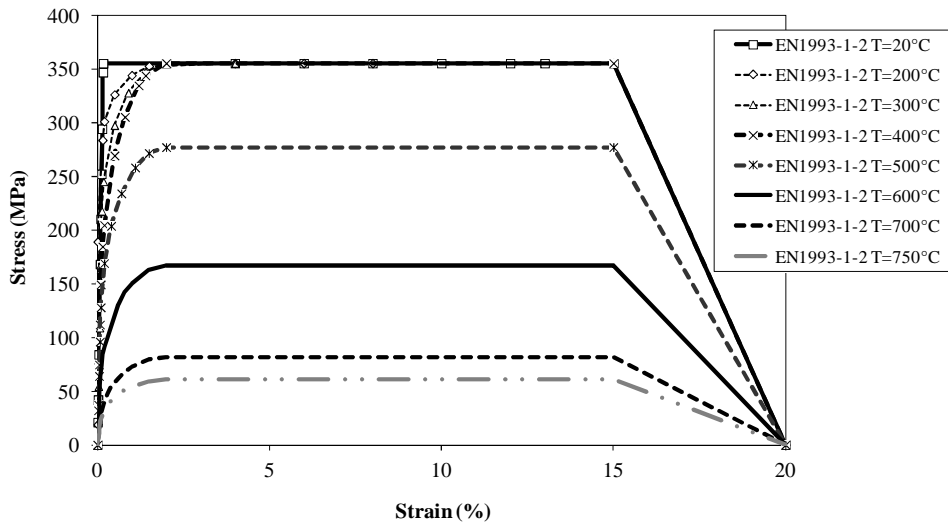


Fig. 1.4 Stress-strain constitutive law from Eurocode 3 – Steel S355

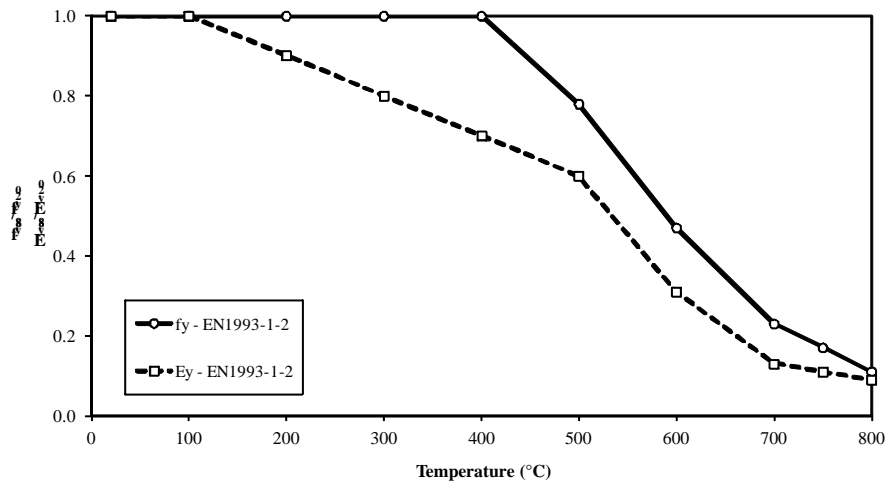


Fig. 1.5 Reduction factors for yield strength $f_{y,\theta}$ and modulus of elasticity $E_{y,\theta}$ at temperature θ from Eurocode 3

A sensitivity analysis was performed for both the total number of finite elements and the representation of fire temperatures developed in the beams. The analysis included the calculation of the member response using 5, 8, 10, 14 three-noded elements. Asymptotic convergence of the results was achieved with 10 elements, so the four benchmark analyses were conducted with this

discretization. Fig. 1.6 presents the chosen discretization scheme with the disposition of the finite elements.

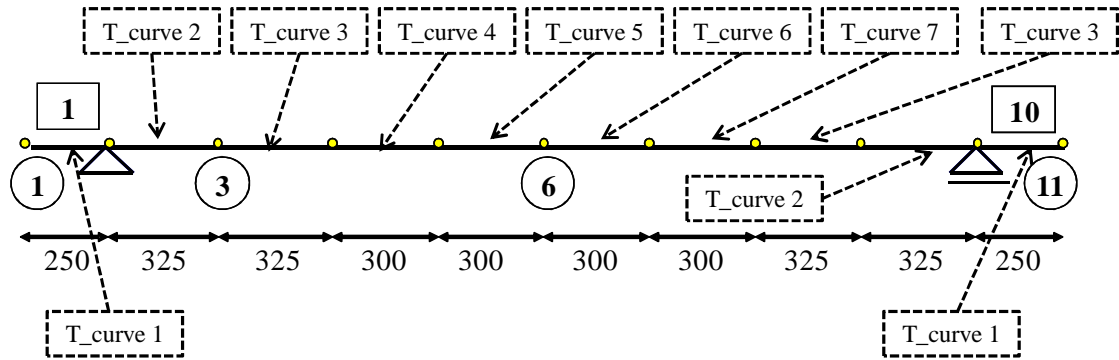
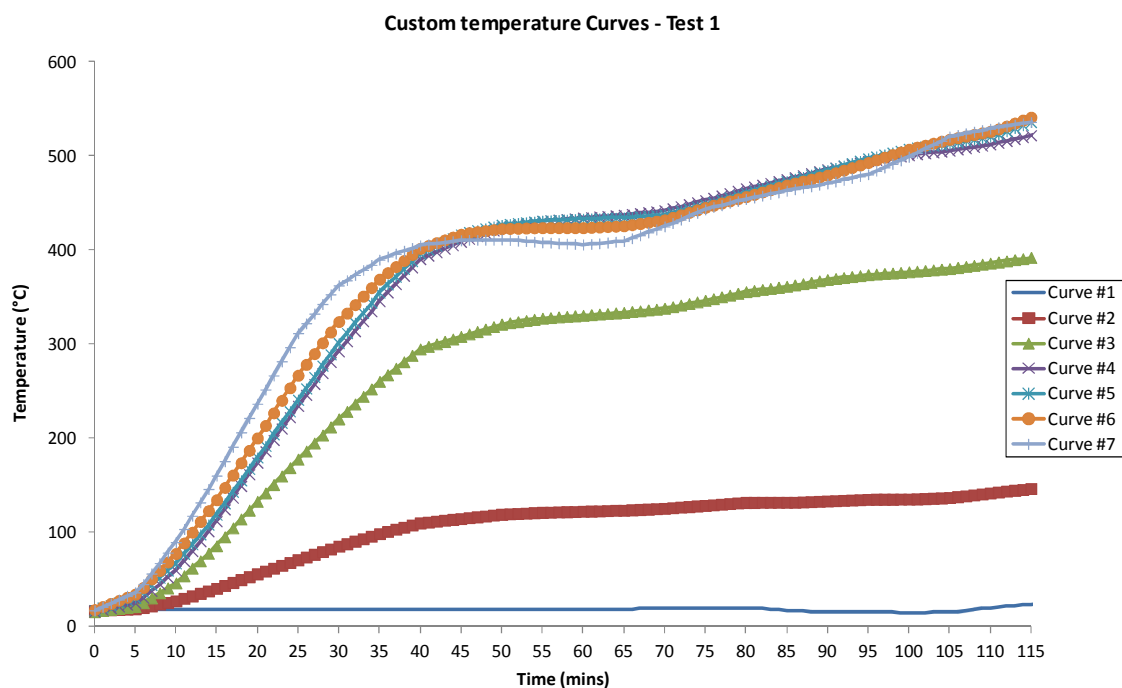
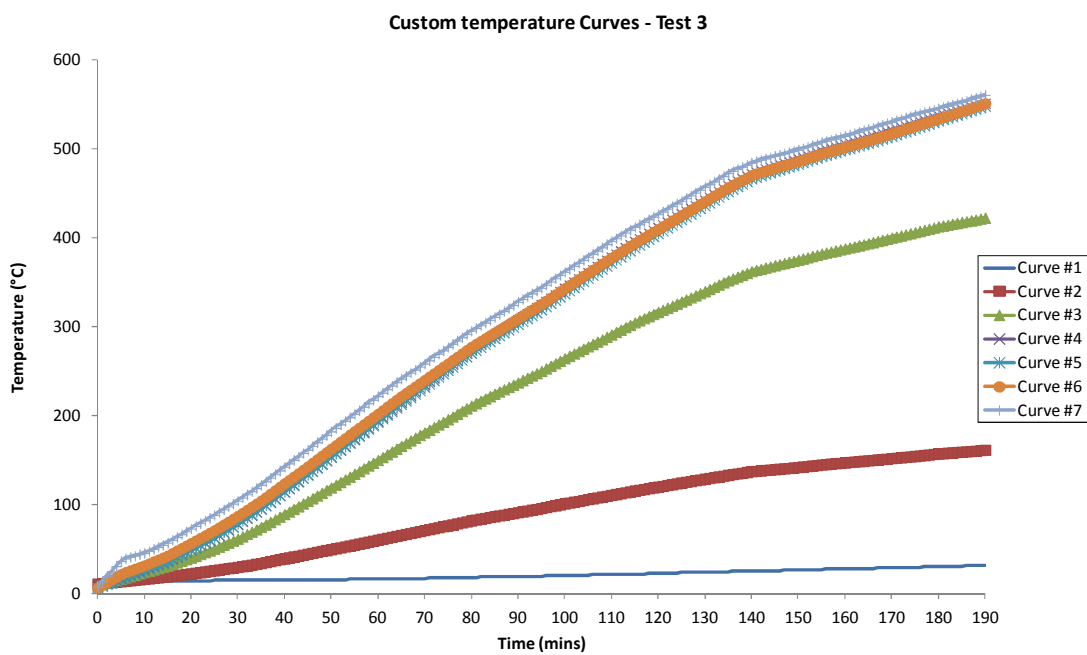
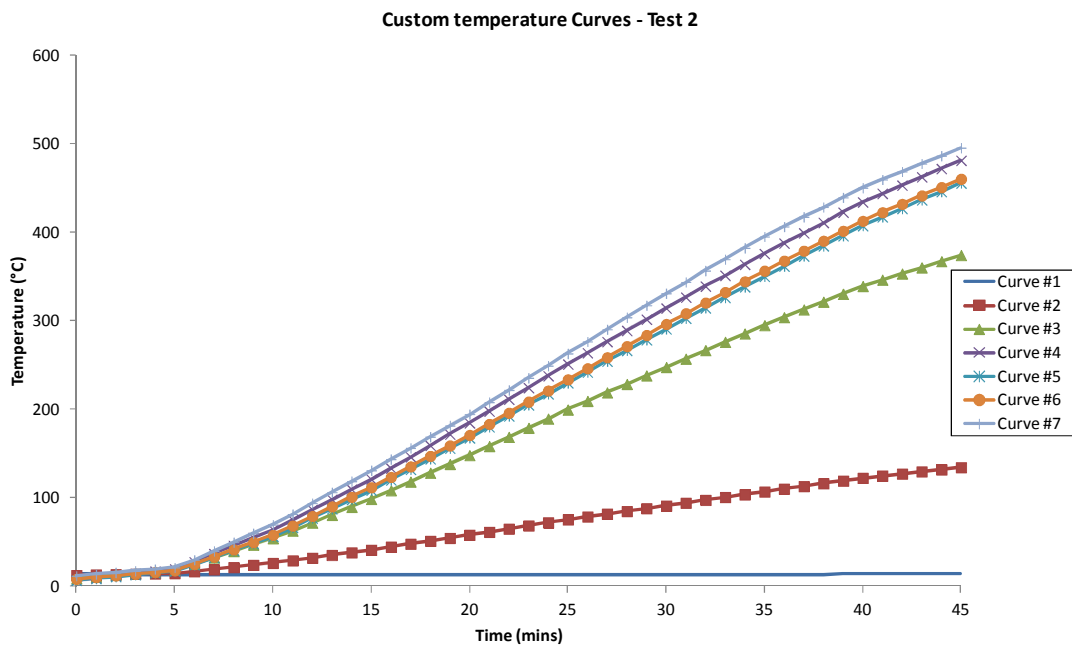


Fig. 1.6 Discretization scheme for partially heated steel beam

A basic requirement of the software is manual input of the temperatures of the structure. The input temperatures used in the benchmarks are based on the average temperatures of the cross section measured during fire tests; for example the temperature of the cross section at 0,25 m from the end of the member is determined as the average of the temperatures at points 11&12 (Fig. 1.2). Mean values of temperature at different parts of the cross-section are presented in the input spreadsheet files, together with the details of loading and boundary conditions. A uniform temperature profile was used for each of the elements to represent the temperature action. Fig. 1.6 also shows which of the temperature curves is assigned to a certain finite element. Fig. 1.7 presents the temperature input for all of the fire tests.





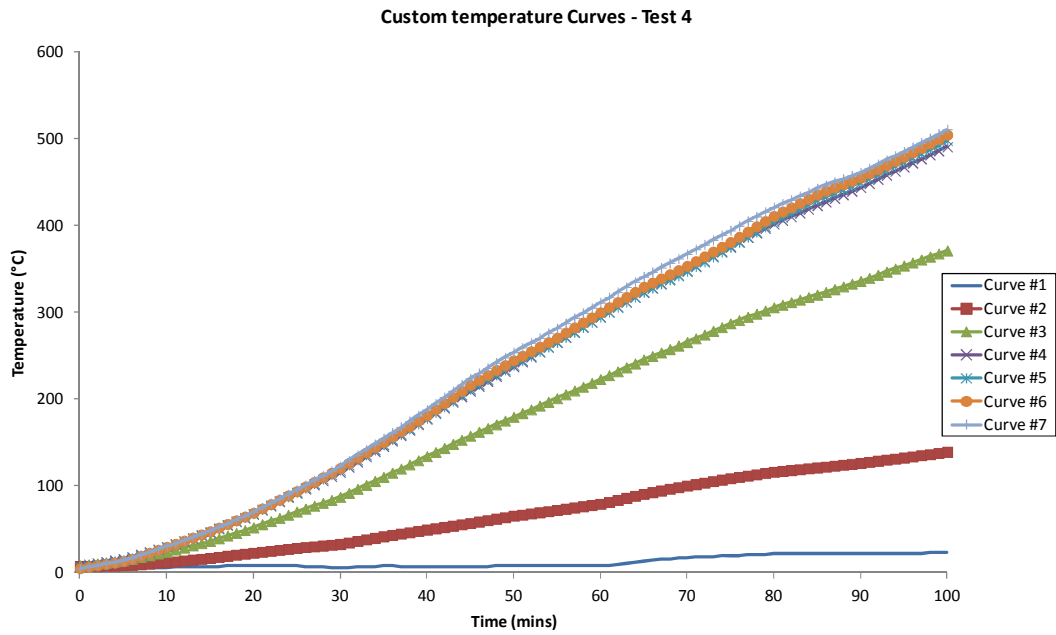
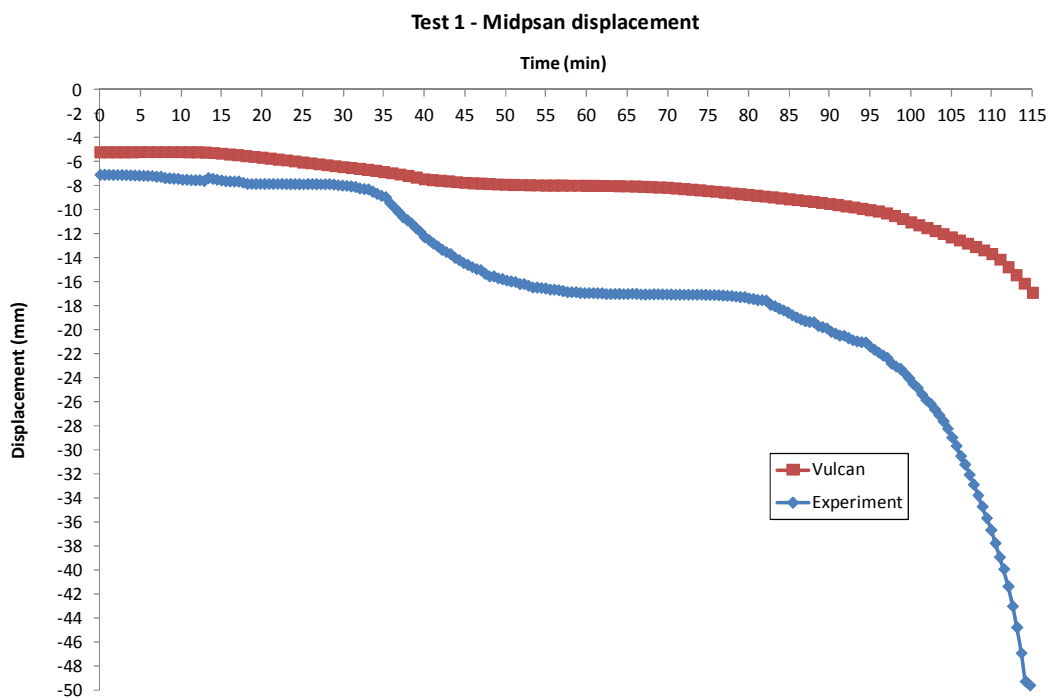


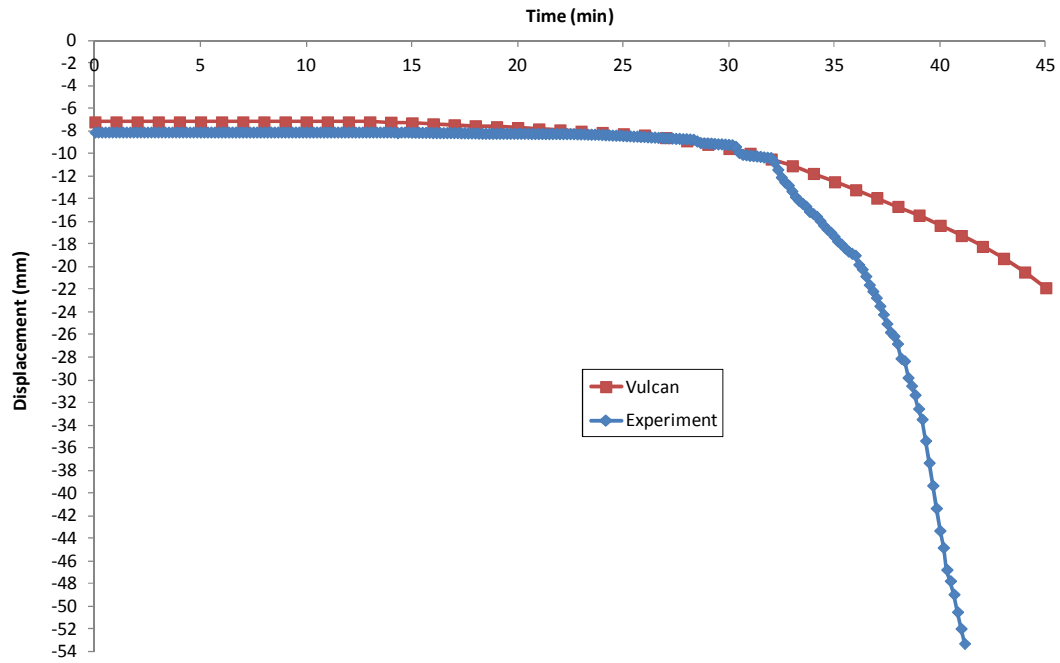
Fig. 1.7 Plot of temperature curves used as a heating curve for steel beams

1.3 SUMMARY OF RESULTS

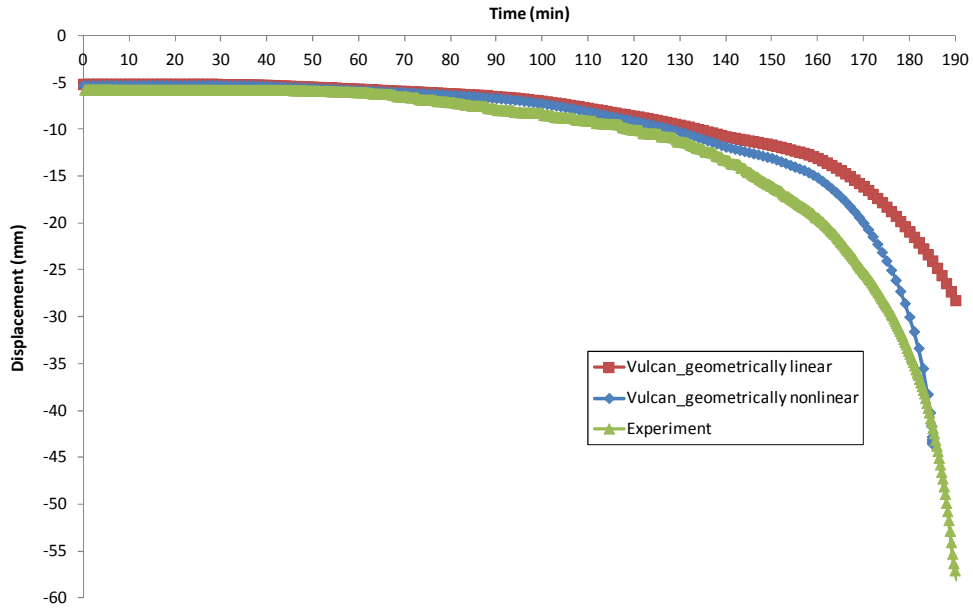
Fig. 1.8 presents the midspan deflections predicted by Vulcan and a comparison with the experimental displacement for the four tests. Vulcan deflection predictions for tests 3&4 are given in the spreadsheet for geometrically linear and nonlinear analyses, to permit other researchers' wish to conduct different types of analysis.



Test 2 - Midspan displacement



Test 3 - Midspan displacement



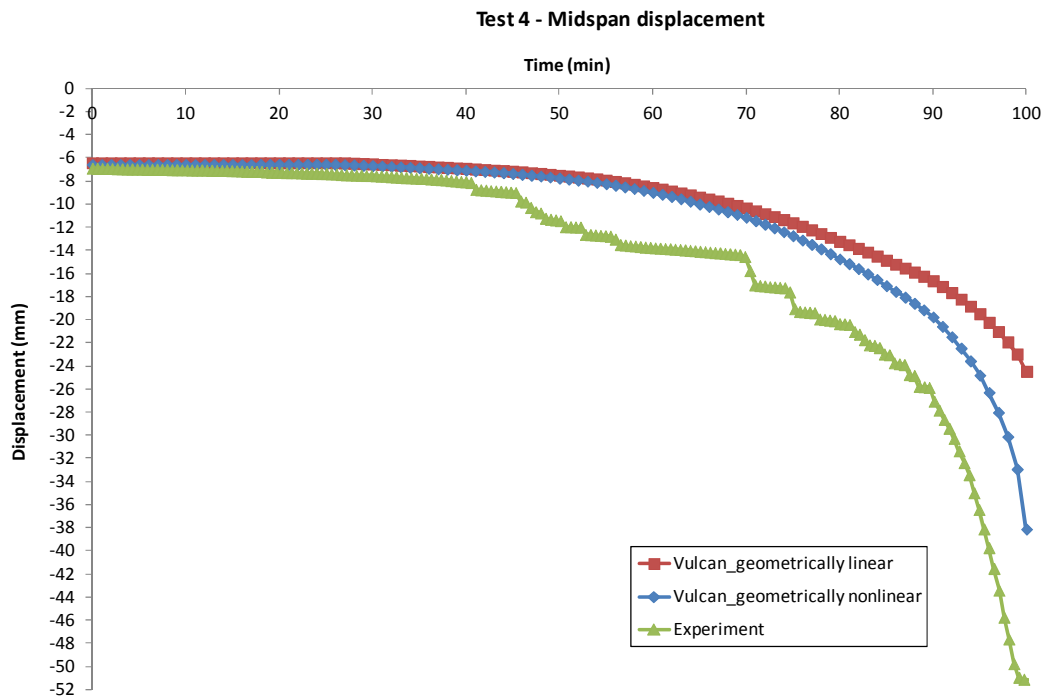


Fig. 1.8 Comparison of results between Vulcan predictions and the experiment

1.4 GENERAL REMARKS

A discrepancy between the results obtained by Vulcan and the experiment is observable for tests 1&2. Several factors can be attributed to this, but the important ones are connected with the simplified treatment of temperature field in the beams, usage of reduction factors and material constitutive law from Eurocode 3 and neglecting the realistic creep strain analysis (Eurocode curves consider creep strains implicitly in the material constitutive law). Since the members are partially heated, a moving 3D temperature field exists in the member, thus only a 3D heat transfer model can provide an adequate temperature field description in the member (Torić et al., 2013b). Realistic material properties have been determined for the steel grade of the beams, pointing to larger reduction of yield strength and modulus of elasticity at high temperature if compared to Eurocode 3 reduction factors (Boko et al., 2012). Creep analysis is necessary if steel members are exposed to temperature above 400°C for a prolonged time period, which is precisely the case for Tests 1,3&4. Member deflections tend to increase in case of simply supported axially unrestrained beams due to creep (Torić et al., 2013b). Therefore, implicit creep in the Eurocode 3 material curves might be inadequate to account for additional deflections recorded in the experiment.

References

- Boko, I., Torić, N. and Peroš, B., 2012, Structural fire design parameters and procedures – analysis of the potential of Eurocode 3, *Materialwissenschaft und Werkstofftechnik*, 43 (12), pp.1036-1052, ISSN 0933-5137.
- Torić, N., Harapin, A., Boko, I., Peroš, B. and Ban, M., 2013a, Modelling of the influence of creep strains on the fire response of steel elements, *Applications of Structural Fire Engineering*, CTU Publishing House, Prague, pp. 480-485, ISBN 978-80-01-05204-4.
- Torić, N., Harapin, A., Boko, I., 2013b, Experimental verification of a newly developed implicit creep model for steel structures exposed to fire, *Engineering Structures*, 57, pp.116-124, ISSN 0141-0296.
- Huang, Z., Burgess, I.W. and Plank, R.J., 2000, Three-Dimensional Analysis of Composite Steel-Framed Buildings in Fire, *ASCE Journal of Structural Engineering*, 126 (3), pp 389-397, ISSN 0733-9445.
- Cai J., Burgess, I.W. and Plank, R.J., 2003, A generalised steel/reinforced concrete beam-column element model for fire conditions, *Engineering Structures*, 25(6), pp.817-833, ISSN 0141-0296.
- Huang, Z., Burgess, I.W. and Plank, J.R., 2009, Three-dimensional analysis of reinforced concrete beam-column structures in fire, *ASCE Journal of Structural Engineering*, 135 (10), pp.1201-1212, ISSN 0733-9445.
- Dong, G., Burgess, I.W., Davison, J.B. and Sun, R., 2013, Development of a general component-based connection element for structural fire engineering analysis, *Applications of Structural Fire Engineering*, CTU Publishing House, Prague, pp. 207-213, ISBN 978-80-01-05204-4.
- EN 1993-1-2: 2005 – Eurocode 3: Design of steel structures - Part 1-2: General rules - Structural fire design, CEN Brussels.

Martin Prachař, martin.prachar@fsv.cvut.cz

WG3 - Nuno Lopes, nuno.lopes@ua.pt

WG1 - Carlos Couto, ccouto@ua.pt

WG3 - Michal Jandera, michal.jandera@fsv.cvut.cz

WG3 - Paulo Vila Real, pvreal@ua.pt

WG2 - František Wald, wald@fsv.cvut.cz

2 LATERAL TORSIONAL-BUCKLING OF CLASS 4 STEEL PLATE GIRDERS UNDER FIRE CONDITIONS: EXPERIMENTAL AND NUMERICAL COMPARISON

Summary

This paper presents a validation of numerical model of the lateral torsional-buckling of Class 4 steel plate girders under fire conditions. In the framework of the RFCS project FIDESC4 - Fire Design of Steel Members with Welded or Hot-rolled Class 4 Cross-sections, three simple supported beams, one of them non-uniform (tapered), submitted to two point loads were tested with different temperatures at the Czech Technical University in Prague. Detailed information on the geometric data, measured geometrical imperfections and actual mechanical properties are given. The design of the test set-up and description of the experiment is given, as well as verification of numerical model. The experimental load-displacement diagrams and the ultimate loads were compared with the numerical results obtained with the FE software ABAQUS and SAFIR.

2.1 INTRODUCTION

This paper deals with lateral-torsional buckling (LTB) of slender steel I beams under fire conditions. The fire behaviour of three beams is analysed by means of experimental tests and numerical analyses.

Steel members with thin-walled cross-sections are commonly used in buildings due to its lightness and long span capacity. However the understanding of the fire resistance of these structural elements can still be further developed and increased.

The structural steel elements with thin walled cross-sections (Class 4 section according to Eurocode 3 (CEN, 2005) subjected to uniform bending diagram, are characterized by having the possibility of occurrence of failure by both local and global buckling modes (LTB). These instability phenomena and their influence on the ultimate strength are of utmost importance to characterize the behaviour of these members. The local buckling occurs due to the compression of thin plates in profiles cross-sections (see Fig. 2.1a). The LTB is an instability phenomenon that in I-sections is induced by the

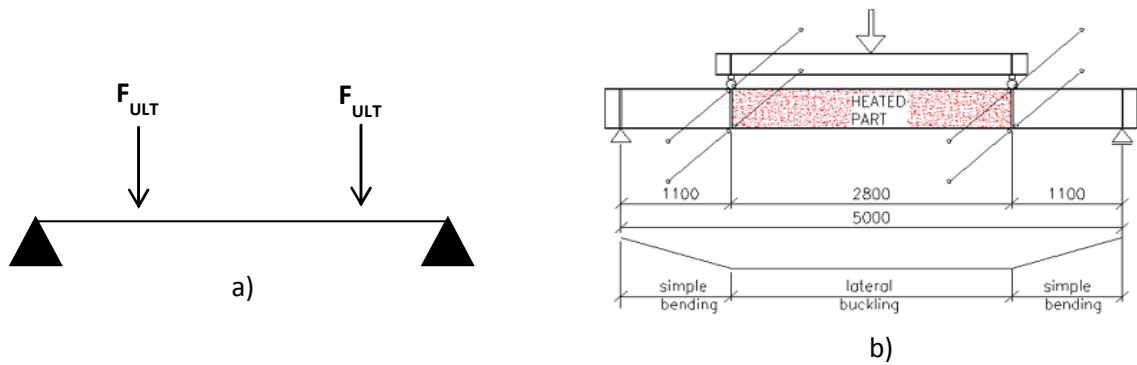


Fig.2.2 Tested beam: a) scheme; b) test set-up

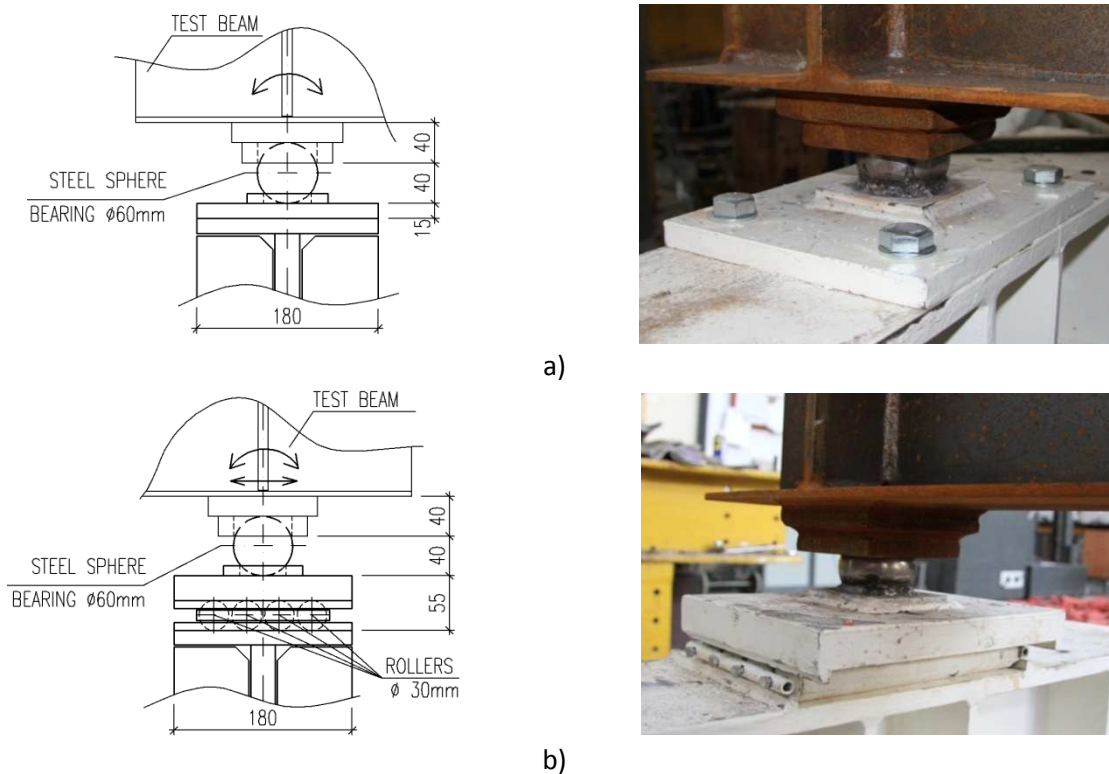
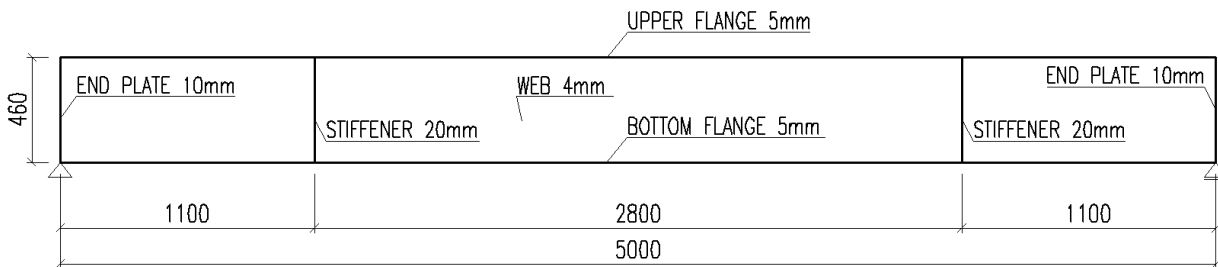


Fig. 2.3 Pinned point supports: a) fixed; b) free

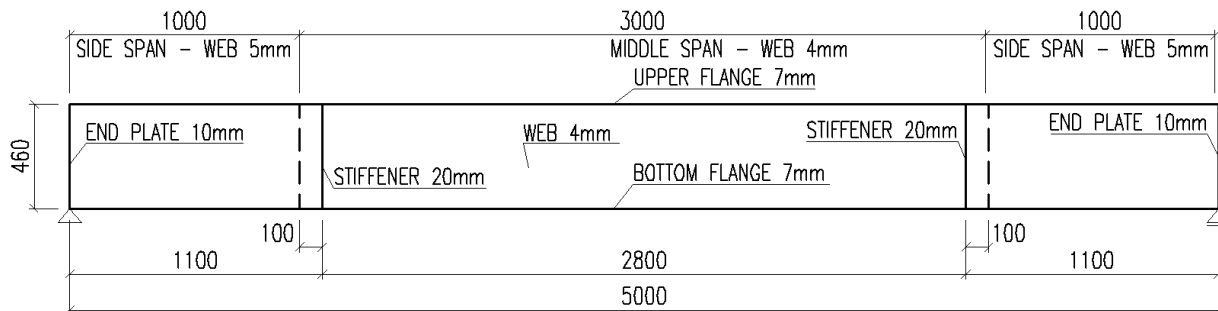
The three tests differ in the cross-sections and applied temperatures. Tab. 2.1 presents the used cross-sections which were fabricated by welding of different steel plates for the flanges and webs. The test 3 was performed on a non-uniform beam. The tests 1 and 2 were set to be at 450°C and test 3 at 650°C. End plates were used with thicknesses of 10 mm and stiffeners at the load application points had 20 mm of thickness. Figure 2.4 summarises the beams dimensions.

Tab. 2.1 Cross-sections

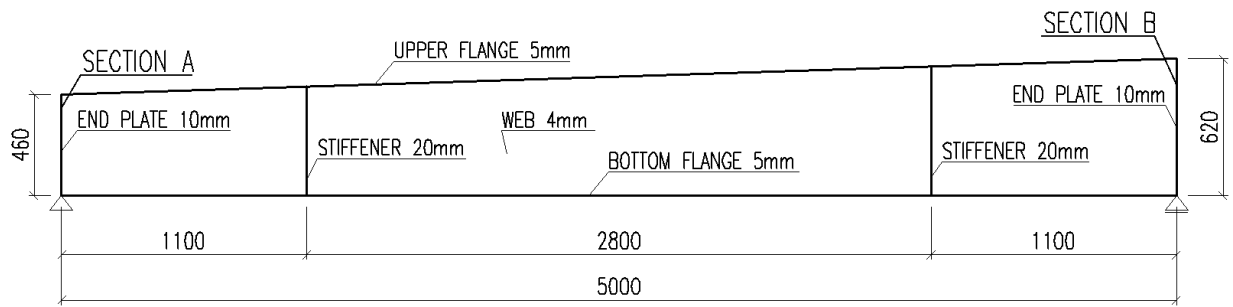
| | Heated Cross-section [mm] | | Non-heated Cross-section [mm] | |
|----------------------------------------------------|-------------------------------------------------------------------|----------------------------|----------------------------------------------------------------------------------|----------------------|
| | Dimensions [mm] | Idealized dimensions (FEM) | | |
| Test 1 (450°C) | $h = 460$ $b = 150$ $t_f = 5$ $t_w = 4$ | | The same as in the heated part See Fig. 2.4a | |
| Test 2 (450°C) | Middle span $h = 460$ $b = 150$ $t_f = 7$ $t_w = 4$ | <u>MIDDLE SPAN</u> | Side span $h = 460$ $b = 150$ $t_f = 7$ $t_w = 5$ (see Fig. 2.4b) | <u>SIDE SPAN</u> |
| Test 3 (650°C) (Tapered beam, see Fig. 2.4c) | $h_A = 460$ $h_B = 620$ $b = 150$ $t_f = 5$ $t_w = 4$ | <u>SECTION A</u> | <u>SECTION B</u> | |



a)



b)



c)

Fig. 2.4 Beams: a) test 1 and 2; b) test 3

The real geometric imperfections, steel temperatures and mechanical properties of the steel plates were measured, as described in the following section.

2.3 EXPERIMENTS

In this section the tests set up and tests procedures are given in detail (see Figure 2.5). The mechanical properties, restraint conditions, geometric imperfections, temperatures in the steel and all other important parameters measurements are described. The load application on the tests was deflection controlled.

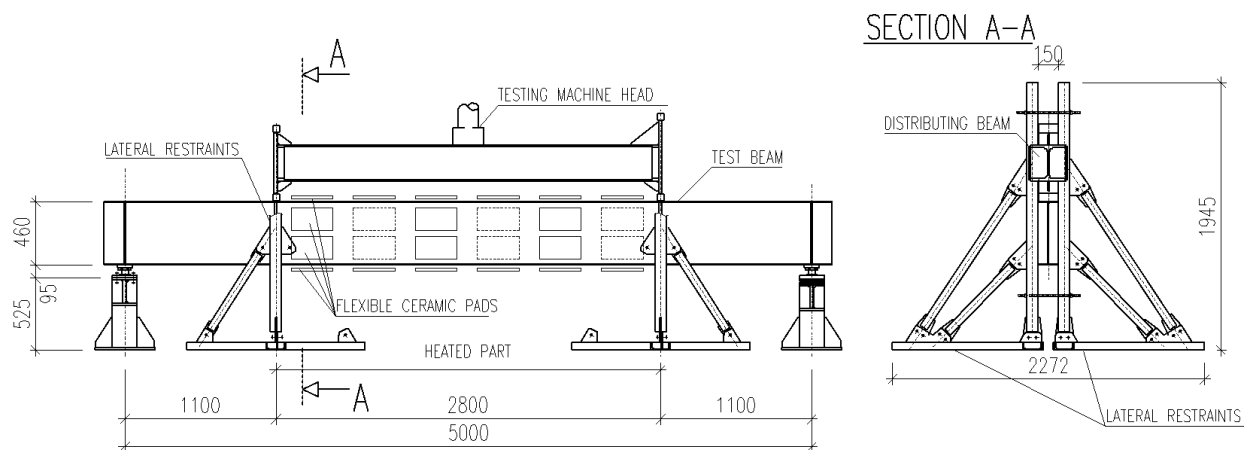


Fig. 2.5a Detailed experimental test set-up



Fig. 2.5b Detailed experimental test set-up

Within the experiment, the material properties of the plates used on the profiles were measured. Number of coupon tests was performed to determination of yield strength and young's modulus for each thickness. The real values of yield strength are presented in Table 2.2

Tab. 2.2 Steel plates yield strength

| Beam parts | Yield strength [MPa] |
|------------------|----------------------|
| Test 1 | |
| Flanges | 385 |
| web | 394 |
| Test 2 | |
| Flanges | 435 |
| web | 394 |
| Web in side span | 376 |
| Test 3 | |
| Flanges | 385 |
| web | 394 |

Before the experiment, after placing the beam on the support, (2) the initial geometry of the specimens was established by manual measurements. It consists of amplitude measurement for global and local imperfection. Amplitude of global imperfection was measured as a deviation from a string spanned between the stiffeners. For measurements of local imperfection amplitude, a special device set with a centesimal displacement meter was used. The investigation was made in compression zone of the beams only. Figure 2.6 shows the position of the measurement. Table 2.3 shows the maximum amplitude of the local and global imperfections.

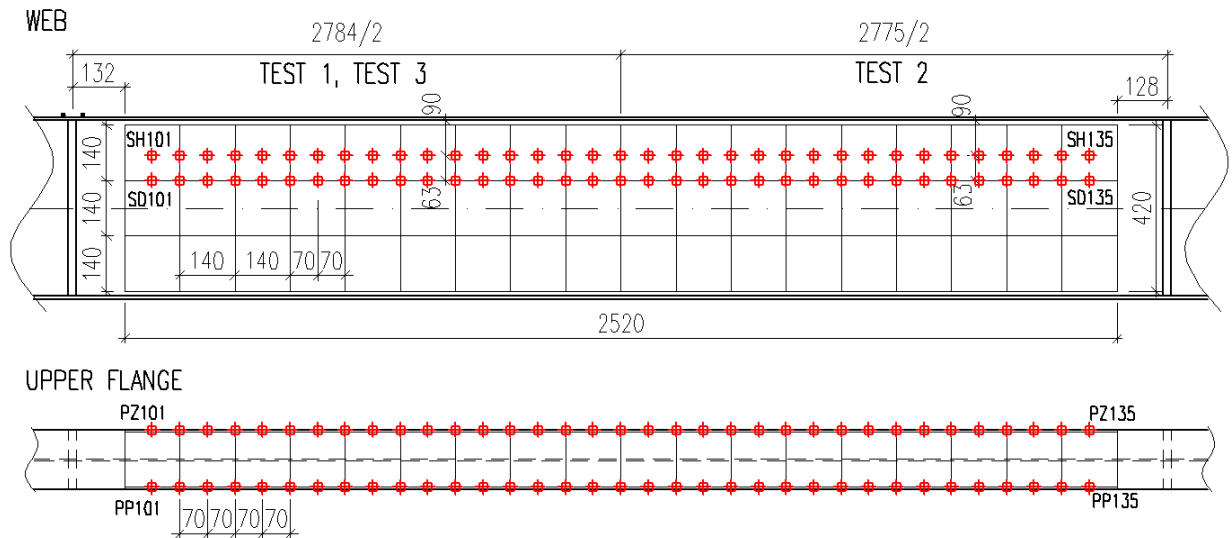


Fig. 2.6 Measured geometric imperfections - position of the measurements

Tab. 2.3 Local and global imperfections amplitudes

| Imperfection | Amplitude [mm] |
|---------------------|----------------|
| Test 1 | |
| Local | 7.36 (web) |
| Global (y-y axis) | 2.5 |
| Test 2 | |
| Local imperfections | 5.8 (web) |
| Global (y-y axis) | 1.5 |
| Test 3 | |
| Local | 7.59 (web) |
| Global (y-y axis) | 1.5 |

Mannings 70kVA heat power units with 6 channels were used to heat the specimens. Cable connection of 70kVA consists of 6 triple cable sets and 4-way splitter cables can accommodate 24 flexible ceramic pads attached. Maximum connected load for the 70kVA unit is 64.8kW. One size of the ceramic pads was used: 305 x 165mm. The power output of the pad was 2.7kW. Ceramic pads were placed as shown in Figure 2.7. In the first step, the pads were put on the rod rack in order to maintain the position of the heating elements on the web. On the bottom flange, the pads were fixed with the steel wires. On the top flange, the pads were fixed by adhesive tape only.

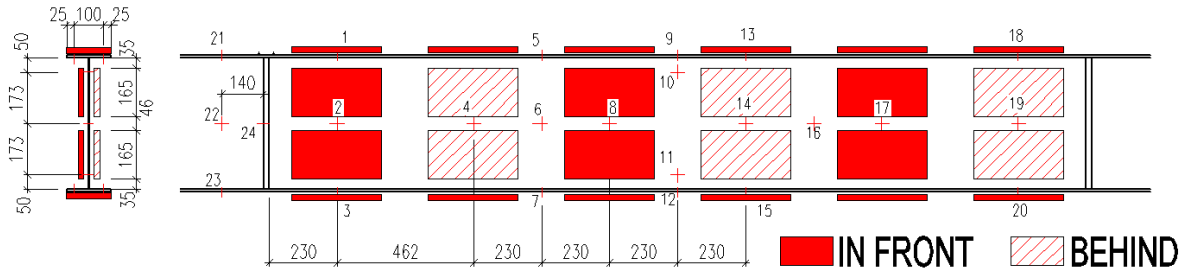


Fig. 2.7 Layout of flexible ceramic pads and thermocouples



Fig. 2.8 Test specimen

Two types of material were used for beams isolation. In the first step, the space between the flanges was filled with standard wool. The space on the flange and below the flange was insulated using standard wool too (ROCKWOOL Airrock HD). The wool was fixed on the beam with steel wires. In the following step, the middle span was wrapped by super wool insulation material.

Twenty-four thermocouples were used for the temperature measurement. Twenty were placed in the middle span and four were placed in the side spans for monitoring of the temperature in not-heated section. The thermocouples were distributed on the beam according to position of ceramic pads, as shown and numbered in Fig. 8. Beam temperatures were recorded from the beginning of heating to the end of experiment. The temperatures varied during the test slightly and were not uniform for the whole section. The average measured temperatures from each part of the beams can be found in Table 2.4.

Tab. 2.4 Steel temperatures

| Beam parts | Average temperature (°C) |
|---------------|--------------------------|
| Test 1 | |
| Upper flange | 457 |
| Web | 444 |
| Bottom flange | 354 |
| Test 2 | |
| Upper flange | 481 |
| Web | 443 |
| Bottom flange | 369 |
| Test 3 | |
| Upper flange | 624 |
| Web | 567 |
| Bottom flange | 416 |

2.4 NUMERICAL ANALYSES

To consider the local buckling of thin walls in members with Class 4 cross-sections, shell finite elements were used instead of the beam finite elements, due to the fact that it is one of the dominant failure modes.

As mentioned before, two finite element programs were used, ABAQUS and SAFIR. The software SAFIR (Franssen, 2005) is a geometrical and material non-linear finite element code especially developed, at the University of Liège, to model the behaviour of structures in case of fire.

The boundary conditions applied to the model followed the degrees of freedom provided by the supports on Fig. 2.3 and the lateral restraints on Fig. 2.2b as it is presented in Fig. 2.8. On the supports, only the displacements were restrained and the rotations were set to be free.

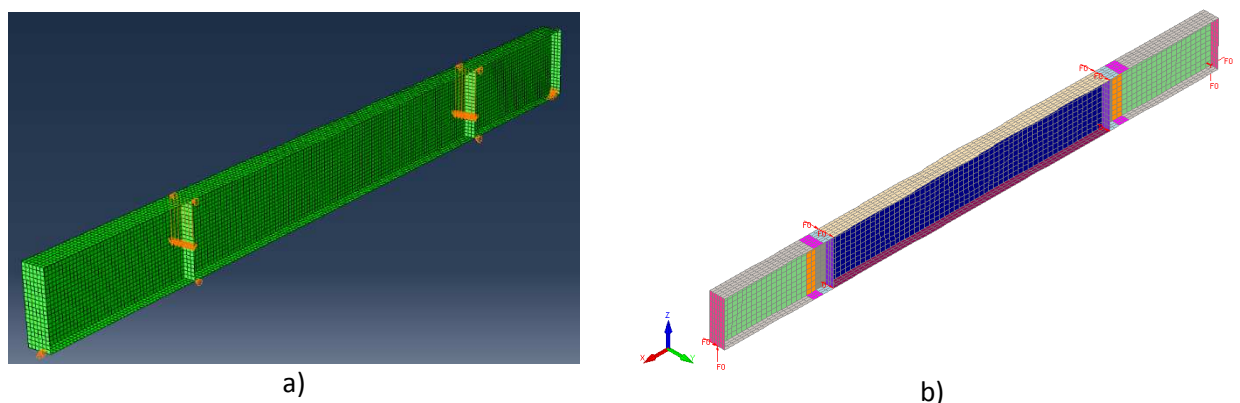


Fig. 2.9 Numerical model used: a) in ABAQUS b) in SAFIR

To obtain the models shown in Figure 2.9, a mesh convergence study was performed. The optimal number of shell elements, in the flanges and in the web, was studied. It is presented in Figure

2.10, the variation of the ultimate bearing load in function of the number of shell elements in the model. On the chosen model ten divisions on the flanges and on the web were used, the beam length was divided by 100 (Safir). Despite this mesh was found to be fine enough, width of the element (in direction of the beam length) was 25 mm for the model in ABAQUS. The welding filets were not taken into account.

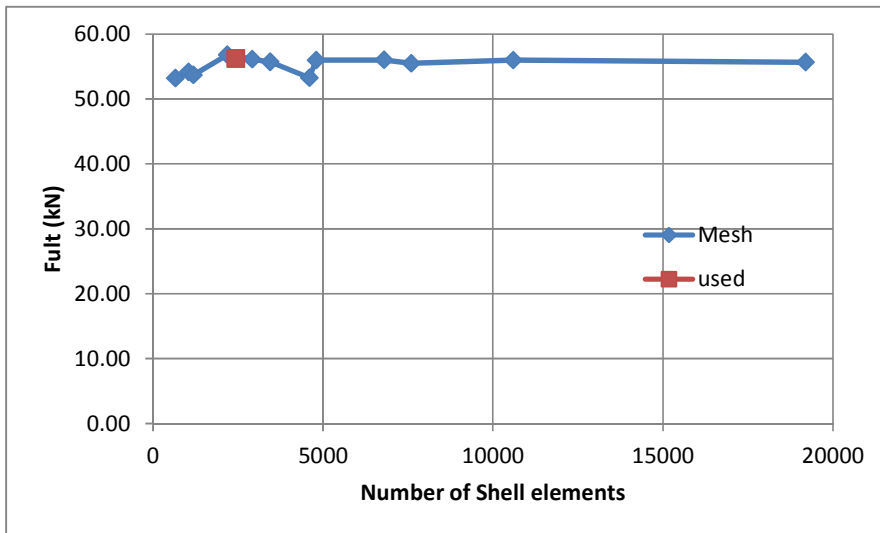
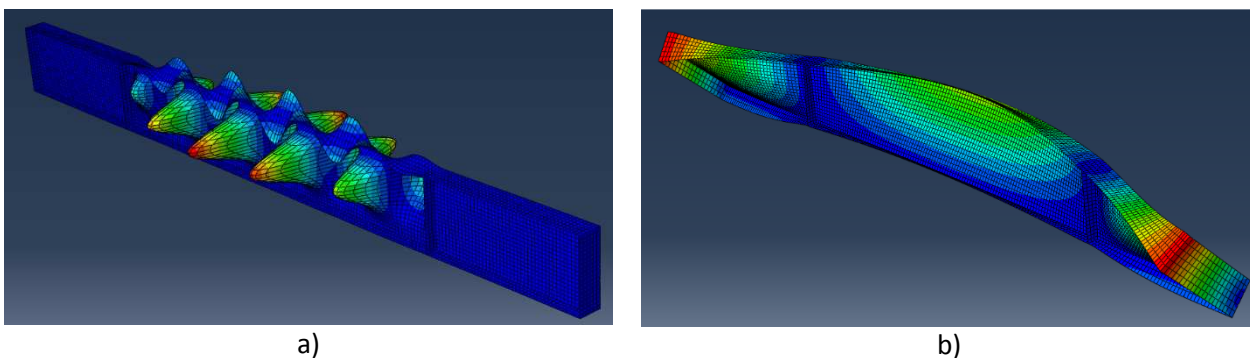


Fig. 2.10 Ultimate bearing load in function of the number of shell elements

Initial geometric imperfections were applied following the beams eigen modes. Two shapes were chosen: the beam 1st local buckling mode and 1st global buckling mode (LTB) shapes (Figure 2.11). For the imperfection amplitudes, the measured values were used (see the previous section).



a) b)
Fig. 2.11 Beams buckling modes shape: a) local; b) global

In these numerical models it was considered that the applied loads were controlled by forces and by displacements. The consideration of the steel thermal expansion was also tested but is neglected in the study shown here. The measured values of the steel mechanical properties (yield strength and

young modulus) and the measured temperatures were adopted in the models. No residual stresses were considered.

2.5 DISCUSSION OF THE RESULTS

Fig. 2.12 shows the failure deformed shape of the test 1 obtained on the experimental test and on the numerical analyses.

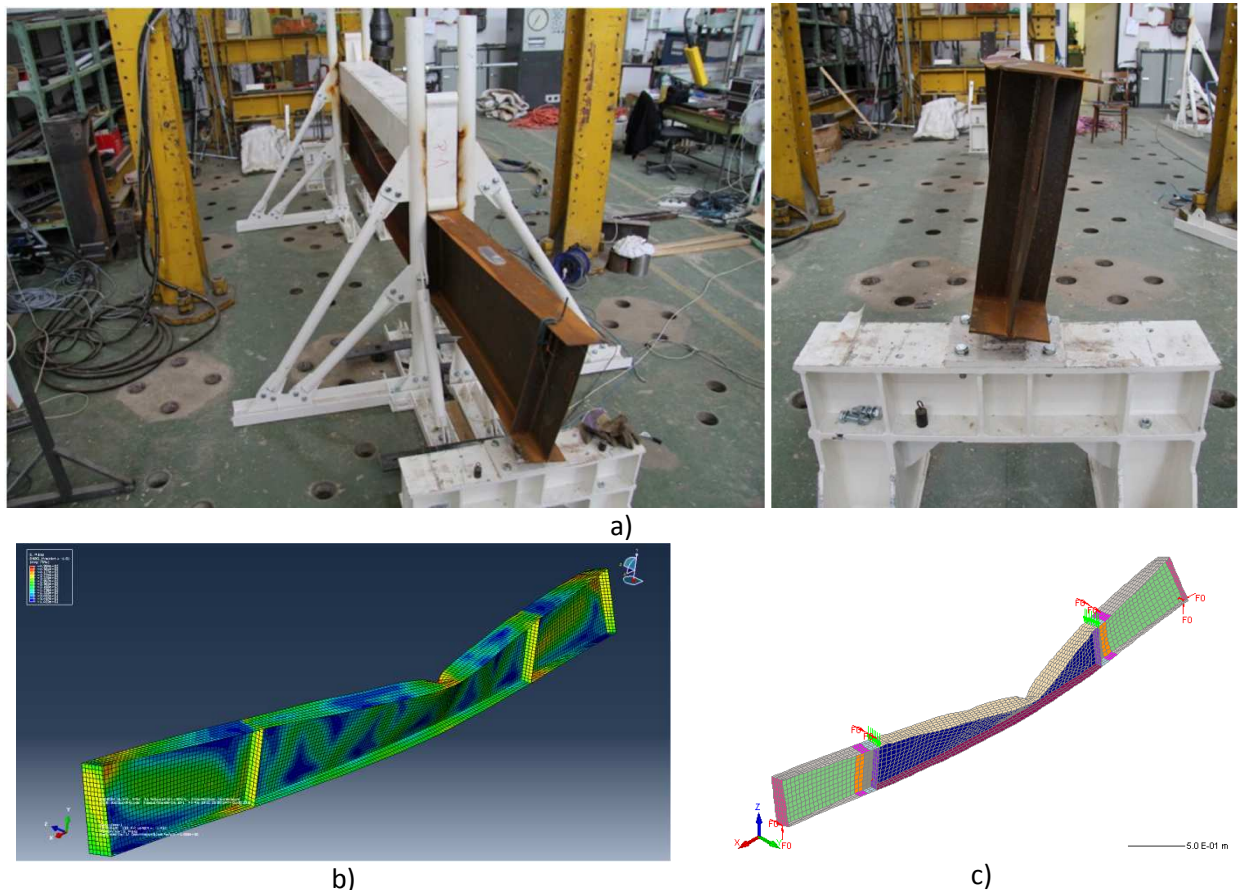


Fig. 2.12 Failure deformed shape on the: a) experimental test; b) ABAQUS analysis; c) SAFIR analysis

The numerical models approximation to the experimental tests is analysed in Figure 2.13. This figure shows the load-displacements relationship comparisons between the experimental test and the numerical analyses. The load corresponds to the total force imposed on the two load application points. The shown displacement corresponds to the vertical displacement at the bottom flange at mid span. In the graphs the curves corresponds to the results of the models with:

- DC – Controlled by displacement;
- FC – Controlled by force;
- No exp - without thermal expansion;
- exp Yes - including thermal expansion;

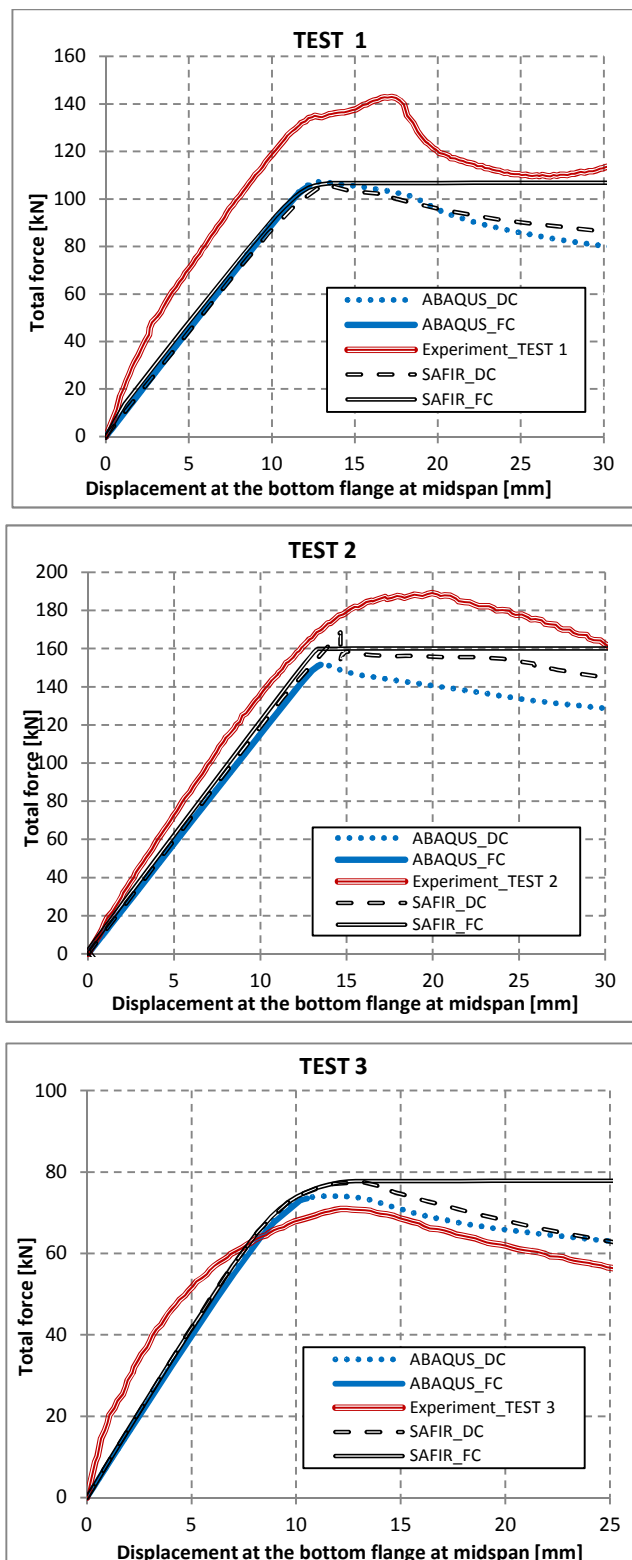


Fig. 2.13 Load-displacement relation for the three beams: experimental and numerical

From the graphs it can be concluded that the two programs give results and mechanical behaviours at high temperatures that are close from each other. The obtained experimentally initial

tangent of the curve is different from the numerical curves mainly in test 1 and 3. The maximum loads in the tests 1 and 2 are higher than the corresponded numerical tests values. Overall the approximations are reasonable considering the nature of the different parameters involved in the presented tests, as for instance the heating process.

2.6 SUMMARY

The paper presents numerical modelling using two different FEM software packages on three fire resistance tests to steel beams with slender I-cross-sections. The results were compared to tests and found reasonably close. Therefore, it can be concluded that the mechanical behaviour during the complete duration of the fire tests to the beams was fairly predicted by the numerical models.

Acknowledgement

The authors would like to thank the financial support by the European Commission through the Research Fund for Coal and Steel for research project FIDESC4 "Fire Design of Steel Members with Welded or Hot-rolled Class 4 Cross-section".

References

- ABAQUS, 2010: Abaqus, Analysis user's manual, Volumes I-IV, version 6.10. Hibbitt, Karlsson & Sorensen, Inc., Providence, R.I, USA, 2010.
- Franssen, 2005: Franssen JM, "SAFIR A Thermal/Structural Program Modelling Structures under Fire", *Engineering Journal* vol 42/3, 143-158, 2005.
- CEN, 2005: CEN European Committee for Standardisation, EN 1993-1-1, Eurocode 3, Design of Steel Structures - Part 1-1: General rules and rules for buildings, Brussels, Belgium, 2005.
- CEN, 2006: CEN European Committee for Standardisation, EN 1993-1-5, Eurocode 3: Design of Steel Structures - Part 1-5: Plated structural elements, Brussels, Belgium, 2006.
- CEN, 2011: CEN European Committee for Standardisation, EN 1090-2:2008+A1, Eurocode 3: Execution of steel structures and aluminium structures - part 2: Technical requirements for steel structures, Brussels, Belgium, 2011.
- Fidesc4 - Fire Design of Steel Members with Welded or Hot-rolled Class 4 Cross-sections, Six-monthly Report for the Research Programme of the Research Fund for Coal and Steel, September 2012.

Jan Hricák, jan.hricak@fsv.cvut.cz

WG3 - Michal Jandera, michal.jandera@fsv.cvut.cz

WG2 - František Wald, wald@fsv.cvut.cz

3 LOCAL BUCKLING OF CLASS 4 SECTIONS AT ELEVATED TEMPERATURE

Summary

A significant progress in fire engineering research was made in the last decade. This resulted in more precise structural fire design and higher reliability of steel structures. However, for design of very slender sections (Class 4 cross-sections according to the Eurocode 3), where elevated temperature affects also behaviour of elements subjected to local buckling, no wide research was published.

This article describes the course of the experiment and validation of a numerical model based on the data obtained.

3.1 INTRODUCTION

A common practice in recent years, thanks to the introduction of European design standards for building construction has become not only an assessment of the structure at normal design situation, but also in the fire (Buchanan, 2001), (CEN, 2001). The area of slender cross-sections research is very important, because the assessment and design principles of Class 4 cross-sections are very specific and usually more difficult than for normal cross-sections. Along with any global problems their behaviour includes also local buckling of the compressed parts of the cross-section (Trahair, 2001), (CEN, 2004).

The research is focused on the behaviour of steel beams made from welded class 4 cross sections of I and H shape exposed to high temperatures.

3.2 DESIGN AND EXECUTION OF EXPERIMENTS

The focus of the project is to carry out experiments with I - beams with slender cross-sections, which belong to the Class 4. The load capacity of these sections is not directly affected by the yield strength of the steel, but by deformations of the compressed areas of the cross-section, i.e. upper part the web and the upper flange. It was necessary to choose the appropriate cross-sectional shape to reach this way of the deformation of the samples during the planned experiments, beam load form and force. Four tests with two types of cross-section loaded by four-point bending were be carried out. (see Fig. 3.1).

Beams were heated to a constant temperature by an electric heating pads. Increasing load was applied until exhaustion of the load capacity. Each section was heated to a temperature of 450 °C and 650 °C. These experiments were complemented by a number of material tests at normal temperature.

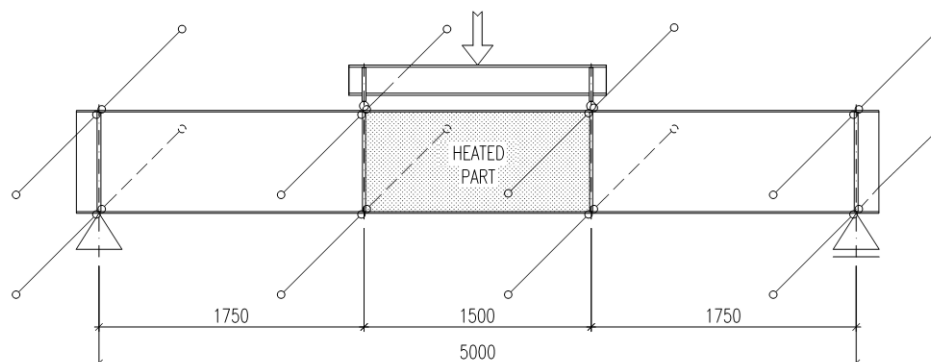


Fig. 3.1 Static scheme of the experiment

For these experiments, there were two types of welded cross-sections chosen. They represent Class 4 cross-sections and they are sufficiently burdened by the problematic of local stability of the walls.

- The Cross-Section A (IW 680/250/12/4) has the web in the Class 4 and the flanges are in Class 3, see Fig. 3.2a.
- The Cross-Section B (IW 846/300/8/5) has the web in the Class 4 and the flanges are in Class 4, see Fig. 3.2b.

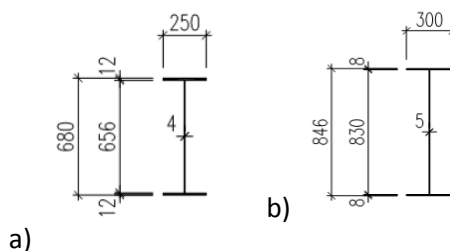


Fig. 3.2 Cross sections designed for experiment: a) Cross-section A, b) Cross-section B

Steel test fixtures were designed and manufactured to ensure smooth running of the experiment and proper introduction of all the boundary conditions according to the static scheme (see Fig. 3.1). steel test fixtures were designed and manufactured. The scheme of the test fixtures layout including the location of the test beam is shown in the following figure (see Fig. 3.3).

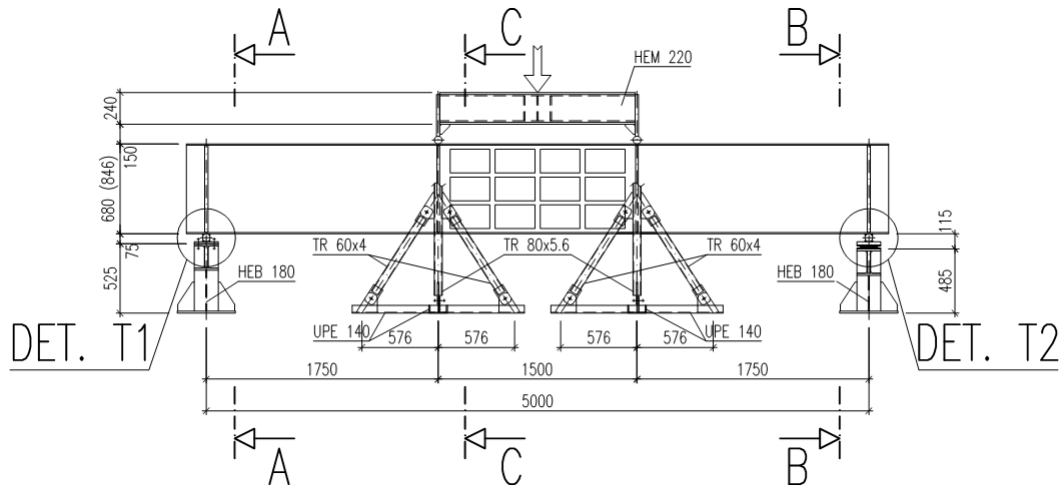


Fig. 3.3 Scheme of the experiment set-up

3.2.1 The test fixtures for ensuring the torsional stability

The principle of the test fixtures for ensuring the torsional stability at the support points and at the point of the load input is shown in the section views A-A, B-B and C-C (see Fig. 3.4).

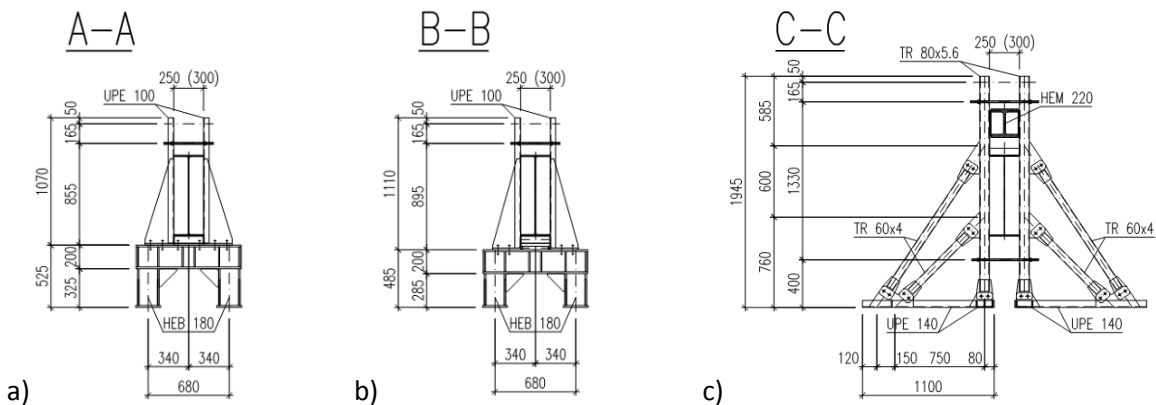


Fig. 3.4 Sections: a) at the point of the firm joint support, b) at the point of the sliding joint support, c) at the point of the load introduction

The construction of the test fixtures at the support (see Fig. 3.4a, b) is formed by two vertical guide profiles. The test fixtures for ensuring the torsion stability at the point of the load introduction (see Fig. 3.4c) are formed by the struts, which hold a vertical pair of guide profiles. After placing the test beam to the support, the individual test fixtures will clamp the cross-section of the beam with a small allowance, therefore free movement in the vertical and longitudinal directions is not obstructed, but the lateral and the torsional stability was ensured.

3.2.2 The design of the supports

The test beams were, according to the scheme (see Fig. 3.3), placed on the fixed articulated support from the left side (see Fig. 3.5a) and on the sliding joint support (see Fig. 3.5b) from the right side. The sliding articulated support is designed as a rolling bearing.

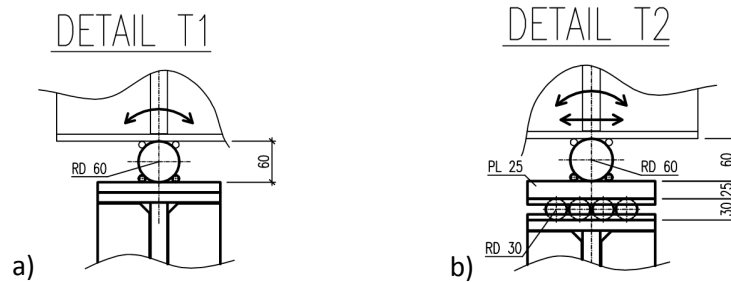


Fig. 3.5 Construction detail: a) Fixed articulated support, b) Sliding articulated support

3.3 Measurement of imperfections of the beams

Values of imperfections were determined by manual measurements in a precisely defined grid (see Fig. 3.6). The values of individual readings are shown in the graphs (see Figs. 3.7-3.10). The maximal amplitudes were chosen from the summary of the readings (see Tab. 3.1).

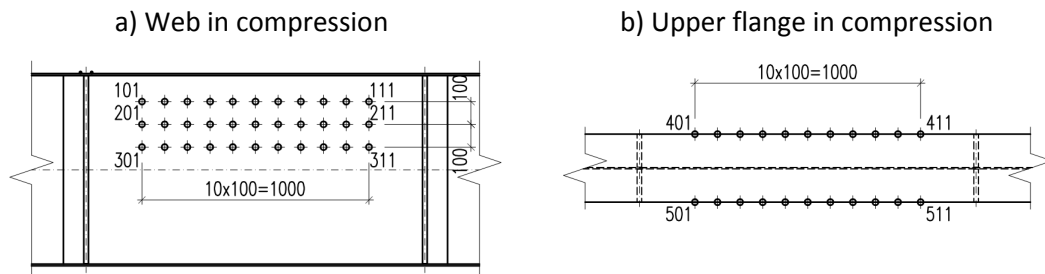


Fig. 3.6 Defined grid of in the central heated part of the beam

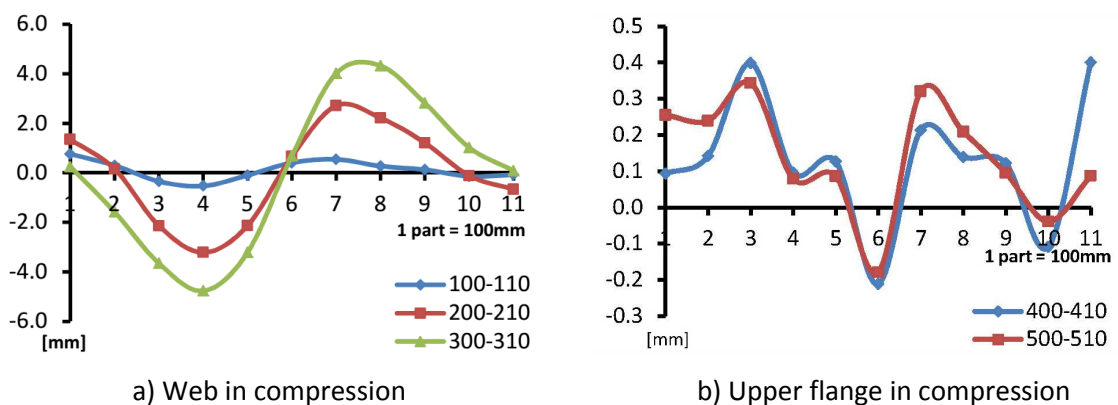


Fig. 3.7 Changing the amplitude imperfections for beam A1 (IW 680/250/12/4)

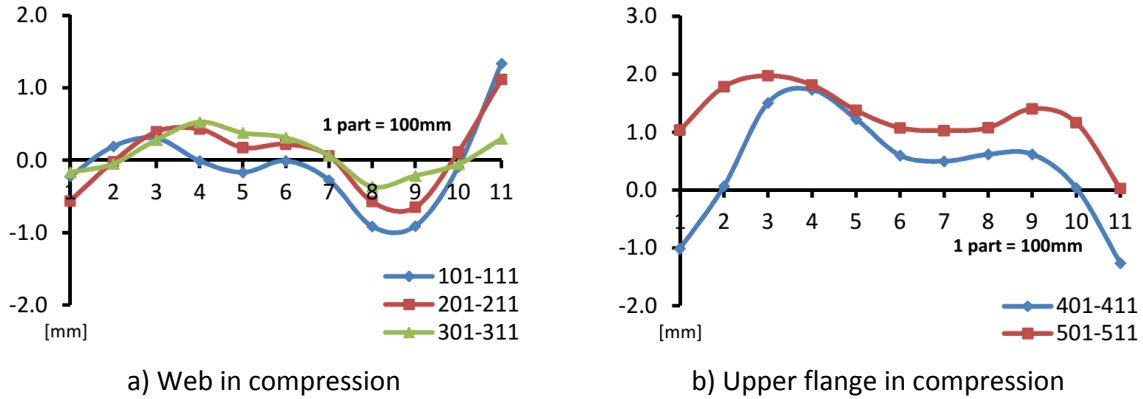


Fig. 3.8 Changing the amplitude imperfections for beam A2 (IW 680/250/12/4)

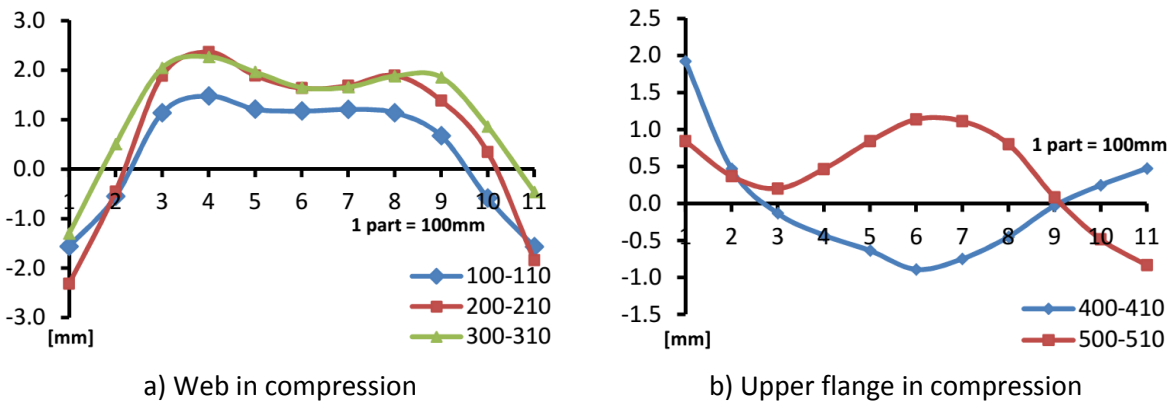


Fig. 3.9 Changing the amplitude imperfections for beam B1 (IW 846/300/5/8)

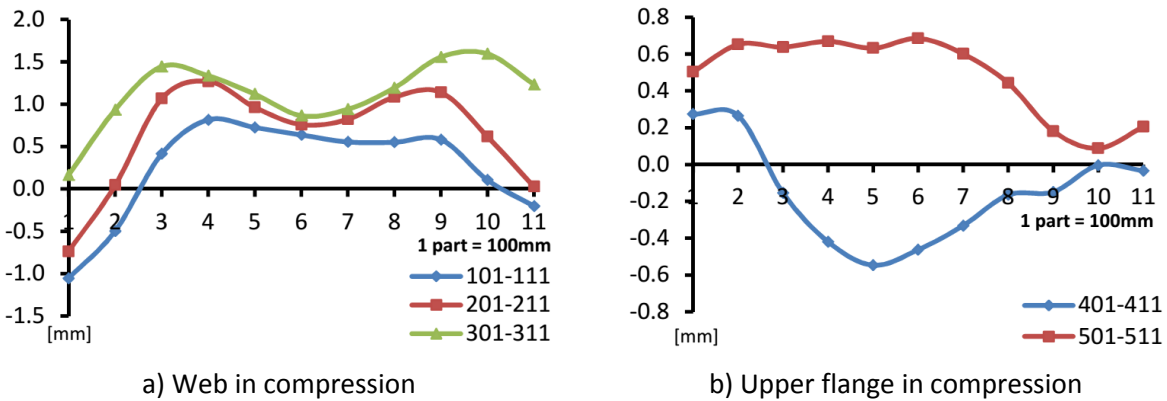


Fig. 3.10 Changing the amplitude imperfections for beam B2 (IW 846/300/5/8)

Tab. 3.1 Maximum amplitudes of the imperfection from the manual measurement

| Beam | Cross-Section | Web [mm] | Flange [mm] |
|------|---------------------|-------------|----------------|
| A1 | A (IW 680/250/4/12) | 4.765 | 1.200 |
| A2 | A (IW 680/250/4/12) | 1.340 | 1.975 |

| | | | |
|----|--------------------|-------|-------|
| B1 | B (IW 846/300/5/8) | 2.364 | 1.924 |
| B2 | B (IW 846/300/5/8) | 1.595 | 0.685 |

3.4 PROGRESS OF THE EXPERIMENT

After connecting all sensing devices (thermocouples, potentiometers, dynamometer in a hydraulic jack) to the central measuring equipment and after connection of the heating pads to the transformer, the beam was ready for the experiment (see Fig. 3.11).

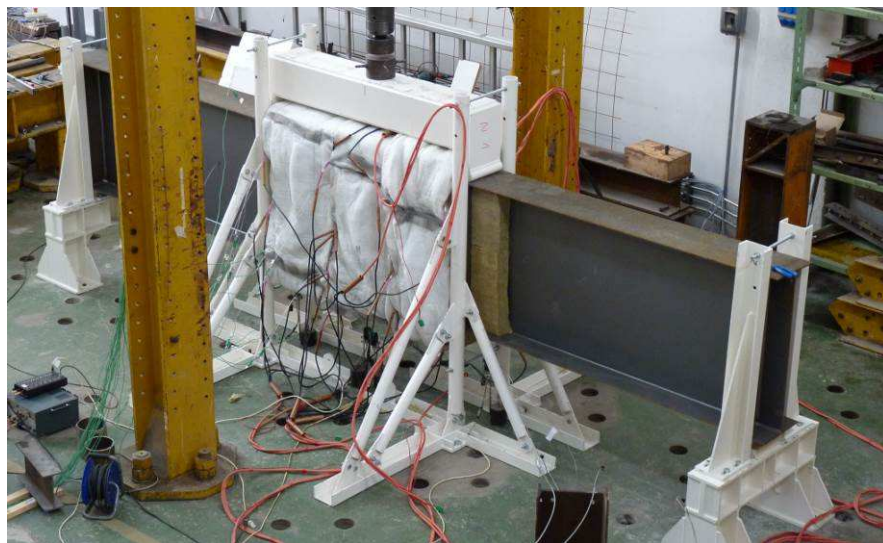


Fig. 3.11 The prepared test beam prior the experiment

Warm-up time for the temperature $T \approx 450 \text{ }^{\circ}\text{C}$ was ~ 45 minutes and ~ 65 minutes for the temperature $T \approx 650 \text{ }^{\circ}\text{C}$. After reaching the desired temperature in the heated part of the beam, the application of the mechanical loading was started. The hydraulic jack, which was controlled by a constant proportion of the deflection path in the middle part of the heated beam, was affecting the test beam through the load beam. The test beam was thus loaded by four-point bending. The following load-deflection diagrams for Tests 1-4 (see Fig. 3.12) show the dependence of the applied load and the deflection in the middle of the heated part of the test beam. Summary of the results is shown in Tab. 3.2.

The behaviour of proposed Class 4 cross-sections in the experiments corresponded to expectations and there was significant buckling of the compressed part of the section observed, see Figs. 3.18 b, 3.19 b, 3.21b and 3.22b.

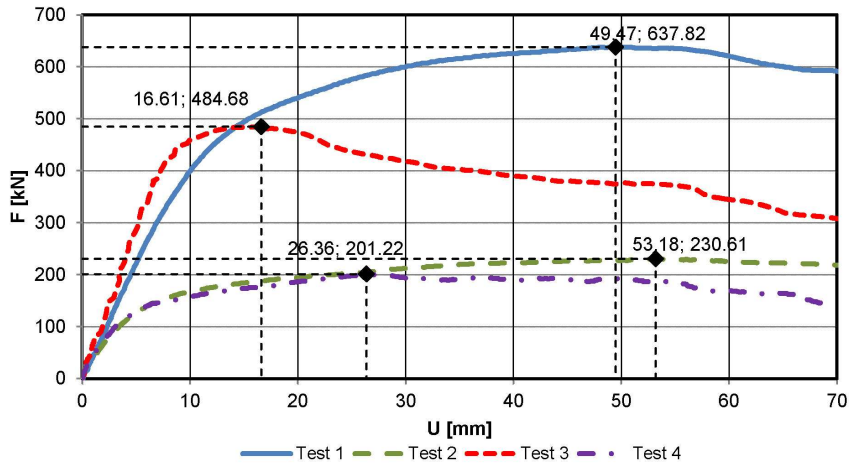


Fig. 3.12 Load-deflection diagram for Tests 1-4

Tab. 3.2 Load capacity of the Test beams

| Test | Cross-Section | Temperature [°C] | Load capacity [kN] |
|------|----------------------|---------------------|-----------------------|
| 1 | A1 (IS 680/250/4/12) | ~ 450 | 637 |
| 2 | A2 (IS 680/250/4/12) | ~ 650 | 230 |
| 3 | B1 (IS 846/300/5/8) | ~ 450 | 484 |
| 4 | B2 (IS 846/300/5/8) | ~ 650 | 201 |

3.5 NUMERICAL SIMULATION OF EXPERIMENTS

This part of the study includes description of a numerical model created by a finite element method (FEM) and its validation. The numerical model was created in ABAQUS software (ABAQUS, 2010). The model was compared to the experiments. It should be noted that the influence of residual stress is not included in the analysis.

3.5.1 Meshing of the beams

It is advantageous to use shell elements for the modelling of thin-walled elements. These elements are suitable for the wall of the slenderness of more than 10 (the width / thickness ratio). Element S4 (see Fig. 3.13) was used for the comparative study of the shell elements.

The shell element S4 has four nodes with six degrees of freedom (three displacements and three rotations), linear approximations and full integration (4 integration points on the surface of the element). Element S4 can be used in the calculation of large deformations and large rotations. For each model of the beam, web is formed by 200 elements along the length and by 16 elements along the

height of the cross-section. Upper and lower flanges are formed by 6 elements along the width of the cross-section. The structural mesh is shown in Fig 3.16.

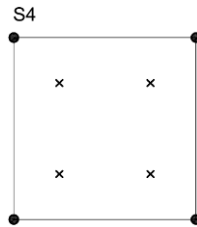


Fig. 3.13 Shell element S4

3.5.2 Geometric imperfections

After set-up of the experiment, initial imperfections in the heated part of the beam were measured as described above (see paragraph 3.3). Initial imperfections were entered for the numerical model to correspond the real beams from the experiments. The individual curves describing the shape imperfections (see Figs. 3.7 - 3.10) were replaced by a sinusoidal function for simplification with the maximum amplitude taken from Tab. 3.1.

3.5.3 Material modelling

Mechanical properties of steel at normal temperature were determined from the mechanical tests for each thickness of the plate. Mechanical properties at high temperatures were obtained with the help of the reduction factors dependent on temperature, which are listed in EC 3 Part 1- 2 (CEN, 2004). Material behaviour at high temperature is defined by the elastic-plastic non-linear stress-strain relationship (see Fig. 3.15). Mechanical properties (yield stress and modulus of elasticity) for the individual plates according to the scheme (see Fig. 3.14) are shown in the Tab. 3.3.

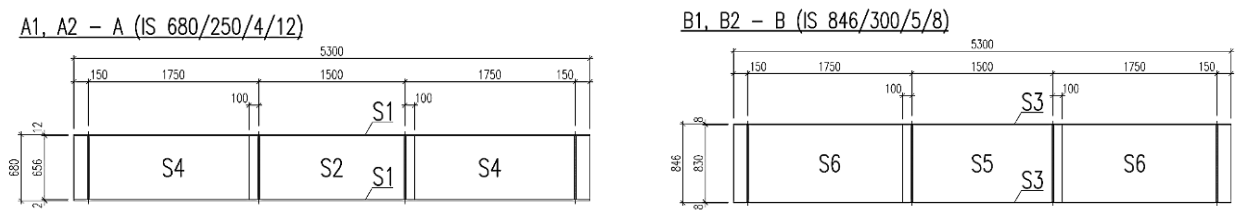


Fig. 3.14 Layout scheme of each plate

Tab 3.3 Material properties for the individual plates

| Part | [MPa] | S1 | S2 | S3 | S4 | S5 | S6 |
|--------------------|----------|--------|--------|--------|--------|--------|--------|
| Upper Yield Stress | R_{eH} | 430 | 394 | 341 | 376 | 385 | 435 |
| Lower Yield Stress | R_{eL} | 424 | 391.67 | 338 | 361 | 378 | 408 |
| Elastic Modulus | E | 178399 | 176897 | 194375 | 199200 | 209988 | 208900 |

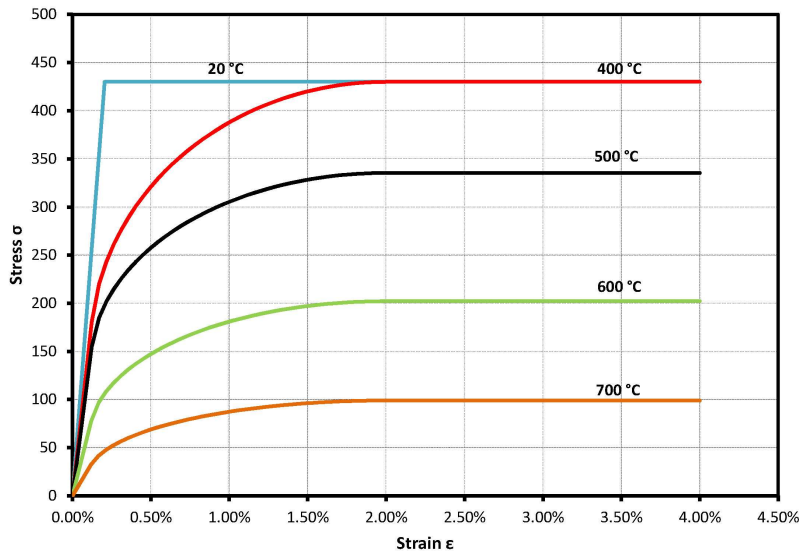


Fig. 3.15 Stress–strain relationship for S1

3.5.4 Boundary conditions and loading

For the simulation of the boundary conditions according to the static scheme (see Fig. 3.1), the fixed articulated support was chosen on the left side of the model (the point "a") and the sliding articulated support was chosen on the right side (the point "d"), see Fig. 3.16. On the left side, shift in the direction of the X, Y, Z axis and the rotation about the X axis are blocked, the rotation about the Z axis is not restrained. On the right side, the shift in the direction of the Y, Z axis and rotation about the X axis are blocked, the shift in the direction of the X axis and the rotation about the Z axis are not restrained. In the point of the load application (the points "b", "c"), shift in the direction of the Z axis is blocked, shift in the direction of the X and Y axes is not restrained.

The static structural analyses (load–displacement analysis) were performed to predict the load–deflection behaviour of the steel beams. Regarding the application of load, the two concentrated loads were applied incrementally by means of equivalent displacements to overcome convergence problems and to facilitate the capture of the post-buckling behaviour of the models. Displacement loads were applied at 1/3 span of the steel beams (see Fig. 3.1) and the load step increments were varied in order to avoid potential numerical problems. The region between the two loading points ($L = 1500$ mm) is the tested part where uniform bending moment acts. Loading points are shown in Fig. 3.16.

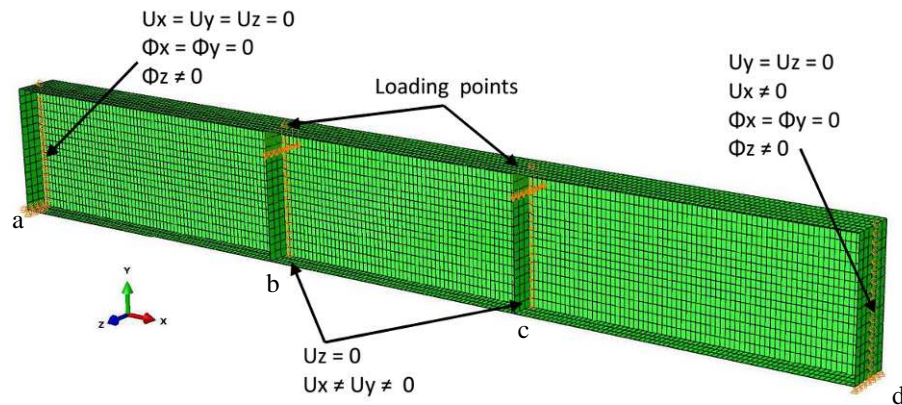


Fig. 3.16 Loading and boundary conditions for beams

3.5.5 Steel temperature distribution in numerical modelling

The real temperatures attained in steel cross sections during the experiments were evenly introduced at each node of the heated part of the shell elements in the finite element structural models. The following data provide the distribution of temperature used for the numerical simulations, see Fig. 3.17 and Tab. 3.4.

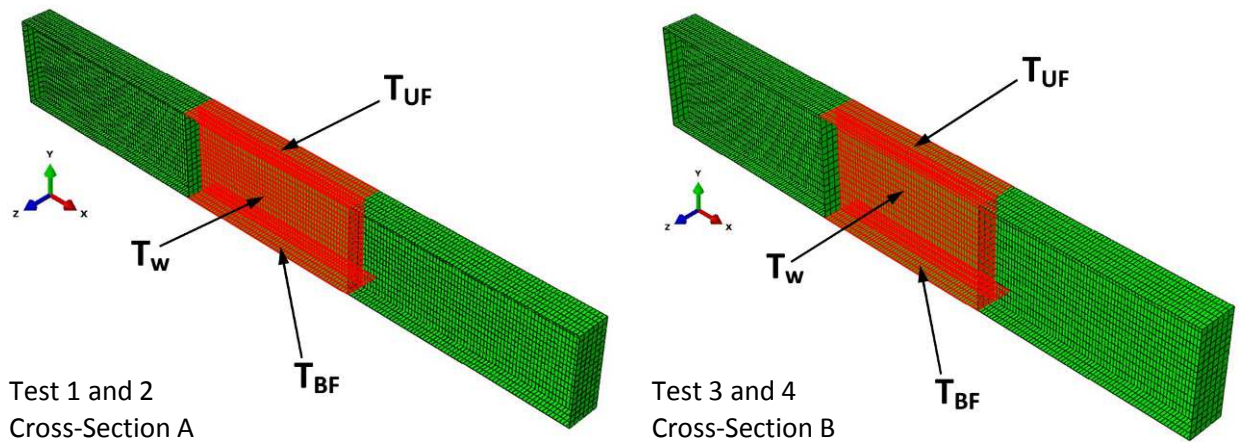


Fig. 3.17 Temperature distribution in numerical model

Tab 3.4 Temperatures for Tests 1-4

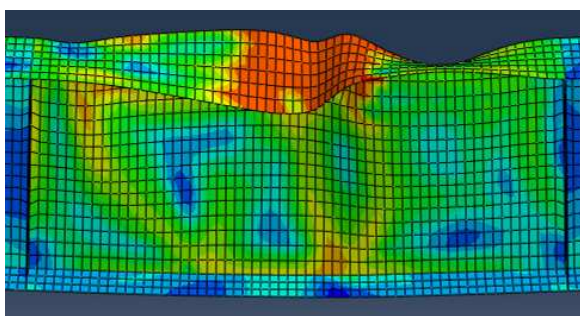
| T [°C] | A (IW 680/250/4/12) | | B (IW 846/300/5/8) | |
|----------|---------------------|-----|--------------------|-----|
| Test | 1 | 2 | 3 | 4 |
| T_{UF} | 444 | 654 | 481 | 661 |
| T_{BF} | 469 | 636 | 425 | 631 |
| T_w | 458 | 649 | 431 | 641 |

3.6 RESULTS OF THE NUMERICAL SIMULATION vs. TEST RESULT

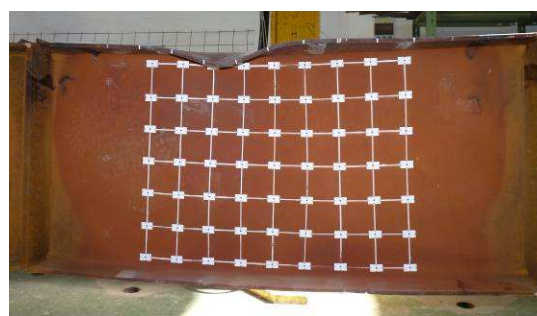
In the next table and figures, the results obtained in the fire tests are compared to the results obtained in the numerical simulations. Failure mode of the tests and the numerical model is also compared in the figures.

3.6.1 Model for Test 1 and Test 2 (IS 680/250/4/12)

The following figures (Fig. 3.18 and 3.19) show the deformed shape of the central heated part of the beam from the numerical simulation and from the experiment for Test 1 and Test 2.

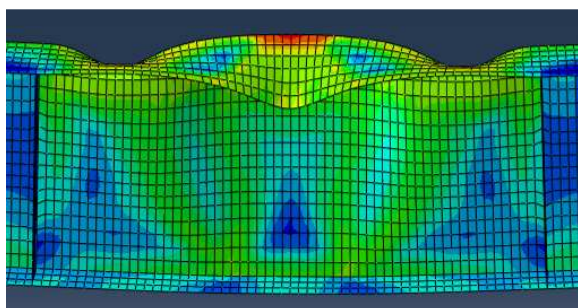


a) Numerical simulation



b) Experiment

Fig. 3.18 Deformed shape for Test 1



a) Numerical simulation



b) Experiment

Fig. 3.19 Deformed shape for Test 2

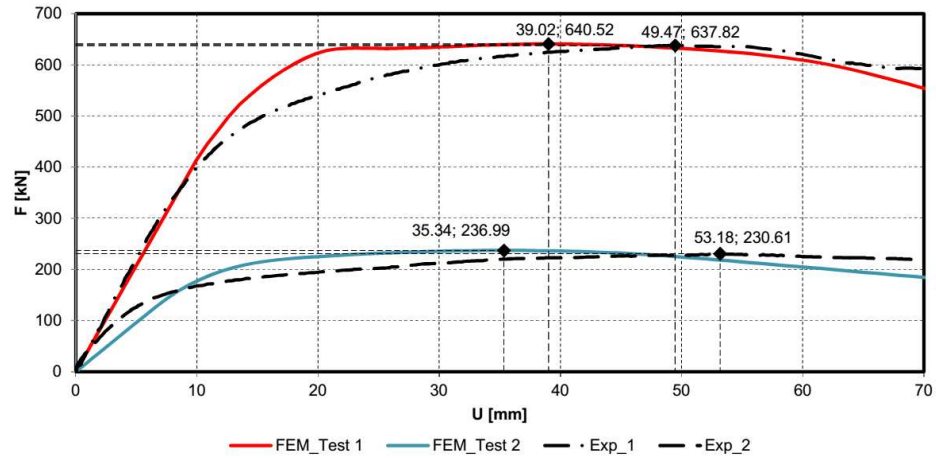
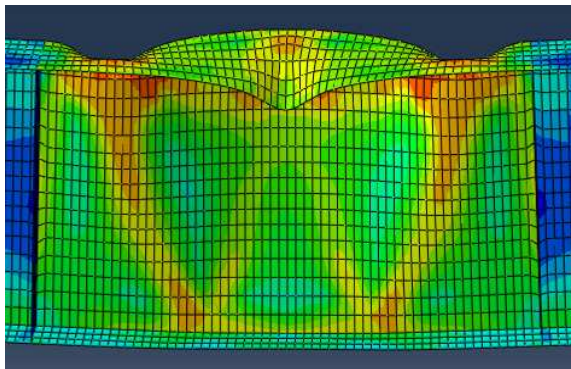


Fig. 3.20 Load-deflection diagram for Test 1 and 2

3.6.2 Model for Test 3 and Test 4 (IS 846/300/5/8)

Figs. 3.21 and 3.22 show the deformed shape from the numerical simulation and from the experiment for Test 3 and Test 4.

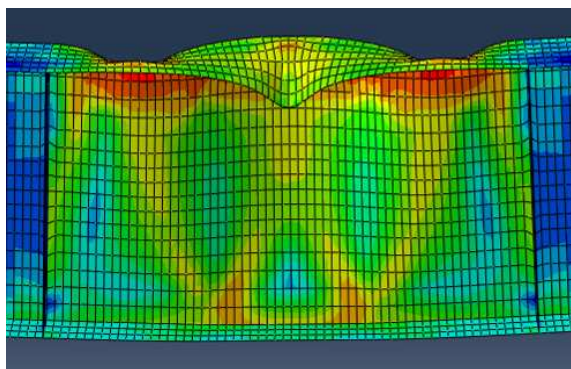


a) Numerical simulation



b) Experiment

Fig. 3.21 Deformed shape for Test 3 and 4



a) Numerical simulation



b) Experiment

Fig. 3.22 Deformed shape for Test 3

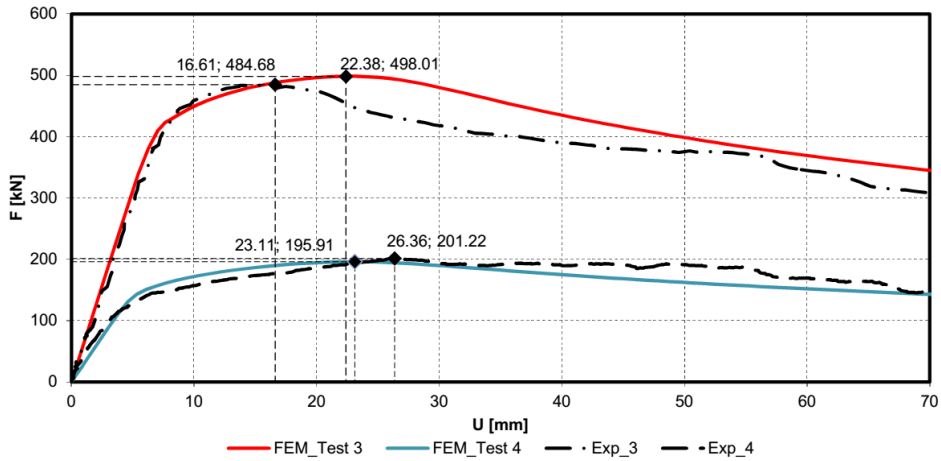


Fig. 3.23 Load-deflection diagram for Test 3 and 4

3.6.3 Comparison

The following table and figure summarize the numerical results and compare them to the test results.

Tab. 3.5 Summary of tests results vs. numerical results

| Test | Cross-Section | Load capacity [kN] | | ϵ [%] |
|------|----------------------|--------------------|--------|----------------|
| | | Experiment | FEM | |
| 1 | A1 (IS 680/250/4/12) | 637.82 | 640.52 | 0.42 |
| 2 | A2 (IS 680/250/4/12) | 230.61 | 236.99 | 2.69 |
| 3 | B1 (IS 846/300/5/8) | 484.68 | 498.01 | 2.68 |
| 4 | B2 (IS 846/300/5/8) | 201.22 | 195.91 | 2.64 |

3.7 CONCLUSION

Numerical simulations exhibit similar behaviour as the test beams in the experiment. As seen in Tab. 3.5 and Fig. 3.24, the difference between the results of numerical model in ABAQUS and ultimate resistance obtained from the experiment is smaller than 3%. Therefore, we can say that the material model at high temperatures is suitable for creating numerical simulation of steel beams with Class 4 cross-sections exposed to fire.

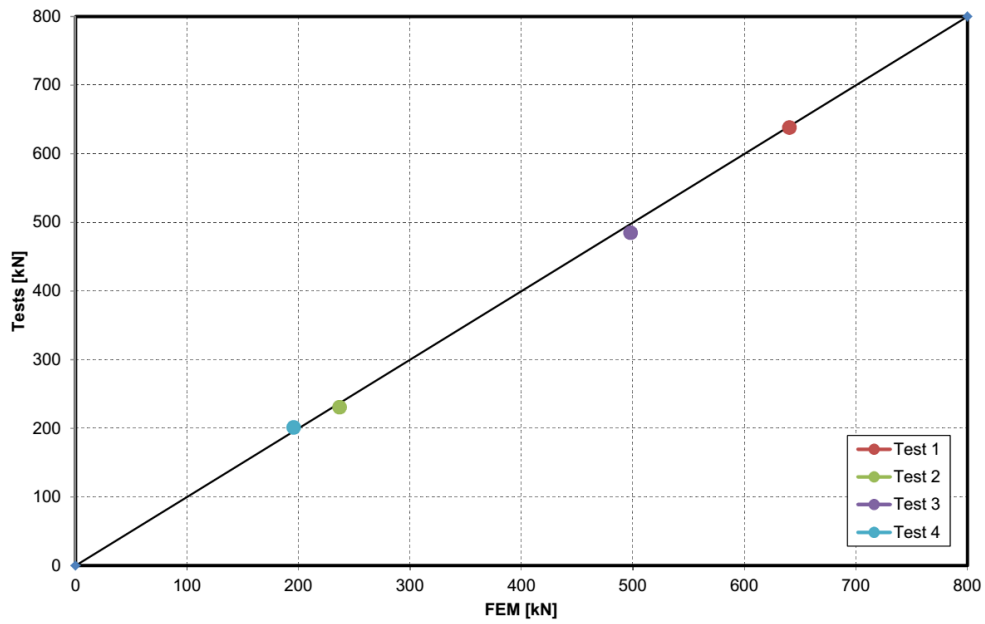


Fig. 3.24 Comparison of test results with numerical results

References

- Buchanan, 2001: Buchanan A. H., Structural Design for Fire Safety, New Zealand, 2001.
- Trahair, 2001: Trahair, N. S., Bradford, M. A., Nethercot, D. A., The Behaviour and Design of Steel Structures, London, 2001.
- CEN, 2001: CEN. Eurocode 3: design of steel structures, part 1.2: general rules—structural fire design (EN 1993-1-2:2001). Brussels: European Committee for Standardization; 2001.
- CEN, 2004: CEN. Eurocode 3: design of steel structures, part 1.5: plated structural elements (EN 1993-1-5:2004). Brussels: European Committee for Standardization; 2004.
- ABAQUS, 2010: Analysis user's manual, Volumes I-IV, version 6.10. (2010). Hibbitt, Karlsson & Sorenses, Inc., Providence, R.I, USA.

WG2- Meri Cvetkovska, cvetkovska@gf.ukim.edu.mk

Milivoje Milanovic, pbarhisnp@gmail.com

WG2- Ljupco Lazarov, lazarov@gf.ukim.edu.mk

WG2- Koce Todorov, todorov@gf.ukim.edu.mk

4 NUMERICAL AND EXPERIMENTAL ANALYSIS OF RC BEAMS EXPOSED TO DIFFERENT FIRE MODELS

Summary

In 1987 six reinforced concrete beams were cast at the Construction Technology Laboratories of the Portland Cement Association. All beams were designed according to ACI Standard 318. Three beams were tested using the ASTM E119 fire exposure and the other beams were exposed to a short duration, high intensity (SDHI) expose. Specimens were tested to simulate the end span of a continuous beam. The results from the experimental investigation were published in 1991 in “Journal of the structural engineering” by Ellingwood B. and Lin T.D.

The results from this investigation were used as benchmark example for validation the finite element program FIRE (homemade program). The experimental and numerical results for the thermal and mechanical responses are compared and presented in this paper. In same time all results from the program FIRE are compared with the corresponding one from the program SAFIR.

4.1 INTRODUCTION

This paper presents a computational procedure for the nonlinear analysis of a reinforced concrete elements and plane frame structures subjected to fire. The program FIRE (Cvetkovska, 2002) carries out the nonlinear transient heat flow analysis (modulus FIRE-T) and nonlinear stress-strain response associated with fire (modulus FIRE-S). The solution technique used in FIRE is a finite element method coupled with time step integration. The used analysis procedure does not account for the effects of large displacements on equilibrium equations.

4.2 NONLINEAR STRESS-STRAIN ANALYSIS

The response of a reinforced concrete elements and plane frame structures exposed to fire is predicted by modulus FIRE-S (Cvetkovska, 2002). This modulus that is a modification of the computer program FIRES-RC II (Iding et al. 1977), accounts for: dimensional changes caused by temperature differences, changes in mechanical properties of materials with changes in temperature, degradation of sections by

cracking and/or crushing and acceleration of shrinkage and creep with an increase of temperature. To define the fire response of reinforced concrete structure is thus a complex nonlinear analysis problem in which the strength and stiffness of a structure as well as internal forces continually change due to restraints imposed by the structural system on free thermal expansion, shrinkage, or creep. Because linear elements and frames are modelled as an assemblage of members connected to joints, the basic analytical problem is to find the deformation history of the joints $U(t)$ when external loading at the joints $R(t)$ and temperature history within the members $T(t)$ are specified. Since only linear elements and two dimensional frames are considered, each joint has three degrees of freedom, two translations and one rotation. Likewise, there are two forces and a moment at each joint.

The overall system stiffness matrix of a structure is assembled by incorporating the stiffness contribution of each member. Each member is treated as a linear beam element modeled by simple beam theory and is composed of a linear elastic material. In a reinforced concrete, the first condition holds if members are of usual properties, but the second condition is violated for virtually all loading conditions. The materials in a reinforced concrete structure are nonlinear and detailed knowledge of the strain states existing within members is necessary in order to obtain the member stiffness matrix. Hence, the member must be further discretized. Structure members are subdivided into a number of segments such that by calculating segment properties, it is possible to determine overall member properties. Each segment is treated as a standard beam element in which axial force is assumed to be constant and bending moment to vary linearly along the length of a segment. However, in order to calculate section properties and internal forces and moments within a segment, it is necessary to discretize cross sections further into subslices (Fig. 4.1a).

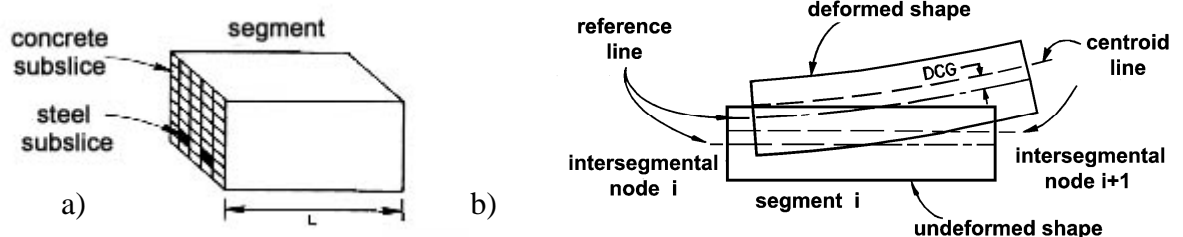


Fig. 4.1 a) cross-section of a segment discretized to subslices, b) deformation mode of segment

The subslices associated with each segment can be envisioned as uniaxially loaded prisms. Therefore, only uniaxial stress states are considered, equivalent to the assumption that the effect of multiaxial stress components is negligible. This type of prismatic model allows only the effects of axial and flexural stiffness to be considered in modeling structural behavior, neglecting the effect of shear in member idealization. Local effects near member ends are not considered. However, in most linear

structures these effects are of secondary importance and principal structural action is due to flexure and axial deformation. Internal axial force and bending moment at each end of a segment are found by summing the force and moment contributions of subslices discretizing the cross section. The mechanical strain in each subslice can be found directly from the extension and curvature of a cross section:

$$\epsilon_i^{r,j} = \epsilon_a + \phi(y - DCG) \quad (1)$$

where $\epsilon_i^{r,j}$ = total mechanical strain in the subslice r for time step i and iteration j ; ϵ_a = total strain in the reference plane; y = distance from subslice to reference plane; ϕ = curvature; DCG = distance from the reference plane to centroidal plane (Fig. 1b). In order to find current stress in each subslice, that part of the current total mechanical strain which gives rise to stress, must be determined:

$$\epsilon_i^j = \epsilon_i^{r,j} - \epsilon_i^f \quad (2)$$

where: ϵ_i^j = stress related strain for time step i and iteration j ; ϵ_i^f = free strain for time step i .

Free strains are determined for each subslice at the beginning of a time step and do not vary during iteration within a time step. For the concrete, or the steel subslice they are calculated according to the following equations:

$$\epsilon_i^{f,c} = \epsilon_{i-1}^{f,c} + \Delta\epsilon_i^{cr,c} + \Delta\epsilon_i^{tr,c} + \Delta\epsilon_i^{th,c} \quad (3)$$

$$\epsilon_i^{f,s} = \epsilon_{i-1}^{f,s} + \Delta\epsilon_i^{cr,s} + \Delta\epsilon_i^{th,s} \quad (4)$$

where ϵ_i^f = free strain for concrete, or steel subslice, for time step i ; $\Delta\epsilon_i^{cr}$ = free creep strain accumulated over current time step i ; $\Delta\epsilon_i^{tr,c}$ = transient strain accumulated only in concrete subslice over current time step i ; $\Delta\epsilon_i^{th}$ = free thermal expansion accumulated over time step i .

The “ $\sigma - \epsilon$ ” relations, recommended by Eurocode 2, part 1.2, take into account the creep of concrete and steel at elevated temperatures. It is done by moving the maxima in the stress-strain curves to higher strains with higher temperatures. When compressed concrete is heated for the first time, the total strain is different from the total strain measured in constant temperature creep tests and an additional irrecoverable “transient strain” must be taken into account. This transient strain is a function of the level of stress and the thermal expansion (Anderberg et al. 1986). The increment of transient strain at any given time step can be computed as:

$$\Delta \varepsilon_i^{tr,c} = -2.35 \frac{\sigma_c}{f_c'} \Delta \varepsilon_i^{th,c} \quad (5)$$

where $\Delta \varepsilon_i^{tr,c}$ = transient strain accumulated over current time step i ; $\Delta \varepsilon_i^{th,c}$ = free thermal expansion accumulated over current time step i ; σ_c = applied compressive stress; f_c' = compressive strength at ambient conditions.

When the transient strain is not included in the structural analysis, the result is stiffer structural model at elevated temperatures, in which the computed thermal stresses become very large and failure is predicted to occur much earlier than experimentally observed (Ellingwood & Lin 1991).

4.2.1 Stress-strain laws at high temperatures

The current level of stress in a subslice can be determinate while the stress-strain law for current temperature is defined. The program enables use of temperature dependant $\sigma - \varepsilon$ curves for steel and concrete based on experimental data, or use of theoretical curves. A stress-strain law for concrete under uniaxial loading consists of two parts: a compressive part and a tensile part. The stress-strain curve in compression (Fig. 4.2a) consists of ascending and descending branch. The ascending branch is defined by equation (6), recommended by Popovic (Bazant, 1996) (Fig. 4.2b) and the descending branch, equation (7), is assumed to be linear. Parameters that completely define this curve are temperature dependant and for various temperature intervals they are given in Eurocode 2, part 1-2.

$$\frac{\sigma_c}{f_c} = \frac{\varepsilon_c}{\varepsilon_{c1}} \cdot \frac{m}{m-1 + (\varepsilon_c / \varepsilon_{c1})^m} \quad \text{for } \varepsilon_c \leq \varepsilon_{c1} \quad (6)$$

$$\frac{\sigma_c}{f_c} = \frac{\varepsilon_{cu} - \varepsilon_c}{\varepsilon_{cu} - \varepsilon_{c1}} \quad \text{for } \varepsilon_{c1} \leq \varepsilon_c \leq \varepsilon_{cu} \quad (7)$$

where: f_c is the compressive strength of the concrete and the value decrease with temperature, ε_{c1} is the strain at compressive strength and the value increase with temperature, ε_{cu} is the ultimate crushing strain and the value increase with temperature, m is empirical coefficient ($m=2$ or 3 , which applies to lower or higher strength concretes). According to Eurocode 2, part 1-2, the coefficient m is the same for lower or higher strength concretes and $m=3$.

When concrete reaches ultimate tensile strain, primary cracks form at finite intervals along the length of an element. Total load is transferred across these cracks by reinforcement. However, concrete between cracks is still capable of carrying stress due to bond between concrete and steel. This phenomenon, involved by the descending branch in tension, is called the tension-stiffening effect. As EC2 recommends, tensile strength $f_{c,t}$ decrease linearly with temperature, and the descending branch

might be neglected. During the cooling phase, the concrete does not recover its initial strength because of initial degradation and chemical decomposition of the cement past. In this research the values of f_c , ϵ_{c1} , ϵ_{cu} and $f_{c,t}$, during the cooling phase are assumed to be the same as their values at maximum temperatures of concrete reached.

Fig. 4.2c represents the stress-strain law for steel in the phase of loading and unloading. This model is used in the computer modulus FIRE-S (Bazant, 1996), while the temperature in the steel subslice is changed from t_1 (lower) to t_2 (higher value). The stress-strain curve (recommended by EC2) is the same for compression and tension and is completely defined by: $\sigma_{spr}(T)$ - stress at the end of the proportional domain; $f_y(T)$ - yield strength, $E_s(T)$ -Young's modulus of elasticity; ϵ_{s1} -yield strain (constant); ϵ_{su} -ultimate strain (constant).

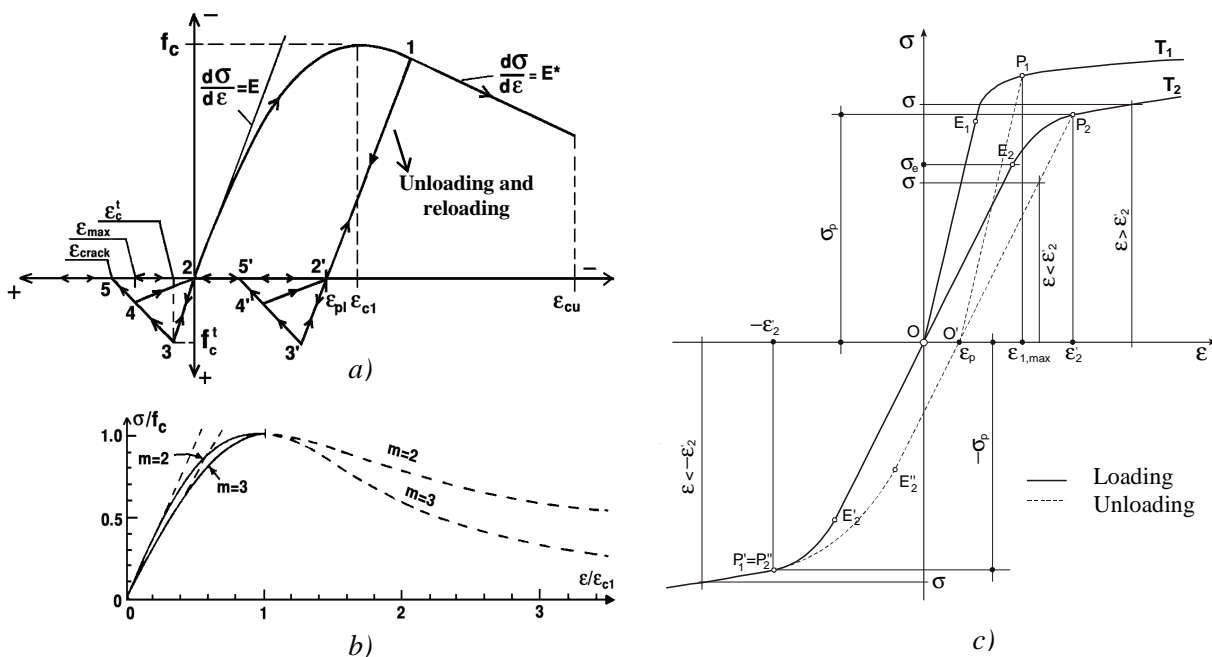


Fig 4.2 a) Stress-strain law for concrete, b) “ $\sigma - \epsilon$ ” curve by Popovic, c) Stress-strain law for steel

4.3 Fire resistance of RC beams

In 1987 six reinforced concrete beams were cast at the Construction Technology Laboratories of the Portland Cement Association (Ellingwood, 1991). All beams were designed according to ACI Standard 318. Beams were fabricated using normal-weight carbonate concrete and Grade 60 deformed reinforcing bars. Only four of them are analyzed in this example. Figure 4.3 and Table 4.1 provide details of the beam specimens. Beams B1 and B3 were tested using the ASTM E119 fire exposure and beams B5 and B6 were exposed to a short duration, high intensity (SDHI) expose.

Specimens were tested to simulate the end span of a continuous beam. This was accomplished by maintaining the cantilever end of the beam at a constant elevation during the course of the fire test by changing the cantilever load F_o as required. In program FIRE it was simulated by prescribing a constant vertical displacement at the end of the cantilever beam, equal to the vertical displacement before the fire action. In program SAFIR a three span continuous beam was analyzed and the fire was applied only in the first span.

The loads applied to the simply supported span were held constant during the test ($F= 44.48$ KN).

Beams are analyzed using the computer programs FIRE and SAFIR. Since the actual coefficient of thermal conductivity λ_c and specific heat ρc for the carbonate aggregate concrete used in fabricating the beams were not known, comparative thermal analysis are performed using the relations recommended by EC2, part 1.2 and by other authors. In program SAFIR all material properties are according to EC2, and in program FIRE the thermal conductivity λ_c is taken as it is recommended by Lin.T.D (Ellingwood, 1991), equation (8):

$$\begin{aligned}\lambda_c &= 1.78 \quad (T = 20^\circ C) \\ \lambda_c &= 1.78 - 0.005 * (T - 20) \quad (20^\circ C < T \leq 140^\circ C) \\ \lambda_c &= 1.18 - 0.002 * (T - 140) \quad (140^\circ C < T \leq 430^\circ C) \\ \lambda_c &= 0.6 - 0.005 * (T - 430) \quad (430^\circ C < T \leq 830^\circ C) \\ \lambda_c &= 0.4 \quad (T > 830^\circ C)\end{aligned} \tag{8}$$

Figure 4.4 and Figure 4.5 compares the measured and numerically achieved reinforcement temperatures for beams B1 and B5, exposed to ASTM E119 and SDHI fires. The comparison is satisfactory except for the reinforcement no.1, but the thermocouples at the exposed surface might not give accurate readings, since they are often damaged by oxidation at extremely high temperatures.

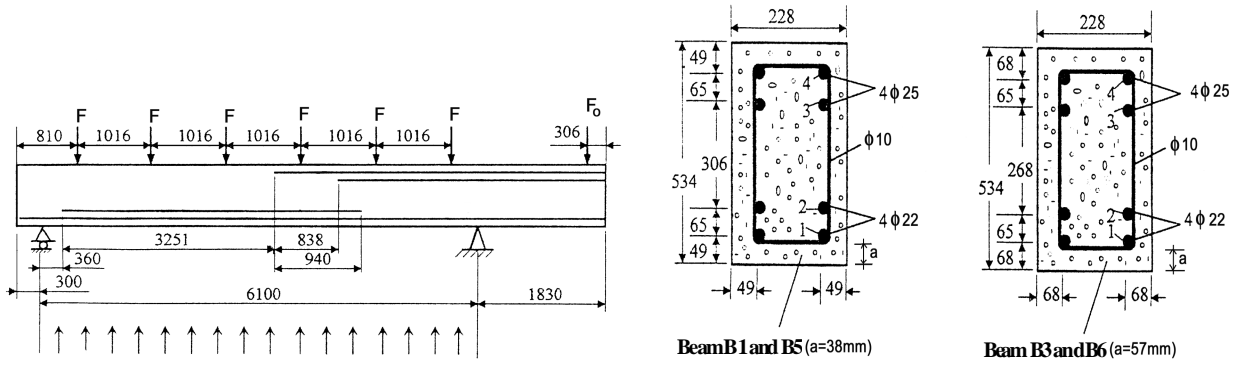


Fig. 4.3 Reinforcement details and cross sectional geometry of the beam specimens

Table 4.1

| beam | $f_c(20^\circ C)$ (Mpa) | $f_y(20^\circ C)$ (Mpa) | F_o (KN) | Fire model |
|------|----------------------------|----------------------------|---------------|------------|
| B1 | 27.8 | 410 | 114.6 | ASTM |
| B3 | 29.5 | 440 | 111.2 | ASTM |
| B5 | 33.5 | 410 | 114.6 | SDHI |
| B6 | 34.5 | 440 | 111.2 | SDHI |

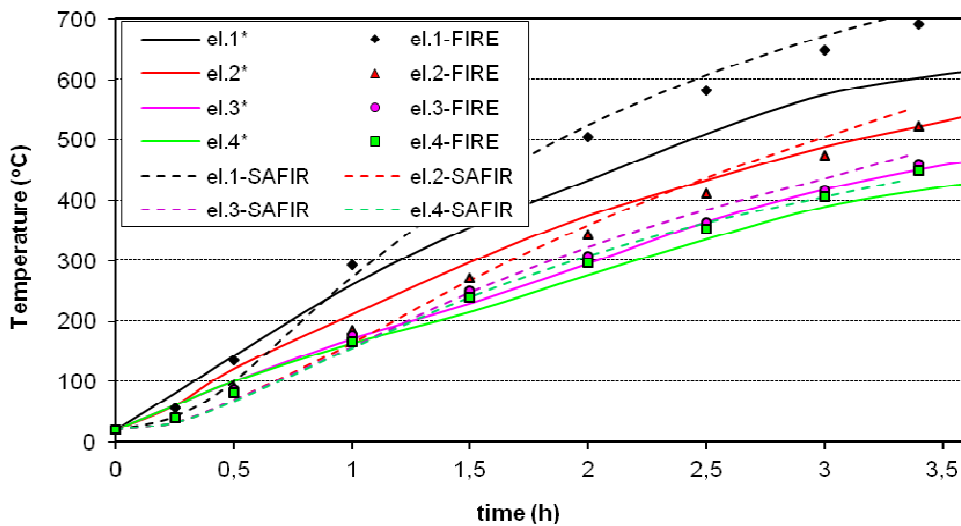


Fig. 4.4 Comparison of measured reinforcement temperatures (marked with *) and predicted by programs FIRE and SAFIR for the beam B1 (ASTM fire)

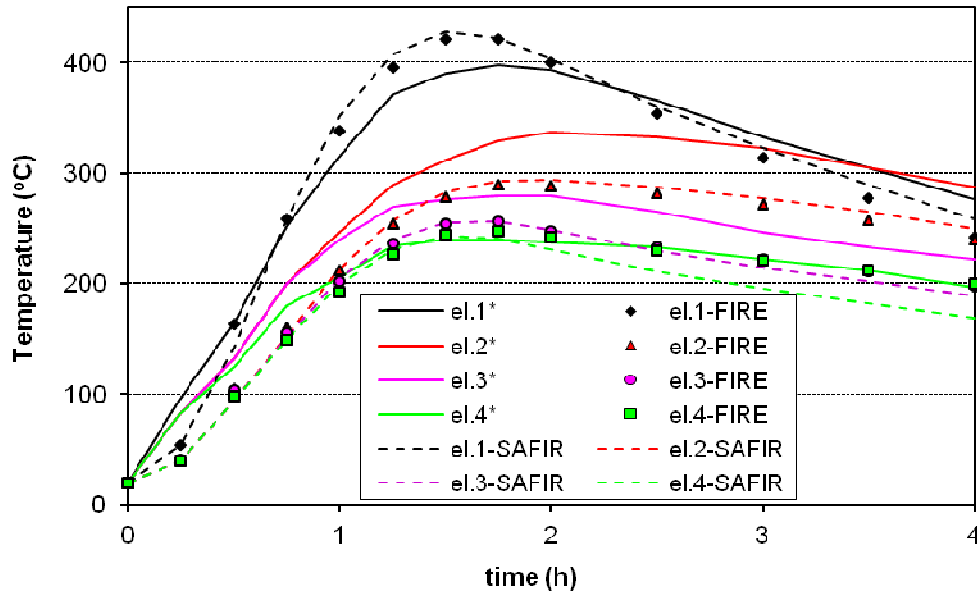
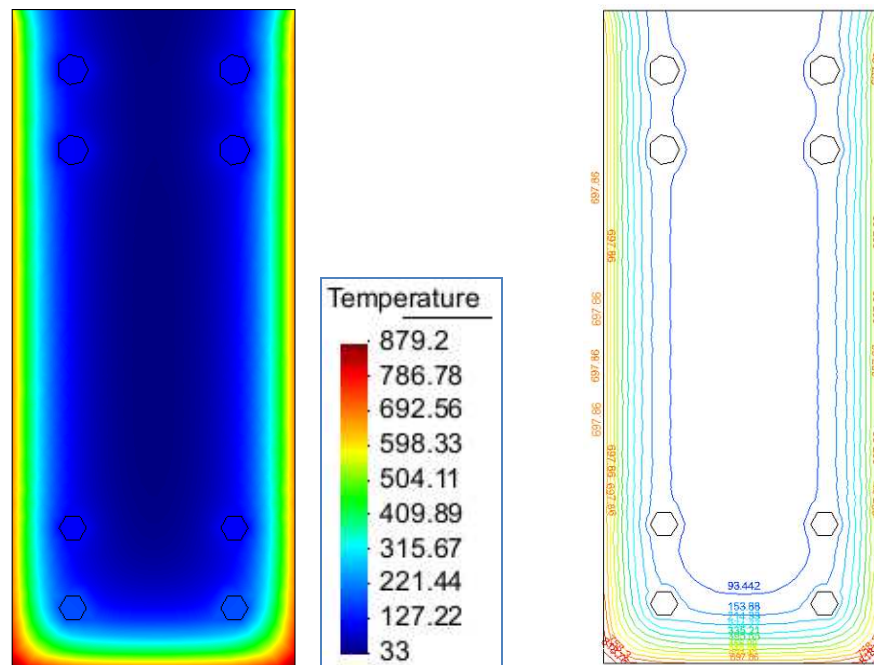


Fig. 4.5 Comparison of measured reinforcement temperatures (marked with *) and predicted by programs FIRE and SAFIR for the beam B5 (SDHI fire)

Temperature distribution (isotherms) in the cross section of the beam B1 exposed to ASTM E 119 fire, for two different times are presented on Fig. 4.6 and Fig. 4.7.



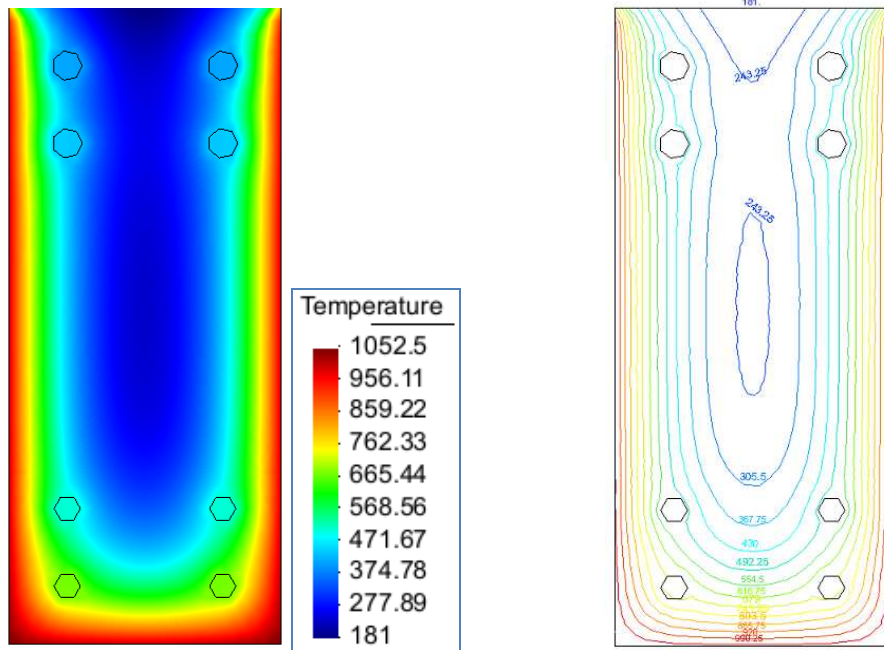


Fig. 4.7 Isotherms in the cross section of the beam B1 (ASTM fire), at moment $t=3h$

Ellingwood & Lin (1991) had modified the computer program FIRES-RC (Iding et al. 1977) by involving the transient strains according to Equation 5 and this program was used to perform the structural analysis of the beams. All six beams developed significant shear cracks near the continuous support early in the fire, but eventually failed from excessive flexural cracking and deformation, so the effect of the shear forces was neglected in this program. The same procedure is used in the computer program FIRE. Huang & Platten (Huang, 1997) had developed a nonlinear finite element model based on the “plane stress” theory, so the program FPPRCM-S involved the effect of shear forces.

Fig. 4.8 and Fig. 4.9 compare the measured and numerically achieved maximum deflections of beams B1 and B5, using different computer programs. In first three cases the structural analysis models of the beams analyzed were stiffer than the beams actually tested, leading to predicted deflections at ambient temperature (time $t = 0$) that were less than those measured. The apparent reason for this difference is the presence of several flexural cracks in the beams that appeared in the vicinity of the continuous support during the period before the fire test.

This cracking caused a slight loss of rotational stiffness and a concentration of curvature in the vicinity of the support, leading to an increase in deflection in the exposed span. During the fire test the high thermal gradient in the cross section of the beams caused more cracks and the rotational stiffness of the beam models became more close to the real one, so the predicted and measured deflections became close too. Only in program SAFIR the initial deflections were set as the measured one.

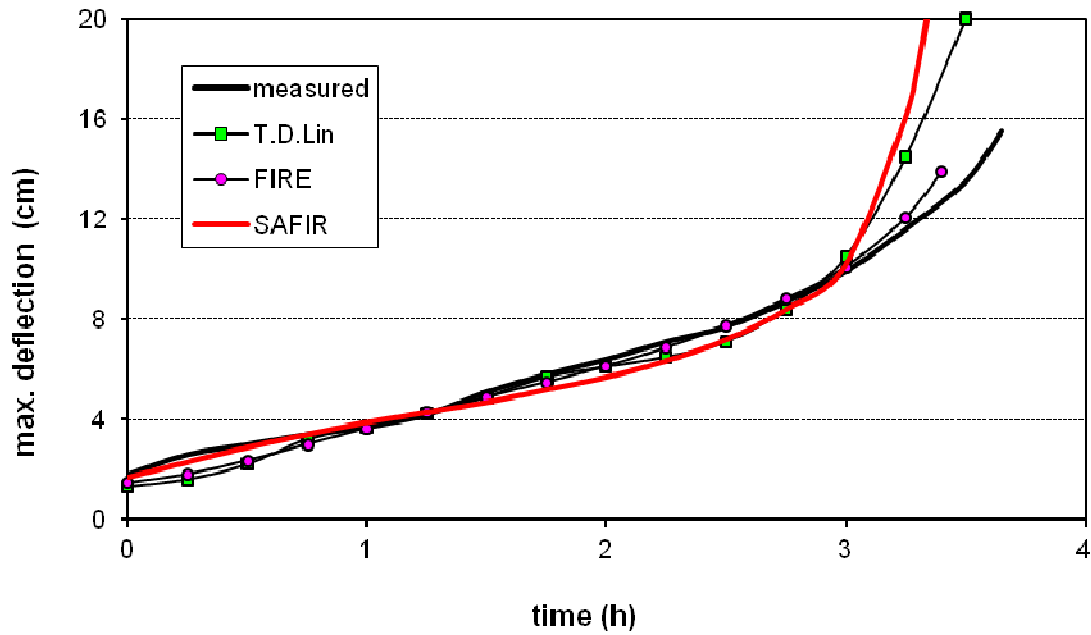


Fig. 4.8 Comparison of maximum deflections, measured and predicted by different computer programs for the beam B1 (ASTM fire)

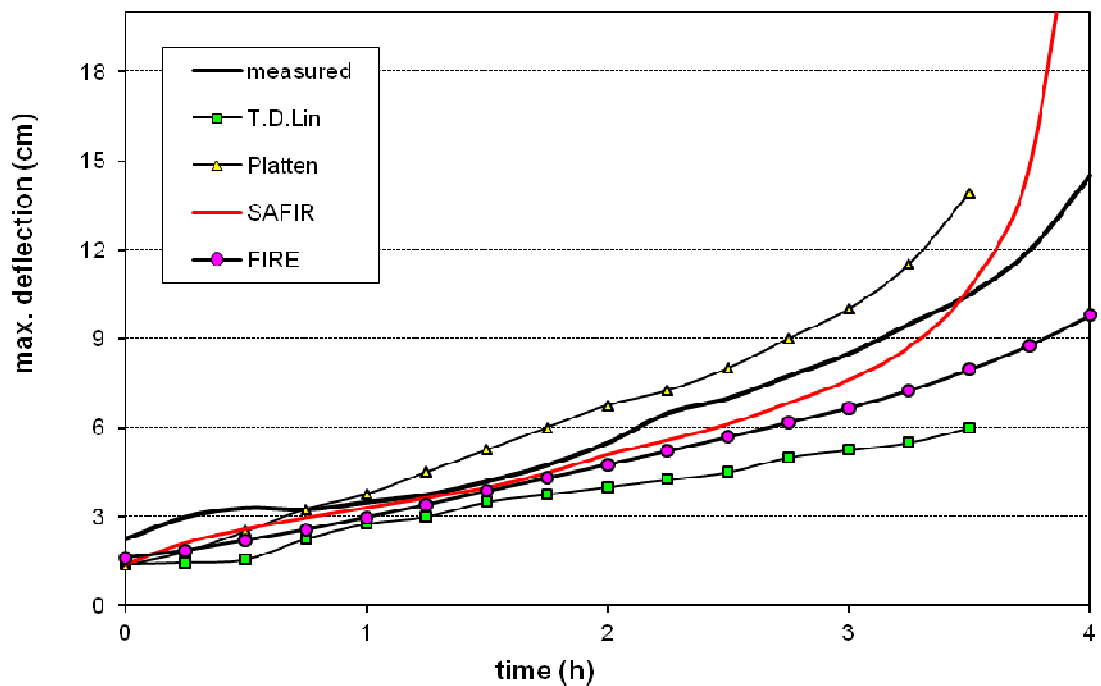


Fig. 4.9 Comparison of maximum deflections, measured and predicted by different computer programs for the beam B3 (ASTM fire)

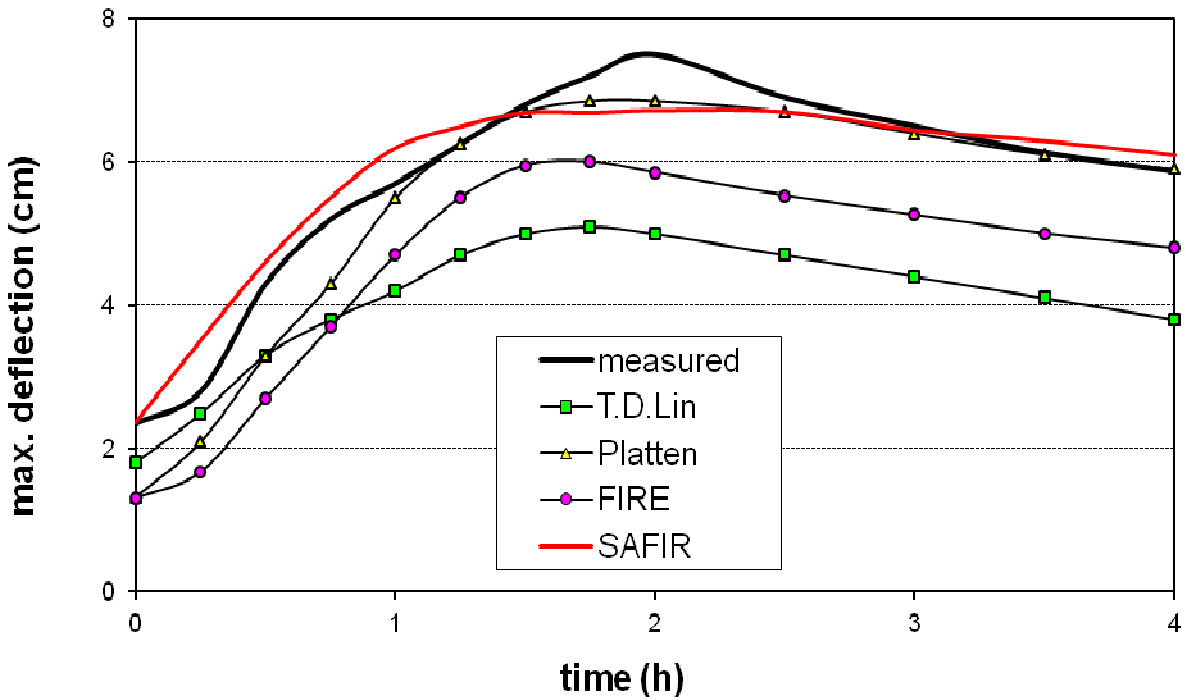


Fig. 4.10 Comparison of maximum deflections, measured and predicted by different computer programs for the beam B5 (SDHI fire)

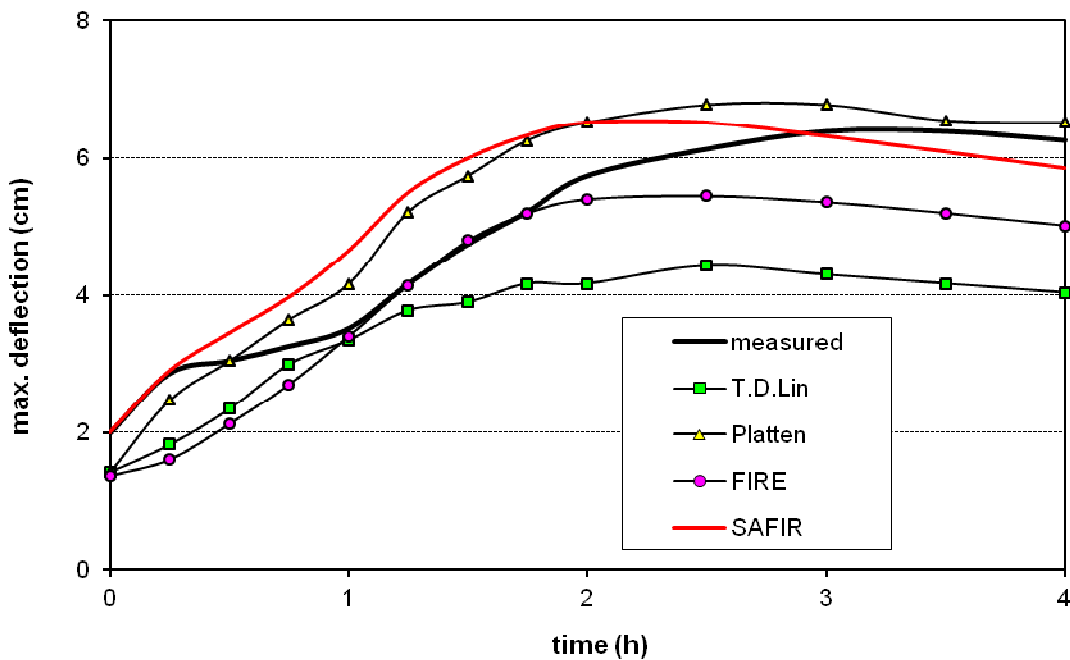


Fig. 4.11 Comparison of maximum deflections, measured and predicted by different computer programs for the beam B6 (SDHI fire)

The effect of creep at elevated temperatures in the program FIRE and SAFIR is involved by the temperature dependent stress-strain relationships for concrete and steel, recommended in EC2. They

are defined while specimens are subjected to ASTM E119 (or ISO 834) fire model, so they are not adequate for SDHI fire model. The other two programs, mentioned above, use a different approach. They involve the creep strains based on a temperature compensated time model that reflected the thermal acceleration of creep. The approach used in FIRE provides better agreement between the calculated and experimentally achieved deflections in case when ASTM fire model is used (Fig. 4.8 and Fig. 4.9), but that is not a case during the cooling phase, when beams are subjected to SDHI fire model (Fig. 4.10 and Fig. 4.11).

4.4 CONCLUSIONS

The model proposed in this study is capable of predicting the fire resistance of planar reinforced concrete structural members with a satisfactory accuracy. The computer program FIRE has been developed as analytical tool to study the fire response of reinforced concrete frame structures. Histories of: displacements, internal forces and moments, stresses and strains in concrete and steel reinforcement, as well as current states of concrete (cracking and crushing) and steel reinforcement (yielding) are calculated subject to temperature field development in the thermal time history of the structure. Since a physical testing program for investigating the response of a large variety of structural elements under differing restraint, loading, and fire conditions is impractical and expensive, analytical studies supported by the results of physical experiments could efficiently provide the data needed to resolve questions related to the design of structures for fire safety. Parametric studies, helping to identify important design considerations, could be easily achieved throughout implementation of this program. The time response capability of FIRE can also be used to assess potential modes of failure more realistically and to define the residual capacity of structure after attack of fire.

References

- Cvetkovska, 2002: Cvetkovska M., Nonlinear stress strain behaviour of RC elements and RC frames exposed to fire, Phd. thesis, Skopje, University St.Cyril and Methodius, 2002.
- Bazant, 1996: Bazant Z.P., Kaplan M.F., Concrete at high temperature: Material properties and mathematical models, London: Longman Group Limited, 1996.
- Ellingwood, 1991: Ellingwood B. and Lin T.D., Flexure and shear behavior of concrete beams during fires, *Journal of the Structural Engineering*, Vol.117, No.2, 1991, pp. 440-458.
- Huang, 1997: Huang Z. and Platten A., Nonlinear Finite Element Analysis of Planer reinforced Concrete Members Subjected to Fire, *ACI Structural Journal*, Vol.94, No.3, 1997, pp. 272-282.

WG2 - Aldina Santiago, aldina@dec.uc.pt

WG2 - Cécile Haremza, haremza@dec.uc.pt

WG3 - Fernanda Lopes, fernanda@dec.uc.pt

WG1 - Jean-Marc Franssen, jm.franssen@ulg.ac.be

5 NUMERICAL BEHAVIOUR OF STEEL COLUMNS UNDER LOCALIZED FIRE LOADING

Summary

This paper presents a benchmark example based on the paper published in 1995 about a natural fire test on a fully loaded, two dimensional, unprotected steel framework carried out in a purpose-built compartment in Cardington (Franssen, 1995). The main objective of this benchmark is to validate the utilization of the following finite element (FEM) programs for steel structures subject to elevated temperatures: i) the commercially available program, ABAQUS, and ii) the specialised homemade program dedicated to the analyses of structures subject to fire, SAFIR (Franssen, 2005). The validation is performed by comparing thermal and mechanical results against the experimental results and the numerical results obtained by the software CEFICOSS (Franssen, 1987). The influence of the model definition, axial restraint to beam, frame continuity and non-uniform temperature is discussed, and the differences between the results of the FEM programs, as well as the experimental results are illustrated.

5.1 INTRODUCTION

The benchmark example presented in this paper was prepared within the European RFCS ROBUSTFIRE project, and it refers to numerical simulations of a steel frame subject to fire. This report presents comparisons between the FEM programs: the specialized homemade FEM software dedicated to the analyses of structures subject to fire, SAFIR, and its predecessor CEFICOSS, and the commercially available program ABAQUS. The main objective was to validate the utilisation of the SAFIR and ABAQUS programs for steel structures subject to fire. This benchmark example is based on the paper published by Franssen in 1995 about a natural fire test on a fully loaded, two dimensional, unprotected steel framework carried out in a purpose-built compartment in Cardington (Franssen, 1995). The influence of the model definition, axial restraint to beam, frame continuity and non-uniform temperature is discussed, and the differences between the results of the two numerical software's SAFIR and ABAQUS are illustrated. The study cases are listed in Table 5.1. The experimental results as well as the numerical

results presented by Franssen (Franssen, 1995) with the FEM program CEFICOSS, the predecessor of SAFIR, are also showed.

Table 5.1 Overview of the considered study cases

| | Parameter | Study Cases |
|---|-------------------------|-------------------------------------------------------------------|
| 1 | Reference structure | Modelling of a half structure with account of the symmetry |
| 2 | Model definition | Complete Cardington structure modelling |
| 3 | Axial restraint to beam | a) Half structure without horizontal spring |
| | | b) Entire Cardington structure without horizontal springs |
| 4 | Frame continuity | Beam analysed as a separate member |
| | | Column analysed as a separate member |
| 5 | Thermal expansion | Half structure without expansion coefficient |
| 6 | Non-uniform temperature | Half structure with uniform temperature within the cross-sections |

5.2 DESCRIPTION OF THE BENCHMARK STUDY

The natural fire test reported by Franssen (1995) was carried out by British Steel in collaboration with the Fire Research Station. A fully loaded, two dimensional steel framework was tested in fire in a purpose-built compartment of typical size for office accommodation. Dimensions of the steel framework were specified for a building of two or three storey in height. The beam, 4550 mm long, with a universal beam section of 406 x 178 x 54, Grade 43A, was bolted to two columns of 3530 mm tall, with a universal column section of 203 x 203 x 52, Grade 43A. M20 grade 8.8 bolts were used to provide improved resistance to loss in strength at high temperatures. Columns were pin ended at the base and extended above the beam. Autoclaved aerated concrete blocks were built between the column flanges to protect the web from fire, but there were only considered to give thermal insulation (non-composite behaviour). A concrete slab, which has a cross-section of 1200 x 150 mm, was also represented because of its influence on the temperature distribution in the beam (non-composite behaviour). Lateral and sway instabilities were prevented by a subsidiary framework specially designed for.

5.3 NUMERICAL MODEL

5.3.1 Numerical tools

CEFICOSS (Computer Engineering of the Fire design of Composite and Steel Structures) is a special purpose FEM program developed in Liege, Belgium (Franssen, 1987), for analysing the behaviour of structures in fire. This program integrates thermal and structural analysis and is the predecessor to the SAFIR program.

SAFIR is a special purpose computer program for the analysis of structures under ambient and elevated temperature conditions. The program, which is based on the Finite Element Method (FEM), can be used to study the behaviour of one, two and three-dimensional structures. The program (SAFIR) was developed at Liege University, Belgium, and is today viewed as the second generation of structural fire codes developed in Liege, the first generation being the computer program CEFICOSS. As FEM program, SAFIR accommodates various elements for different idealization, calculation procedures and various material models for incorporating stress-strain behaviour.

ABAQUS is an American general commercial finite element package. It provides a complete and flexible solution for a large range of problems, including the analysis of structures subjected to fire. All modes of structural behaviour involved in fire can be simulated thanks to a large library of finite elements which enables the creation of an efficient and detailed model, in which relevant material properties at high temperatures are included (Wang, 2002). ABAQUS is able to simulate the detailed behaviour of connections in fire and user defined subroutines enable modelling many of the special features of structural behaviour in fire.

5.3.2 Mechanical and thermal material properties

All material properties used in ABAQUS at high temperature are based on the EN 1993-1-2:2005. At ambient temperature, the yield stress f_y considered by Franssen to simulate the experimental test is 408MPa. The elastic modulus considered is 210 GPa, which decreases at high temperatures according to the reduction factor $k_{E,\theta}$ (EN 1993-1-2:2005). A Poisson ratio constant equal to 0.3 is used. Franssen also used a convective heat transfer coefficient and an emissivity given by the EN 1993-10:1990 and respectively equal to 25W/m²K and 0.5. However, for the column flange facing the wall of the fire compartment, the emissivity is taken equal to 0.3 to account for some degree of radiative shadowing. The conductivity and the specific heat of the concrete slab are defined according to the EN 1992-1-2:2004. The concrete blocks insulating the column have particular properties: a density equal to 677kg/m³, a constant specific heat of 1050J/kgK and a thermal conductivity given by 0.20 + 0.0004 θ_c W/mK, where θ_c is the concrete temperature (Franssen, 1995). The concrete is not modelled in the mechanical analysis.

5.4 THERMAL ANALYSIS

In the present study, a thermal analysis is performed for each different type of structural elements met within the considered structure, i.e. the beam with the concrete slab and the column with the concrete between the flanges. The heat-transfer problem analysed in CEFICOSS, SAFIR and ABAQUS involves conduction and boundary radiation. In these analyses, the stress/deformation state is not studied, only

the temperature field is computed. With SAFIR, boundary conditions (i.e. temperatures or heat fluxes) are imposed and the temperature is computed at each point of integration of each finite element. The applied temperatures correspond to the gas temperature measured during the experimental test (Franssen, 1995). In SAFIR, the thermal analyses are made using 2-D SOLID elements to determine the distribution of the temperature within the element cross-sections. In ABAQUS, the two models (beam and column) are developed using 2D deformable element DC2D4, and are simplified taken into account the symmetry of the section. The FE mesh is similar to the mesh used by Franssen (Franssen, 1995) in CEFICOSS program. Figure 5.1 shows the evolution of the temperatures in flanges and in web centroid of a) the beam section and b) the column section. Numerical results show good agreement with the measured temperatures, as well as with the computed temperatures of CEFICOSS.

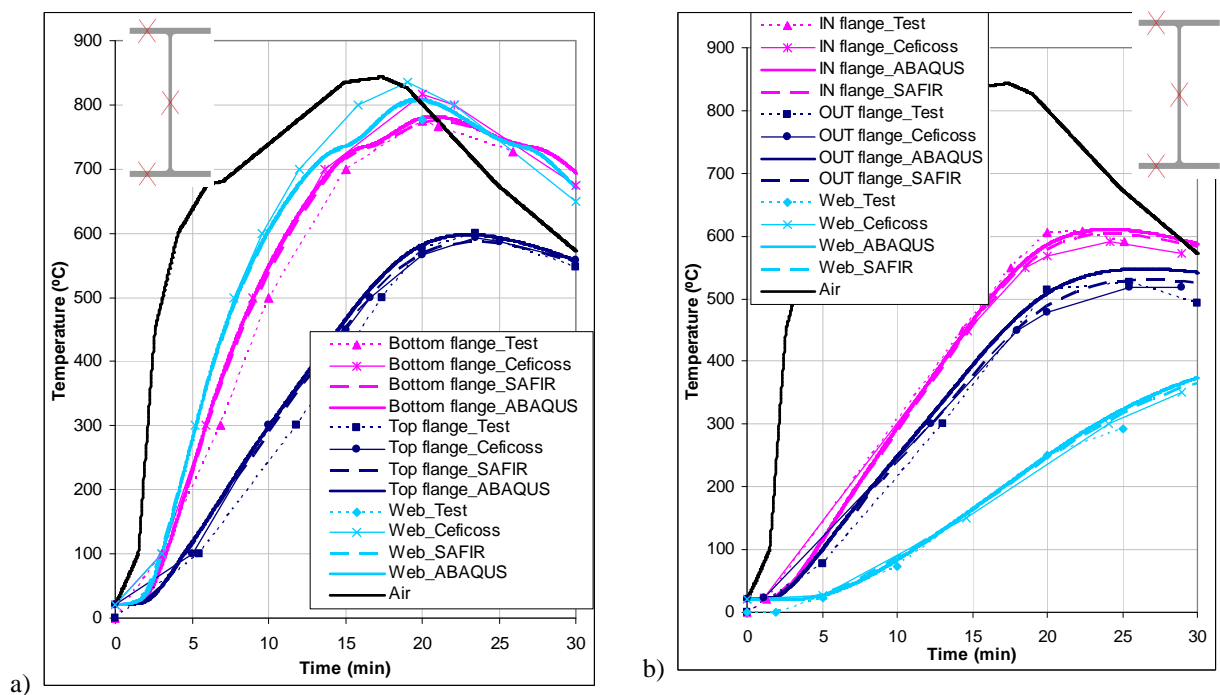


Fig. 5.1 Temperatures a) in the beam and b) in the column

5.5 MECHANICAL ANALYSIS

5.5.1 General modelling assumptions

Nonlinearities arise from large-displacement effects and material nonlinearities, and are taken into account on the numerical models. Moreover, temperature dependent material properties and nonlinear temperature gradient over the cross-section are also considered. Figure 5.2a presents the steel frame structure for which symmetry conditions are taken into account. Two dimension beam elements are used to define the beam and the column. As the concrete slab and the concrete blocks in the column only provide thermal boundary conditions for the temperature, they are not modelled in the structural analysis. According to Cooke and Latham (Cooke and Latham, 1987), during the experimental test, no

relative rotation at the connection occurred and the temperature around the connection remained lower than elsewhere in the compartment during the fire. It is then allowed to suppose a rigid beam-to-column connection. In order to represent the restraint offered by the secondary steelwork, a bi-linear spring is modelled with a nonlinear force-displacement behaviour (Figure 5.2b).

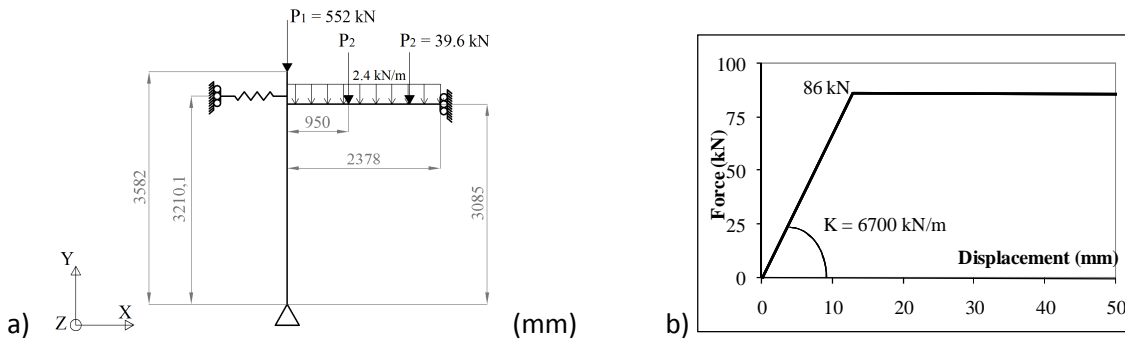


Fig. 5.2: a) Reference frame; b) behaviour of the spring

The mechanical loads are applied at ambient temperature and maintained constant during the fire. They correspond to: i) the self-weight, ii) a vertical load on the column equal to 552 kN (P1), iii) two vertical load on the beam equal to 39.6 kN (P2), iv) a uniform loading of 2.4 kN/m distributed along the beam to represent the self-weight of the concrete slab.

In ABAQUS, temperatures are specified at the three specific points through the section (ABAQUS, 2007): i) centroid of the top flange; ii) centroid of the web and iii) centroid of the bottom flange. Only one amplitude curve defining the evolution of the temperature in function of the time can be introduced for each section type. The thermal gradients applied in the beam and column cross-sections are shown in Figure 5.3. The amplitude curve corresponds to the web temperatures for the beam and to the inner flange temperatures for the column.

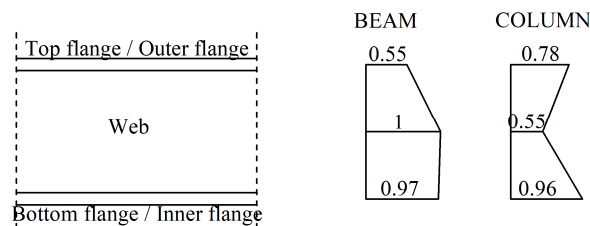


Fig. 5.3 Thermal gradient within the beam and column cross-sections in ABAQUS

Because the measured temperatures of the combustion gases were slightly lower in the vicinity of the beam-to-column connection (Franssen, 1995), the beam has also a temperature variation along its length. In SAFIR, a reduction function of the temperatures along the longitudinal beam axis, $f(x)$, with a sinusoidal shape (Figure 5.4), is taken into account (with a value of $0.90 \theta_a$ at the beam/column interconnection and $1.00 \theta_a$ at mid-span node of beam).



Fig. 5.4 Coefficients of reduction of the temperatures along the beam used in SAFIR

In order to approximate this variation in ABAQUS, the half of the beam is divided into five parts where the temperature along each length part is constant (Figure 5.5).

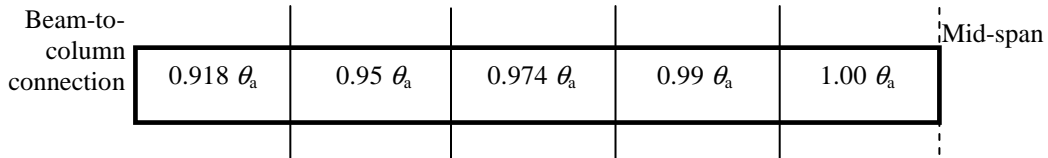


Fig.5.5 Temperature gradient along the beam span used in ABAQUS

5.5.1 Reference case

The model of the reference structure (Figure 5.2a) is validated by comparing beam mid-span vertical displacements, beam axial load and column lateral displacements with the experimental and CEFICOSS results. Figure 5.6 shows the frame deformation after 16 minutes, compared to the lateral deformation of the column obtained during the experimental test. One aspect which can explain the difference observed between the measured lateral displacements for the column and the computed ones is the presence of the concrete between the column flanges which is neglected for the mechanical analysis performed with the two programs. The evolution of the lateral horizontal displacement at mid-height of column is shown in Figure 5.7. Due to the elongation of the beam, the column bows laterally up to the buckling at about 19-20 min. The two FEM programs SAFIR and ABAQUS obtain quite close results.

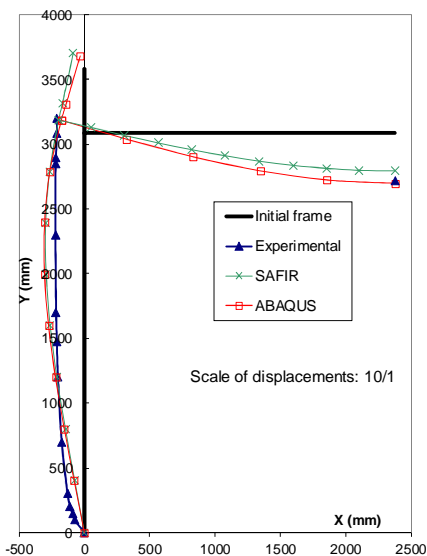


Fig. 5.6 Deformation of the frame after 16 minutes (case 1)

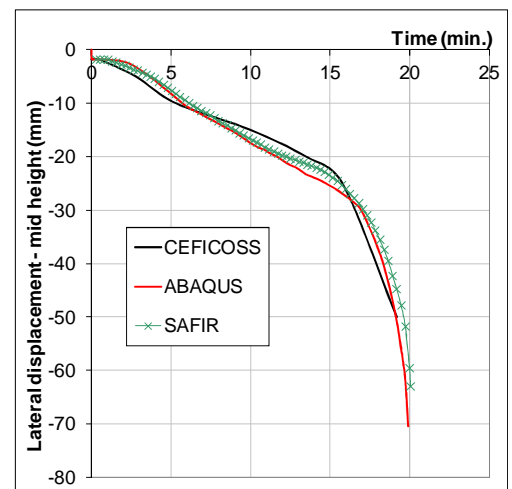


Fig. 5.7 Calculated horizontal displacement at mid height of column (case 1)

Figure 5.8 and Figure 5.9 show respectively the vertical displacement at the mid-span of the beam and the axial compression force in the beam. A very good agreement between SAFIR and ABAQUS is observed for the fire resistance time, equal to about 20 minutes as observed during the fire test (see Table 5.2). The beam vertical displacement calculated by ABAQUS increases slightly faster than with the other numerical programs (Figure 5.8). Finally, it can be concluded that a good agreement between SAFIR and ABAQUS is observed, as well as for the resistance time than for the internal forces or the displacements calculations.

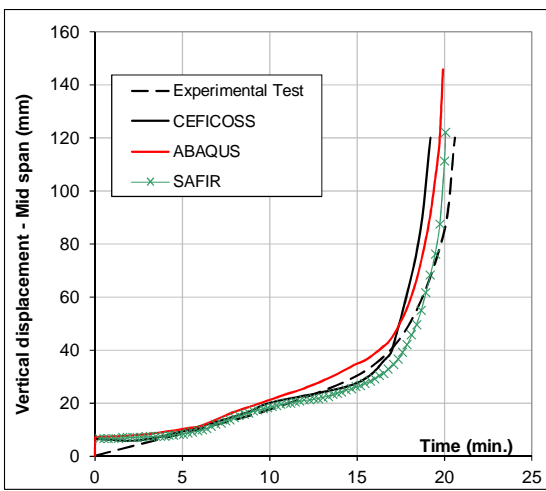


Fig. 5.8 Case 1 - Vertical displacement of the beam in the fire test

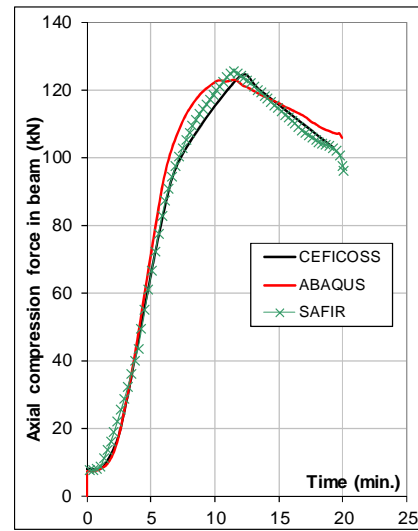


Fig. 5.9 Case 1 - Calculated axial force in the beam

5.5.2 Influence of the model definition

In order to verify that satisfactory results are obtained by simulating only one half of the frame (case 1 – Figure 5.2a), the complete frame is modelled assuming the presence of two springs (case 2 – Figure 5.10). According to Franssen, an initial (sway) imperfection of $0.8 H_c/1000$ is considered, where H_c is the column height (Franssen, 1995). Results of fire resistances are shown in Table 5.2 and a good agreement is obtained. The failure mode is exactly the same than for half of the frame (Figure 5.16), and the fire resistances are very close, so satisfactory results are obtained by simulating only one half of the frame.

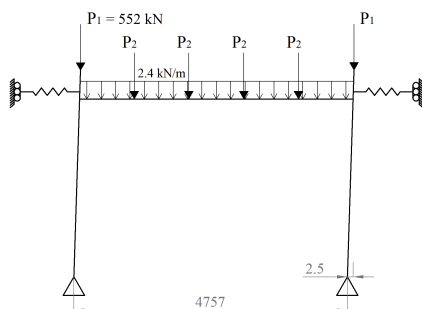


Fig. 5.10 Complete frame (case 2)

Table 5.2 Fire resistance time (R_f) calculated by SAFIR and ABAQUS

| | R_f SAFIR | R_f ABAQUS |
|--------------------------------|---------------|---------------|
| Case 1 (half of the frame) | 20'04" | 19'55" |
| Case 2 (complete frame) | 17'55" | 19'51" |

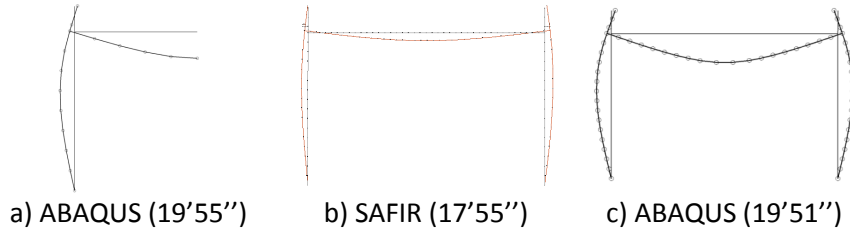


Fig. 5.11 Failure modes (scale 4/1) of the complete frame models in (b) SAFIR and (c) ABAQUS compared to the reference case failure mode in (a) ABAQUS

5.5.3 Influence of the axial restraint to beam

Mainly due to the axial restraints, the beam cannot expand with the increasing of temperature, leading to the development of axial compressive forces. In order to see if the frame stability is influenced or not by these restraints, the half of the frame and the complete frame are modelled without springs (Figure 5.12). For half of the frame, the beam axial compressive forces of both restrained (case 1) and unrestrained (case 3a) frames are shown in Figure 5.13a. It is also showed that the results from the two programs SAFIR and ABAQUS present a good correlation.

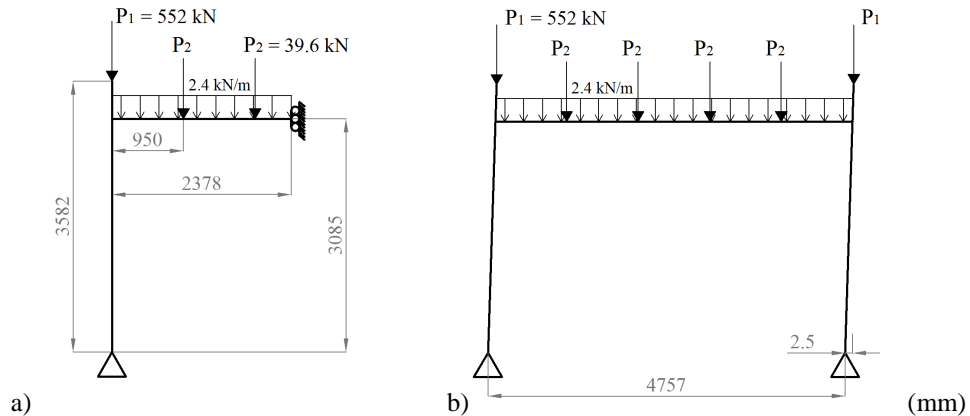


Fig. 5.12 Cases 3a and 3b – No axial restraint

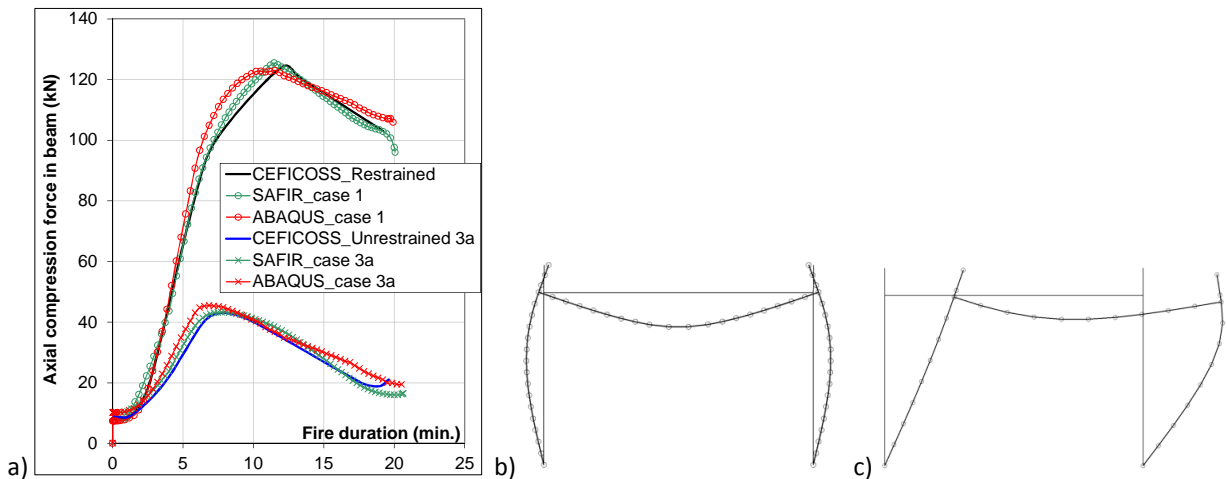


Fig. 5.13 Calculated axial force in the beam (half of the frame); Calculated failure mode of the sway frame (scale of displ. 4/1): b) with / c) without lateral restraints

The peak values reached by the axial compression forces in the beam are equal to 125.40 kN and 43.23 kN with SAFIR and 122.92 kN and 45.43 kN with ABAQUS when restraint is present and absent respectively, as shown in Table 5.3. At failure, the axial compression force in the beam is reduced from 95.97 kN to 16.43 kN with SAFIR and 105.83 kN to 19.38 kN with ABAQUS, when axial restraint is removed. However, it can be seen that the beam axial force does not significantly influence the fire resistance and the stability of the structure. Table 5.3 also shows that a good correlation is found between the fire resistance times.

Table 5.3 Axial compression forces (N), and Fire resistance time (R_f) calculated by SAFIR and ABAQUS

| | | N SAFIR | N ABAQUS | R _f SAFIR | R _f ABAQUS |
|---------------|------------------------------|-----------|-----------|----------------------|-----------------------|
| Peak value | Case 1 (restrained frame) | 125.40 kN | 122.92 kN | 20'04'' | 19'55'' |
| | Case 3a (unrestrained frame) | 43.23 kN | 45.43 kN | 20'38'' | 20'31'' |
| Failure value | Case 1 (restrained frame) | 95.97 kN | 105.83 kN | | |
| | Case 3a (unrestrained frame) | 16.43 kN | 19.38 kN | | |

However, the failure mode of the complete frame without spring and with account of an initial imperfection (case 3b) is completely different from the one observed in the previous modelling (case 3a) (Figure 5.13 b and c). Without spring and with the 0.8 H_c/1000 of initial imperfection, a non-symmetrical response of the frame can be developed. This leads to a significant reduction of the fire resistance, from 20 min. with the axial restraint to 12 min. without restraint (Table 5.4). The FEM programs obtain very close results.

Table 5.4 Fire resistance time (R_f) calculated by SAFIR and ABAQUS

| | R _f SAFIR | R _f ABAQUS |
|----------------------------------------------|----------------------|-----------------------|
| Case 1 (restrained frame) | 20'04'' | 19'55'' |
| Case 3b (complete unrestrained frame) | 12'08'' | 12'17'' |

5.5.4 Influence of the frame continuity

The influence of the frame continuity is studied simulating the beam and the column on their own (cases 4a and 4b respectively). For the beam considered on its own, at room temperature, a bending moment and a horizontal force are introduced by the column at the extremity of the beam (Figure 5.14).

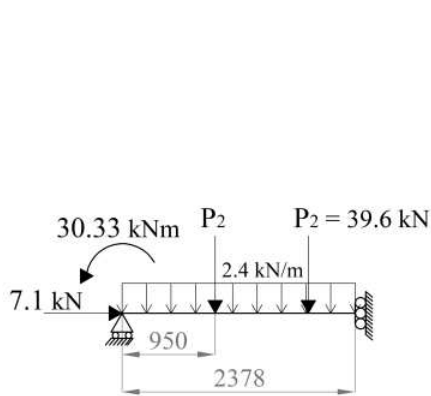


Fig. 5.14 Beam as a separate member – Case 4a

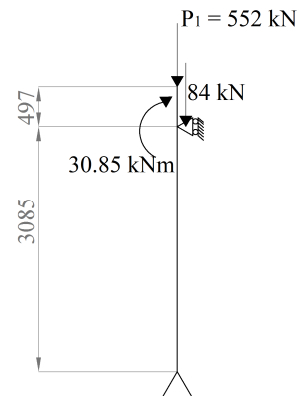


Fig. 5.15 Column considered on its own – Case 4b

Table 5.5 presents the fire resistance times and Figure 5.16 presents the evolution of the beam mid-span vertical displacement computed by the FEM programs for the beam as a separate member. These displacements are compared with the vertical displacement of the beam as part of the frame measured during the experimental test. It clearly shows that the fire resistance time reduces and the vertical displacement is higher in the absence of beneficial restraints from the column.

Table 5.5 Fire resistance time (Rf) calculated by SAFIR and ABAQUS

| | Rf SAFIR | Rf ABAQUS |
|-------------------------------------|----------|-----------|
| Case 1a (restrained frame) | 20'04" | 19'55" |
| Case 4a (beam as a separate member) | 17'29" | 17'00" |

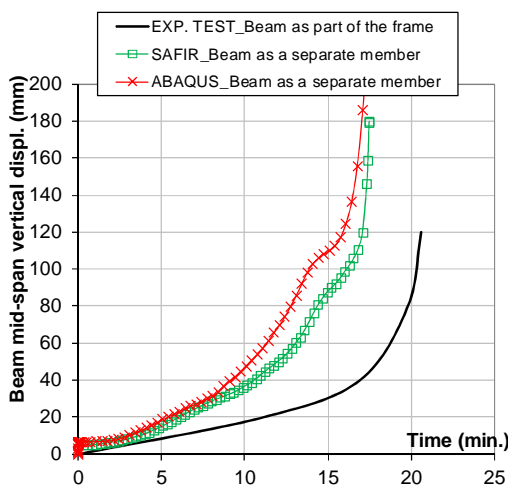


Fig. 5.16 Beam mid-span displacement – case 4a

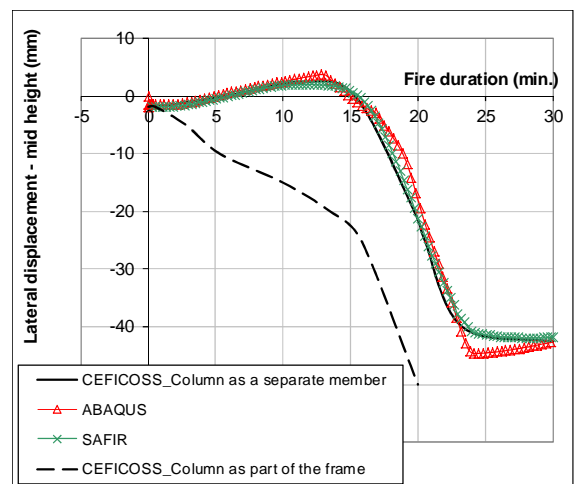


Fig. 5.17 Calculated horizontal displacement at mid height of column – case 4b

For the column considered on its own (Figure 5.23), effects of the beam are taken into account by applying a bending moment and a vertical force at the top of the column. All FEM programs obtain fire resistances of at least 30min. The lateral displacement behaviour of the column as a separate

member is presented in Figure 5.17 and compared to the behaviour of the column modelled as part of the frame. It is showed that modelling the column on its own provides completely different results of the behaviour of the column and the fire resistance time. It remains safe until the end of the analysis, against the failure at $t = 20\text{min.}$ observed with the complete frame.

5.5.5 Influence of the non-uniform distribution of temperature

Uniform temperatures throughout the beam and column cross-sections are calculated using the simplified calculation method proposed in EN 1993-1-2:2005 (EC3). According to Franssen (1995), an average emissivity equal to 0.4 can be used to calculate the uniform temperature. In Figure 5.18, the uniform temperatures (EC3) are compared to the mean temperatures calculated by the heat transfer analysis in CEFICOSS, SAFIR and ABAQUS. They are higher because the heat transfer from the steel to the concrete is not considered by the simplified calculation method.

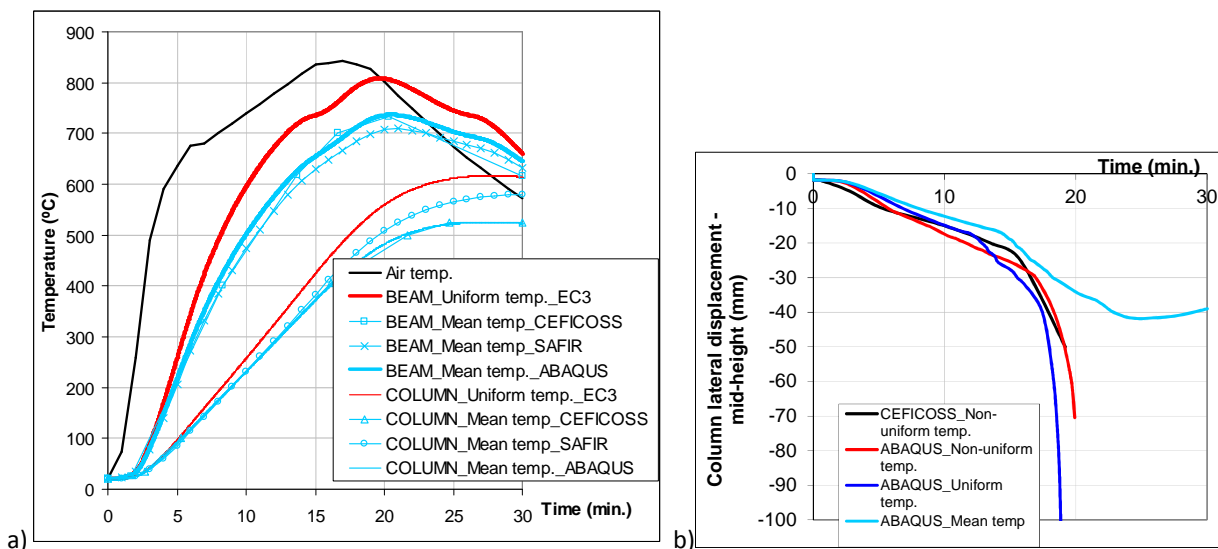


Fig. 5.18 Calculated uniform and mean temperatures

Results and comparisons of the fire resistance obtained by the numerical tools using uniform temperatures (case 5) and temperature gradients in the cross-section (case 1) are presented in Table 5.6. The mechanical models with uniform temperature in the beam and column sections, calculated according EN 1993-1-2:2005, give a lower fire resistance time than with a thermal gradient (case 1). It can be explained by the fact that the mean temperatures computed through the programs are lower than the uniform temperatures computed with EN 1993-1-2:2005.

Table 5.6 Fire resistance time (R_f) calculated by SAFIR and ABAQUS

| | R_f SAFIR | R_f ABAQUS |
|-------------------------------------|----------------|----------------|
| Case 1 (gradient of temperature) | 20'04'' | 19'51'' |
| Case 5 (uniform temperature) | 19'16'' | 19'00'' |

Figure 5.18b shows the vertical mid-span displacement of the beam for three different applications of the cross-section temperatures. The uniform temperature calculated using EC3 method leads to conservative results (premature failure) while the ABAQUS average temperature leads to unsafe results (no failure is observed until the end of the analysis).

5.6 CONCLUDING REMARKS

This document presented a comparison between three finite element programs, CEFICOSS, SAFIR and ABAQUS. The main objective was to validate the utilization of the SAFIR and ABAQUS programs for steel structures subject to fire. The FEM results obtained were also compared to experimental results.

The simple 2D steel frame studied in this document was based on the paper of Franssen published in 1995 about a natural fire test on a fully loaded, two dimensional, unprotected steel framework carried out in a purpose-built compartment in Cardington (Franssen, 1995). The influence of the model definition, axial restraint to beam, frame continuity and non-uniform temperature were discussed.

SAFIR and ABAQUS performed well the heat transfer analysis to obtain temperature distributions in structures. They also showed a good ability to simulate steel structural behaviour under fire conditions using beam elements. Some of the differences between the different results could be explained by: i) the temperature gradients in cross-sections were approximated in ABAQUS as they only could be defined into three dependant points in the cross-section; ii) the difficulty to simulate the behaviour of springs with SAFIR (no dedicated finite element), in particular when investigating the behaviour of the complete structure, and iii) ABAQUS fire resistances were defined as the beginning of the strongly decrease of the beam axial compression-time curve. In reality, ABAQUS stops a few times after. So the precision of the fire resistance value depends of the increment sizes, but also of the appreciation of the person.

Acknowledgement

The authors would like to thank the European Community's Research Fund for Coal and Steel (RFCS) under grant agreement n° RFSR-CT-2008-00036.

References

- ABAQUS Theory Manual & Users Manuals, Version 6.7, Hibbitt, Karlsson and Sorensen, Inc. USA, 2007.
- Cooke G.M.E., Latham D.J. "The inherent fire resistance of a loaded steel framework". *Steel Construction Today*, 1, 49-58, 1987.
- EN 1992-1-2:2004. "Eurocode 2: Design of concrete structures – Part 1-2: General rules – Structural fire design". European committee for standardization, December 2004.
- EN 1993-10:1990. "Eurocode 3: Design of Steel Structures, Part 10: Structural Fire Design". Draft April 1990.
- EN 1993-1-2:2005. "Eurocode 3: Design of steel structures – Part 1-2: General rules – Structural fire design". European committee for standardization, April 2005.
- Franssen, 1987: Franssen J.M. "Etude du comportement au feu des structures mixtes acier béton". PhD Thesis, University of Liège, 1987.
- Franssen, 1995: Franssen J.M., Cooke G.M.E., Latham D.J. "Numerical Simulation of a Full Scale Fire Test on a Loaded Steel Framework". *Journal of Constructional Steel Research*, 35, 377-408, 1995.
- Franssen J.M., Kodur V.K.R., and Mason J. "User Manual for SAFIR 2001, A computer program for analysis of structures submitted to the fire". University of Liège, Belgium, 2000.
- Franssen, 2005: Franssen J.-M. "SAFIR. A Thermal/Structural Program Modelling Structures under Fire", *Engineering Journal*, A.I.S.C., Vol 42, No. 3, 143-158, 2005.
- Izzuddin, B.A. "Nonlinear Dynamic Analysis of Framed Structures". PhD Thesis, Department of Civil Engineering, Imperial College, University of London, London, UK, 1991.
- Lim L., Buchanan A., Moss P., Franssen J.M. "Numerical modelling of two-way reinforced concrete slabs in fire". *Engineering Structures*, 26, 1081-1091, 2004.
- Liu T.C.H. "Theoretical Modelling of Steel Bolted Connection under Fire Exposure". *Proceedings of International Conference of Computational Methods in Structural and Geotechnical Engineering Mechanics*, Hong Kong, 1994.
- Liu T.C.H. "Finite element modelling of behaviour of steel beams and connections in fire". *Journal of Constructional Steel Research*, 36(2), pp.181-199, 1996.
- Wang Y.C. "Steel and composite structures – Behaviour and design for fire safety". Spon Press, 2002.

Luís Laím, luislaim@hotmail.com

Hélder David S. Craveiro, heldercraveiro.eng@gmail.com

WG1- João Paulo C. Rodrigues, jpaulocr@dec.uc.pt

6 BASELINE STUDY ON THE BEHAVIOUR OF COLD-FORMED STEEL ELEMENTS SUBJECTED TO FIRE

Summary

In this paper is presented a state-of-the-art and future research pathways on cold-formed steel (CFS) elements (beams and columns) subjected to fire, the experimental set-ups built at the University of Coimbra for testing CFS elements and some preliminary results obtained comparing them with the ones existing in the literature when it is possible. The main objective of the experimental research already carried out was to assess the critical temperature and time, investigate the effect of section geometry, characterize the failure modes under different boundary conditions, provide experimental data for future numerical studies and develop simplified calculation methods for fire design of CFS elements.

6.1 INTRODUCTION

Recently the demand of cold-formed steel structures (CFS) has increased significantly, especially for residential, commercial and industrial buildings due to a high strength to weight ratio and an ease to erect when compared to hot rolled-steel structures. In some cases, CFS structures are required to be fire resistant however they present poor fire behaviour because of a combination of the high thermal conductivity of steel and the elevated section factor of the structural member. Despite increasing use there is a lack of research on their behaviour under fire situation. Therefore it is extremely important to investigate and assess the structural behaviour of CFS beams and columns subjected to fire.

Due to experimental limitations, so far, most of the experimental studies were performed on stub columns, resulting in a lack of knowledge on the behaviour of CFS slender columns subjected to fire.

A state-of-the-art review is presented in this paper, as well as the experimental set-ups developed at University of Coimbra for testing CFS slender columns and beams with restrained thermal elongation subjected to fire and also some preliminary experimental results obtained, comparing them with some existing ones in the literature.

6.2 STATE-OF-THE-ART REVIEW

As mentioned there has been little research on the behaviour of CFS slender columns subjected to fire being most of the studies on stub columns. However these studies are very important and are here presented as baseline studies for future investigations.

A study performed at the Swedish Institute of Steel Construction (Ranby, 1998), for developing structural fire design of thin-walled cold-formed steel sections, was presented in order to find out the steel temperature, how it varies across the steel cross-section and the effect on the load bearing resistance. It was intended to develop a method for designing thin walled cold formed steel sections and to show that limiting the maximum temperature to 350°C for class 4 cross sections, as mentioned in the EN 1993-1.2 (2005), is too restrictive. Results showed that initial deflections have the same influence on the load bearing capacity at ambient and high temperatures and that the calculation of the plate buckling resistance according to EN1993-1.3 (2005) considering the reduced yield strength and elastic modulus is accurate at elevated temperatures. Results also showed that the 350°C limitation for class 4 cross section is too restrictive.

Feng et al. (2003) performed a total of 52 load-bearing capacity tests at ambient and elevated temperatures on compressed short CFS lipped channels, with and without service holes and unlipped channels to assess the physical behaviour and failure modes of this type of structures. The column was heated in an electric furnace and the longitudinal distribution of temperature and displacements were measured. Elevated temperatures tests, without thermal restraint, were carried out under steady state condition for four temperature levels (250, 400, 550 and 700°C). When the temperature reached the desired level the axial compression loading was applied until failure. This experimental study showed that depending on the initial imperfections the failure mode of nominally identical columns can be different at both ambient and elevated temperatures. Despite the difference in failure modes the failure loads of nominally identical columns were very close. A numerical analysis was also performed (Feng et al., 2003) based on the experimental work using the design methods presented in some international standards such as the EN 1993-1.3 (2006), and a finite element analysis (FEA) using the commercial software ABAQUS (2004) considering geometrical and material non-linearities. Stress-strain relationship of steel at high temperature was determined according to EN 1993-1.2 (2005), with a suitable modification in order to use the mathematical equations for the stress-strain relationships at elevated temperatures, or the ones proposed by Outinen et al. (1999). It was found that ambient temperature design guidelines can be used at elevated temperatures providing the reduced yield strength based on 0,2% proof stress and the reduced elastic modulus.

Heva and Mahendran (2008) performed a series of local buckling tests of CFS short compression members at elevated temperatures. The tests were carried out at predefined temperatures (100, 200, 300, 400, 500, 600 and 700°C) using a small electric furnace and a special loading set-up made to fit the

furnace using 253MA (has increased contents of silicon and nitrogen, and is microalloyed with rare earth metals (REM) providing better performance at elevated temperatures up to 1100°C) stainless steel and a Tinius Olsen Testing Machine. Ultimate loads were calculated using the available design rules, emphasizing the EN 1992-1.2 (2005) using the effective width method for the local buckling capacity of compression members at elevated temperatures. The yield stress reduction factors at elevated temperatures determined by Ranawaka (2009) and Dolamune Kankanamge (2011) were used since the recommended yield stress reduction factors for both cold-formed and hot-rolled steels were identical in this standard. It was found that using the reduced mechanical properties at elevated temperatures with ambient temperature design guidelines is possible to predict approximately the axial compression capacity of CFS short columns. This study showed once again that limiting the temperature to 350°C as in EN 1993-1.2 (2005) is too restrictive since the CFS columns presented significant capacities beyond this limiting temperature.

Ranawaka and Mahendran (2009) carried out a research based on experimental studies to investigate the distortional buckling behaviour of CFS short compression members under fire conditions. Two types of cross section were tested with different nominal thicknesses, both with low and high strength steels, G250 and G550. Steady state tests were carried out and three types of distortional buckling failure modes were observed at elevated temperature tests, namely by both flanges moving inwards or outwards and by one flange moving outward while the other moving inward. Comparing the ultimate load results with the ones obtained using the direct strength method it was found that they are reasonably accurate when the appropriate reduced mechanical properties are used. Based on this experimental research a numerical study on CFS compression members subjected to distortional buckling at elevated temperatures was developed, considering geometric imperfections, residual stresses and the reduced mechanical properties at elevated temperatures (Ranawaka and Mahendran, 2010). Comparing numerical and experimental results it was found out that the developed finite element models considering accurate mechanical properties and stress-strain characteristics of steels, initial geometric imperfections and residual stresses as a function of temperatures were able to simulate the failure modes, load deflection and ultimate loads.

Ju Chen and Ben Young (2007) developed a numerical study on CFS lipped channel stub and slender columns at elevated temperatures using a finite element software ABAQUS (2004) to investigate the behaviour and design of CFS lipped channel columns at elevated temperatures considering the effects of initial local and overall geometrical imperfections. The nonlinear model was verified against experimental results obtained in the research performed by Young and Rasmussen (1998) at ambient temperature and in the research performed by Feng et al. (2003) at ambient and elevated temperatures, and then the strength prediction of columns was compared with the design strengths using the effective width and direct strength method. It was found that the estimated column strengths

using FEA is in good agreement with experimental results both at ambient and elevated temperatures and that the effective width and direct strength method using the reduced material properties conservatively predicted the columns strength.

On the other hand, studies on CFS beams under fire conditions are still fewer and are also mostly numerical. Some studies concluded that the increase of the magnitude of the local imperfections may lead to a relatively straightforward decrease of initial stiffness of the member and that the magnitude of global imperfections may have more influence on the ultimate load of the member. For instance, Kaitila (2002) observed that the compressive ultimate load of a C column may be reduced by 5.1% when the global imperfection magnitude increases from $L/1000$ to $L/500$ and may also be reduced by 3.9% when the local imperfection magnitude increases from $h/200$ to $h/100$ at 600°C (where, L is the beam length and h its height). Nevertheless, the failure by distortional buckling may still be further affected by the initial geometric imperfections. Ranawaka and Mahendran (2010) noted that the maximum load capacity of a C column may be reduced by 20 and 30% when the distortional imperfection magnitude increases from zero to $2t_n$ (two times the thickness of section) at 20°C and 500°C , respectively. In addition, it seems that the design method given in EN1993-1.2 is over-conservative for all the temperatures excepted for CFS beams with very high slenderness values (Kankanamge, 2010). With regard to the maximum temperature in CFS members, EN1993-1.2:2005 has enforced a limit of 350°C , which also seems again to be overly conservative (Lu et al., 2007, Laím and Rodrigues, 2011). Therefore, there is a long trek to go in the clarification of this behaviour before developing simplified calculation methods that can be used in fire design.

With regard to the residual stresses of CFS members, it is important to remember that coiling, uncoiling, cold bending to shape, and straightening of the formed member lead to a complicated set of initial stresses and strains in the cross-section (Schafer and Peköz, 1998, Moen et al., 2008). It is also noticed that both residual stress and cold-work of forming effect (where the yield stress of the material in the corners is increased above the virgin yield stress) should not be modelled independent of one another because they are derived from the same process. However, this effect in the corners is generally small since the corners are usually just a small proportion of the overall cross-sectional area (Ranawaka and Mahendran, 2010). These residual stresses vary across the steel sheet thickness as membrane (constant) and bending (linear variation) components, in opposition to the hot-rolled members. The membrane residual stresses are reasonably small and can be ignored. As well as that, Ranawaka and Mahendran (2010) observed in their study that the influence of flexural residual stress in a press-braked C-section was negligible. This may occur because the members may buckle at a stress level lower than the yield point of steel. Hence, members with high values of steel yield strength and / or low values of the steel sheet thickness are little susceptible to residual stresses and, on the other hand, in those cases, the own residual stresses also have the tendency to be low (Quach et al., 2004).

Lastly, the residual stresses are not often considered at elevated temperatures since they decrease rapidly with increasing temperatures (Ranawaka and Mahendran, 2010).

So far, the absence of experimental fire resistance studies in slender CFS columns and beams is clear. Establishing the presented studies as a starting point and aiming to respond to the existing challenges in this research field a new experimental set-up was developed in order to perform fire resistance tests on cold-formed steel slender elements with restrained thermal elongation.

6.3 FIRE RESISTANCE TESTS ON CFS ELEMENTS

6.3.1 Test specimens

6.3.1.1 CFS columns

The experimental programme was carried out on CFS slender columns with different types of cross-sections, namely single sections, C, open built-up cross-sections, I, and closed built-up cross-sections, R and 2R (Fig. 6.1) with pin-ended support conditions and 3 kN/mm of axial restraining provided by a 3D surrounding structure. All specimens were fabricated with structural steel S280GD+Z (EN 10147:2000), hot dip galvanized with zinc on each side. All these profiles also had the same nominal thickness, 2.5 mm, and the nominal web width was 150 mm for the C profiles and 155 mm for the U profiles. Built-up cross-sections were assembled with self-drilling screws Hilti S-6.3×19 MD03Z spaced from 725 mm. Each column was 2950 mm tall. The thermocouples were placed in the flanges and in the web of each cross-section (Fig. 1) and in five different sections throughout the length of the column, in order to evaluate the longitudinal temperature distribution.

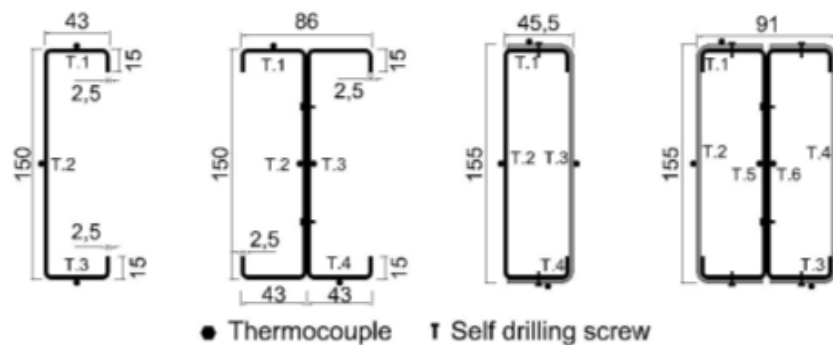


Fig. 6.1 CFS cross sections of columns tested and thermocouple's position in each cross section

6.3.1.2 CFS beams

The same kind of cross sections used in columns was also adopted for beams. However, the nominal web width of the C and U profiles was of 150 and 155 mm, respectively. The beam span was 3.0 m for all specimens and the distance between the screws along beam was about 1 m. These profiles were built by PERFISA S.A. company which is specialized in the fabrication of CFS profiles, and the choice of the

cross-sections and the distance between the screws was based on the observation of CFS structures and design projects for this kind of buildings representing commonly used details in several countries.

The actual axial stiffness imposed by the surrounding structure was about 15kN/mm. The restraining systems intended to reproduce as faithful as possible the actual boundary conditions of an element when is inserted in a real CFS building structure, making it possible to understand how the surrounding structure effects the element when it is subjected to fire.

6.3.2 Experimental set-ups

6.3.2.1 CFS columns

The experimental setup (Fig. 2) developed at the University of Coimbra comprises a 2D reaction steel frame (nº1) and a 3D restraining steel frame of variable stiffness (nº2) in order to simulate the axial stiffness of a surrounding structure to the CFS column subjected to fire. The restraining frame was composed by four columns and four beams (2 in the top and 2 in the bottom) placed orthogonally. The connections between columns and the top beams were made using M24 threaded rods in order to allow the vertical adjustment of the vertical position of the top beams. The hydraulic jack (nº3) used to apply the service load, N_b, R_d , was placed in the 2D reaction frame. The loading intended to simulate the serviceability load of a column inserted in a real building structure. The thermal action was applied using a vertical modular electric furnace (nº4) programmed to reproduce the standard fire curve ISO 834. To measure the restraining forces generated during the heating process a special device was built (nº5), consisting on a hollow steel cylinder with a load cell inside where a solid steel cylinder, that was connected to the top of the column, slides through it. The temperatures in each specimen were measured by type K thermocouples placed in the cross-section and throughout the length of the column. The axial displacements of the columns were measured using Linear Variable Displacement Transducers (L.V.D.T.) placed on top and bottom of the column. Lateral displacements were measured using linear wire displacement transducers (L.W.T.) placed throughout the length of the column in specified positions (Fig. 6.2).

6.3.2.2 CFS beams

Fig. 6.3 shows many views of the test set-up for beam which consisted essentially of a reaction frame (nº1) and a hydraulic jack (nº2) to impose loading, a modular electric furnace (nº3) to simulate fire conditions, a roller and pinned support (nº 4) to provide a simply supported beam. Hence, the test specimens (nº 5) were loaded at two points 1.0 m (one-third of the beam span) from the supports of the beam in such a way that between the two loading points the beam was under pure bending state (four point bending test). The loading was applied by a hydraulic jack (nº 2), which was hung on a two-dimensional reaction frame (nº 1). This hydraulic jack had a maximum loading capacity in compression

of 295 kN and a maximum stroke length of 360 mm and was controlled by a servo hydraulic central unit. Additionally, beneath the hydraulic jack a 250 kN load cell (n° 6) was mounted in order to monitor the applied load during the test. This loading was transferred from the hydraulic jack to the specimen by an HEA160 column (n° 7) and applied at two points on the specimen by means of a HEB140 load distribution beam (n°8).

These specimens were also heat with a horizontal modular electric furnace (n° 3). A spherical plain bearing and a spherical hinge (respectively ns° 9 and 10) were also assembled in the loading system in such a way that the load applied on the beams could easily follow the local and global deformations of the beams during the tests. Furthermore, the instrumentation of the beams still included linear variable displacement transducers (LVDTs) for vertical displacement measurements. Finally, the experimental system still comprised two simply supported steel beams placed orthogonally to the testing beam with the goal of simulating the axial restraint to the thermal elongation of that beam (Fig. 6.4). Note that the specimen was connected to the axial restraining beams by means of a HEB220 profile (near the pinned support) and a threaded rod system (near the roller support) which allowed eliminating the clearances between the specimen and those beams. At the end of this HEB220 profile and this threaded rod system, a steel semi-sphere (covered with a thin layer of Teflon) was placed, so that the displacements were measured without friction.



Fig. 6.2 Test set-up for CFS slender columns with restrained thermal elongation subjected to fire

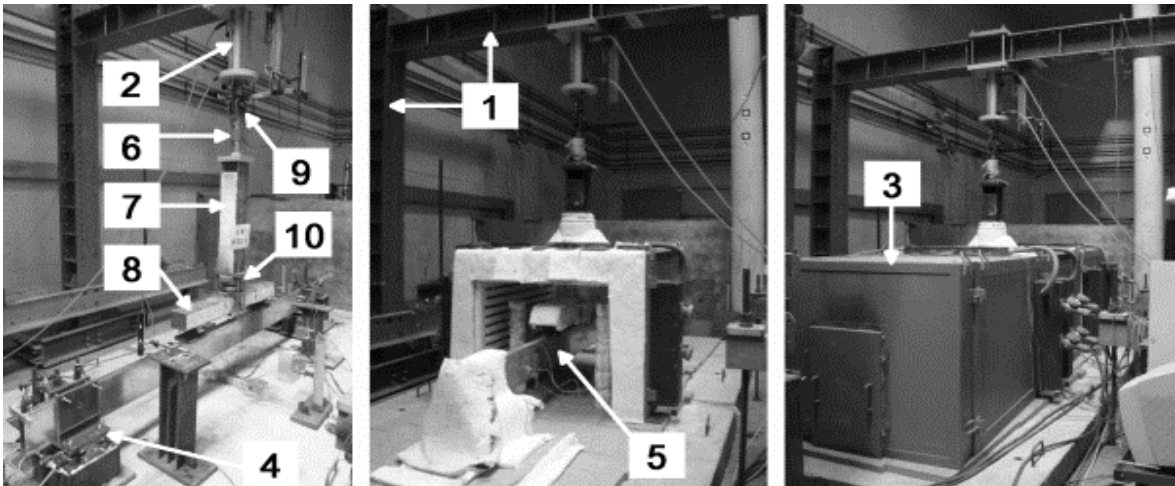


Fig. 6.3 Test set-up for CFS beams

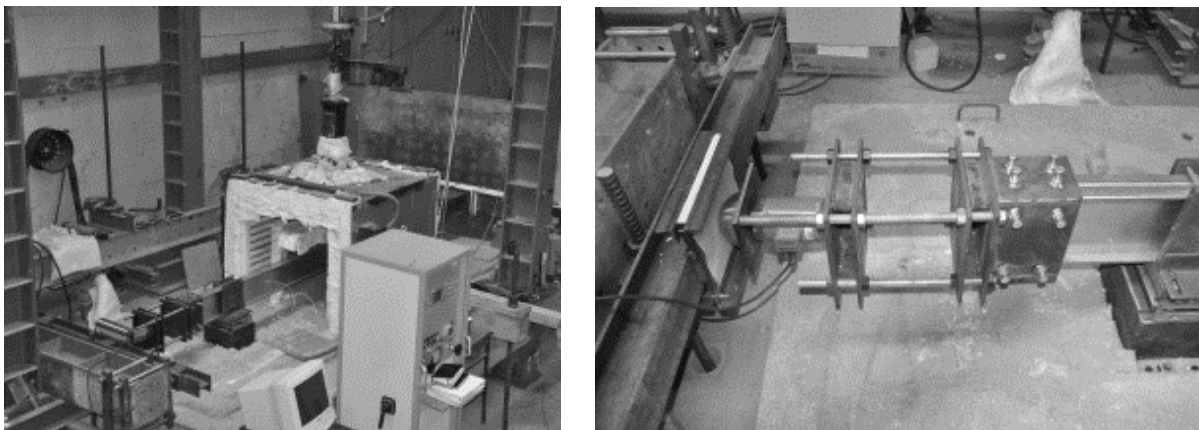


Fig. 6.4 Detail of axial restraining system

6.3.3 Test procedure

To achieve the goals of this scientific investigation, these fire resistance tests were performed in two stages: loading and heating stage. First, the specimens were loaded up to the target force under load control at a rate of 0.1 kN/s. The load level applied on the elements was 50 % of the design value of the load-bearing capacity of the respective element at ambient temperature, calculated in accordance with the methods proposed in EN 1993-1.1 (2004) and EN 1993-1.3 (2006). Finally, the heating stage was started after the desired load was reached. Thus, the specimens were heated according to the standard fire curve ISO 834. During this period of heating, the load was kept constant until the specimen failed, in other words when the restraining forces on it returned to the value of the initial applied axial load, where the deterioration of mechanical properties of steel is so high that the element no longer has any load carrying capacity against the restraining forces (failure criteria in terms of strength).

6.4 RESULTS

6.4.1 Temperature

It was found that the temperature in each cross-section was nearly uniform, except for the closed built-up cross-section, 2R, where it was found that the temperature in the inner web was significantly lower (Fig. 6.5). The evolution of temperature depended on the cross-section shape. It is clear that for single and open built-up cross-sections the rate of temperature rise was higher than in closed built-up cross-sections such as, R and 2R, due to the existence of confined air in their interior which has low thermal conductivity and due to the fact that only the external sections (U in the 2R cross-section) were directly exposed to radiation.

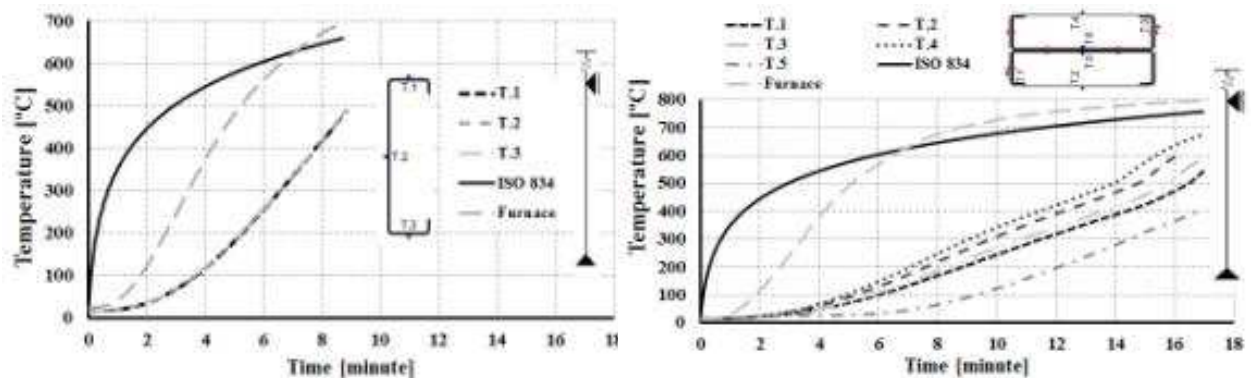


Fig. 6.5 Evolution of temperatures in each cross-section at mid-section of the columns

6.4.2 Restraining forces

The obtained results for the evolution of restraining forces in function of mean temperature throughout the length of the CFS columns with 50% load level and different end support conditions, namely, pin-ended and semi-rigid, are presented in Figure 6. It was found out that for the C cross-section the restraining forces increased up to 2.7 times the initial axial load while for I, R and 2R they increased approximately up to 1.6, 1.5 and 1.2, times respectively, for the 50% load level and pin-ended support conditions. It is worth mentioning that for the 2R cross-section with a 50% load level and semi-rigid end support conditions the restraining forces kept almost constant throughout the test. It is clear that for pin-ended columns the critical temperatures were higher than the limiting 350 °C established in the EN 1993-1.2:2005. Fig. X.6 shows that the critical temperature of the pin-ended C, lipped I, R and 2R columns was respectively about 400, 410, 380 and 420 °C, corresponding to a critical time around 8, 9.5, 9.5 and 11.5 minutes. On the other hand, the critical temperature of the C, lipped I, R and 2R columns with semi-rigid end support conditions was respectively about 475, 346, 466 and 364 °C, corresponding to a critical time around 9, 7.5, 9 and 8 minutes. The post-critical behaviour at high temperatures was characterized by a sudden decrease of the restraining forces and followed by a large lateral deformation. For the R and 2R cross sections with semi-rigid end support conditions the critical

temperatures observed were very low when compared with the ones observed in other cross sections. That may be explained by the existence of distortional buckling in the column near the built support system when the initial applied load was applied, causing the failure of the column more rapidly.

The evolution of the axial restraining forces generated in beams as a function of temperature for the different cross-sections is depicted in Fig. 6.7. From these graphs, it can be seen that the fire resistance of the C, lipped I, R and 2R beams was respectively about 11, 13, 15 and 22 minutes, corresponding to the following critical temperatures of 530, 440, 505 and 665 °C. So, the critical temperature of the different cross-sections was almost the same (around 475°C), except for the 2R beam. One reason for that may be due to the fact that the axial stiffness of the 2R beam is significantly higher than the other beams. It is obviously that the critical temperature of the beams is a question of balance between the axial stiffness of the beam and the axial stiffness imposed by the surrounding structure to the thermal elongation of beam. This is why the beam temperatures of the I and R beams are very similar when their axial restraining force is maximum.

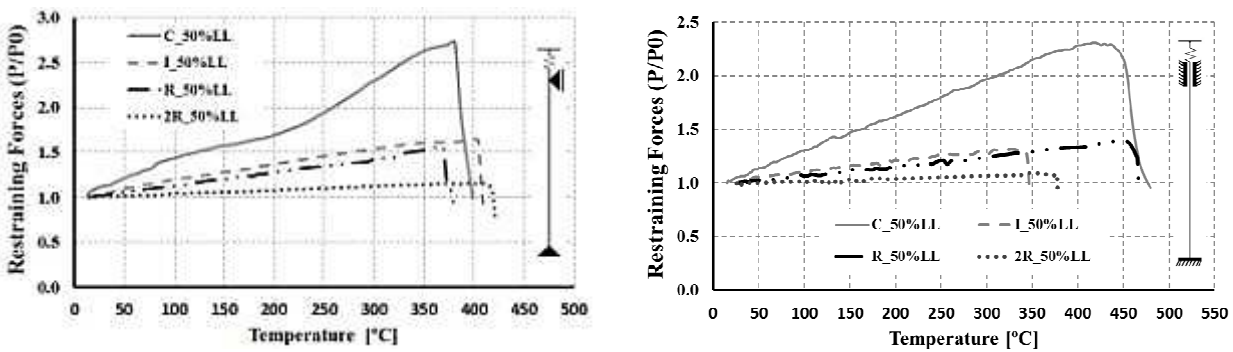


Fig. 6.6 Evolution of restraining forces vs mean temperature in CFS column with pin-ended and semi-rigid end support conditions

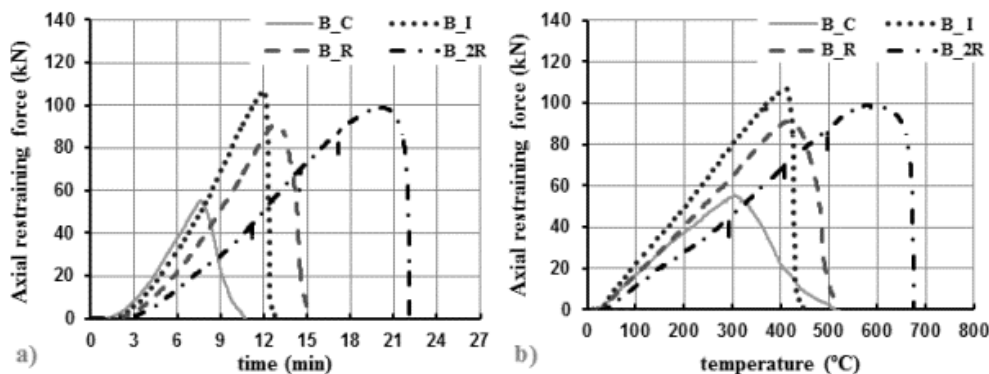


Fig. 6.7 Evolution of axial restraining forces in the CFS beams as a function of time (a) and temperature (b)

6.4.3 Failure modes

As it was expected, cold-formed steel elements are very sensitive to local, distortional and global buckling and also their interactions (Fig. 6.8). It was observed that the flexural global buckling was the main failure mode responsible for the collapse of the open columns (C and I columns), the lateral-torsional buckling for the collapse of the beams with the same last cross-sections mentioned and the distortional buckling for the collapse of the R and 2R elements. For the columns with semi-rigid end support conditions local and distortional buckling were more visible.

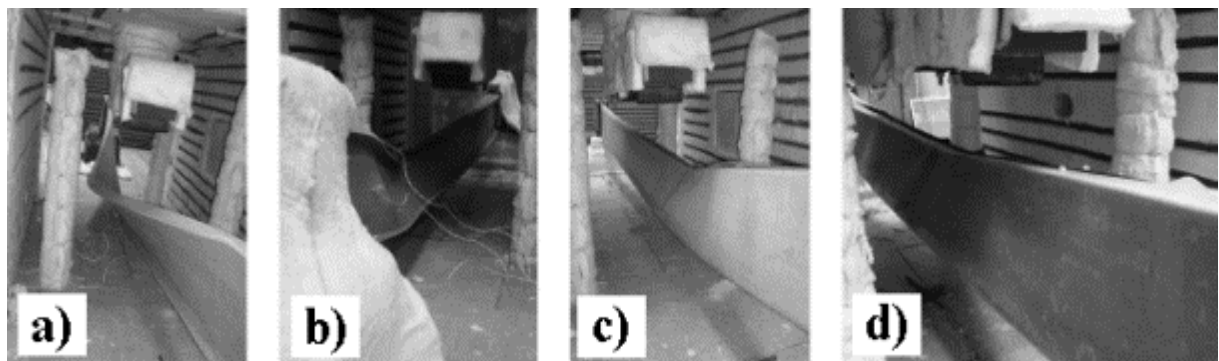


Fig. 6.8 Failure modes of the C (a) I (b) R (c) and 2R (d) beams after fire test

6.5 CONCLUSIONS

This paper has presented a state-of-the-art and future research pathways on cold-formed steel elements (beams and columns) subjected to fire. In addition, it is described the experimental programme, the testing procedures and the test set-up for bending and compression tests in fire, performed at the Department of Civil Engineering of the University of Coimbra. The load applied on the elements, the bending moments, the restraining forces, the vertical and horizontal displacements of the elements, as well as, the temperatures in the furnace and at several points of the elements are shown as preliminary results of these experimental tests so as to characterize the structural behaviour of the CFS elements subjected to fire in the best possible way.

One of the main and expected conclusions of this research work is that all these elements had low fire resistances (less than 30 minutes). However, it was observed that the hollow sections (R and 2R sections) show an enhanced fire behaviour (higher fire resistance) than the open sections (C and lipped-I sections), with the fire resistances of the beams being better than the ones of the columns.

It was found that single and open built-up cross-sections (C and I) presented a higher heating rate than the closed built-up cross-sections (R and 2R) hence the evolution of temperature depended on the cross-section shape. In the closed built-up cross-sections (R and 2R) there was confined air in the interior which has low thermal conductivity and only the external sections (U in the 2R cross-section) were directly exposed to radiation.

Finally, CFS elements can also fail in a variety of buckling modes including local, distortional and global (flexural and lateral-torsional) buckling at high temperatures. It seemed that the global buckling was the main failure mode responsible for the collapse of the open elements and the distortional buckling the main failure mode responsible for the collapse of the closed built-up elements. However, in general it looked like that the failure modes become more complicate in CFS elements with complex boundary conditions.

References

- ABAQUS Analysis User's Manual, Version 5.8.1.5 and Version 6.5, Abaqus, Inc., 2004.
- Chen, 2007: Chen J., Young B., Cold-Formed Steel Lipped Channel Columns at Elevated Temperatures, in: *Engineering Structures*, 2007, Vol. 29, pp. 2445-2456.
- EN 10147, Specification for Continuously hot-dip zinc coated structural steel sheet – Technical Delivery Conditions, 2000.
- EN 1993-1.1, Eurocode 3: Design of steel structures. General rules and rules for buildings. European Committee for Standardization. Brussels, Belgium, 2004.
- EN 1993-1.2, Eurocode 3: Design of steel structures, Part 1.2: General rules, Structural fire design. European Committee for Standardization. Brussels, Belgium, 2005.
- EN 1993-1.3, Eurocode 3: Design of steel structures, Part 1.3: General rules, Supplementary rules for cold formed members and sheeting. European Committee for Standardization. Brussels, Belgium, 2006.
- Feng, 2003: Feng M., Wang Y.C., Davies J.M., Structural Behaviour of Cold-Formed Thin Walled Short Steel Channel Columns at Elevated Temperatures. Part 1: experiments, in: *Thin-Walled Structures*, 2003, Vol. 41, pp. 543-570.
- Feng, 2003: Feng, M., Wang, Y.C., Davies, J.M., Structural Behaviour of Cold-Formed Thin Walled Short Steel Channel Columns at Elevated Temperatures. Part 2: Design Calculations and Numerical Analysis, in: *Thin-Walled Structures*, 2003, Vol. 41, pp. 571-594.
- Heva, 2008: Heva Y.B., Mahendran M., Local Buckling of Cold-Formed Steel Compression Members at Elevated Temperatures. Fifth International Conference on Thin-Walled Structures, Brisbane (Australia), 2008.
- ISO 834, Fire resistance tests – elements of building construction, Part 1: General requirements, International Organization for Standardization ISO 834, Geneva, Switzerland.
- Kaitila, 2002: Kaitila O., Imperfection sensitivity analysis of lipped channel columns at high temperatures, in: *Journal of Constructional Steel Research*, 2002, Vol. 58, pp. 333-351.
- Kankanamge, 2010: Kankanamge N.D., Structural Behaviour and Design of Cold-formed Steel Beams at Elevated Temperatures, PhD thesis, University of Queensland, Brisbane, Australia, 2010.
- Kankanamge, 2011: Kankanamge N.D., Mahendran M., Mechanical Properties of Cold-Formed Steels at Elevated Temperatures, in: *Thin-Walled Structures*, 2011, Vol. 49, pp. 26-44.
- Laím, 2011: Laím L., Rodrigues J.P.C., Comportamento ao fogo de vigas de aço enformado a frio para pavilhões industriais. Proceedings of the 1st Ibero-Latin-American conference on fire safety, Natal, Brasil, 2011, Vol. 1, pp. 53-62.
- Lu, 2007: Lu W., Mäkeläinen P., Outinen J., Numerical simulation of catenary action in cold-formed steel sheeting in fire, in: *Journal of Structural Mechanics*, 2007, Vol. 40, no. 3, pp. 28-37.
- Moen, 2008: Moen C.D., Igusa T., Schafer B.W., Prediction of residual stresses and strains in cold-formed steel members, in: *Thin-Walled Structures*, 2008, Vol. 46, pp. 1274-1289.
- Outinen, 1999: Outinen J., Mechanical Properties of Structural Steels at Elevated Temperatures, Licentiate thesis, Helsinki University of Technology, Laboratory of Steel Structures, Espoo, 1999.

- Quach, 2004: Quach W.M., Teng J.G., Chung K.F., Residual stresses in steel sheets due to coiling and uncoiling: a closed-form analytical solution, in: *Engineering Structures*, 2004, Vol. 26, pp. 1249-1259.
- Ranawaka, 2009: Ranawaka T., Mahendran M., Experimental Study of the Mechanical Properties Of Light Gauge Cold-Formed Steels at Elevated Temperatures, in: *Fire Safety Journal*, 2009, Vol. 44, pp. 219-229.
- Ranawaka, 2009: Ranawaka T., Mahendran M., Distortional Buckling tests of Cold-Formed Steel Compression Members at Elevated Temperatures, in: *Journal of Constructional Steel Research*, 2009, Vol. 65, pp. 249-259.
- Ranawaka, 2010: Ranawaka T., Mahendran M., Numerical Modelling of Light Gauge Cold-Formed Steel Compression Members Subjected to Distortional Buckling at Elevated Temperatures, in: *Thin-Walled Structures*, 2010, Vol. 48, pp. 334-344.
- Ranby, 1998: Ranby A., Structural Fire Design of Thin Walled Steel Sections, Swedish Institute of Steel Construction, *J. Construct. Steel Res.* 1998, Vol. 46, Nos. 1-3, pp. 303-304.
- Schafer, 1998: Schafer B.W., Peköz T., Computational modeling of cold-formed steel: characterizing geometric imperfections and residual stresses, in: *Journal of Constructional Steel Research*, 1998, Vol. 47, pp. 193-210.
- Young, 1998: Young B., Rasmussen K.J.R, Design of Lipped Channel Columns, in: *Journal of Structural Engineering*, ASCE, 1998, Vol. 124, no. 2, pp. 140-148.

David Rush, d.rush@ed.ac.uk

7 BENCHMARK MODELLING OF CONCRETE FILLED STRUCTURAL HOLLOW SECTIONS

Summary

This benchmark study is from (Rush, 2013) and assesses the inputs parameters required to accurately predict the fire resistance time of historical furnace tests on unprotected concrete filled structural hollow (CFS) sections. This study proceeds in three stages: (1) thermal tests on 14 unprotected concrete filled structural hollow sections (CFS); (2) the development of a thermal modelling approach to predict the observed temperatures within the cross-sections of the thermal tests; and (3) a meta-analysis of the predicted fire resistance of four exemplar structural furnace tests using the EC4 Annex H (CEN, 2005).

7.1 THERMAL TESTS

Fourteen thermal furnace tests on unprotected CFS sections were conducted as detailed in Tab. 7.1, and the temperatures at specific points within the cross-section are measure and predicted, again using ABAQUS. A number of parameters were considered included the shape of the section, the overall size of the section, the wall thickness, the type of concrete infill, and the type of thermal insult (fire). The temperatures within the sections were predicted using both the *Combi EC4c* and *Combi ω* thermal modelling approaches and compared to the observed temperatures. More details of the tests are available in (Rush, 2013). The main parameters assessed were used to identify the individual tests using a naming scheme as outlined below. Details of the specimens tested are given in Fig. 7.2 and Tab. 7.1.

The concrete infill in the majority of the specimens was a commercial, high strength, hybrid steel (45 kg/m³) and polypropylene fibre (2 kg/m³) reinforced mix (FIB). One specimen (C11HIN) was filled with high strength concrete (HSC) using the same mix design as the FIB concrete mix but without added fibres. The concrete strength at the time of testing (> 6months old) was approximately 50 MPa and had a moisture content of 4.8 % by mass (determined by the use of cylinder tests). More details of the concrete mix and strengths are available in (Rush, 2013). The steel tubes were Grade S355 (355 MPa nominal yield strength). Two pairs of vent holes and a pair of lifting holes were included to allow vapour pressure to escape during heating and also to enable easy handling (Fig. 7.2).

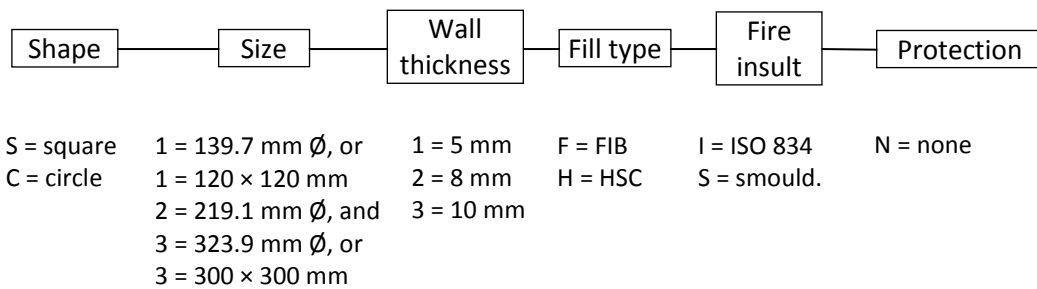


Fig. 7.1 Details of six-character naming and identification scheme for the columns tested herein

All specimens were heated for 120 minutes. Two thermal regimes were selected, the ISO 834 (ISO, 1999) standard fire and the slow heating smouldering curve (*Smould.*) (CEN, 2009). These two heating regimes were selected to advance understanding of the heat transfer in a cross-section under different heating rates. Temperature readings were taken at two heights ($L/3$ and $2L/3$) At each height; four thermocouples at each height measuring steel temperatures (denoted “St”); four thermocouples measured the temperature as close as possible to the steel-concrete boundary (denoted “CF”, approximately 2.5 mm from the steel); two thermocouples measured temperatures within the concrete 35 mm from the steel concrete boundary (denoted “35 mm”); and one thermocouple measures the concrete temperature at the centre of the cross-section (denoted “CC”). No load was applied during heating or cooling.

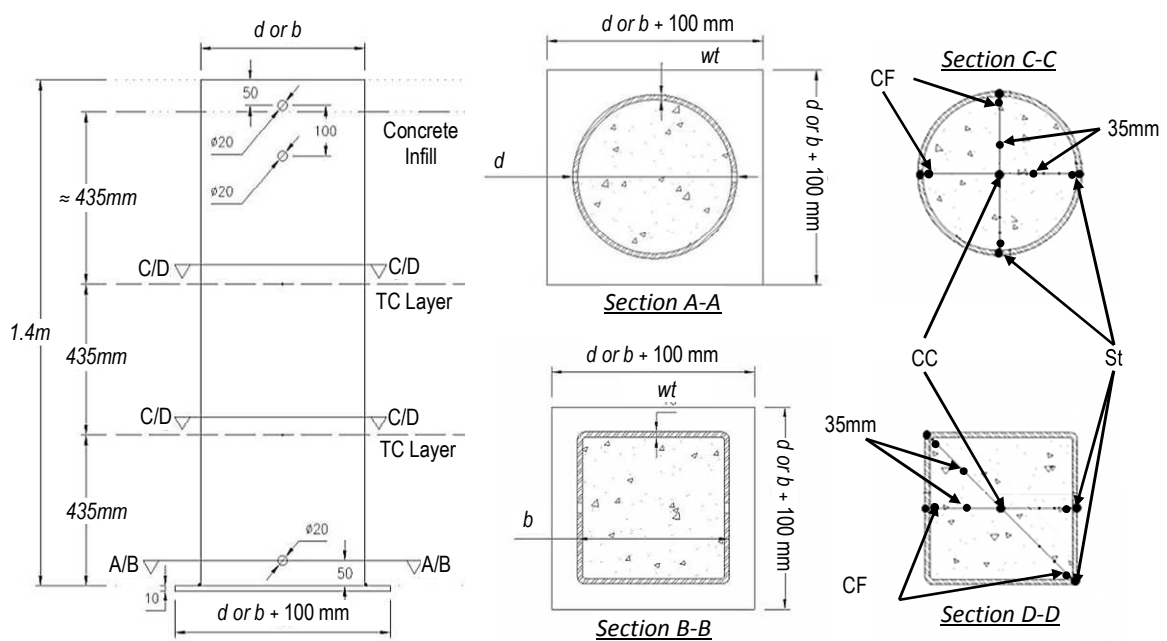


Fig. 7.2 Plan, elevation and sections of thermal test sections

7.1.1 Results of thermal tests

Selected temperatures recorded during the two hours of heating are given in Tab. 7.1. For the circular sections, single temperatures are given at each thermocouple layer. For the square sections, temperatures are given in both the orthogonal and diagonal directions (highlighted grey), apart from at the centre of the cross-section thermocouple (CC) where only one thermocouple can exist. The positions of the thermocouples are within ± 2.5 mm of the desired location.

7.1.2 Temperature predictions in unprotected specimens

To ensure accurate predictions at each thermocouple location, a mesh convergence analysis was required. Fig. 7.3 shows the mesh diagram used for the mesh convergence analysis for circular sections. The two-dimensional (2-D) mesh employed small triangular elements near centre of element to converge at a point and is divided into 4 element regions; region D represents the steel tube; region C represents the initial 5 mm of concrete; region B represents the subsequent 30 mm of concrete; and region A the remaining concrete core to the centre of the cross-section, which in this analysis is approximately 35 mm in radius.

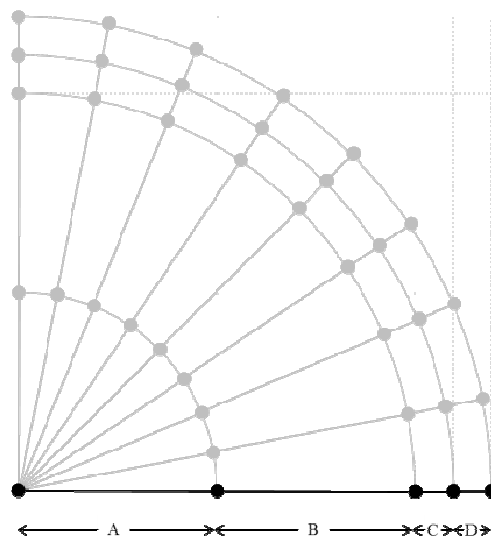


Fig. 7.3 Mesh region diagram for thermal predictions

The numbers of elements in each region (A, B, C, or D in Figure 4) were varied so as to produce a difference in predicted temperatures of less than 5°C within ABAQUS, with plain heat transfer elements (DC2D4) adopted in the finite element analysis. Tab. 7.2 shows the results of the mesh convergence analysis reporting temperatures at selected locations within the cross-section at specific time intervals, using the *Combi EC4c* thermal modelling approach (outlined below).

The *Combi EC4c* modelling approach assumes:

1. the emissivity of the fire is 1.0; convection coefficient is $25\text{W/m}^2\text{C}$ (CEN, 2009);
2. the emissivity of the steel is 0.7, (CEN, 2005);
3. EC4 (CEN, 2005) specified temperature dependant values for thermal conductivity (lower limit), λ , and heat capacity, c , (including 10% moisture content as permissible in EC4); and
4. perfect contact at the steel tube-concrete core interface, (CEN, 2005).

7.2 DEVELOPMENT OF A THERMAL MODELLING APPROACH

Tab. 7.2 shows that a good level of convergence can be obtained when using 9/8/4/4 elements in the regions A/B/C/D, respectively. This mesh density was therefore used in all subsequent 2-D predictions for the square (same mesh density as shown in Fig. 7.3) and circular (i.e. x1xxxN) sections; an additional eight elements were used between regions A and B for C2xxxN and x3xxxN sections to account for the additional size these sections.

Using the meshes outlined above, a thermal modelling approach, *Combi γ* , for prediction of temperatures within unprotected CFS sections, was developed in (Rush, 2013) to take into account the variable thermal and mechanical interactions and properties that are present within CFS sections. *Combi γ* used the recorded furnace temperatures, to predict temperatures with the CFS sections. The recorded furnace temperatures were applied to the cross-section via a series of elements outside of the steel which simulates the furnace environment. A GAPCON.f sub-routine was used to analyse the heat transfer from the furnace elements to the steel, and a heat transfer through the cross-section was conducted.

The *Combi γ* thermal modelling approach assumes:

1. the emissivity of the fire is 0.38 (calibrated to fire tests); convection coefficient is $25\text{W/m}^2\text{C}$, (CEN, 2009);
2. temperature dependant emissivity from Papoloski and Liedquist (Paloposki, 2005);
3. temperature dependant values for thermal conductivity (EC4 upper limit (CEN, 2005)), λ , and heat capacity, c with a new concrete specific heat capacity model (A-11) ; and
4. The gap conductance between the steel tube and concrete core is assumed as suggested by Ghojel (Ghojel, 2004).

Tab. 7.1 Specimen details and average temperatures at thermocouple locations after 30, 60 and 120 minutes of heating

| Test no. ^a | Specimen details | | | | | | Temperatures (°C) ^e | | | | | | | | | | | |
|-----------------------|--------------------|--------------------------|---------------------|-----------------------|-------------------|-------------------|--------------------------------|-----|------|------------|-----|-----|-------------|-----|------|-----|------|-----|
| | Shape ^b | Size (b and h OR d) (mm) | Wall thickness (mm) | Length of column (mm) | Fill ^c | Fire ^d | 30 minutes | | | 60 minutes | | | 120 minutes | | | | | |
| | | | | | | | St | CF | 35mm | CC | St | CF | 35mm | CC | St | CF | 35mm | CC |
| C11FIN | C | 323.9 | 10 | 1000 | FIB | ISO 834 | 489 | 241 | 109 | 22 | 727 | 531 | 252 | 78 | 949 | 828 | 412 | 121 |
| C12FIN | C | 323.9 | 8 | 1000 | FIB | ISO 834 | 479 | 250 | 101 | 22 | 709 | 534 | 224 | 57 | 931 | 828 | 380 | 119 |
| C21FIN | C | 219.1 | 10 | 1400 | FIB | ISO 834 | 513 | 272 | 120 | 48 | 765 | 562 | 269 | 130 | 981 | 869 | 452 | 193 |
| C22FIN | C | 219.1 | 8 | 1400 | FIB | ISO 834 | 503 | 285 | 131 | 47 | 748 | 587 | 296 | 130 | 971 | 885 | 487 | 180 |
| C23FIN | C | 219.1 | 5 | 1400 | FIB | ISO 834 | 531 | 323 | 141 | 50 | 753 | 600 | 307 | 126 | 973 | 892 | 482 | 178 |
| C31FIN | C | 139.7 | 10 | 1400 | FIB | ISO 834 | 554 | 444 | 283 | 145 | 825 | 783 | 591 | 412 | 1005 | 995 | 807 | 684 |
| C32FIN | C | 139.7 | 8 | 1400 | FIB | ISO 834 | 529 | 394 | 179 | 116 | 800 | 738 | 543 | 389 | 991 | 977 | 792 | 737 |
| C33FIN | C | 139.7 | 5 | 1400 | FIB | ISO 834 | 532 | 371 | 136 | 123 | 799 | 691 | 384 | 286 | 997 | 954 | 647 | 564 |
| C33HIN | C | 139.7 | 5 | 1400 | HSC | ISO 834 | 553 | 380 | 157 | 138 | 806 | 698 | 408 | 313 | 996 | 952 | 651 | 574 |
| C33FSN | C | 139.7 | 5 | 1400 | FIB | Smould. | 320 | 187 | 86 | 66 | 712 | 583 | 255 | 146 | 980 | 935 | 543 | 448 |
| S11FIN | S | 300 | 10 | 1000 | FIB | ISO 834 | 506 | 218 | 95 | 21 | 759 | 507 | 215 | 63 | 966 | 782 | 346 | 116 |
| S21FIN | S | 120 | 10 | 1400 | FIB | ISO 834 | 506 | 291 | 139 | 145 | 760 | 644 | 354 | 400 | 975 | 928 | 556 | 698 |
| S23FIN | S | 120 | 5 | 1400 | FIB | ISO 834 | 458 | 320 | 155 | 139 | 768 | 687 | 435 | 354 | 987 | 961 | 719 | 556 |
| S23FSN | S | 120 | 5 | 1400 | FIB | Smould. | 479 | 356 | 169 | 78 | 785 | 722 | 468 | 192 | 995 | 977 | 741 | 529 |
| | | | | | | | 465 | 317 | 147 | 139 | 757 | 649 | 384 | 354 | 974 | 932 | 653 | 556 |
| | | | | | | | 513 | 305 | 161 | 78 | 792 | 641 | 445 | 192 | 984 | 928 | 696 | 529 |
| | | | | | | | 296 | 175 | 90 | 78 | 725 | 559 | 247 | 192 | 990 | 935 | 569 | 529 |
| | | | | | | | 260 | 206 | 94 | 78 | 714 | 661 | 268 | 192 | 987 | 978 | 592 | 529 |

^a test numbering system *Shape* – size – wall thickness- fill type – fire insult – protection type;

^b C = circle, S = square;

^c HSC = high strength concrete, FIB = fibre reinforced concrete; and

^d ISO 834 = standard fire insult, Smould = slow heating curve

^e averaged temperatures at each thermocouple layer (i.e. St=steel, CF=concrete face, 35mm= 35 mm depth, CC= concrete centre)

Tab. 7.2 Temperature results of the mesh convergence analysis at various locations and instances in time

| | No. of elements A/B/C/D | Time (min) | | | | |
|-------------------------|----------------------------|------------|-------|-------|-------|--------|
| | | 10 | 20 | 30 | 60 | 120 |
| Steel (°C) | 3/1/1/1 | 294.4 | 585.9 | 727.7 | 912.3 | 1039.1 |
| | 4/2/2/2 | 310.6 | 595.1 | 727.9 | 910.7 | 1038.7 |
| | 9/4/4/4 | 327.3 | 596.6 | 728.1 | 910.3 | 1038.6 |
| | 16/8/4/4 | 330.3 | 597.3 | 728.1 | 910.2 | 1038.6 |
| | 9/8/4/4 | 331.6 | 597.8 | 728.2 | 910.2 | 1038.6 |
| Concrete 5 mm (°C) | 3/1/1/1 | 147.2 | 446.6 | 603.6 | 835.0 | 1007.2 |
| | 4/2/2/2 | 183.5 | 449.0 | 604.3 | 829.6 | 1005.4 |
| | 9/4/4/4 | 216.6 | 454.8 | 603.9 | 828.2 | 1005.0 |
| | 16/8/4/4 | 213.7 | 455.9 | 603.5 | 827.8 | 1004.9 |
| | 9/8/4/4 | 215.3 | 456.7 | 603.7 | 827.9 | 1005.0 |
| Concrete centre (°C) | 3/1/1/1 | 34.7 | 84.4 | 110.1 | 373.3 | 780.5 |
| | 4/2/2/2 | 30.9 | 74.4 | 104.9 | 372.5 | 780.7 |
| | 9/4/4/4 | 29.1 | 70.5 | 102.5 | 373.0 | 780.8 |
| | 16/8/4/4 | 28.9 | 69.5 | 102.0 | 372.7 | 781.0 |
| | 9/8/4/4 | 29.4 | 69.9 | 102.2 | 373.2 | 781.3 |

Tab. 7.3 shows that in general the errors are less than 20°C and follow the observed trends from experiments as shown in Fig. 7.4. Similar accuracy in temperature predictions is found for all the specimens.

Whilst the predicted temperatures using the *Combi* γ modelling approach shows good agreement with the observed test data, an area of concern is the appropriate modelling of heat transfer to CFS sections from the furnace. In order to calibrate the predicted temperatures to those observed in the thermal tests, an emissivity of the furnace ($\epsilon_{m,fi}$) of 0.38 was required, which may be only appropriate for the specific floor furnace in which the specimens were tested and may not be realistic of other furnaces. Large scale loaded furnace tests conducted and modelled by the NRCC (e.g. Lie, 1992a), quote emissivities of the furnaces used as 0.75; twice that required in the *Combi* γ modelling approach.

Tab. 7.3 Predicted temperatures and errors of predictions of unprotected tests at 60 and 120 minutes, using *Combi γ* modelling approach with applied furnace temperatures, at the St, CF and CC thermocouple locations.

| Test | 60 minutes | | | | | | 120 minutes | | | | | |
|---------|------------|------|-------|------|-------|------|-------------|------|-------|------|-------|------|
| | St | | CF | | CC | | St | | CF | | CC | |
| | Pred. | Err. | Pred. | Err. | Pred. | Err. | Pred. | Err. | Pred. | Err. | Pred. | Err. |
| C11FIN | 708 | -19 | 523 | -8 | 54 | -24 | 958 | 9 | 829 | 1 | 133 | 1 |
| C12FIN | 724 | 15 | 544 | 10 | 54 | -3 | 962 | 31 | 836 | 8 | 133 | -1 |
| C21FIN | 723 | -42 | 554 | -8 | 125 | -5 | 980 | -1 | 874 | 5 | 364 | -13 |
| C22FIN | 733 | -15 | 571 | -16 | 125 | -5 | 984 | 13 | 879 | -6 | 361 | 31 |
| C23FIN | 757 | 4 | 596 | -4 | 126 | 0 | 988 | 15 | 886 | -6 | 357 | 26 |
| C31FIN | 740 | -85 | 613 | -170 | 301 | -111 | 1012 | 7 | 956 | -39 | 734 | -110 |
| C32FIN | 758 | -42 | 628 | -110 | 301 | -88 | 1013 | 22 | 957 | -20 | 726 | -156 |
| C33FIN | 805 | 6 | 664 | -27 | 303 | 17 | 1014 | 17 | 958 | 4 | 715 | -41 |
| C33FHIN | 805 | -1 | 664 | -34 | 303 | -10 | 1014 | 18 | 958 | 6 | 715 | -39 |
| C33FSN | 679 | -33 | 509 | -74 | 160 | 14 | 976 | -4 | 904 | -31 | 627 | -56 |
| S11FIN | 707 | -27 | 484 | -23 | 53 | -10 | 951 | 1 | 776 | -6 | 132 | -7 |
| | 749 | -36 | 677 | 33 | | | 996 | 5 | 959 | 31 | | |
| S21FIN | 755 | -13 | 604 | -83 | 369 | -31 | 1018 | 31 | 951 | -10 | 791 | -74 |
| | 779 | -6 | 712 | -10 | | | 1024 | 29 | 1001 | 24 | | |
| S23FIN | 826 | 69 | 653 | 4 | 363 | 9 | 1019 | 45 | 950 | 18 | 765 | 66 |
| | 851 | 59 | 781 | 140 | | | 1028 | 44 | 1006 | 78 | | |
| S23FSN | 687 | -38 | 481 | -78 | 176 | -16 | 981 | -9 | 894 | -41 | 678 | -88 |
| | 712 | -2 | 622 | -39 | | | 992 | 5 | 964 | -14 | | |

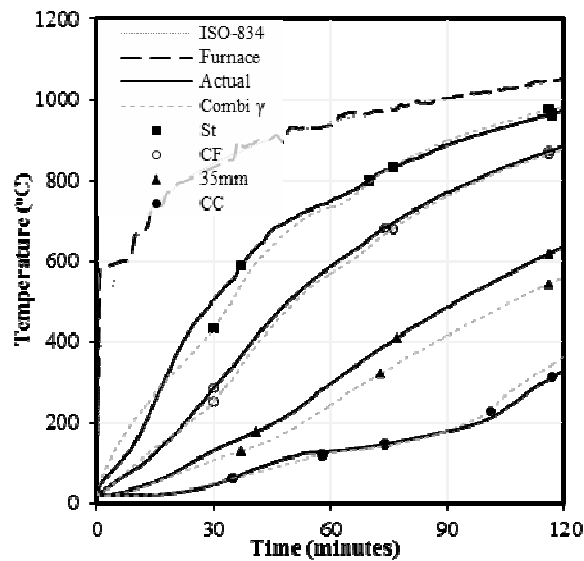


Fig. 7.4 Representative thermal profile (C22FIN) and predictions of temperatures using the *Combi γ* thermal modelling approaches

7.3 META-ANALYSIS OF FOUR EXEMPLAR COLUMNS

The meta-analysis of four example full scale structural furnace test columns is to assess whether the thermal modelling approach developed from the thermal tests can be used to predict the failure of CFS columns in fire. The thermal modelling for the cross-sections uses the same material and interaction properties as used in Combi {gamma} but with the fire emissivity set to 0.75 as calibrated by the NRCC and appropriate to be used with column furnace tests. The modified thermal modelling approach is designated *Combi alpha*. Tab. 7.4 shows the details of the four example columns to be assessed.

Tab. 7.4 Details of example columns assessed and observed fire resistance from furnace tests

| Example | [REF] | C/S | d or b | t _w | L | l _ϕ | f _y | E _s | Fill | f _{ck} | # bars x ϕ | Cover | As/Ac | Fixity | N _{fi, Rd} | N _{Rd} | N _{fi, Rd} / N _{Rd} | FR | Surface temp. |
|---------|-----------------|-----|--------|----------------|------|----------------|----------------|----------------|------|-----------------|---------------|-------|-------|--------|---------------------|-----------------|------------------------------------------|-----|---------------|
| | | | mm | mm | m | m | MPa | GPa | | MPa | mm | | | | mm | kN | kN | | mins |
| 1 | Lie, 1992b | C | 273.1 | 5.6 | 3.81 | 2 | 350 | 2.05 | PC | 28.6 | - | - | - | FF | 574 | 2243 | 0.26 | 112 | 960 |
| 2 | Lie, 1992b | C | 168.3 | 4.8 | 3.81 | 2 | 350 | 2.05 | PC | 35.5 | - | - | - | FF | 218 | 965 | 0.23 | 56 | 896 |
| 3 | Grandjean, 1981 | S | 350 | 10 | 3.6 | 2.52 | 326 | 2.05 | RC | 36.2 | 8x19 | 40 | 2.10% | FF | 4560 | 8520 | 0.54 | 51 | 749 |
| 4 | CIDECT, 1976 | S | 160 | 3.6 | 3.6 | 2.52 | 368 | 2.05 | RC | 40.1 | 4x12 | 27 | 2.00% | FF | 820 | 1720 | 0.48 | 25 | 670 |

C = circle, S = square; d = diameter, b = breadth; t_w = wall thickness; L = actual column length, l_ϕ = effective length; f_y = steel yield strength; E_s = young's modulus; PC = plain concrete, RC = reinforced concrete; f_{ck} = concrete strength; FF = fixed-fixed end conditions; N_{Rd} = ambient design strength; FR = fire resistance.

The four example columns to be assessed are from a large database presented in (Rush, 2013) and are applicable for assessment using the design approach in EC4 Annex H (CEN, 2005), which is a relatively simple calculation model.

The EC4 Annex H (CEN, 2005) approach represents a simplified sectional analysis technique which has two distinct steps: first, a temperature distribution over the cross-section is determined (using one of a number of applicable methods) for a given duration of fire exposure, and second, from this thermal analysis a calculation of the design axial buckling/crushing capacity of the column is made.

The heat transfer analysis was conducted again using ABAQUS finite element software to predict the temperature distribution for each example column at one-minute intervals. The input parameters to the analysis, apart from the cross-sectional dimensions, were the thermal properties and interactions of steel and concrete (thermal modelling approach *Combi alpha*), and the thermal insult (fire exposure). The thermal insults used in the vast majority of the tests were ISO 834 (ISO, 1999) standard fires (or similar) and was applied using the method adopted earlier, with a subroutine to assess the heat flux to the surface of the steel from an array of elements representing the furnace environment.

Once the temperature profile within the section at a given time of fire exposure has been established, the cross-section is discretized into elements in which the temperature is assumed to be uniform, and, using a simple spreadsheet analysis, relatively simple equations can be used to check that the design resistance of the column, $N_{fi,Rd}$, at the given time (and temperature profile) is greater than the design load in fire, $N_{fi,Sd}$.

The steel tube is assumed to have uniform temperature and the concrete cross-section is divided into ringed segments of equal thickness. This is shown schematically in Fig. 7.5, where six concrete layers have been chosen.

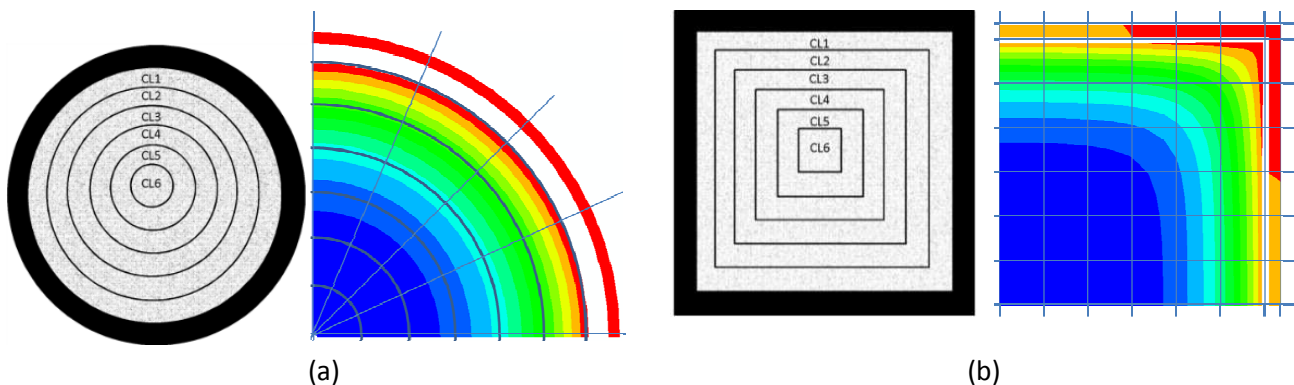


Fig. 7.5 (a) Circular and (b) square segmentation used in EC4 Annex H (CEN, 2005) analysis (CL_i = concrete layer *i*) and quarter section heat transfer analysis (steel separated for visual clarity)

Each of the concrete rings is assumed to have a uniform temperature at any given instant in time, based on heat transfer analysis. The determination of the midpoint temperature for the concrete layers in circular sections is straightforward due to axisymmetry. The situation in a square section is more complicated; in a square section the temperature at the corners is higher than at the middle of the flat faces. However precedence exists (Aribert, 2008) to assume an equivalent uniform temperature in each concrete layer in the square section, provided that the uniform temperature chosen for the layer leads to the same (or smaller) contribution to either the plastic resistance in compression or the cross-section's flexural stiffness as would a more complete summation of a 2D grid of concrete elements. A heat transfer analysis was therefore performed (again using ABAQUS) and showed that the average temperature for the layer provides an accurate estimate for the load capacity analysis. Thus a full two dimensional discretization of square sections was not required.

The temperatures of the reinforcing steel within the cross section were taken to be the same as the temperature of the concrete layer in which it resides. A thermal model was also developed to assess whether the reinforcement has an effect on the temperature profile within a CFS section, and it was found not to have an effect on the concrete layer temperatures.

After the temperature of each layer was determined, the layer mechanical properties were found by interpolation of tables 3.1 through 3.4 of EC4 (CEN, 2005), and these properties were then applied within equations 1 to 4 to determine the design resistance of the column, $N_{fi,Rd}$, and thus the columns fire resistance, using a simple spreadsheet analysis.

The design resistance of the column, $N_{fi,Rd}$, is determined from the design axial buckling load of the column during fire. This is found by assuming that all materials experience the same strain at a given time and temperature and then calculating the strain at which the elastic critical or Euler buckling load, $N_{fi,cr}$, is equal to the plastic (crushing) resistance to compression of the cross section, $N_{fi,pl,Rd}$ (CEN, 2005):

$$N_{fi,Rd} = N_{fi,cr} = N_{fi,pl,Rd} \quad (1)$$

$N_{fi,cr}$ is the summation of the elastic flexural rigidities of the steel tube (subscript a), the concrete (subscript c), and any internal steel reinforcement (subscript s):

$$N_{fi,cr} = \pi^2 [E_{a,\theta,\sigma} I_a + E_{c,\theta,\sigma} I_c + E_{s,\theta,\sigma} I_s] / l_\theta^2 \quad (2)$$

The true levels of fixity, and therefore effective lengths of the columns (l_θ), are difficult to determine with different heated lengths of specimens (e.g. Kodur, 1999) and various methods of creating the idealised end-conditions. The effective lengths that are employed in Equation 2 are, where available, those quoted in the respective test reports; otherwise the design values imposed by the codes (CEN, 2005) are used.

$N_{fi,pl,Rd}$ is the summation of the crushing strength contributions of the respective materials:

$$N_{fi,pl,Rd} = (A_a \sigma_{a,\theta} / \gamma_{M,fi,a}) + (A_c \sigma_{c,\theta} / \gamma_{M,fi,c}) + (A_s \sigma_{s,\theta} / \gamma_{M,fi,s}) \quad (3)$$

In the above equations, l_θ is the buckling length in the fire situation, $E_{i,\vartheta,\sigma}$ is the tangent modulus of the stress-strain relationship for the material i at temperature ϑ and for a stress $\sigma_{i,\vartheta}$, I_i is the second moment of area the material i , and A_i is the cross-sectional area of material i . The above parameters are calculated as the summation of the contributions from all of the respective elements in the column's cross-section at a given instant of fire exposure. In this study the values of $\gamma_{M,fi,i}$ are assumed to be 1.0.

Tab. 7.5 Example columns selected temperatures from heat transfer analysis and calculated fire resistances, steel tube failure temperature and strain

| Combi α | | | | | | | | | | | |
|-------------------------------------------------------------------|--------------|--------|-------|---------|----------|-------------------------------------------------------------------|--------------|--------|-------|--------|---------|
| Temperatures | | | | | | | | | | | |
| Column | Time | St | CL1 | CL3 | CL6 | Column | Time | St | CL1 | CL3 | CL6 |
| Example column 1 – 273.1 x 5.56 mm Ø (Actual FR = 112 mins) | 0 | 20.0 | 20.0 | 20.0 | 20.0 | Example column 3 – 350 x 350 x 10 mm (Actual FR = 51 mins) | 0 | 20.0 | 20.0 | 20.0 | 20.0 |
| | 10 | 256.4 | 82.1 | 25.6 | 20.2 | | 10 | 200.7 | 59.7 | 21.6 | 20.0 |
| | 20 | 404.8 | 154.4 | 47.6 | 23.0 | | 20 | 337.7 | 119.9 | 30.5 | 20.3 |
| | 30 | 628.8 | 286.2 | 79.1 | 32.5 | | 30 | 508.1 | 203.2 | 46.6 | 21.6 |
| | 60 | 857.6 | 555.6 | 179.3 | 95.0 | | 60 | 819.3 | 473.8 | 115.4 | 40.4 |
| | 90 | 954.6 | 703.2 | 302.1 | 141.6 | | 90 | 945.8 | 649.3 | 185.0 | 79.1 |
| | 120 | 1012.8 | 798.2 | 421.2 | 199.3 | | 120 | 1007.0 | 747.1 | 269.1 | 119.1 |
| | Predicted FR | | | | 117 mins | | Predicted FR | | | | 45 mins |
| Pred. Steel Temp | | | | 1008 °C | | Pred. Steel Temp | | | | 726 °C | |
| Strain | | | | 4.6 µε | | Strain | | | | 1.9 µε | |
| Example column 2 – 168.3 x 4.78 mm Ø (Actual FR = 56 mins) | 0 | 20.0 | 20.0 | 20.0 | 20.0 | Example column 4 – 160 x 160 x 3.6 mm (Actual FR = 25 mins) | 0 | 20.0 | 20.0 | 20.0 | 20.0 |
| | 10 | 276.0 | 104.8 | 42.2 | 24.2 | | 10 | 298.5 | 115.2 | 44.2 | 23.6 |
| | 20 | 458.0 | 203.7 | 94.5 | 52.2 | | 20 | 517.2 | 234.3 | 97.4 | 48.6 |
| | 30 | 661.4 | 363.8 | 148.7 | 95.6 | | 30 | 686.9 | 400.8 | 153.1 | 89.7 |
| | 60 | 877.1 | 663.1 | 384.0 | 205.7 | | 60 | 885.5 | 684.8 | 385.6 | 189.9 |
| | 90 | 969.9 | 820.8 | 590.9 | 460.8 | | 90 | 973.2 | 831.3 | 581.1 | 427.2 |
| | 120 | 1026.7 | 919.3 | 734.5 | 621.0 | | 120 | 1028.4 | 924.8 | 721.5 | 586.5 |
| | Predicted FR | | | | 55 mins | | Predicted FR | | | | 29 mins |
| Pred. Steel Temp | | | | 854 °C | | Pred. Steel Temp | | | | 676 °C | |
| Strain | | | | 2.2 µε | | Strain | | | | 2.3 µε | |

7.4 SUMMARY

The chapter summarises the benchmark modelling study for concrete filled structural hollow sections and has assessed the input material properties and the steel-furnace interface models possible to calculate the heat transfer through CFS sections. The ability to predict the thermal profile within CFS columns exposed was compared to 14 unprotected thermal tests conducted on CFS sections. The thermal modelling approaches were also used in the assessment of the EC4 Annex H simple calculation method for CFS columns, by comparing the predicted fire resistance of four example columns to the actual fire resistances observed in tests.

Acknowledgement

The author would like to thank acknowledge the support of Arup (Fire Engineering), The Ove Arup Foundation, The Royal Academy of Engineering, and the Engineering and Physical Sciences Research

Council. The authors gratefully acknowledge the support of the School of Engineering at the University of Edinburgh, which is part of the Edinburgh Research Partnership in Engineering.

References

- Rush, 2013: Rush D., Fire performance of unprotected and protected concrete filled structural hollow sections, University of Edinburgh, 2013.
- CEN, 2005: CEN, BS EN 1994-1-2: Eurocode 4: Design of composite steel and concrete structures; Part 1-2: Structural Fire Design, Brussels, Belgium, 2005.
- ISO, 1999: ISO 834: Fire resistance tests-elements of building construction, Geneva, Switzerland, 1999.
- CEN, 2009: CEN, BS EN 1991-1-2: Eurocode 1: Actions on structures; Part 1-2: General Actions - Actions on structures exposed to fire, Brussels, Belgium, 2009.
- Paloposki, 2005: Paloposki T., Liedquist L., Steel emissivity at high temperatures - Research notes. Tampere, Finland: Technical Research Centre of Finland, 2005.
- Ghojel, 2004: Ghojel J., Experimental and analytical technique for estimating interface thermal conductance in composite structural elements under simulated fire conditions, *Experimental Thermal and Fluid Science*, vol. 28, no. 4, pp. 347–354, Mar. 2004.
- Lie, 1992a: Lie T. T., Chabot M., Irwin R. J., Fire resistance of circular hollow steel sections filled with bar-reinforced concrete - *Internal Report No. 636*. Ottawa, Canada: National Research Council Canada, 1992.
- Lie, 1992b: Lie T. T., Chabot M., Experimental studies on the fire resistance of hollow steel columns filled with plain concrete - *Internal Report No. 611*, National Research Council Canada, Ottawa, Canada, 1992.
- Grandjean, 1981: Grandjean G., Grimault J. P., Petit L., CIDECT 15B Part 1 - Determination de la duree au feu des profils creux remplis de beton, CIDECT, Paris, France, 1981.
- CIDECT, 1976: CIDECT, Fire resistance of structural hollow sections: Final Report - CIDECT Programme 15 A, Croydon, UK, 1976.
- Aribert, 2008: Aribert J. M., Renaud C., Zhao B., Simplified fire design for composite hollow-section columns, in *Proceedings Of The Institution Of Civil Engineers - Structures and Buildings*, 2008, vol. 161,6, no. December, pp. 325–336.
- Kodur, 1999: Kodur V., Performance-based fire resistance design of concrete-filled steel columns, *Journal of Constructional Steel Research*, vol. 51, no. 1, pp. 21–36, 1999.

WG2- Meri Cvetkovska, cvetkovska@gf.ukim.edu.mk

WG2- Ljupco Lazarov, lazarov@gf.ukim.edu.mk

WG2- Milica Jovanoska, m.jovanoska@hotmail.com

Milivoje Milanovic, pbarhisnp@gmail.com

8 NUMERICAL AND EXPERIMENTAL ANALYSIS OF RC COLUMNS EXPOSED TO FIRE

Summary

In 1987 a test program was conducted by the Portland Cement Association (PCA) and the National Research Council of Canada (NRCC) to determine the fire resistance of centrally and eccentrically loaded reinforced concrete columns. The results from the experimental investigation were published by T.D. Lin, R.I. Zwierny, R.G. Burg, T.T. Lie & R.J. McGrath in 1992.

The results from this investigation were used as benchmark example for validation the finite element program FIRE (homemade program). The experimental and numerical results for the thermal and mechanical responses are compared and presented in this paper and the influences of different parameters are discussed. In same time all results from the program FIRE are compared with the corresponding one from the program SAFIR.

8.1 INTRODUCTION

Today, as a result of many years of investigations, there are three basic methods for determination of fire resistance of structural elements and their assemblies. The oldest method is the performance of a fire test of loaded elements, in compliance with the national regulations and standards, or comparison of the elements with the results from already performed tests on similar or identical elements. The second method implies the use of empirical formulae that are based on the results from performed fire tests and holds for a certain combination of: structure, material and protective coating. Lately, the latter method has more frequently been in use due to the high cost of the fire test. The third method represents an analytically elaborated approach to design elements with a predefined fire resistance and it is based on the principles of Structural Mechanics and Theory of Heat Transfer. This method enables obtaining of the structural response under conditions of fire, which opens a new prospective for more extensive investigations in this field.

To define the fire resistance of structures as assemblies of structural elements, experimental investigations of models are almost impossible. The time dimension of spreading of the temperature field is practically impossible to be simulated on a model of small proportions. Hence, model investigations can hardly be accepted due to the high cost. For the last twenty years, particular importance has therefore been given to analytical definition of the problem. Generally, analytical computation of the whole structure for the case of fire means proof that the structure, or its elements, loaded by a defined load and exposed to thermal effect, satisfies certain functional requirements, expressed through the ultimate state of bearing capacity and usability.

This paper presents experimental results for the fire resistance of different types of RC columns and these data were used as a benchmark example for validation the finite element program FIRE (homemade program). The experimental and numerical results for the thermal and mechanical responses are presented and compared with the corresponding results from the program SAFIR.

8.2 FIRE RESISTANCE OF RC COLUMNS

8.2.1 Experimental investigation of fire resistance of RC columns

In 1987 a test program was conducted by the Portland Cement Association (PCA) and the National Research Council of Canada (NRCC) to determine the fire resistance of centrally and eccentrically loaded reinforced concrete columns (Lin, 1992). Columns were 3.8m long, and had 38mm concrete cover to the tie bars (Fig. 8.1). They were fabricated with either siliceous or carbonate aggregate concrete. The specified yield strength of the reinforcement was 400 Mpa (deformed bars). The columns were exposed to the standard fire ASTM E119 from all sides. Basic characteristics of the centrally loaded columns are listed in Table 8.1, and for the eccentrically loaded columns in Table 8.2.

For comparative purposes, test loads N were divided by the maximum factored axial load allowed by ACI 318, $N_d = \Phi N_n$, and the load/strength ratio α' was defined as: $\alpha' = N / N_d$. For columns reinforced with tie reinforcement the equation for N_d is:

$$N_d = \Phi N_n = 0.8\Phi \left[0.85 f'_c (A_g - A_s) + f_y A_s \right]$$

In the above equation f'_c is the strength of the concrete, f_y is the specified yield strength of the reinforcement, A_g is the gross area of the section, A_s is the area of the reinforcement, Φ is the strength reduction factor which is equal to 0.7, for members with tie reinforcement, and to 0.75, for members with spiral reinforcement.

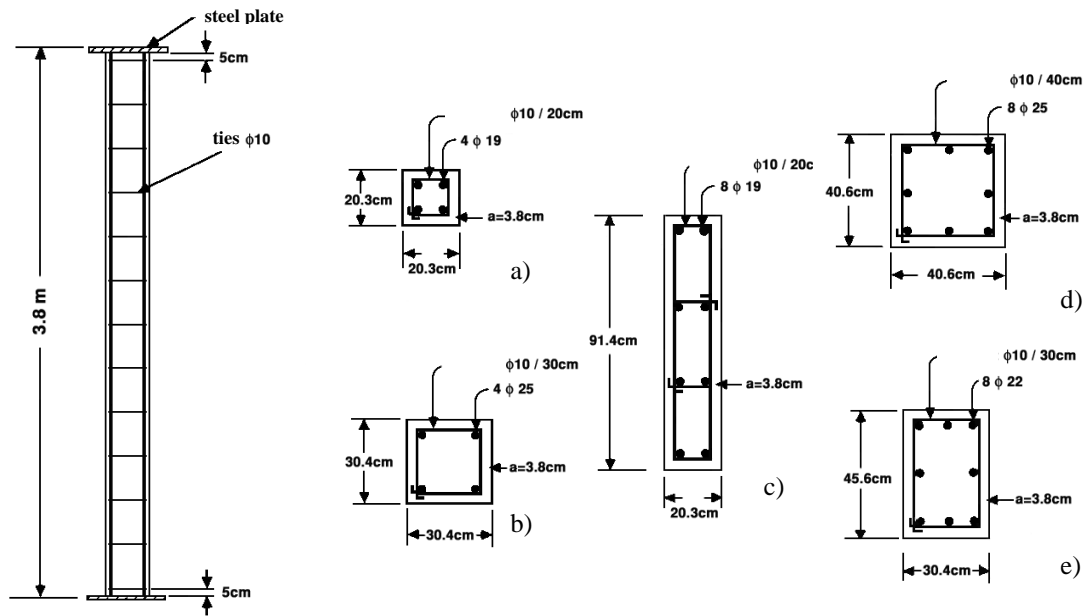


Fig. 8.1 Cross-sectional geometry and reinforcement details for the column specimens

8.2.2 Numerical analysis of RC columns-programs FIRE and SAFIR

The fire resistance of the columns was predicted by the computer programs FIRE (homemade program) and commercial program SAFIR. When program FIRE was used the columns were discretised by three elements and each element was further discretised by five subelements. Because of the symmetry of the cross sections and the symmetry of the fire load, only one half of the column was analyzed. The cross section was discretised by isoparametric 4 node rectangular elements (subslices). For the surface layers a finer discrete mesh was adopted because of the high temperature gradient ($\Delta x = 1.9\text{cm}$), while for the inner layers the size of the subslices was $2.5 \leq \Delta x \leq 3.5\text{cm}$. The time step was $\Delta t = 0.025h$ and it was adopted to the size of the subslices according to equation:

$$\Delta t \leq \frac{c_{min} \rho_{min}}{4 \lambda_{max}} \Delta x^2$$

8.2.2.1 Material model

A stress-strain law for concrete under uniaxial loading, used in the program FIRE consists of two parts: a compressive part and a tensile part. The stress-strain curve in compression (Fig. 8.2) consists of ascending and descending branch. The ascending branch is defined by Equation (8.1), recommended by Popovic (Fig. 8.3) and the descending branch is assumed to be linear. Parameters that completely define this curve are temperature dependant and for various temperature intervals they were given in ENV 2-1-2:1995.

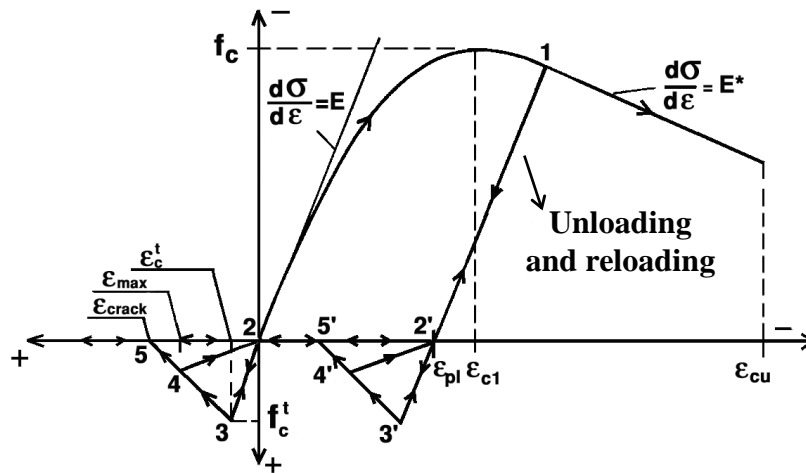


Fig. 8.2 Stress-strain law for concrete subslice

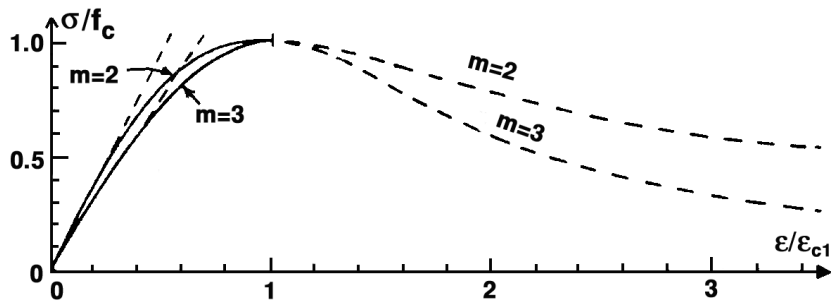


Fig. 8.3 "σ - ε" curve by Popovic

$$\frac{\sigma_c}{f_c} = \frac{\epsilon_c}{\epsilon_{c1}} \cdot \frac{m}{m-1 + (\epsilon_c / \epsilon_{c1})^m} \quad \text{for } \epsilon_c \leq \epsilon_{c1} \quad (8.1)$$

Where:

f_c is the compressive strength of the concrete and it's value decrease with temperature

ϵ_{c1} is the strain at compressive strength and it's value increase with temperature

ϵ_{cu} is the ultimate crushing strain and it's value increase with temperature

m is empirical coefficient ($m=2$ or 3 , which applies to lower or higher strength concretes)

Figure 8.4 represents the stress-strain law for steel in the phase of loading and unloading. This model is used in the computer modulus FIRE-S for structural analysis, while the temperature in the steel subslice is changed from t_1 (lower) to t_2 (higher value).

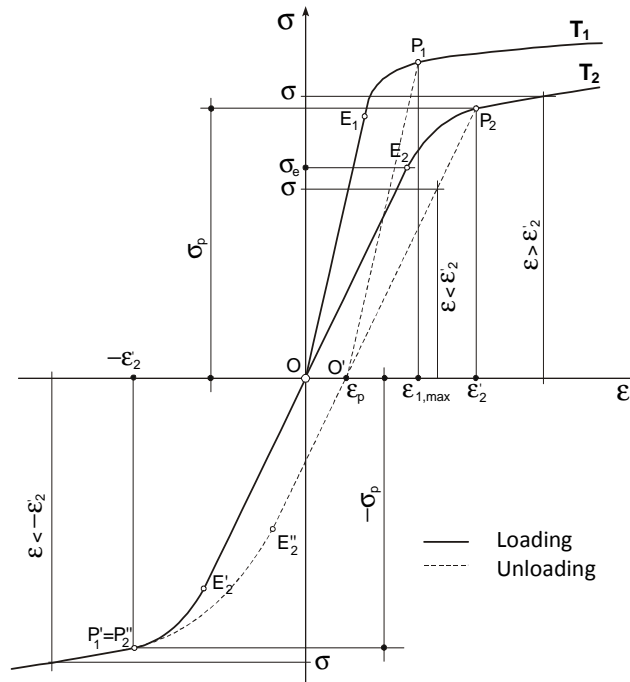


Fig. 8.4 Stress-strain law for steel subslice

The parameters that define the stress-strain curve for the steel used in the computer program FIRE, are according to ENV 2-1-2:1995, and in SAFIR according to EN 2-1-2:2004.

8.2.2.2 Mechanical and thermal properties properties

No data existed for the temperature dependent thermal and mechanical properties of concrete and steel, so in program FIRE they were taken as it was recommended by ENV 1992-1-2:1995 and in SAFIR according to the new revised version of EN 1992-1-2: 2004. The differences between the ENV and EN are the main reasons for the deferences in the results obtained with these two different programs, specially in case when columns are made of carbonate agregate concrete.

8.3 Comparison of the experimental and numerical results for the fire resistance of RC columns

Tab. 8.1 Test data for centricly loaded columns

| Column No. | Concrete strength (Mpa) | Concrete relative humidity, % | Test load (KN) | load/strength ratio α | Test duration Hr : min. | Predicted fire resist. (FIRE) | Deviation FIRE/experim | Predicted fire resist. (SAFIR) | Deviation SAFIR/exper. in % | Deviation SAFIR/FIRE in % |
|---------------------------------------------------------------------------------------|-------------------------|-------------------------------|----------------|------------------------------|-------------------------|-------------------------------|------------------------|--------------------------------|-----------------------------|---------------------------|
| Cross section: 304×304mm, steel: 2.19% (4φ25), siliceous aggregate (Figure 1b) | | | | | | | | | | |
| S1 | 34.1 | 65 | 0 | 0.00 | 4:00 | 6:00 | / | / | / | / |

| | | | | | | | | | | |
|---------------------------------------------------------------------------------------|------|----|------|------|------|-------|-------|------|-------|-------|
| S13 | 40.3 | 63 | 340 | 0.15 | 5:40 | 5:45 | +1.5 | 5:52 | +3.5 | +2 |
| S4 | 35.0 | 60 | 710 | 0.36 | 3:40 | 4:00 | +9.1 | 4:03 | +10.4 | +1.3 |
| S25 | 39.6 | 75 | 800 | 0.37 | 4:02 | 4:00 | -0.8 | 4:00 | -0.8 | 0 |
| S17 | 50.3 | 70 | 1070 | 0.41 | 3:54 | 3:51 | -1.3 | 3:50 | -1.7 | -0.4 |
| S3 | 34.0 | 75 | 800 | 0.41 | 3:38 | 3:42 | +1.8 | 3:43 | +2.2 | +0.4 |
| S16 | 52.9 | / | 1180 | 0.43 | 3:47 | 3:45 | -0.9 | 3:42 | -2.2 | -1.3 |
| S31 | 41.5 | 67 | 1024 | 0.45 | 3:41 | 3:36 | -2.3 | 3:32 | -4.0 | -1.7 |
| S26 | 39.3 | 74 | 1000 | 0.46 | 3:40 | 3:30 | -4.5 | 3:38 | -0.9 | +3.6 |
| S7 | 36.0 | / | 1070 | 0.53 | 3:28 | 3:12 | -7.7 | 3:17 | -5.2 | +2.5 |
| S9 | 38.3 | 15 | 1335 | 0.63 | 3:07 | 2:51 | -8.6 | 2:54 | -6.9 | +1.7 |
| S2 | 36.8 | / | 1335 | 0.65 | 2:50 | 2:43 | -4.1 | 2:42 | -4.7 | -0.6 |
| S8 | 34.8 | | 1780 | 0.90 | 2:26 | 1:57 | -19.8 | 2:01 | -17.1 | +2.7 |
| Cross section: 304×304mm, steel: 2.19% (4φ25), carbonate aggregate (Figure 1b) | | | | | | | | | | |
| S10 | 40.8 | 75 | 800 | 0.36 | 8:30 | 5:00 | -41.2 | 5:11 | -39.0 | +2.2 |
| S11 | 36.8 | 75 | 1070 | 0.52 | 6:06 | 4:06 | -32.8 | 4:32 | -25.7 | +7.1 |
| S12 | 40.0 | | 1780 | 0.81 | 3:35 | 3:00 | -16.3 | 3:39 | +1.9 | +18.2 |
| Cross section: 304×304mm, steel: 4.38% (8φ25), siliceous aggregate | | | | | | | | | | |
| S20 | 42.5 | 80 | 980 | 0.36 | 4:12 | 3:54 | -7.0 | 3:56 | -6.3 | +0.7 |
| S21 | 37.0 | | 1335 | 0.53 | 3:45 | 3:10 | -15.5 | 3:16 | -12.9 | +2.6 |
| Cross section: 203×203mm, steel: 2.75% (4φ19), siliceous aggregate (Figure 1a) | | | | | | | | | | |
| S6 | 42.3 | | 169 | 0.16 | 3:05 | 3:27 | +11.9 | 2:56 | -4.9 | -16.8 |
| Cross section: 406×406mm, steel: 2.47% (8φ25), siliceous aggregate (Figure 1d) | | | | | | | | | | |
| S5 | 40.7 | 70 | 0 | 0.00 | 5:00 | >5:00 | / | / | / | / |
| S22 | 38.8 | | 2420 | 0.62 | 4:22 | 4:20 | -0.8 | 4:17 | -1.9 | -1.1 |
| Cross section: 304×456mm, steel: 2.22% (8φ22), siliceous aggregate (Figure 1e) | | | | | | | | | | |
| S27 | 42.4 | | 1415 | 0.41 | 5:56 | 4:50 | -18.5 | 5:00 | -15.7 | +2.8 |
| Cross section: 203×914mm, steel: 1.22% (8φ19), siliceous aggregate (Figure 1c) | | | | | | | | | | |
| S28 | 42.0 | / | 756 | 0.16 | 5:35 | 5:12 | -6.8 | 5:49 | +4.2 | +11 |

Tab. 8.2 Test data for eccentrically loaded columns

| Column No. | Concrete strength (Mpa) | Axial force (kN) | Moment (kNm) | load/strength ratio ρ' | Test duration Hr : min. | Predicted fire resist. (FIRE) | Deviation experim/FIRE in % | Predicted fire resist. (SAFIR) | Deviation Exper/SAFIR in % | Deviation FIRE/SAFIR in % |
|---------------------------------------------------------------------------------------|-------------------------|------------------|--------------|-----------------------------|-------------------------|-------------------------------|-----------------------------|--------------------------------|----------------------------|---------------------------|
| Cross section: 304×304mm, steel: 2.19% (4φ25), carbonate aggregate (Figure 3b) | | | | | | | | | | |
| S1 | 39.3 | 1000 | 25.4 | 0.46 | 3:02 | 3:24 | +12.1 | 2:57 | -2.7 | -14.8 |
| Cross section: 304×304mm, steel: 2.19% (4φ25), siliceous aggregate (Figure 3b) | | | | | | | | | | |
| S2 | 42.0 | 1023 | 25 | 0.45 | 2:50 | 2:40 | -5.9 | 2:52 | +1 | +6.9 |
| S3* | 42.7 | 1037 | 25 | 0.45 | 3:45 | 3:39 | -2.7 | 3:51 | +2.7 | +5.4 |
| S4* | 44.8 | 940 | 25 | 0.39 | 3:30 | 3:54 | +11.4 | 3:42 | +5.7 | -5.7 |
| S5 | 38.6 | 980 | 22.6 | 0.46 | 2:47 | 2:39 | -4.8 | 2:58 | +6.5 | +11.3 |

* restrained to initial rotation

There is no information for the measured temperatures in the carbonate aggregate columns. The difference between the measured and predicted fire resistance for the columns S10, S11 and S12

(Tab. 8.1) indicates that the values for the thermal conductivity and the specific heat of the carbonate aggregate concrete, recommended in EC2, are not adequate, but the predicted results are on the side of safety. In the literature there is a considerable scatter in the recommended values for these two parameters. For all other columns there is a good agreement between the calculated and experimentally achieved fire resistance (max. deviation is -8.9%). It is not the case only for columns S4 and S8, but probably the reason is the dispersion of the experimental results.

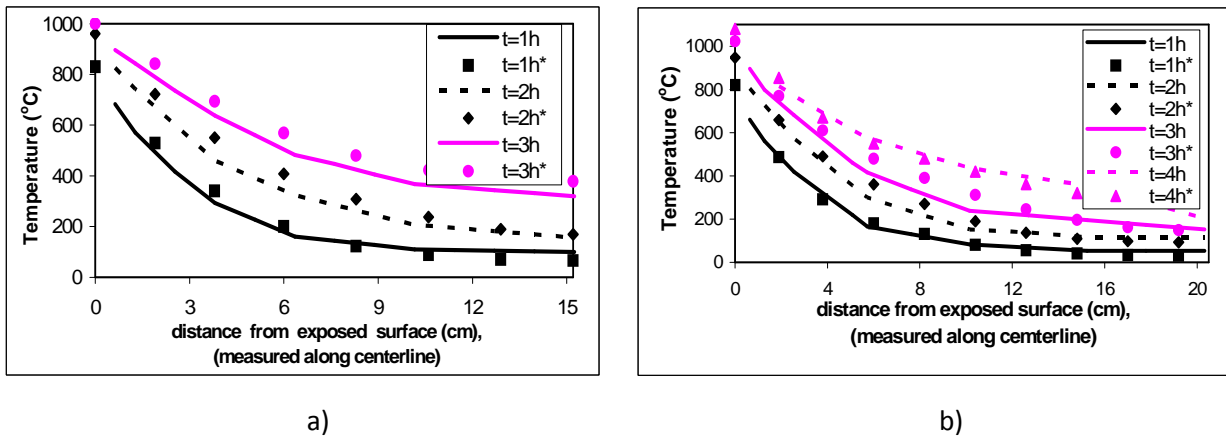


Fig. 8.4 Predicted* and measured concrete temperatures in the cross section of:
 a) 304x304mm, b) 406x406 mm, siliceous aggregate columns

Test data indicate that the end conditions and the effective length of the columns were not significant factors for the fire resistance of the columns. All the columns failed in compression, and only S6 failed in a buckling mode. The reason is the high slenderness of this column. The computer program FIRE does not account for the effects of large deformations, so the numeric results are 12% higher than experimentally achieved. The effect of restraining was also considered. While constant loads were maintained on the reference columns, the initial load was increased as required to prevent expansion. The average decrease in test time due to fully restraining the columns during the fire test was 6%. The effect of concrete strength was evaluated by comparing results for high strength siliceous aggregate column S17 with results for the reference column S3. For the same load/strength ratio the difference is only 4%.

The type of the aggregate, the cross sectional geometry and the load/strength ratio α' are significant factors affecting fire resistance of centrally loaded columns. Since it was anticipated that both carbonate and lightweight aggregate concrete columns would have a better fire resistance than the siliceous aggregate concrete columns, most of the tests were performed on the last one. A relationship of fire resistance of siliceous columns to load/strength ratio was obtained and presented on Fig. 8.5.

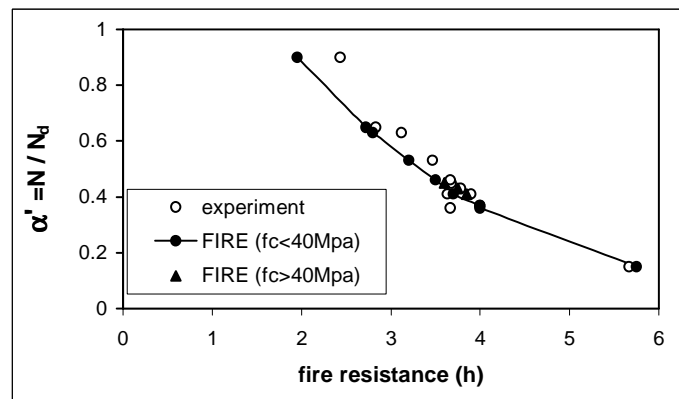


Fig. 8.5 Fire resistance of 304×304mm siliceous aggregate columns

The fire resistance of five eccentrically loaded columns (small eccentricity) was determined in this investigation. Test results were analyzed to evaluate the effects of load/moment interaction, end conditions and aggregate type upon the performance of eccentrically loaded columns. Numerically and experimentally achieved results are presented in Tab. 8.2. Columns S1, S2 and S5 were pin-ended, while for columns S3 and S4 both top and bottom eccentric loads were adjusted to maintain constant end rotations throughout the test. The end rotations correspond to the initial rotations of the pin-ended columns when the full load was applied at ambient conditions. This procedure enables simulation of restraint conditions that occur in actual buildings due to column interaction with surrounding building components.

8.4 SUMMARY

As a result of parametric studies, the following conclusions are made: dimensions of the cross section, intensity of the axial force (load ratio α) and the type of the aggregate (siliceous or carbonate) are significant factors affecting fire resistance of centrally loaded columns exposed to standard fire from all sides. When dimensions of the cross section are small temperature penetrates deeper in a short time period and the fire resistance is lower. If carbonate aggregate concrete is used instead of siliceous aggregate concrete, the fire resistance is increased.

With the increase of the strength of concrete, the fire resistance increases in proportion to the assigned load capacity. The steel ratio has a negligible effect on the fire resistance of the centrally loaded columns, exposed to fire from all sides. As a result of that the concrete cover thickness has a negligible effect. Because of the symmetry of the axial load and fire exposure, support conditions and height of the column have no influence on the fire resistance (the used analysis procedure does not account for the effects of large displacements on equilibrium equations). The effect of axial restraint on the fire resistance is negligible. Experimental results indicated that fully restrained column didn't significantly decrease its fire resistance, and only columns with high slenderness ratio failed in buckling.

References

- Bazant, 1996: Bazant Z.P., Kaplan M.F., Concrete at high temperature: Material properties and mathematical models, London: Longman Group Limited, 1996.
- Cvetkovska, 2002: Cvetkovska M., Nonlinear stress strain behaviour of RC elements and RC frames exposed to fire, Phd Thesis, Skopje: University St.Cyril and Methodius, 2002.
- Iding, 1977: Iding R., Bresler B., Nizamuddin Z., FIRES-RC II A computer program for the fire response of structures-reinforced concrete frames, Report No. UCG FRG 77-8, Berkeley, University of California, 1977.
- Lin, 1992: Lin T.D., Zwiers R.I., Burg R.G., Lie T.T., McGrath R.J., Fire resistance of reinforced concrete columns, PCA Research and Development Bulletin RD101B, Skokie, Illinois, Portland Cement Association, 1992.

9 TEMPERATURE DISTRIBUTION IN R/C CROSS-SECTION SUBJECTED TO HEATING AND THEN FREELY COOLED DOWN IN AIR

Summary

This paper deals with the comparison between tests and calculation results of temperature distribution inside heated concrete specimens. Three types of specimens with the cross section of 20 x 20, 30 x 30 and 40 x 40 cm corresponding to the cross section of concrete columns were tested. Concrete C25/30 with siliceous aggregate was used. Specimens were put into an electric furnace heated up to a temperature of 850 o C, and kept there until the temperature in the middle of them exceeded 500 o C. After that specimens were removed from the furnace and cooled freely in air. The temperature of concrete was measured during the whole period of heating and cooling. The calculations of a two dimensional problem of transient heat transfer were solved using ANSYS program on the base of concrete thermal properties recommended in Eurocode 2-1-2. Good conformity of calculations to experimental results was obtained.

9.1 INTRODUCTION

At the present time probably no one has doubts how important and complete are basic requirements for construction works introduced nearly a quarter of a century ago [1, 2]. In practice these requirements have been replicated in the Regulation of The European Parliament [3] issued two years ago. Amongst the basic requirements for construction works [1, 3] the safety in case of fire is mentioned second only after mechanical resistance and stability. From the structural designer's point of view the most important fire safety requirement [2, 3] is that in the event of an outbreak of fire the load-bearing capacity of the construction can be assumed for a specific period of time. Formally this time is identified with the structure or structural element fire resistance [4]. The most reliable method for determining fire resistance of structural elements is execution of experimental tests. However this method is expensive and can be only applied to elements of limited size.

Currently in highly developed countries fire hazard is commonly considered as an accidental design situation [5], where ultimate limit states of the structure are analysed. The Eurocode [6], amongst others gives basic requirements for predicting fire resistance of reinforced concrete structures. The value of this parameter can be determined at the level [6]: (1) member analysis isolated from the structure, (2) analysis of parts of the structure (3) global structural analysis. Depending on the level of

performed analysis one can use [6]: (1) tabulated data, (2) simplified calculation methods or (3) advanced calculation methods. Comments on requirements [6], and remarks on calculations of reinforced concrete structures exposed to fire conditions can be found amongst others in papers [7-12].

Irrespective of whatever analysis detail level is used in both methods, using simplified and advanced calculation one of the key calculation stages important for adequateness of the obtained results is determination of temperature field in the structure exposed to fire conditions. This paper presents results of experimental research where concrete specimens were exposed to high temperature and then freely cooled in air.

9.2 EXPERIMENTAL PROGRAM

The experimental program included heating of three series of rectangular concrete specimens with cross sections 20 x 20, 30 x 30 and 40 x 40 cm, height 20 cm. Three equal specimens were tested in each of the series. Specimens were made from ordinary concrete C25/30 with siliceous aggregate. Table 9.1 shows the composition of used concrete mixture.

Tab. 9.1 Concrete mixture

| | |
|------------------------------------------------|--------|
| Portland cement CEM 32.5 | 300 kg |
| Siliceous gravel 8 – 16 mm | 695 kg |
| Siliceous gravel 2 – 8 mm | 570 kg |
| Sand 0.1 – 2 mm | 710 kg |
| Water | 155 kg |
| Plasticiser Woerment FM21 (per 1 kg of cement) | 4 ml |

After casting, specimens were placed in a chamber with controlled humidity of 95% and temperature of 18 °C. The specimens were removed after 28 days and stored in ordinary dry place until testing day. Average concrete compressive strength, tested after 28 days on six cubes with 15 cm side was 38.9 MPa. Testing specimens in high temperature was conducted about five months from casting. At that time the average concrete compressive strength tested on six cubes with 15 cm side was 52.5 MPa, and moisture content in concrete, determined on four cubes with 15 cm side was 3.8%.

The author's idea of the specimen's size was an attempt to map the existing cross-sections i.e. reinforced-concrete columns (sizes 20 x 20, 30 x 30 and 40 x 40 cm). In order to secure such a mapping the top and bottom specimen surfaces were isolated by a 6 cm thick rockwool panels normally used for fire protection of construction elements. Without detailed analysis it can be estimated that the thermal resistance of a 6 cm rockwool layer is about 12 times greater than the thermal resistance of a 20 cm

concrete layer. Due to the application of this isolation heat could only penetrate from the lateral areas of the specimens, thus access of heat to the top and bottom was practically eliminated.

Temperature measurements were made in nine places inside the specimens and in four on the lateral sides (at half of their height) and in the middle of the top and bottom surfaces under the rockwool isolation (Fig. 9.1). K type thermocouples were used for measurements. In order to take measurements inside, 5 mm holes were drilled in the specimens, thermocouples were inserted and then filled up with fine grained dry sand and closed with rockwool. This enabled of precise location for the thermocouples and their multiple use. Figure 9.2 shows examples of specimens ready for the experiment.

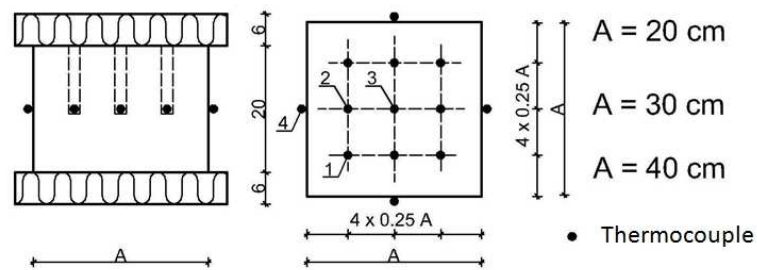


Fig. 9.1 Thermocouples location in specimens



Fig. 9.2 Photographs of specimens with cross sections of 20 x 20, 30 x 30 and 40 x 40 cm

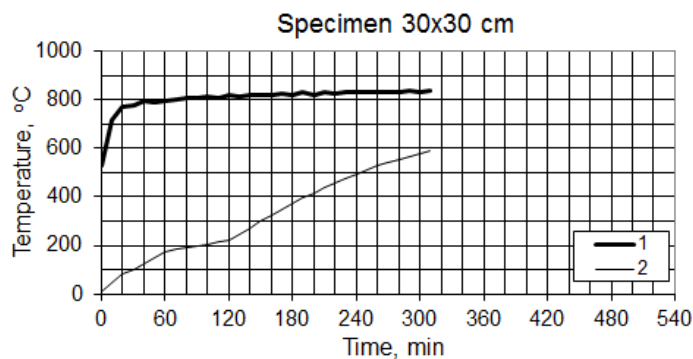
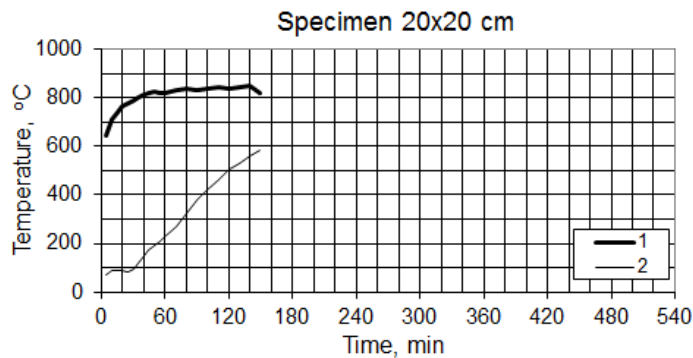
The experiment was executed in an electric furnace with chamber dimensions of 75 x 120 cm, height 50 cm and heating power of 50 kW. Specimens were placed on a specially constructed steel stand, and then inserted into the furnace initially heated to the temperature of 850 °C. Figure 9.3 presents photos of a specimen with cross section of 30 x 30 cm inserted into the furnace.

After placing the specimens in the furnace they were heated until the temperature measured in their middle point exceeded 500 °C. Figure 9.4 presents temperature graphs on surface of tested specimens. The thick continuous line shows the average temperature value at lateral surfaces. Determination of this value was first calculated from an arithmetic median on values measures at four

lateral surfaces of each specimen and then the arithmetic median was calculated from results obtained in three equal specimens. The thin continuous line shows the average temperature value at middle of the cross section, on upper and bottom parts between the concrete and rockwool plates. Here to calculate the arithmetic median value the measurement results from top and bottom were taken first and then the arithmetic median was calculated from results obtained in three equal specimens.



Fig. 9.3 Sample photos of a specimen 30 x 30 cm in the furnace chamber



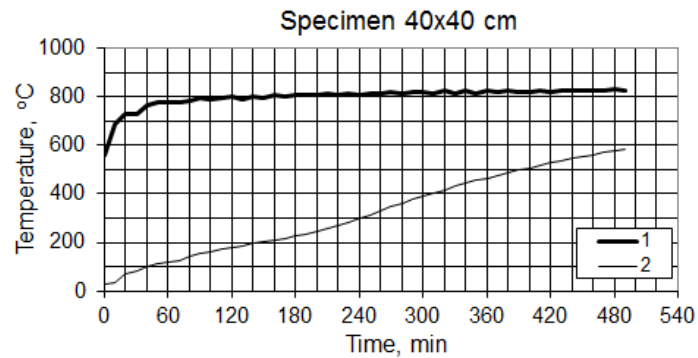


Fig. 9.4 Temperature on surface of specimens (1 – lateral surface, 2 – upper/bottom surface)

In all cases after placing specimens in the furnace the temperature measured on their lateral surfaces reached a value slightly exceeding 800°C in a short time, and was then maintained for the whole heating period. The temperature on lateral surfaces of the specimens was smaller than the temperature under the furnace chamber ceiling reaching 850°C .

Temperature measured between the concrete and shielding rockwool increased slowly. It is undoubted that to some extent the increase of temperature was related to the heat penetration through the rockwool plates. It must be underlined that the temperature on the top and bottom surfaces of the specimens mainly increased due heat penetration to inside of the specimen from the lateral areas. This fact can be confirmed by comparing temperature increase on the top and bottom surfaces of examined specimens (Fig. 9.4) with relative temperature increase inside the specimens (Fig. 9.7).

After termination of heating, the specimens were removed from the furnace and freely cooled down in air with temperature near 10°C . Figure 9.5 presents an example of the specimen inside the furnace chamber immediately before end of heating. Figure 9.6 shows a specimen after removing from furnace chamber (cooling).



Fig. 9.5 Specimen in the furnace chamber



Fig. 9.6 Specimen cooled after removing from furnace chamber

9.3 TEMPERATURE INSIDE THE SPECIMENS

Figure 9.7 presents temperatures measured in each place of the specimens. Placement and numeration of points is shown on Fig. 9.1. Temperature values at points 1 and 2 have been averaged according to rule described in paragraph 2. Temperature values at point 3 (middle of specimen) are arithmetic median values taken from three repetitive experiments of the same specimens. Vertical line stands for time when the furnace was opened to take out the specimens for free cooling. Appendix 1 shows tabulated data of average values of test results.

The time required to reach a temperature exceeding 500 °C differed depending on the size of their cross-section. In case of specimens with cross-section of 20 x 20 cm the heating lasted about two and half hours, in case of specimens with cross-section of 30 x 30 cm – slightly greater than five hours, and for specimens with cross-section of 40 x 40 cm – a little above eight hours. The time required for free cooling was significantly different for specimens of various sizes.

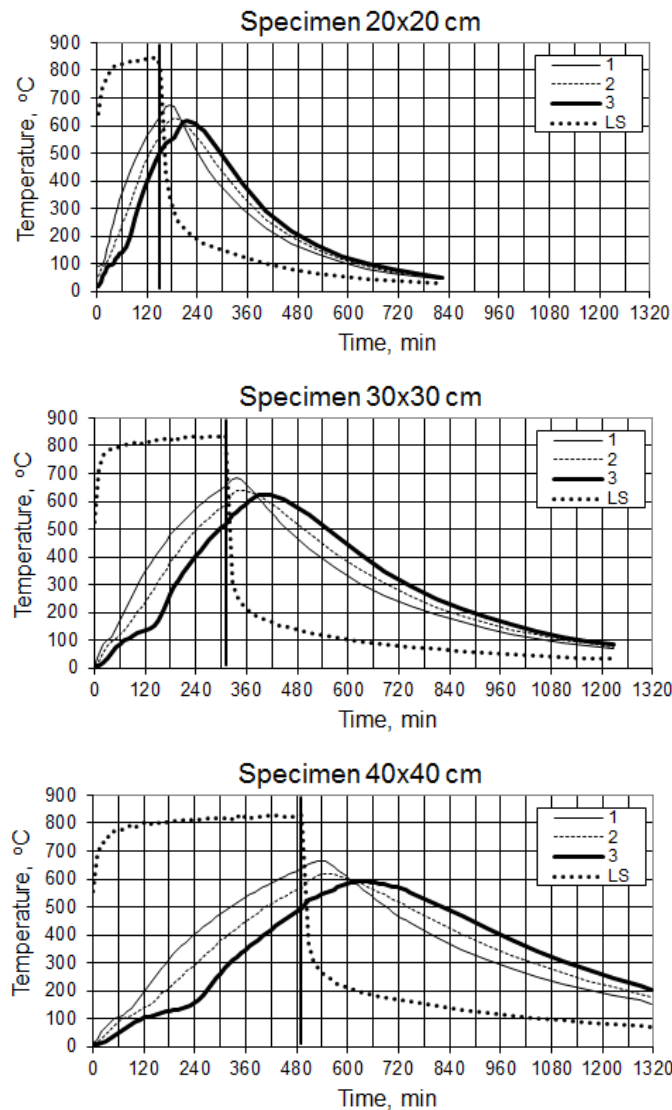


Fig. 9.7 Temperature in specimen cross-sections (placement of points 1-3 – see Fig. 1; LS – lateral surface)

A similar phenomenon related to concrete thermal inertia occurred in all types of specimens. At the beginning of the cooling process the temperature in the middle of the specimen was slightly higher than 500 °C, temperature at points close to corners – slightly below 700 °C, and about 600 °C in intermediate points. Next, temperatures in near corner points nearly immediately started falling, while the temperature in middle part of the specimens still increased for some time. Temperature equalization in particular points of the specimen's cross-section occurred only after some time from heating termination. The time when temperature values inside the specimens reached maximum, that is time after temperature in all places of the specimen's cross-section started decreasing was even longer. In specimens with cross-section of 20 x 20 cm it was about 50 minutes, in specimens with cross-section of 30 x 30 cm – about one hour and 20 minutes, and in specimens with cross-section of 40 x 40 cm about two and half hours.

In all three types of examined specimens the temperature inside them increased about 80 °C (to about 600 °C) from the moment of heating termination to the moment of maximal temperature values. This range of temperature increase may cause significant decrease in concrete compressive strength. On the base on [6] it can be evaluated that concrete with siliceous aggregate in temperature of 500 °C maintains about 60% of its virgin compressive strength, while in temperature of 600 °C only 45%.

Referring the experimental program results to a practical behaviour of reinforced concrete elements after the fire ends, it can be predicted that in the initial stage of the element's cooling the destruction of concrete structure can still be active in the internal parts of the element's cross-section. The biggest load bearing capacity decrease i.e. of reinforced concrete columns will most probably occur not during the time of fire but only after some time after fire termination. The time will increase with bigger element cross-section sizes.

9.4 CALCULATIONS OF TEMPERATURE FIELD IN EXAMINED SPECIMENS

The author's goal was to prepare a simple quick calculation used to determine the temperature field helpful during usage of simplified structural analysis methods and then compare them with temperature values obtained in the experimental program.

Calculations were done using the ANSYS program. Three two-dimensional problems calculating temperature fields after the determined heating time in square specimens with sizes 20 x 20, 30 x 30 and 40 x 40 cm were executed. Calculations used square four nod elements available in the program. Each of the examined squares was divided into 400 equal elements.

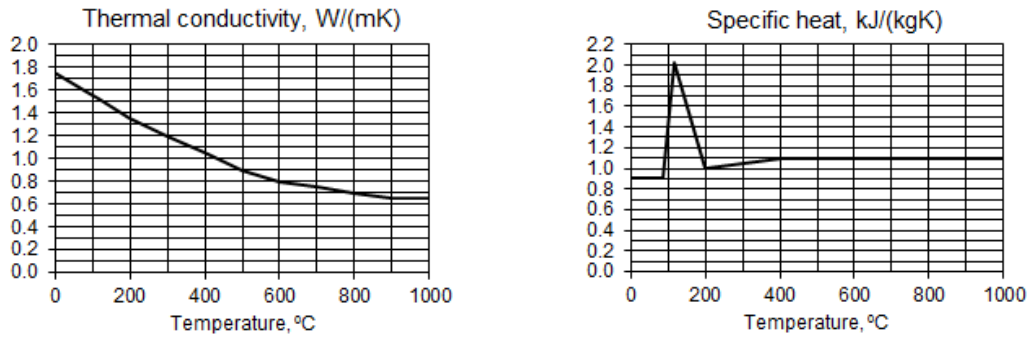


Fig. 9.8 Values of concrete thermal conductivity and concrete specific heat used for calculations

It was assumed that the concrete volumetric density is 2400 kg/m^3 , irrespective of the temperature. Concrete thermal conductivity was assumed as a median of minimal and maximal values given in [6]. In order to determine the concrete specific heat the relation given in [6] for concrete with 3.0% moisture content was used. This relation was slightly modified to ensure a convergence with the MES solution. Figure 9.8 presents graphs of concrete thermal conductivity and concrete specific heat values relative to temperature which were used for calculations.

Calculations were performed assuming that the concrete temperature at the edge of the examined area was at a constant $810 \text{ }^\circ\text{C}$ (compare. Fig. 9.4). No attempt was made to determine the boundary conditions considering heat transfer between the furnace chamber and the concrete surface of examined specimens due to convection and radiation. It was acknowledged that it would be inexpedient because the possibly obtained values would only refer to conditions in this specific furnace.

Figures 9.9-11 show examples of temperature field in the examined specimens after various heating duration. Borders of the areas with different shades determine locations of successive isotherms relating to temperature values from 100 to $800 \text{ }^\circ\text{C}$.

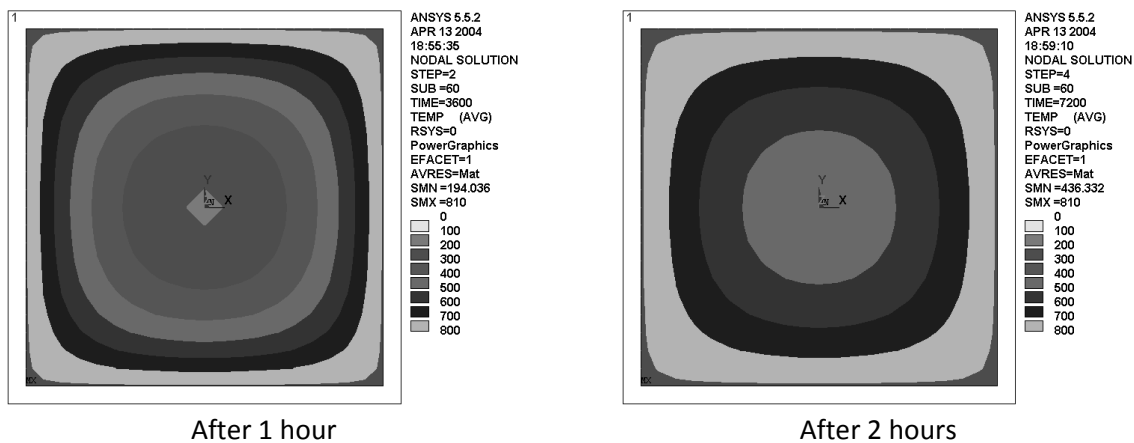


Fig. 9.9 Examples of temperature field in specimen 20 x 20 cm – calculation results

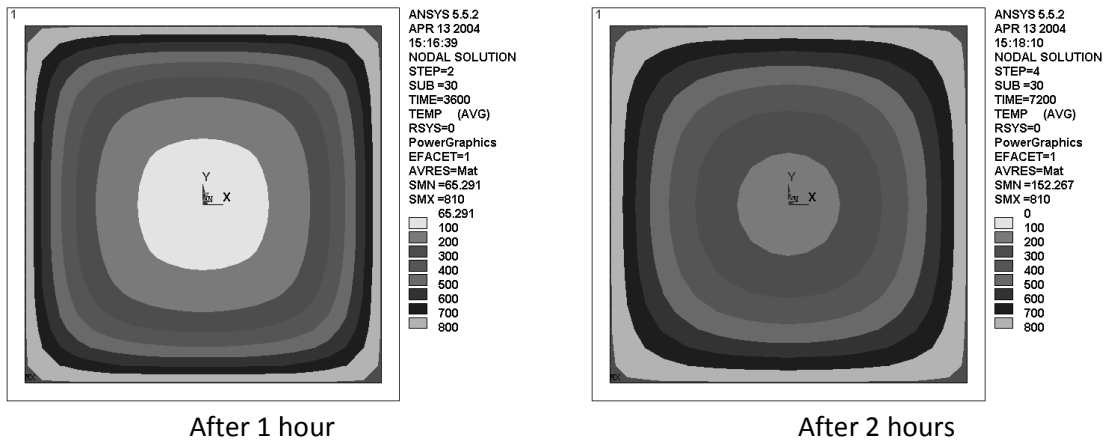


Fig. 9.10 Examples of temperature field in specimen 30 x 30 cm – calculation results

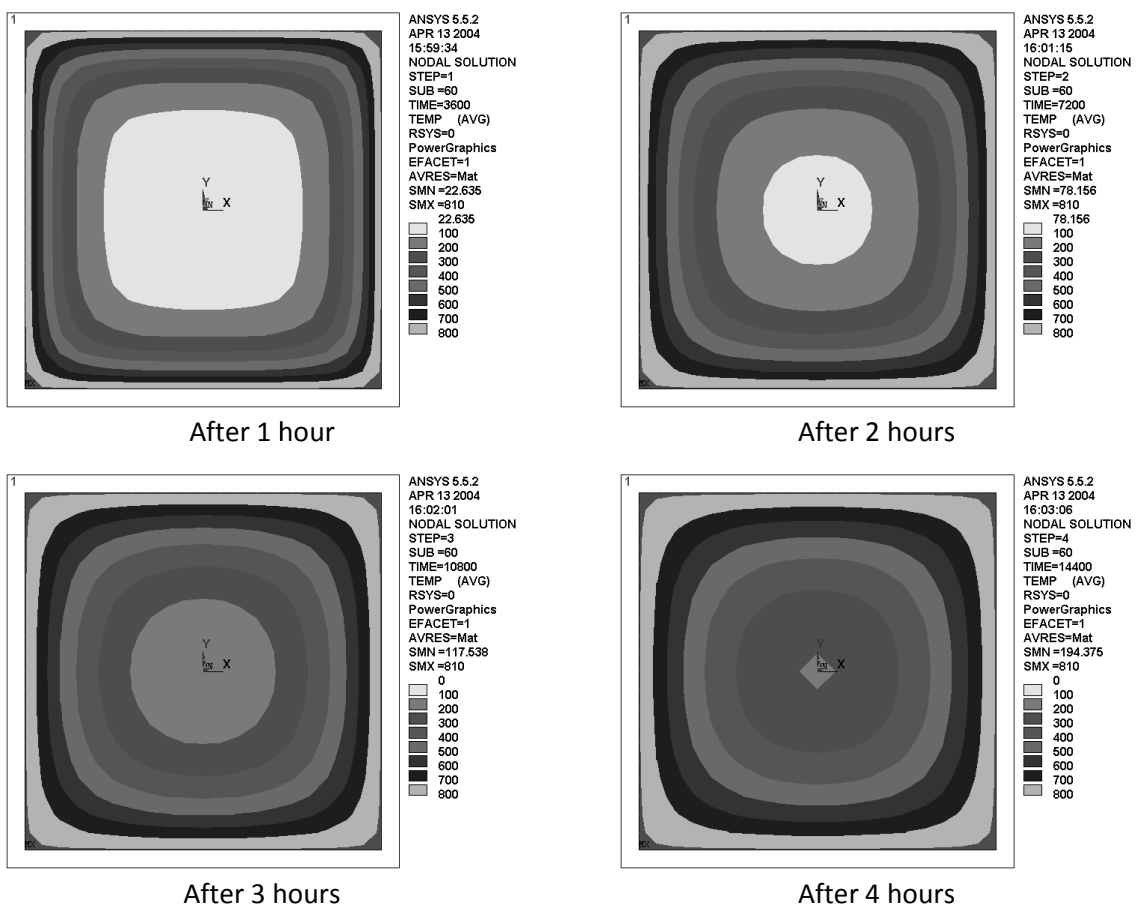


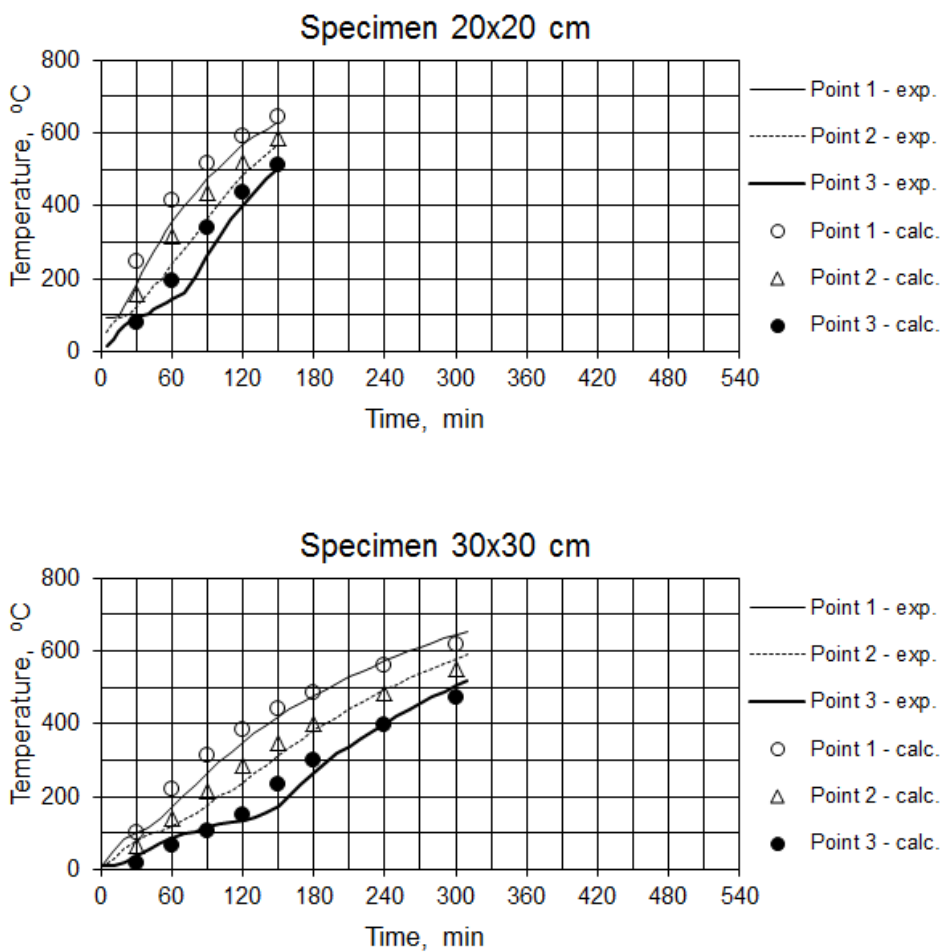
Fig. 9.11 Examples of temperature field in specimen 40 x 40 cm – calculation results

Figure 9.12 presents comparisons of test and calculation results. Points (circles and triangles) show temperature values calculated in measurement points (Fig. 9.1). Lines (continuous and dashed) show median temperature values determined experimentally. At first the arithmetical median was calculated from temperature values at points located symmetrically to the middle of the specimen and secondly

the median values from three equal tests of each specimen were taken in order to determine the median temperature in the given cross-section.

Figure 9.12 shows quite a good conformity of experimental and calculated results. The calculations could have used a modified set of concrete thermal properties and thus could allow to obtain a much better conformity of calculations to experimental values. However it was considered inadequate to try and “match” the calculation results to results of just a few experiments.

The author's goal was to check to what extent results of simple calculations using parameters of heat transfer in concrete taken from Eurocode [6], will conform to experimental results. From this point of view the results can be considered as satisfactory. Results obtained from solving a simple two dimensional problem using the finite element method may be assumed as precise enough for practical analysis of ultimate limit state in cross-sections of reinforced concrete elements subject to fire conditions.



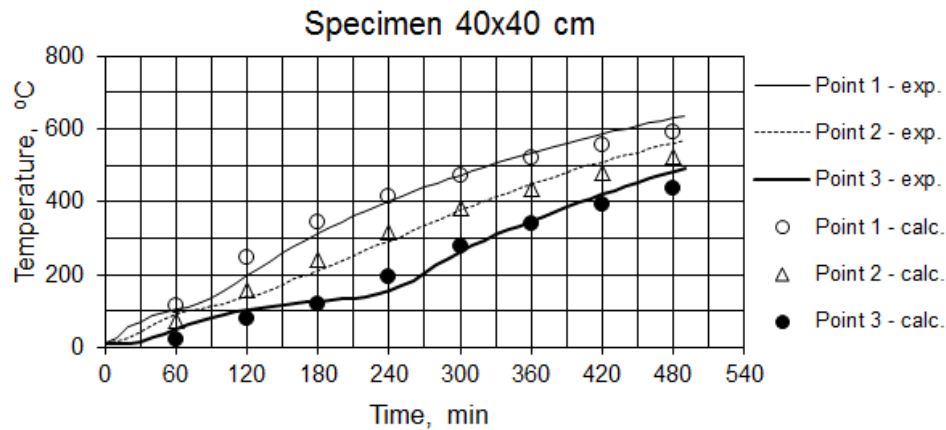


Fig. 9.12 Temperature in specimens – comparison of experiment and calculation results
 (points location – see Fig. 1)

9.5 FINAL REMARKS

This paper presents a description and results of an experimental test on heating and cooling of concrete specimens which is an attempt to resemble cross-sections of reinforced concrete columns used in practice. Specimens were heated to temperature exceeding 500 °C, and then freely cooled in air, making temperature measurements in various locations of the cross-sections.

Results of simple calculations of a two dimensional transient heat transfer problem performed by ANSYS program using concrete thermal properties taken from Eurocode 2-1-2, can be assumed as precise enough for practical use in simplified analysis of reinforced concrete elements subject to fire conditions.

Free cooling of reinforced concrete elements heated to high temperatures may last even over a dozen hours. In this time further degradation of concrete mechanical properties inside the element's cross-section may take place due to the concrete thermal inertia. This may cause that a reduced load bearing capacity of reinforced concrete columns subject to fire conditions may occur even a few hours after fire termination.

References

- Council Directive 89/106/EEC of 21 December 1988 on the approximation of laws, regulations and administrative provisions of the Member States relating to construction products.
- Interpretative Document (to Council Directive 89/106/EEC), Essential Requirement No 2 "Safety in Case of Fire".
- Regulation (EU) No 305/2011 of the European Parliament and of the Council of 9 March 2011 laying down harmonised conditions for the marketing of construction products and repealing Council Directive 89/106/EEC. Official Journal of the European Union, 04.04.2011.
- EN 1991-1-2: 2002: Eurocode 1: Actions on structures – Part 1-2: General actions – Actions on structures exposed to fire.

- EN 1990: 2002: Eurocode: Basis of structural design.
- EN 1992-1-2: 2004: Eurocode 2: Design of concrete structures – Part 1-2: General rules - Structural fire design
- fib Bulletin 38/2007. Fire design for concrete structures – materials, structures and modelling. State-of-art report. International Federation for Structural Concrete (fib), April 2007; 97 p.
- fib Bulletin 46/2008. Fire design of concrete structures – structural behaviour and assessment. State-of-art report. International Federation for Structural Concrete (fib), July 2008; 209 p.
- Taerwe, 2008: Taerwe L.R., Fire Design of Concrete Structures According to the Eurocodes, A Review, SP-255-4, p. 75-96 in: *Design of Concrete Structures for Fire Safety*, ACI SP-255, ACI, Detroit 2008.
- Kowalski, 2009: Kowalski R., Calculations of reinforced concrete structures fire resistance, Architecture Civil Engineering Environment, in: *Journal of the Silesian University of Technology*, Vol. 2, No. 4/2009, p. 61-69.
- Kordina, 2010: Kordina K., Design of concrete buildings for fire resistance, Chapter 6, in: *Structural concrete. Textbook on behaviour, design and performance. Second edition*, Vol. 4, fib bulletin 54, 2010.
- Kowalski, 2012: Kowalski R., Abramowicz M., Chudzik P., Fire design of reinforced structures according to Eurocode prescriptions. Theoretical Foundations of Civil Engineering. XXI Russian-Slovak-Polish-Seminar. Moscow-Archangelsk, Russia. Publishing House of Warsaw University of Technology 2012, ISBN 978-83-7814-021-4, p. 303-312.

APPENDIX 1. Average values of test results

Tab. 9. A.1 Specimen 20 x 20 cm; thermocouples location – see Fig. 1

| Time, min. | | Temperature, °C | | | | |
|----------------------|-------|--------------------|----------------|----------------|----------------|---------------------|
| Heating/ /cooling | Total | Lateral surface | Point No. 1 | Point No. 2 | Point No. 3 | Top/bot. surface |
| 5 | 5 | 643 | 92 | 53 | 18 | 70 |
| 10 | 10 | 708 | 94 | 79 | 34 | 86 |
| 15 | 15 | 741 | 98 | 91 | 56 | 88 |
| 20 | 20 | 763 | 122 | 99 | 73 | 86 |
| 25 | 25 | 776 | 154 | 108 | 86 | 85 |
| 30 | 30 | 790 | 186 | 122 | 94 | 93 |
| 35 | 35 | 802 | 217 | 142 | 97 | 119 |
| 40 | 40 | 812 | 248 | 158 | 102 | 148 |
| 45 | 45 | 819 | 276 | 184 | 117 | 171 |
| 50 | 50 | 822 | 305 | 196 | 127 | 190 |
| 55 | 55 | 821 | 332 | 216 | 136 | 210 |
| 60 | 60 | 820 | 357 | 244 | 144 | 229 |
| 70 | 70 | 828 | 399 | 278 | 162 | 269 |
| 80 | 80 | 835 | 438 | 323 | 203 | 326 |
| 90 | 90 | 830 | 476 | 367 | 263 | 380 |
| 100 | 100 | 837 | 504 | 406 | 314 | 420 |
| 110 | 110 | 842 | 539 | 452 | 363 | 465 |
| 120 | 120 | 836 | 567 | 485 | 404 | 502 |
| 130 | 130 | 844 | 590 | 514 | 441 | 531 |
| 140 | 140 | 848 | 611 | 543 | 474 | 556 |
| 150 | 150 | 819 | 633 | 568 | 504 | 581 |
| 0 | 165 | 426 | 668 | 608 | 537 | 643 |
| 10 | 175 | 338 | 674 | 618 | 544 | 628 |
| 20 | 185 | 284 | 669 | 626 | 555 | 606 |
| 30 | 195 | 252 | 640 | 623 | 589 | 594 |
| 40 | 205 | 232 | 607 | 613 | 611 | 583 |
| 50 | 215 | 217 | 575 | 598 | 618 | 569 |
| 60 | 225 | 204 | 546 | 581 | 615 | 552 |
| 70 | 235 | 192 | 517 | 564 | 606 | 534 |
| 80 | 245 | 183 | 491 | 545 | 594 | 516 |
| 90 | 255 | 175 | 465 | 524 | 580 | 496 |
| 100 | 265 | 167 | 441 | 503 | 562 | 475 |
| 110 | 275 | 161 | 420 | 482 | 542 | 455 |
| 120 | 285 | 155 | 399 | 461 | 520 | 434 |
| 180 | 345 | 126 | 301 | 345 | 395 | 325 |
| 240 | 405 | 100 | 228 | 260 | 293 | 244 |
| 300 | 465 | 82 | 175 | 198 | 219 | 185 |
| 360 | 525 | 66 | 135 | 151 | 167 | 142 |
| 420 | 585 | 55 | 105 | 118 | 128 | 110 |
| 480 | 645 | 47 | 83 | 93 | 100 | 87 |
| 540 | 705 | 40 | 66 | 73 | 79 | 69 |
| 600 | 765 | 35 | 55 | 59 | 64 | 57 |
| 660 | 825 | 32 | 46 | 50 | 53 | 48 |

Tab. 9. A.2 Specimen 30 x 30 cm; thermocouples location – see Fig. 1

| Time, min. | | Temperature, °C | | | | |
|----------------------|-------|--------------------|----------------|----------------|----------------|---------------------|
| Heating/ /cooling | Total | Lateral surface | Point No. 1 | Point No. 2 | Point No. 3 | Top/bot. surface |
| 0 | 0 | 527 | 10 | 10 | 9 | 10 |
| 10 | 10 | 717 | 48 | 27 | 10 | 48 |
| 20 | 20 | 769 | 85 | 57 | 18 | 83 |
| 30 | 30 | 778 | 100 | 79 | 36 | 103 |
| 40 | 40 | 794 | 113 | 96 | 57 | 125 |
| 50 | 50 | 792 | 143 | 105 | 74 | 148 |
| 60 | 60 | 797 | 172 | 121 | 88 | 175 |
| 70 | 70 | 802 | 202 | 138 | 100 | 187 |
| 80 | 80 | 806 | 235 | 157 | 105 | 193 |
| 90 | 90 | 805 | 266 | 176 | 117 | 199 |
| 100 | 100 | 815 | 296 | 202 | 126 | 205 |
| 110 | 110 | 807 | 324 | 217 | 131 | 213 |
| 120 | 120 | 819 | 350 | 239 | 136 | 224 |
| 130 | 130 | 812 | 374 | 266 | 143 | 243 |
| 140 | 140 | 820 | 397 | 286 | 155 | 267 |
| 150 | 150 | 819 | 419 | 315 | 175 | 297 |
| 160 | 160 | 820 | 439 | 335 | 205 | 326 |
| 170 | 170 | 826 | 459 | 355 | 237 | 351 |
| 180 | 180 | 819 | 477 | 383 | 267 | 374 |
| 190 | 190 | 830 | 495 | 400 | 294 | 396 |
| 200 | 200 | 821 | 512 | 420 | 318 | 417 |
| 210 | 210 | 831 | 528 | 443 | 340 | 437 |
| 220 | 220 | 825 | 544 | 458 | 361 | 456 |
| 230 | 230 | 830 | 558 | 478 | 381 | 475 |
| 240 | 240 | 831 | 572 | 495 | 401 | 493 |
| 250 | 250 | 830 | 586 | 508 | 420 | 510 |
| 260 | 260 | 833 | 598 | 524 | 439 | 527 |
| 270 | 270 | 831 | 611 | 539 | 457 | 542 |
| 280 | 280 | 833 | 622 | 550 | 474 | 555 |
| 290 | 290 | 834 | 633 | 565 | 489 | 568 |
| 300 | 300 | 831 | 644 | 578 | 504 | 579 |
| 310 | 310 | 836 | 654 | 590 | 518 | 591 |
| 0 | 327 | 304 | 678 | 628 | 551 | 610 |
| 10 | 337 | 260 | 682 | 637 | 560 | 597 |
| 20 | 347 | 233 | 677 | 641 | 576 | 589 |
| 30 | 357 | 220 | 666 | 639 | 589 | 586 |
| 40 | 367 | 203 | 650 | 635 | 603 | 582 |
| 50 | 377 | 196 | 632 | 629 | 614 | 579 |
| 60 | 387 | 186 | 614 | 622 | 621 | 575 |
| 70 | 397 | 179 | 596 | 613 | 624 | 571 |
| 80 | 407 | 171 | 579 | 603 | 625 | 565 |
| 90 | 417 | 167 | 562 | 594 | 623 | 559 |
| 100 | 427 | 160 | 545 | 583 | 619 | 552 |
| 110 | 437 | 155 | 528 | 570 | 613 | 545 |
| 120 | 447 | 151 | 512 | 559 | 607 | 537 |
| 180 | 507 | 129 | 427 | 487 | 553 | 478 |

| | | | | | | |
|-----|------|-----|-----|-----|-----|-----|
| 240 | 567 | 111 | 360 | 416 | 481 | 415 |
| 300 | 627 | 98 | 307 | 356 | 413 | 356 |
| 360 | 687 | 86 | 262 | 303 | 348 | 303 |
| 420 | 747 | 76 | 224 | 259 | 295 | 258 |
| 480 | 807 | 68 | 192 | 220 | 250 | 220 |
| 540 | 867 | 60 | 165 | 189 | 212 | 188 |
| 600 | 927 | 54 | 142 | 162 | 182 | 161 |
| 660 | 987 | 48 | 123 | 139 | 155 | 139 |
| 720 | 1047 | 43 | 106 | 120 | 133 | 119 |
| 780 | 1107 | 39 | 92 | 103 | 114 | 103 |
| 840 | 1167 | 35 | 79 | 89 | 98 | 89 |

Tab. 9. A.3 Specimen 40 x 40 cm; thermocouples location – see Fig. 1

| Time, min. | | Temperature, °C | | | | |
|----------------------|-------|--------------------|----------------|----------------|----------------|---------------------|
| Heating/ /cooling | Total | Lateral surface | Point No. 1 | Point No. 2 | Point No. 3 | Top/bot. surface |
| 0 | 0 | 559 | 12 | 12 | 10 | 26 |
| 10 | 10 | 686 | 27 | 16 | 11 | 34 |
| 20 | 20 | 729 | 56 | 28 | 12 | 71 |
| 30 | 30 | 730 | 73 | 46 | 17 | 82 |
| 40 | 40 | 765 | 88 | 63 | 27 | 99 |
| 50 | 50 | 774 | 99 | 78 | 39 | 111 |
| 60 | 60 | 778 | 104 | 91 | 50 | 120 |
| 70 | 70 | 779 | 112 | 100 | 62 | 126 |
| 80 | 80 | 782 | 125 | 107 | 72 | 143 |
| 90 | 90 | 795 | 138 | 114 | 81 | 152 |
| 100 | 100 | 788 | 156 | 120 | 90 | 161 |
| 110 | 110 | 793 | 177 | 132 | 97 | 171 |
| 120 | 120 | 800 | 197 | 140 | 104 | 179 |
| 130 | 130 | 791 | 218 | 147 | 108 | 188 |
| 140 | 140 | 803 | 238 | 160 | 113 | 195 |
| 150 | 150 | 797 | 259 | 172 | 118 | 202 |
| 160 | 160 | 806 | 278 | 191 | 122 | 209 |
| 170 | 170 | 800 | 296 | 197 | 125 | 216 |
| 180 | 180 | 807 | 314 | 210 | 127 | 225 |
| 190 | 190 | 805 | 330 | 227 | 131 | 234 |
| 200 | 200 | 806 | 346 | 237 | 133 | 244 |
| 210 | 210 | 811 | 360 | 250 | 136 | 255 |
| 220 | 220 | 805 | 375 | 270 | 140 | 268 |
| 230 | 230 | 811 | 389 | 281 | 147 | 282 |
| 240 | 240 | 810 | 402 | 291 | 155 | 298 |
| 250 | 250 | 814 | 415 | 306 | 168 | 314 |
| 260 | 260 | 812 | 427 | 324 | 185 | 330 |
| 270 | 270 | 816 | 440 | 336 | 205 | 346 |
| 280 | 280 | 814 | 451 | 348 | 226 | 363 |
| 290 | 290 | 817 | 463 | 361 | 245 | 377 |
| 300 | 300 | 818 | 474 | 381 | 262 | 391 |
| 310 | 310 | 815 | 485 | 388 | 279 | 405 |
| 320 | 320 | 822 | 495 | 404 | 295 | 417 |

| | | | | | | |
|-----|------|-----|-----|-----|-----|-----|
| 330 | 330 | 813 | 506 | 416 | 309 | 430 |
| 340 | 340 | 826 | 516 | 424 | 323 | 442 |
| 350 | 350 | 813 | 525 | 437 | 335 | 454 |
| 360 | 360 | 827 | 535 | 451 | 348 | 465 |
| 370 | 370 | 817 | 544 | 458 | 360 | 476 |
| 380 | 380 | 825 | 553 | 470 | 373 | 487 |
| 390 | 390 | 822 | 561 | 480 | 385 | 497 |
| 400 | 400 | 820 | 570 | 493 | 397 | 507 |
| 410 | 410 | 827 | 578 | 504 | 409 | 517 |
| 420 | 420 | 821 | 586 | 509 | 421 | 527 |
| 430 | 430 | 826 | 594 | 521 | 432 | 536 |
| 440 | 440 | 824 | 601 | 530 | 443 | 545 |
| 450 | 450 | 823 | 609 | 536 | 454 | 553 |
| 460 | 460 | 827 | 616 | 547 | 464 | 562 |
| 470 | 470 | 822 | 623 | 555 | 474 | 569 |
| 480 | 480 | 828 | 630 | 561 | 484 | 576 |
| 490 | 490 | 827 | 636 | 569 | 494 | 584 |
| 0 | 507 | 366 | 655 | 597 | 523 | 602 |
| 10 | 517 | 313 | 661 | 604 | 531 | 598 |
| 20 | 527 | 285 | 665 | 612 | 538 | 590 |
| 30 | 537 | 266 | 666 | 617 | 544 | 583 |
| 40 | 547 | 253 | 662 | 617 | 551 | 577 |
| 50 | 557 | 242 | 655 | 617 | 557 | 571 |
| 60 | 567 | 233 | 646 | 616 | 564 | 566 |
| 70 | 577 | 225 | 635 | 613 | 570 | 562 |
| 80 | 587 | 219 | 623 | 609 | 577 | 557 |
| 90 | 597 | 212 | 612 | 604 | 582 | 553 |
| 100 | 607 | 208 | 600 | 599 | 586 | 549 |
| 110 | 617 | 203 | 587 | 593 | 589 | 544 |
| 120 | 627 | 198 | 575 | 587 | 590 | 539 |
| 130 | 637 | 194 | 563 | 580 | 590 | 535 |
| 140 | 647 | 190 | 551 | 574 | 590 | 530 |
| 150 | 657 | 186 | 539 | 567 | 589 | 525 |
| 160 | 667 | 183 | 527 | 558 | 587 | 519 |
| 170 | 677 | 180 | 515 | 550 | 584 | 513 |
| 180 | 687 | 176 | 504 | 545 | 581 | 507 |
| 190 | 697 | 174 | 493 | 535 | 578 | 502 |
| 200 | 707 | 172 | 482 | 527 | 574 | 496 |
| 210 | 717 | 169 | 472 | 522 | 571 | 490 |
| 220 | 727 | 166 | 462 | 514 | 565 | 484 |
| 230 | 737 | 163 | 452 | 505 | 560 | 477 |
| 240 | 747 | 160 | 442 | 495 | 554 | 471 |
| 300 | 807 | 146 | 391 | 449 | 513 | 432 |
| 360 | 867 | 134 | 348 | 403 | 469 | 393 |
| 420 | 927 | 123 | 312 | 365 | 425 | 356 |
| 480 | 987 | 113 | 279 | 328 | 382 | 322 |
| 540 | 1047 | 104 | 251 | 295 | 342 | 290 |
| 600 | 1107 | 95 | 226 | 265 | 306 | 261 |
| 660 | 1167 | 88 | 204 | 236 | 274 | 235 |
| 720 | 1227 | 81 | 184 | 214 | 245 | 211 |
| 780 | 1287 | 75 | 167 | 191 | 220 | 191 |

WG2 - Aldina Santiago, aldina@dec.uc.pt

João Ribeiro, joao.ribeiro@uc.pt

M^a Constança Rigueiro, constanca@ipcb.pt

10 NUMERICAL BEHAVIOUR OF T-STUB JOINT COMPONENT AT AMBIENT AND ELEVATED TEMPERATURES

Summary

Current paper presents a three-dimensional finite element model reproducing the structural behaviour of the t-stub component at ambient and elevated temperatures. Validation of the elastic and post-limit behaviour is made against previous experimental results. FE analysis covered the three tested flange thicknesses of 10, 15 and 20 mm under 20 °C, 500 °C and 600 °C. Strain and stress patterns developed during the whole analysis, mainly for the elevated temperature cases where limited instrumentation is possible inside the furnace, are presented. The numerical response is found to be in good agreement with the recorded experimental data although further work in establishing damaged and fracture material behaviour is required. Good agreement for elevated temperature specimens is obtained considering the material reduction factors proposed by the Eurocode 3, Part 1-2.

10.1 INTRODUCTION

After the terrorist attacks that lead to the collapse of the World Trade Center in 2001, the study of steel structures robustness to accidental loadings (impact, explosion and fire hazard) have become major concerns. Connections performance is directly linked to the robustness of steel structures due to the influence of its ductility and rotation capacity, as presented by Papov after Northridge earthquake (Paul Popov, 1998).

Currently, the design of steel joints is based on the “component method” established in the Eurocode 3, Part 1.8 (CEN, 2005a). This method requires the accurate characterization (stiffness, resistance and ductility) of each active component. The main active components in a beam-to-column bolted joint are: i) column web panel in shear; ii) column web in compression iii) column web in tension; iv) column flange in bending; v) end-plate in bending; vi) beam flange and web in compression; vii) beam web in tension and viii) bolts in tension. The t-stub model is used to evaluate the behaviour of components iv) and v), being them the main components that assure the joint ductility due to its high deformation capacity. A t-stub is referred as a partial T-shaped section located in the connection’s tension zone, as shown in Fig. 10.1.

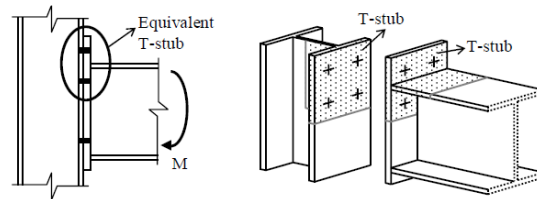


Fig. 10.1 "T-stub" section (Girão, 2004)

Several numerical studies on t-stub component have been developed during the last years. In 2001, Swanson (Swanson, 2002) used ABAQUS software to perform a finite element analysis considering contact and material and geometric non-linear characteristics. Good results in describing the experimental behaviour were obtained with a three-dimensional (3D) model; additionally, due to high computational cost of the 3D model, a 2D simplified model was developed to evaluate the effect of different pre-load levels in the bolts. The results showed that the initial stiffness is improved with increased pre-load force, but the ultimate failure load is not affected.

More recently, experimental tests and numerical studies on welded t-stub component have been conducted by Girão Coelho (Girão, 2004). These studies were developed in order to evaluate the advantages of designing steel-frame buildings with partial strength and semi-rigid joints; several material and geometrical parameters were assessed. The experimental results showed that: (i) the deformation capacity primarily depends on the plate/bolt strength ratio and, (ii) the final collapse is governed by brittle fracture of the bolts, welds, or cracking of the flange near the weld toe. It has been observed that most of the test specimens failed by tension rupture of the bolts after large bending deformation of the flange. The FE models built using LUSAS provided accurate response of the t-stub behaviour up to fracture. It was observed that: (i) the magnitude of bolt and prying forces ratio to the applied load are increased for smaller weld throat thicknesses; (ii) changing the bolt gauge implies that the distance between yield lines also changes eventually shifting the governing plastic mode; (iii) as failure modes progress from mode 1 to mode 3, resistance and initial stiffness increase, while deformation capacity diminishes; (iv) reducing the distance between yield lines produce stiffer behaviour; (v) increasing the flange steel grade would not improve connection stiffness (once elastic modulus remains unchanged) but it will naturally increase the t-stub resistance and eventually the post-limit stiffness, finally, (vi) it is noticed a decrease in the deformation capacity of steel flanges with higher grade, once bolt resistance eventually governs ultimate rupture.

Although at ambient temperature the initial stiffness and the resistance are usually the main requirements for the joint design; at elevated temperatures the rotation capacity and the failure mode are also essential to characterize its behaviour due to the high deformations experienced during a fire (Yu, 2009). In the past, FE analyses of connections under fire have been performed, for example, Liu (Liu, 1996) using a special purpose software FEAST and El-Houssieny et al. (El-Houssieny, 1998) developed 3D

FE models of extended end-plate joints at elevated temperatures. The main purpose of these studies was to assess the influence of the joints on the behaviour of steel structures under fire. Concerning the behaviour of the t-stub component at elevated temperatures, Yu et al. (Yu, 2008) conducted FE analysis, exploring the use of an explicit solver. The evaluation of different loading application times has been studied showing that the explicit solver ensures a quasi-static response if the load application time is higher than the natural period of the system.

The effects of the mesh were also analysed; at least of three elements are suggested in the discretization for the thickness of plates in bending. The numerical results were in good agreement with the test results (Spyrou, 2002) with slight disagreement for temperature of 200 °C due to uncertainty in the properties of steel when subject to low elevated temperatures.

The numerical work on t-stubs at elevated temperatures is limited and it is focused mainly on the calibration of models to be considered on the full joint modelling. Recent focus has been the study of connections subject to fire in which the development of catenary action of the beam requires high ductility demand from connections. Current paper presents FE analyses of the component t-stub subject to static loading at ambient and elevated temperatures. FE models are calibrated with results obtained from experimental tests performed at the University of Coimbra (Barata, 2013). This work is part of the framework of the research project “IMPACTFIRE” which aims to provide further understanding of steel connection behaviour when subject to accidental loads (impact and fire), in order to prevent the progressive collapse of buildings.

10.2 FINITE-ELEMENT MODELLING OF ISOLATED BOLTED T-STUB CONNECTION

10.2.1 Structural Model

The numerical models are drawn from a previous experimental study carried out at University of Coimbra; comprising a set of 3 different geometries of t-stubs, with 10, 15 and 20 mm flange thickness (see Tab. 10.1 and Fig. 10.2). Tests at ambient and elevated temperatures (500 °C and 600 °C) were considered. Tab. 10.1 provides the dimensions of the test specimens and the design values calculated according to the Eurocode 3, Part 1-8 (CEN, 2005a) and Part 1-2 (CEN, 2005b). A detailed description of the experimental work and test results is presented in (Barata, 2013).

Tab. 10.1 Characterization of the t-stub specimens (Barata, 2013).

| Dimensions (mm)(Fig. 10.2) | | | | | | | | | | Design Resistance [kN] | | | Initial Stiffness [kN/mm] | | |
|----------------------------|----------------|----------------|----------------|-----|------|------|----------------|------|-------|------------------------|-------|-------|---------------------------|-------|-------|
| Test | t _p | b _p | h _p | c | n | m | a _w | Bolt | Class | 20°C | 500°C | 600°C | 20°C | 500°C | 600°C |
| T-10 | 10 | 105 | 170 | 110 | 30 | 52.5 | 7 | M20 | 8.8 | 94.8 | 79.8 | 46.3 | 233.8 | 128.2 | 52.4 |
| T-15 | 15 | 105 | 170 | 110 | 30 | 52.5 | 7 | M20 | 8.8 | 209.0 | 133.1 | 63.9 | 385.2 | 207.8 | 81.7 |
| T-20 | 20 | 105 | 185 | 120 | 32.5 | 52.5 | 10 | M24 | 10.9 | 365.3 | 237.0 | 112.7 | 629.6 | 337.1 | 130.6 |

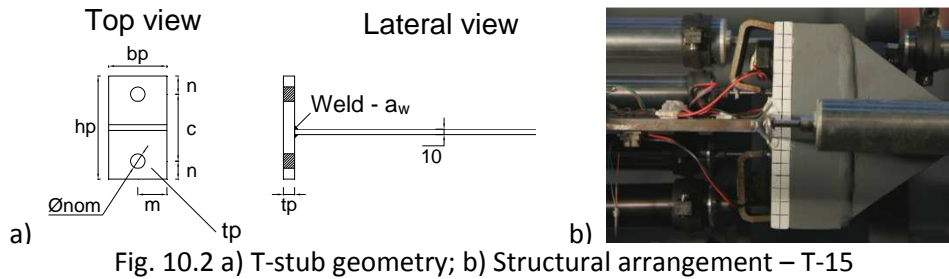


Fig. 10.2 a) T-stub geometry; b) Structural arrangement – T-15

10.2.2 Numerical Model

The FE analyses are conducted with the ABAQUS software making use of the implicit algorithm – ABAQUS\standard (Abaqus, 2006). The three-dimensional FE model is built with solid elements, based on the geometry of the experimental specimens.

10.2.2.1 Description of the FE model

The FE model is composed of four parts: (i) rigid back t-stub; (ii) tested t-stub; (iii) bolt, (head and shank as a single piece) and (iv) pull-out plate, as depicted in Fig. 10.3. Contact conditions are modelled between all the four parts namely: (i) the bottom flange surface with the back t-stub bottom flange; (ii) bolt shank with flanges bolt hole; (iii) top flange surfaces with bolt head; and (iv) pull out plate contact with the tested t-stub once the welds showed very little penetration. The welds have been modelled with tie constraint property linking the pull out plate to the tested t-stub part. Normal contact conditions are accomplished with “hard-contact” property allowing for separation after contact and the tangential behaviour has been assumed with a friction coefficient of 0.2 following “penalty” formulation. Convergence difficulties in the *implicit* procedure, while initializing contact interactions, lead to the need of setting the initial increment to a very small value, $1E-3$, which is allowed to be decreased into a minimum of $1E-12$ during the analysis.

Bolt modelling followed the nominal geometry (bolt shank diameter with 20 mm). Bolts used in the tests had a 2 mm diameter hole in the longitudinal axis to make room for strain gauge placement. Such geometric feature has been included in the bolt model. No pre-load has been considered.

For the analysis at elevated temperature, the following conditions have been assumed: (i) temperature introduced as a pre-defined field in the initial step of the analysis; (ii) high temperature creep effects of steel have not been taken into account. (iii) the temperature has been assumed to be constant throughout the FE models with the exception of the T-20 – 600 °C model; due to the lower massivity of the flange (20 mm) and bolt M24, a temperature of 575 °C was assumed for the bolt.

10.2.2.2 Boundary and loading conditions and specimen discretization

The t-stub model has been simplified by the use of symmetry conditions in axes yy and zz ; therefore, displacements in these directions are restrained at the symmetry surfaces (Fig. 10.3). The mechanical load is applied monotonically by imposing incremental displacement in x direction. The model is generated with solid element type C3D8R, allowing large deformations and non-linear geometrical and material behaviour. C3D8R is a valuable choice due to its reduced integration (only 1 integration point) allowing for reductions in calculation time while it provides hour-glass behaviour control. Generally a structured mesh technique with “Hex” element shape is used, except for the weld zone where a “Wedge” element shape is employed.

Mesh discretization studies were previously conducted assuring that a discretization of 4 elements through the thickness of bending-dominated plates (t-stub flanges), and a concentric mesh around the bolt area with 8x6 (edge x diagonal) elements provides accurate results, whilst optimizing calculation time and reducing convergence problems. This discretization is in accordance with Yu (Yu, 2008). The mesh used in the FE model T-15 has a total of 7864 elements - 5184 elements for the bolt and 2680 elements for the remaining model parts (Fig. 10.3).

10.2.2.3 Material Properties

Material nonlinearity is included by specifying a non-linear stress-strain relationship for material hardening; Von Mises criterion is considered to establish the yield surfaces with the associated plastic flow for isotropic materials (Abaqus, 2006). Stress-strain relationship has been obtained for each plate thickness through uniaxial coupon tests at ambient temperature (Martins, 2012). The mean results are plotted in Fig. 10.4: elastic modulus of $E = 205500$ MPa, elastic strength of $f_y = 385$ MPa; ultimate strength of $f_u = 588$ MPa and an ultimate strain $\epsilon_{cu} = 24\%$ for the steel. Uniaxial tension test on a M20 grade 8.8 bolt yielded an $E = 202500$ MPa; $f_y = 684$ MPa; $f_u = 1002$ MPa and ultimate strain of $\epsilon_{cu} = 3.7\%$. Taking into account the deviation ratio when comparing obtained bolt strength to nominal strength, the material properties for class 10.9 have been exceeded. Once the bolt geometry follows nominal dimensions, bolt material properties have been revised to take into account the reduced tensile shank area.

Material properties for the weld at ambient temperatures have been assumed equal to the base steel plates. For elevated temperature material models proper retention factors reported in Eurocode 3, Part 1-2 (CEN, 2005b) have been used for the mild steel, bolt, and also the weld.

Once large strains and large displacements are expected, material’s constitutive law is included in the numerical model by the *true-stress – logarithmic plastic strain* curves (Abaqus, 2006), (Fig. 10.4).

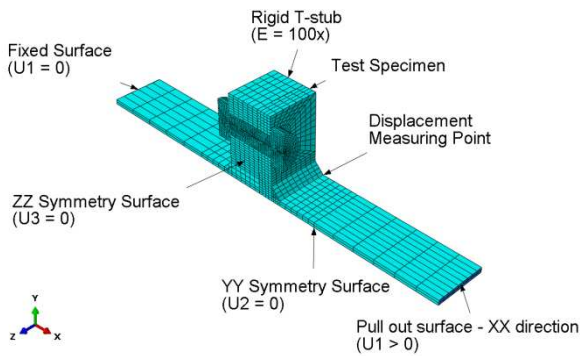


Fig. 10.3 Numerical model, boundary conditions and mesh discretization.

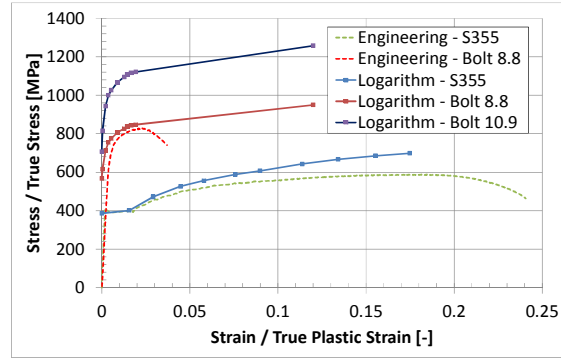


Fig. 10.4 Stress-strain relationships at ambient temperature.

10.2.3 Validation of the numerical model against experimental results

10.2.3.1 Results at ambient temperature

Tab. 10.2 compares the design values obtained from analytical calculation according to Eurocode 3, Part 1.8 (CEN, 2005a) with experimental results and numerical predictions. Estimation of the design resistance (experimental and numerical) is calculated using a bilinear approximation of the force-displacement curve based on the initial and post-limit stiffnesses (K_e , K_p) slopes, as proposed by Jaspart (Jaspart, 1991). Numerical and experimental design resistance predictions are generally under 10% error range. Analytical predictions provide expectedly conservative results. Concerning the initial and post-limit stiffnesses, it is observed that the analytical procedure provides overestimation of these values, with increasing error for increasing flange thickness.

Fig. 10.5 compares the numerical predictions (dashed lines) with the experimental results (solid lines) at ambient temperature. Each t-stub geometry has been tested twice. It can be observed that the numerical models can accurately predict the global behaviour of the t-stub component.

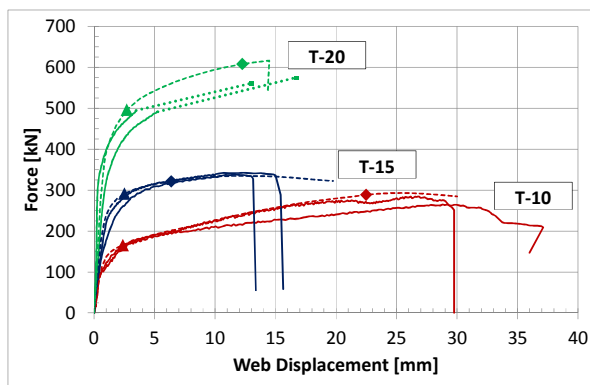
Fig. 10.6 presents the Von Mises stress and plastic strain patterns for the design resistance instant (T-10, T-15 and T-20) and for the failure (T-15) at ambient temperature. Equivalent plastic strain patterns suggest a clear plastic hinge next to the weld toe that is responsible for the knee in the transition from elastic to plastic phase observed in the *force versus web displacement curves* (Fig. 10.5). Comparison of the stress patterns developed in the bolts M20, grade 8.8, confirms the higher solicitation of the bolt demanded in the model T-15 compared with the model with lower flange thickness (T-10). In this study, it is assumed that the fracture initiates when plastic strain reaches the ultimate plastic strain of materials based on the coupon tests (Martins, 2012): $\epsilon_{cu,20^\circ, \text{bolt}} = 3.4\%$ for bolts and $\epsilon_{cu,20^\circ, \text{steel}} = 24\%$ for mild steel. Considering this criteria, bolt rupture is the ultimate numerical failure mode for T-10, T-15 and T-20, identified with diamond marker in Fig. 10.5.

These failure modes are in accordance with the experimental evidences for T-10 and T-15, although with smaller displacement development. Once material properties do not include damage,

web detachment next to the weld in test T-20 is not observed in the model; instead, a descent slope is observed in the end of T-20 model response due to plastification of the web.

Tab. 10.2 Design values and failure modes: Eurocode, experimental and numerical results.

| Test | Design Resist. [kN] | | | Initial Stiffness [kN/mm] | | | Post limit Stiffness [kN/mm] | | | Failure Mode | | | |
|---------|---------------------|-------|-------|---------------------------|-------|-------|------------------------------|-------|-------|--------------|--------|--------|--------|
| | 20°C | 500°C | 600°C | 20°C | 500°C | 600°C | 20°C | 500°C | 600°C | 20°C | 500°C | 600°C | |
| T-10 | Analytic | 101.6 | 79.2 | 46.2 | 130.4 | 78.2 | 40.4 | -- | -- | -- | Mode 1 | Mode 1 | Mode 2 |
| | Exp. | 182.4 | | | 171.4 | | | 3.1 | | | b) | | |
| | | 158.5 | 143.7 | 48.9 | 179.1 | 55.1 | 73.7 | 6.8 | 5.2 | 0.5 | b) | c) a) | c) |
| Numeric | 166.6 | 132.3 | 63.3 | 170.6 | 97.2 | 50.4 | 6.2 | 1.8 | 0.6 | b) | b) | b) | |
| T-15 | Analytic | 212.7 | 132.1 | 63.3 | 336.2 | 201.7 | 104.2 | -- | -- | -- | Mode 2 | Mode 2 | Mode 2 |
| | Exp. | 300.8 | | | 261.0 | | | 3.9 | | | c) b) | | |
| | | 291.0 | 153.3 | 69.1 | 271.0 | 313.1 | 107.8 | 4.7 | 6.2 | 5.5 | b) | c) b) | c) |
| Numeric | 294.0 | 177.8 | 77.6 | 246.0 | 147.9 | 76.6 | 4.6 | 1.4 | 1.0 | b) | b) | b) | |
| T-20 | Analytic | 356.7 | 229.6 | 107.9 | 601.7 | 361 | 186.5 | -- | -- | -- | Mode 1 | Mode 2 | Mode 2 |
| | Exp. | 527.6 | | | 898.6 | | | 2.7 | | | a) | | |
| | | 460.7 | 338.7 | 173.6 | 434.5 | 834.4 | 286.6 | 7.3 | 3.0 | 3.1 | a) | b) | c) |
| Numeric | 503.5 | 340.8 | 185.5 | 356.1 | 203.4 | 170.6 | 9.7 | 3.1 | 6.2 | b) a) | b) | b) | |



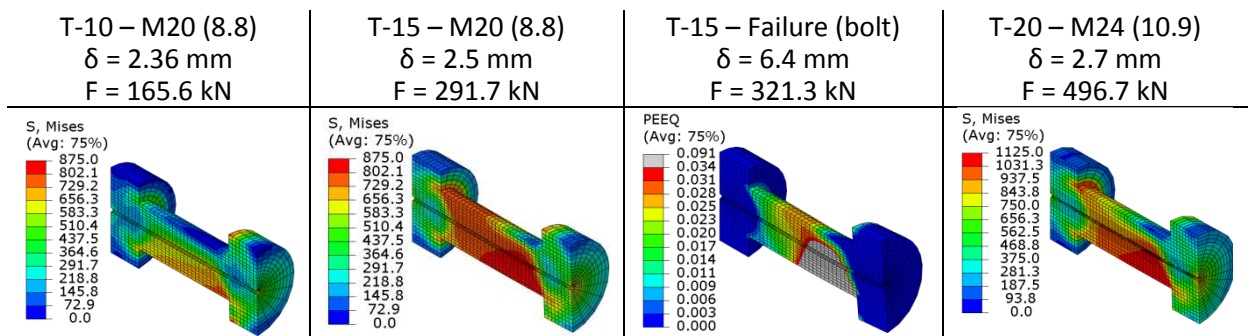
○ Markers legend:

- ◆ Failure
- ▲ Design Resistance

○ Tab. 10. – Failure Mode legend:

- a) Weld fracture;
- b) Bolt fracture;
- c) Crack of flange near the weld toe;

Fig. 10.5 Global response of t-stubs at ambient temperature: numerical *versus* experimental



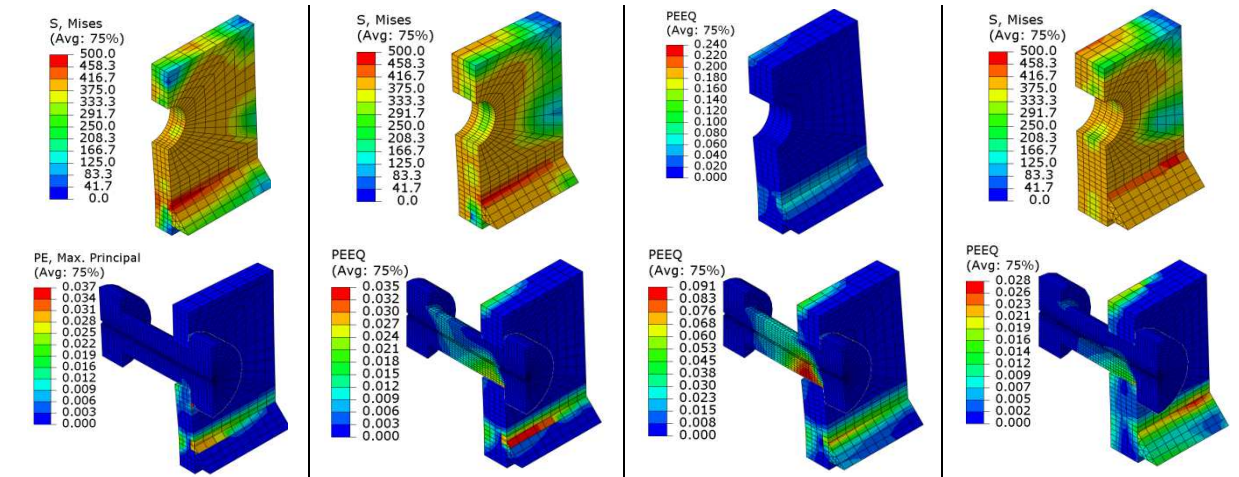
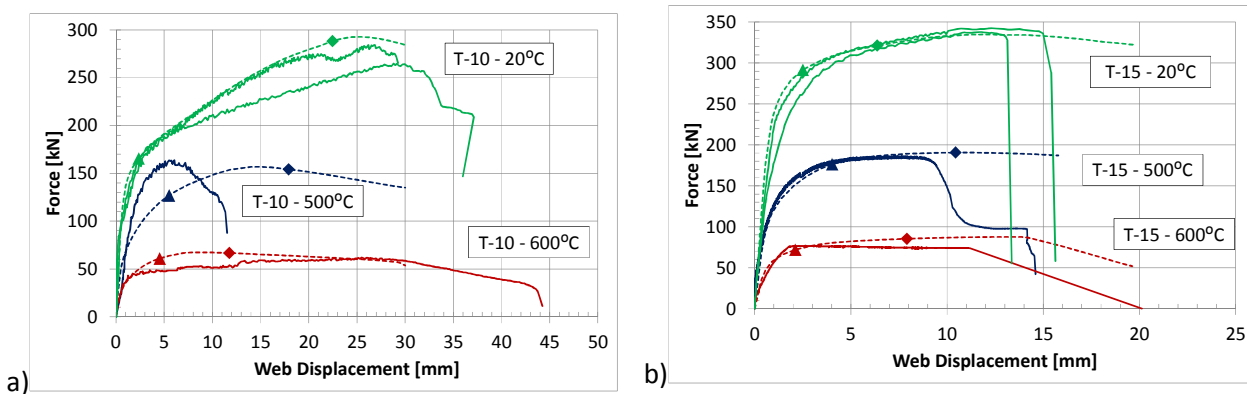


Fig. 10.6 Von Mises stress and equivalent plastic strain patterns for design resistance instant (T-10; T-15 and T-20) and for the failure instant (T-15) at ambient temperature

10.2.3.2 Results at elevated temperature

Fig. 10.7 compares the numerical predictions (dashed lines) with the experimental results (solid lines) under 20 °C, 500 °C and 600 °C. Similarly to the 20 °C models, 500 °C and 600 °C models exhibit stress concentration next to the weld that are responsible for the elasto-plastic transition. Such behaviour is less obvious in the experimental results T-15-600 due to the bolt elongation, identified as a horizontal plastic slope (Barata, 2013). Design resistance values, initial and post-limit stiffnesses and observed failure modes were compared in Tab. 10.2. Excluding the T-10-500, design resistance values predicted by the numerical models provided higher design resistance values than the experimental ones; average differences of 10% are calculated (T-10 models exhibit greater deviation). Again, excluding T-10-500, the elastic and post-limit stiffnesses are similar.



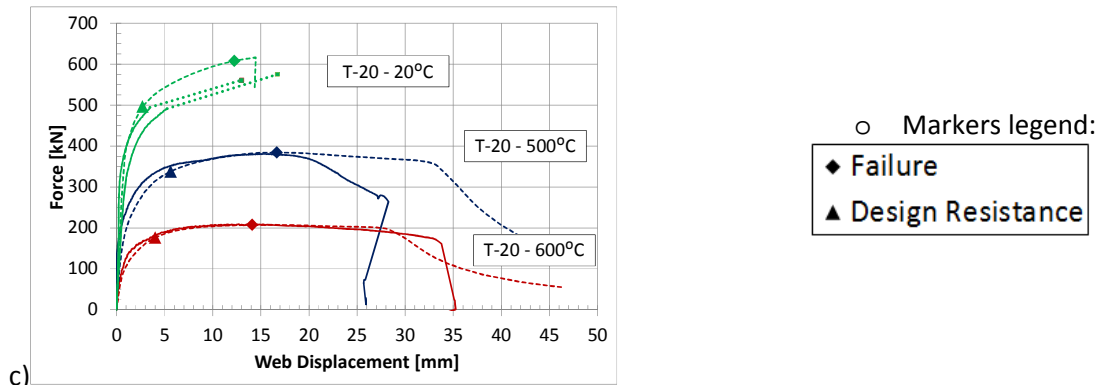
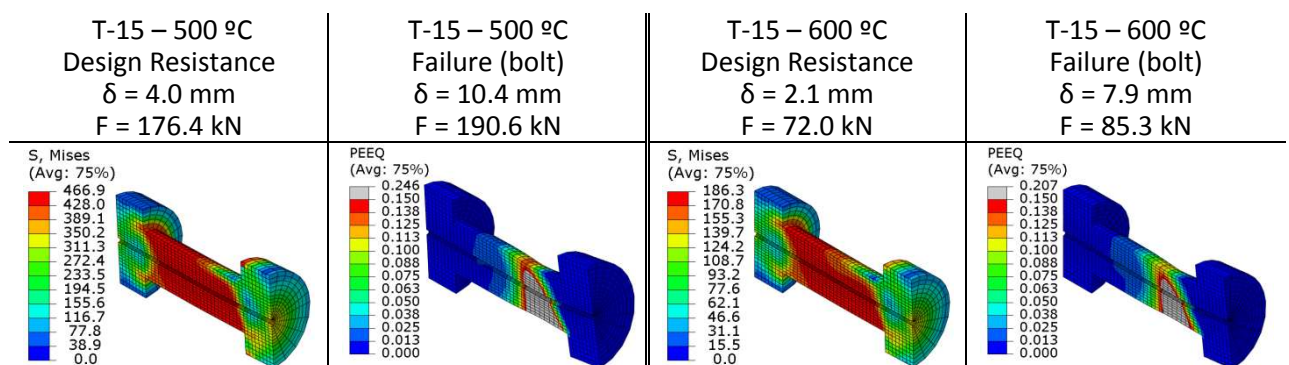


Fig. 10.7 Global response of the t-stubs under 20 °C, 500 °C and 600 °C: numerical *versus* experimental

Numerical failure at elevated temperatures was established based on a procedure similar to that used at ambient temperature, but an ultimate plastic strain for the bolt $\epsilon_{cu,\theta,bolt} = 15\%$ (Hanus, 2011) and for the mild steel $\epsilon_{cu,\theta,steel} = 20\%$ (Martins, 2012) are assumed. Fig. 10.8 depicts Von Mises stress and equivalent plastic strain patterns for T-15 at 500 °C and 600 °C. All numerical models have failed through bolt fracture after high plastic strain concentration on the flange near the weld toe. When the bolt fails, the T-15-500 flange exhibits higher value of equivalent plastic strains than the flange at 600 °C; this is in accordance with the experimental results where T-15–500 exhibited flange cracking next to the weld toe and T-15–600 failed through bolt fracture after long bolt elongation. This shows that from 500 °C to 600 °C the reduction factor in the bolt may assume high importance, leading to imminent plastic failure mode type 3.

Study of stress and strain patterns for T-10 and T-20 models also show higher strain concentration next to the weld toe for 500 °C compared to 600 °C. Therefore it would be expected the 500 °C tests to induce flange or weld cracking more easily than for 600 °C similarly to observations from T-15.



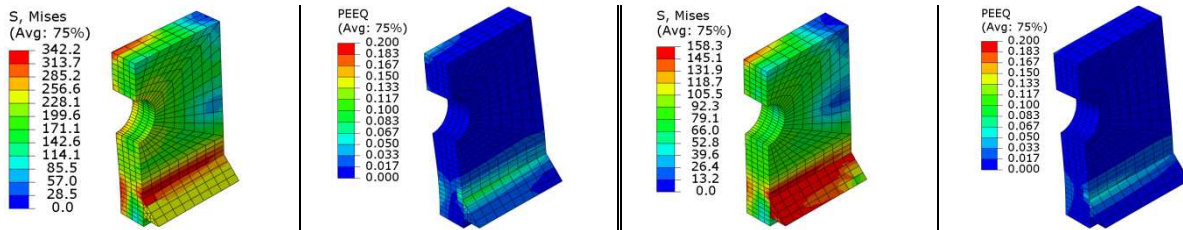


Fig. 10.8 Von Mises stress and equivalent plastic strain pattern evolution – T-15 (500 °C and 600 °C)

10.3 CONCLUSIONS

Current paper presents a three-dimensional finite element model that reproduces the structural behaviour of the t-stub component at ambient and elevated temperatures. Validation of the elastic and post-limit behaviour was made against previous experimental results (Barata, 2013): This numerical model fills in knowledge gaps in the available experimental data concerning to the detailed patterns of strains and stresses developed during the whole analysis, mainly for the elevated temperature cases, where limited instrumentation was possible inside the furnace. The FE models covered the three tested flange thicknesses of 10, 15 and 20 mm under 20 °C, 500 °C and 600 °C. The structural numerical behaviour was in good agreement with the recorded experimental data although further work in establishing damaged and fracture material behaviour was needed. Good agreement was reached at elevated temperature considering the material models with the reduction factors proposed by the Eurocode 3, Part 1-2 (CEN, 2005b).

Numerical simulations predicted bolt fracture as the ultimate failure mode for all analysis; however, observed failure modes in the tests ranged from i) weld fracture; ii) bolt fracture and iii) crack of the flange near the weld toe. Differences in the reduction factor evolution for bolt and steel induced different failure modes as temperature rises; moreover, the same material behaviour was assumed for the material base and for the heated affected zone (HAZ).

Several difficulties dealing with elevated temperature models and test results are drawn: i) the reliability of the assumed constant temperature field; ii) the precision needed to capture such small displacements while in the elastic range may compromise experimental elastic stiffness measurements; iii) eventual creep effects have not been taken into account; iv) variability of the steel mechanical properties at elevated temperatures and v) difficulty in establishing ultimate rupture strain and fracture behaviour. The models may also lack appropriate definition of the heat affected zone by the welding process, where initial stresses can develop and the material is deemed to be rather brittle.

Acknowledgment

The authors acknowledge financial support from Ministério da Educação e da Ciência (Fundação para a Ciência e a Tecnologia) under research project *PTDC/ECM/110807/2009*.

References

- Paul Popov, 1998: Paul Popov E., Yang T.-S., Chang S.-P., Design of steel MRF connections before and after 1994 Northridge earthquake, *Engineering Structures*, 1998.
- CEN, 2005a: Eurocode 3: Design of steel structures Part 1-8 : Design of joints, 2005, Brussels: European Committee for Standardization.
- Swanson, 2002: Swanson J.A., Kokan D.S., Leon R.T., Advanced finite element modeling of bolted T-stub connection components, *Journal of Constructional Steel Research*, no.58, p. 1015-1031, 2002.
- Girão, 2004: Girão, A., Characterization of the ductility of bolted end plate beam-to-column steel connections, 2004, Ph.D. Thesis, Universidade de Coimbra.
- Yu, 2009: Yu H., Burgess I.W., Davison J.B., Plank R.J., Development of a yield-line model for endplate connections in fire, *Journal of Constructional Steel Research*, 2009.
- Liu, 1996: Liu, T.C.H., Finite element modelling of behavior of steel beams and connections in fire, *Journal of Constructional Steel Research*, 1996.
- El-Houssieny, 1998: El-Houssieny O.M., Salam S.A., Attia G.A.M., Saad A.M., Behavior of extended end plate connections at high temperature, *Journal of Constructional Steel Research*, 1998.
- Yu, 2008: Yu H., Burgess I.W., Davison J.B., Plank R.J., Numerical simulation of bolted steel connections in fire using explicit dynamic analysis, *Journal of Constructional Steel Research*, 2008.
- Spyrou, 2002: Spyrou S., Development of a component-based model of steel beam-to-column joints at elevated temperatures, Ph.D. thesis, University of Sheffield; 2002.
- Barata, 2013: Barata P., Santiago A., Rodrigues J.P., Experimental behaviour of t-stub joint component at elevated temperatures, in 2^o CISLACI 2013: Coimbra (paper submitted).
- Abaqus, 2006: ABAQUS analysis : user's manual 2006, Providence, RI: ABAQUS Inc.
- CEN, 2005b: Eurocode 3: Design of steel structures. Part 1-2, General rules - Structural fire design, 2005, Brussels: European Committee for Standardization.
- Martins, 2012: Martins D., Variação das propriedades mecânicas do aço com a temperatura”, Master Thesis, 2012.
- Jaspart, 1991: Jaspart, J-P., Etude de la semi-rigidité des noeuds poutre-colonne et son influence sur la resistance des ossatures en acier (in French), PhD thesis, Department MSM, University of Liège, Belgium.
- Hanus, 2011: Hanus F., Zilli G., Franssen J.M., Behaviour of Grade 8.8 bolts under natural fire conditions – Tests and model, *Journal of Constructional Steel Research*, 2011.

WG1- Guillermo Rein, g.rein@imperial.ac.uk

Wolfram Jahn, w.jahnva@gmail.com

11 MODEL BENCHMARKING THE GROWTH PHASE OF DALMARNOCK

FIRE TEST ONE

Summary

The challenge of modelling a well characterized full-scale fire test using computational fluid dynamics is illustrated in this work comparing a priori and a posteriori simulations. In 2006, The Dalmarnock Fire Tests were conducted in two identical 3.5 m 4.75 m 2.5 m concrete enclosures with a real residential fuel load. This data set provides measured data at the highest spatial resolution available from a fire experiment to date. Prior to the tests, an international study of fire modelling was conducted in order to assess the state-of-the-art of fire simulations using a round-robin approach. Each of the eight round-robin teams independently simulated the test scenario a priori using a common detailed description of the compartment geometry, fuel packages, ignition source and ventilation conditions. Most teams decide to use the numerical code Fire Dynamics Simulator (FDSv4). Comparison to the experimental measurements showed a large scatter and considerable disparity (much larger than the error and variability associated to the experiments). The study showed that the accuracy predicting fire growth is poor. A posteriori simulations of the growth phase were conducted afterwards while having full access to all the measurements. No previous fire simulation had this large amount of data available for comparison. Simulations were compared against average and local measurements. The heat release rate is reconstructed from additional laboratory tests and upper and lower bounds for the fire growth are found. Within these bounds and after adjusting uncertain parameters, the level of agreement reached with the measurements was of 10 to 50% for the evolution of the average hot layer temperatures and between 20% and 200% for local temperatures.

11.1 INTRODUCTION

Modelling of compartment fires using computational fluid dynamics (CFD) has been a research topic since the introduction of computational techniques in fire science in the 1980's (Emmons, 1985). Only in the last decade the available computational power and knowledge of fire dynamics have grown sufficiently to carry out simulations in real-size building enclosures, using grids that are fine enough to reproduce fire-driven flows reasonably well (McGrattan, 2005). Since then, CFD has been used extensively to model enclosure fire dynamics (Ma, 2003, Hasib, 2007, Lattimer, 2003) both in research

and in industrial applications. There are two common industrial uses of CFD. One is for design of the fire safety strategies in the built environment (life safety and structural integrity, and which results are rarely made available for public scrutiny) and the reconstruction of accidental fires as part of forensic investigations (recent examples are the 2001 WTC (McGrattan, Bouldin, 2005), the 2003 Station Nightclub (Grosshandler, 2005) and the 2005 German five-storey apartment (Hofmann)).

The state of the art of fire modelling is such that given a fire of known size and power (evolution of the heat release rate (HRR)), CFD calculates the resulting temperature and smoke concentration fields. The fire source is therefore treated as an input into the model by means of a prescribed HRR as a function of time. This poses a problem in the study of accidental fires where the HRR is unknown. Predicting the evolution of the HRR (i.e., spread rate and growth pattern) instead of measuring it is among the most challenging pending issues in fire research (Rein, 2009, Kwon, 2007).

Most modelling work in the literature corresponds to scenarios with simple fire sources, like pool fires or a single burning item of constant or near constant HRR. This type of scenario avoids the more complex processes of flame spread and fire growth observed in real fires. Little research has been done comparing simulations with real-scale fire tests that use realistic fuel loads. Some important examples using pool and crib fires are presented here. Reneke et al. (Reneke, 2001) conducted a posteriori simulations of fire tests involving crib fires in a full scale single compartment with a zone model obtaining reasonable agreement with the measured average temperatures when the measured HRR is used as an input. Miles et al. (Miles, 2002) obtain good results in average temperatures when performing a posteriori simulations of a series of fire tests involving wood cribs. Although local measurements were available, none of these two simulation papers compared results at the field or local level. Rinne et al. (Rinne, 2007) found temperature profiles, smoke layer heights and gas species concentrations in a 10 by 10 by 5 m compartment predicted by FDSv4 to be in good agreement with experimental data for the burning of pool fires (heptane or toluene) and single cribs (PMMA or wood). The measured mass loss rate of the fuel was used to calculate the HRR, which was then input into the model.

The evaluation of the entire process of fire modelling, in which the mathematical model is only a component, is an important task for the advancement of fire safety engineering. The state-of-the-art of fire modelling is reflected not only in the mathematical model's capabilities, but also on how it is implemented throughout the different stages of fire modelling (Rein, 2008). The assumptions made by the user, the collection of data for input and the selection of the parameter values are crucial components leading to the creation of the input file. This is particularly important when advanced and complex computational tools are used (eg CFD and evacuation modelling). Under the current state of the art, there are many ill-defined and uncertain parameters within the models which cannot be rigorously and uniquely determined. Thus, there is plenty of space for uncertainty and doubt to unravel,

and for curve fitting and arbitrary parameter value selection to take place. This is summarised best in the words attributed to the German scientist Carl Friedrich Gauss (1777 – 1855): “Give me four parameters, and I will draw an elephant for you; with five I will have him raise and lower his trunk and his tail”.

This paper reports a series of CFD simulations (with FDSv4) conducted a posteriori to reproduce the large-scale Dalmarnock Fire Test One that involved several real burning items leading to a complex fire spread process. The interested reader is referred for more details to Jahn et al. (Jahn, 2010) on which this work is largely based.

11.2 DALMARNOCK FIRE TEST ONE

Detailed information about the experimental set-up and the chain of events that occurred during the Test One can be found elsewhere (Rein, 2007, Abecassis-Empis, 2008) but a short summary is given here. Test One was held in a two-bedroom single family flat, with the living room set up as the main experimental compartment. This compartment was 3.50 m by 4.75 m wide and 2.45 m high and made of concrete walls. It had two-pane window as shown in Fig. 11.1.

While the main source of fuel was a two-seat sofa stuffed with flexible polyurethane foam, the compartments also contained two office work desks with computers, each with its own foam-padded chair, three tall wooden bookcases, a short plastic cabinet, three small wooden coffee tables, a range of paper items and two tall plastic lamps. A plastic wastepaper basket filled with crumpled newspaper and 300-500 ml of heptane was the ignition source. The fire spread to a blanket on the sofa hanging into the basket, igniting the seating area of the sofa. After about 275 s the bookshelf next to the sofa ignited and was rapidly engulfed in fire. Within 25 s after ignition of the bookshelf the compartment reached flashover conditions. An estimation for the post-flashover fire results in about 3 MW before the first window breakage, and about 5 MW after the second breakage (Abecassis-Empis, 2008). But the evolution of the HRR during fire growth is unknown. Fig. 11. 2 shows the average temperature of the hot layer d in Test One and Test Two. A detailed presentation of the data can be found in (Rein, 2007, Abecassis-Empis, 2008).

Prior to Test One, laboratory experiments were conducted in order to determine the HRR curves for the sofa and the bookshelves inside the furniture calorimeter (using an exact replica of those used in Test One), see (Rein, 2007). A second series of laboratory experiments was conducted after Test One in order to analyze variations to the ignition protocol (Steinhaus, 2007). These two sets of experiments were the only direct source of information on the HRR in Test One.

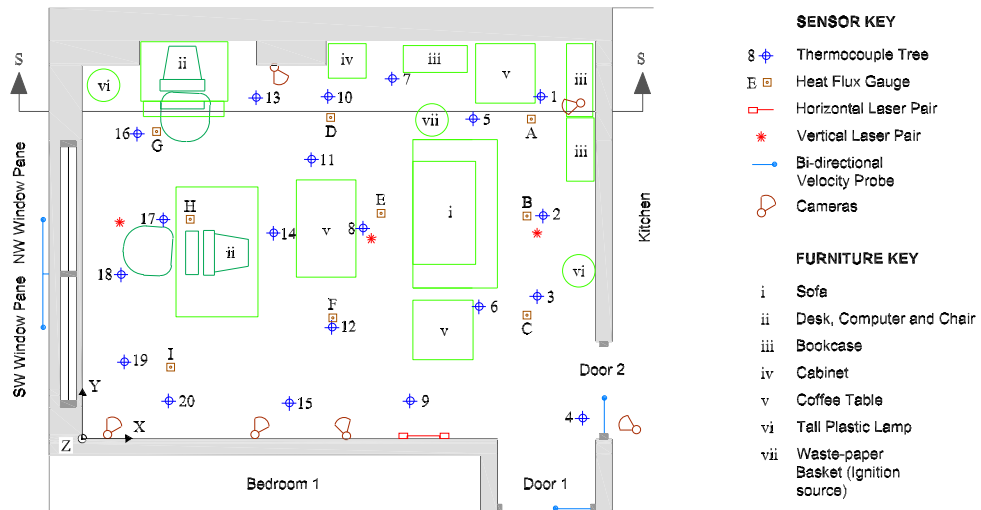


Fig. 11.1 Room layout with location of furniture and sensors (Rein, 2007, Abecassis-Empis, 2008)

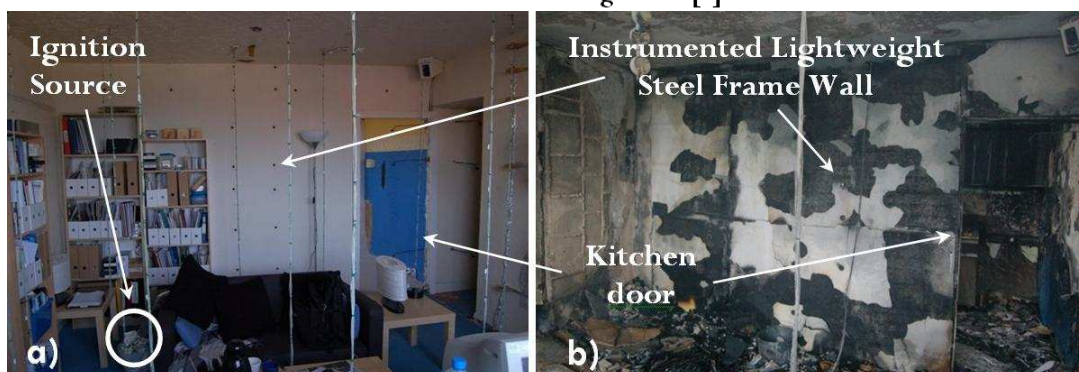
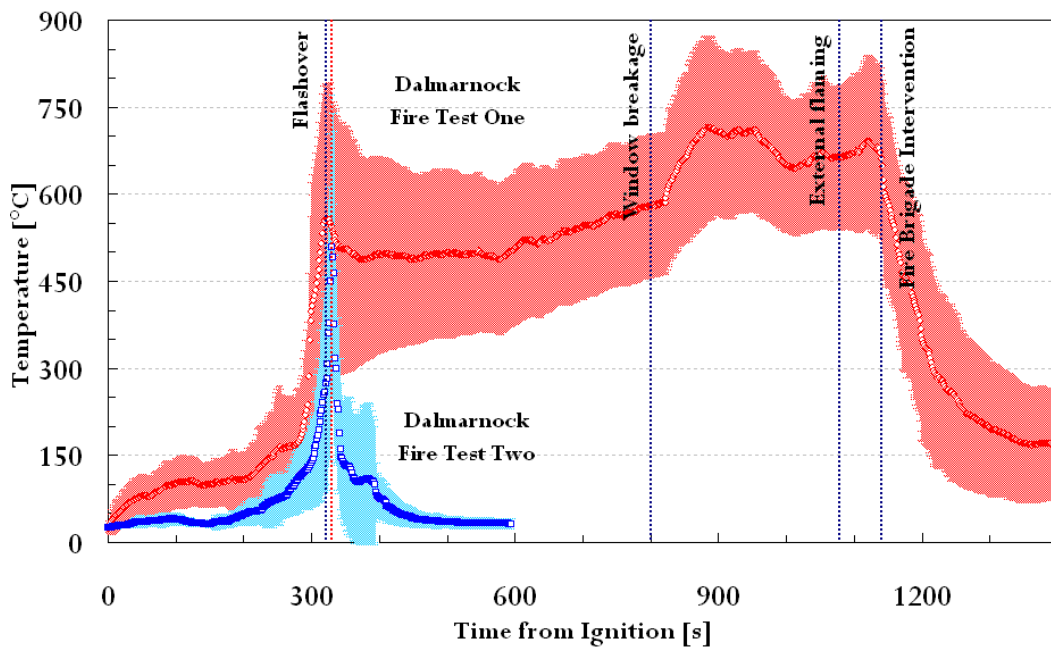


Fig. 11.2 Top) Average of the measured temperatures in the hot layer (corrected for radiation) in the Dalmarnock Test One and Test Two. The shaded areas indicate standard deviation. Test One was allowed to continue burning during the post-flashover stages whereas Test Two was extinguished

immediately after flashover. Bottom) View of the ignition source, the sofa and nearby items in the main compartment: a) before the fire and b) after the fire.

Fig. 11.3 shows the evolution of the HRR of the sofa and the effect of variations to the ignition source. The experiment conducted prior to Test One (referred to as Set 1) consisted of a sofa with two cushions, and a waste paper basket located next to the sofa. Accelerant was poured into the paper basket and the basket was ignited. The fire then spread over the armrest to the sofa and was stopped about 800 s after ignition when approximately one third of the sofa had been burnt. In the experiments conducted after Test One (referred to as Set 2), the exact ignition protocol of Dalmarnock Test One was replicated, which was like Set 1 but including a blanket that had been placed over the armrest of the sofa, and the accelerant distributed between basket and blanket. The presence of the blanket in Set 2 allowed the fire to bypass the armrest fire barrier and led to a faster growth rate involving the cushions. The fire growth rate for Set 2 is equivalent to a t-squared fire with growth constant 1.6 W/s (a medium fire 18). The constant in Set 1 is 0.5 W/s (corresponding to a slow fire 18). The two tests show that the uncertainty in the growth rate of the sofa fire during the early stages is significant and varies between a slow and a medium fire.

Fig. 11.3 suggests two patterns in the burning behaviour; an initial peak that rapidly decreases is followed by a growing fire that resembles a t-squared curve. A similar behaviour can be seen for Set 2. It is conjectured that the initial peak corresponds to the waste paper basket, accelerant and the blanket (in the case of Set 2), while the t-squared fire corresponds to the sofa itself.

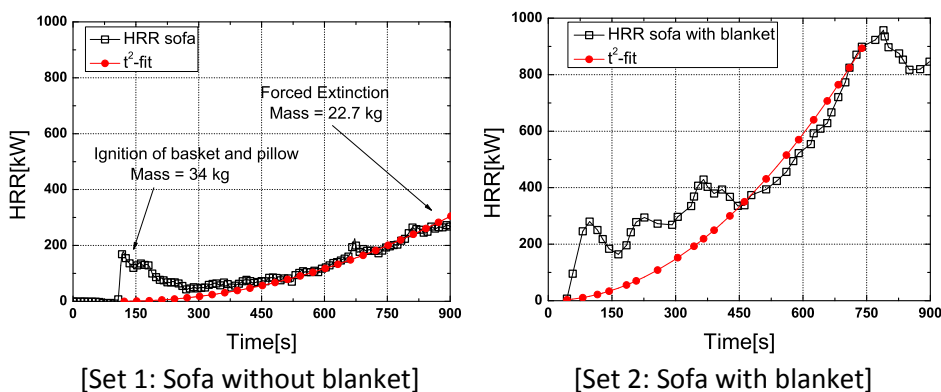


Fig. 11.3 Measured HRR for variations to the ignition source and equivalent t-squared fires: a) measured in the laboratory prior to Test One including sofa and waste basket (Set 1); and b) after Test One including the sofa, waste basket and blanket (Set 2)

11.3 A PRIORI VS. A POSTERIORI MODELLING

Before the Dalmarnock Tests were carried out, a round-robin study of blind predictions (Rein, 2009) was conducted in order to explore the a priori predictive capabilities of fire modelling in realistic scenarios. The aim of the exercise was to forecast the fire development as accurately as possible and compare the results. Comparison of the modelling results showed a large scatter and considerable disparity among the predictions, and between predictions and experimental measurements. The scatter of the simulations was much larger than the error and variability expected in the experiments. The study emphasized on the inherent difficulty of modelling fire dynamics in complex fire scenarios like Dalmarnock, and showed that the accuracy of blind prediction of fire growth (i.e. evolution of the heat release rate) is poor.

During the growth phase, most simulations over-predicted the hot layer temperature in the range of 20% to 500%. During the post flashover, most simulations under-predicted the hot layer temperature between 20 % to 80 %.

The present work revisits the modelling of the Dalmarnock Fire Test One, this time using the large set of measurements available. That is, the work is conducted a posteriori. Many different simulations are conducted and many parameters are adjusted and readjusted until acceptable agreement is reached. Work is focused only on the growth phase of the Dalmarnock fire Test One. The interested reader is referred for more details to Jahn et al. (Jahn, 2010) on which this work is based.

As mentioned before, during the growth phase of Test One the evolution of the HRR is unknown. Moreover, the laboratory experiments of the sofa and similar ignition sources show significant uncertainty. Indeed, this is one of the most important issues addressed in this article. The challenge is to be able to reproduce the HRR such that the fire environment (temperature and smoke) is simulated correctly. The work solves a large and complex inverse problem by trial and error.

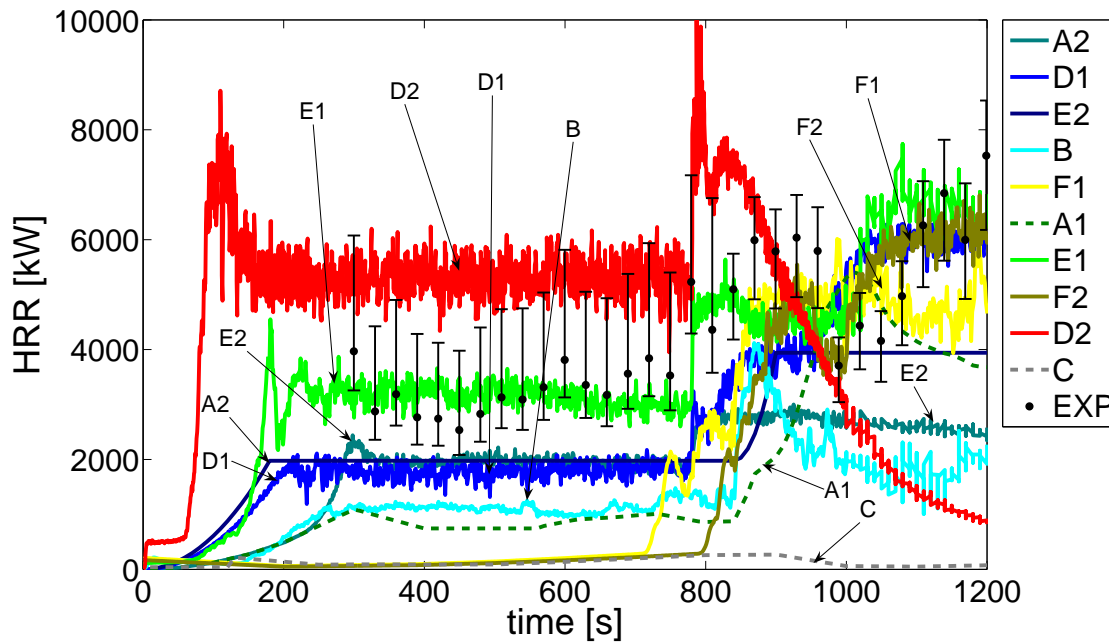


Fig. 11.4 Evolution of the global heat release rate within the compartment. Legend for the different curves: continuous line for CFD simulations; dashed line for zone model simulations; and dotted for the experimental data with error bars. From ignition to growth phase up to flashover and suppression.

11.4 COMPUTATIONAL MODEL

The code Fire Dynamics Simulator v 4.07 (McGrattan, 2003a, McGrattan, 2003b), one of the most commonly used fire CFD codes, is used here. FDS solves a form of the Navier-Stokes equations adequate for low-speed thermally driven flows. While large eddies are solved directly, turbulences at subgrid scale are modelled using Smagorinsky's approach (Smagorinsky, 1963).

FDS is a tool still under active development, and improved versions are released with some frequency. At the time this paper goes to press, FDS v5 had been released and FDSv6 is expected soon. But research has a characteristic time that seems to be longer than the time between version releases of FDS. This means that by the time a research project has been completed and conclusions have been reached, newest versions might be available. While not all of the fine results of this paper might apply directly to FDSv5 or FDSv6, the merit of the study is that the bulk of the conclusions relate to the significant amount of papers in the technical literature where FDSv4 was used, and to current fire safety engineering. This last is particularly important for infrastructure designed, approved and built, and to forensic findings agreed on with the aid of FDSv4.

The computational domain used reproduces in detail the main Dalmarnock compartment and includes the vent openings (two pane windows to the exterior), the nearby kitchen (with another window to the exterior) and the hallway connecting to the apartment entry. The fuel load in the main

compartment was reduced to the fuel elements involved in the growth phase; the sofa, the ignition source and two bookshelves in the corner behind the sofa.

The grid size is one of the most critical parameters in numerical simulations. In the scope of this work a large number of simulations had to be run in order to converge toward good agreement with the measured data and it was therefore necessary to use a sufficiently coarse grid allowing for an efficient use of computational resources. However, too coarse a grid could induce significant numerical errors in the solution. It has been proposed (Dreisbach, 2006, McGrattan, 1998) that to resolve the fire plume properly, the ratio between the characteristic fire diameter and the grid size should be at least 5 to 10.

During the growth phase, the peak of the HRR is ~ 300 kW, and the characteristic diameter of the sofa is around 0.6 m. Hence the grid size should be smaller than 11 cm for an adequate plume resolution. In order to select an adequate grid size, simulation were run with a wide range of different grid sizes: 5 cm, 10 cm, 15 cm and 20 cm edge cubes. The HRR was prescribed according to the laboratory experiment Set 1. Fig. 11.5 shows the temperature vs. height distribution at two different locations in the experimental compartment, one near the burning sofa, and one near the window away from the fire (see Fig. 11.1 for rack locations). The time of comparison is 140 s with data are averaged in time (10 s). The simulations using coarser grids (15 and 20 cm) actually showed better agreement when compared to the measured data, both qualitatively and quantitatively than the finer grids (5 and 10 cm).

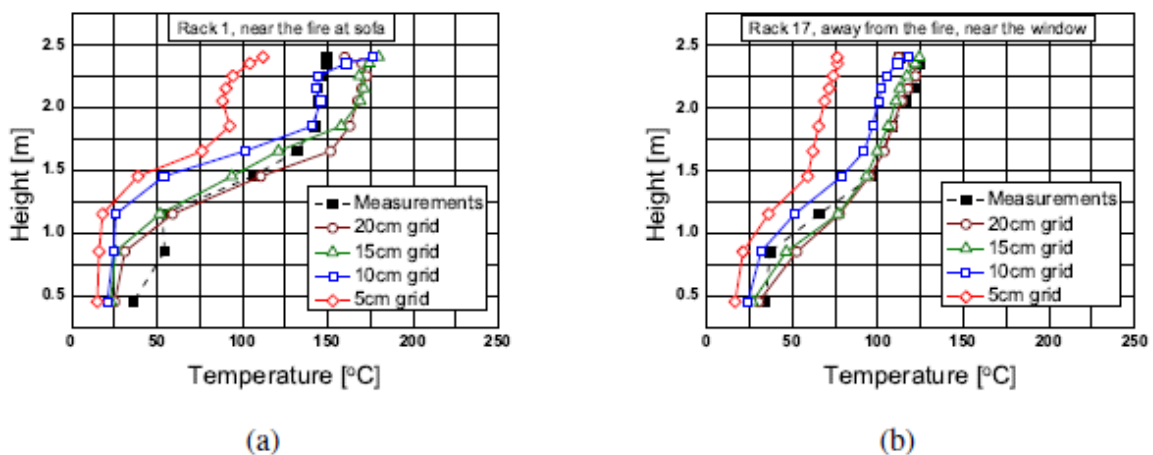


Fig. 11.5 Comparison of results with different grid sizes at 140 s: a) distribution at the north wall next to the bookshelf (rack 1); and b) distribution near the window (rack 17). Data are averaged over 10 s.

Based on this grid dependency study, the 10 cm grid was chosen because it showed good comparison to the experiments, allowed for fast computations and complied with the recommendation associated to the characteristic fire diameter (Dreisbach, 2006, McGrattan, 1998).

11.5 HOT LAYER AVERAGE TEMPERATURE

Two distinct levels of detail are analysed. This section predicts the average hot layer temperature while the next section looks at the distribution of local field temperature and wall heat fluxes. Comparison at detailed level requires a good agreement at averaged level first.

As seen in the Set 1 and Set 2 experiments, the blanket significantly modifies the HRR. A possible HRR of the blanket alone can be estimated assuming quadratic growth and decay phases. The blanket, made of cotton, weighed 1 kg, hence the total combustible energy stored in the blanket including 100 ml of accelerant can be estimated to be around 21 MJ (Jahn, 2008), assuming a heat of combustion of 16.5 MJ/kg for the cotton. The resulting peak HRR would be 150 kW. This is not negligible compared to the measured HRR of the sofa in the early stages, and should therefore be included in the input HRR for the model. Figure 6 shows the reconstructed HRR of the blanket alone and its addition to the HRR of Set 1. The resulting HRR is referred to as Set 1b. Note that here the data is shifted by 150 s compared to Fig. 11.3, so that the ignition occurs at 0 s.

The predicted hot layer average temperature using different HRR and comparison to measurements are shown in Fig. 11.7. For the Set 1 (Fig. 11.7a), the simulated hot layer temperature rise agrees with the measurements during the first 100 s. Results are in lower (up to 50% error) for the simulated average temperatures after $t=100$ s. For Set 1b (Fig. 11.7b), the simulated hot layer temperatures are in good agreement with the measured temperatures (within the instrumental uncertainty) until 200 s into the fire. After that, the simulated temperature decreases in contrast to the measured temperature which rises continually until flashover. For Set 2 (Fig. 11.7c), the average hot layer temperature is overpredicted by about 50% between 25 s and 100 s, and by about 35% between 150 s and 250 s.

Overall, it is seen that Set 1 results in unrealistically low average temperatures for the hot layer, but Set 1b and Set 2 provide predictions closer to the measurements. Thus, it is concluded that Set 1b provides a lower bound to the HRR curve during the growth phase, while Set 2 is an upper bound. This range captures the intrinsic uncertainty of fire growth in real complex scenarios and also includes experimental variability. The uncertainty in the average temperature predictions using these HRR bounds is between 10 and 50%. It confirms that to predict temperatures with reasonable agreement, the HRR must be well characterized.

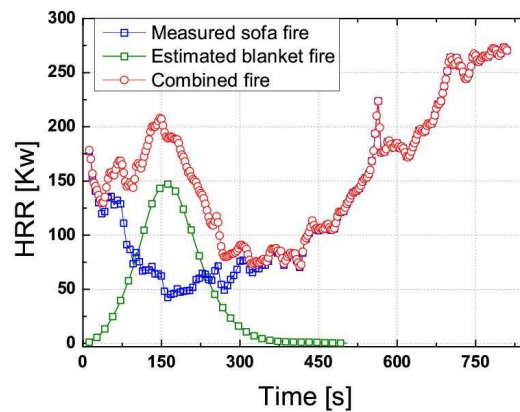


Fig. 11.6 Addition of the blanket to the HRR measured in Set 1 (Measured sofa fire) to obtain Set 1b (combined fire).

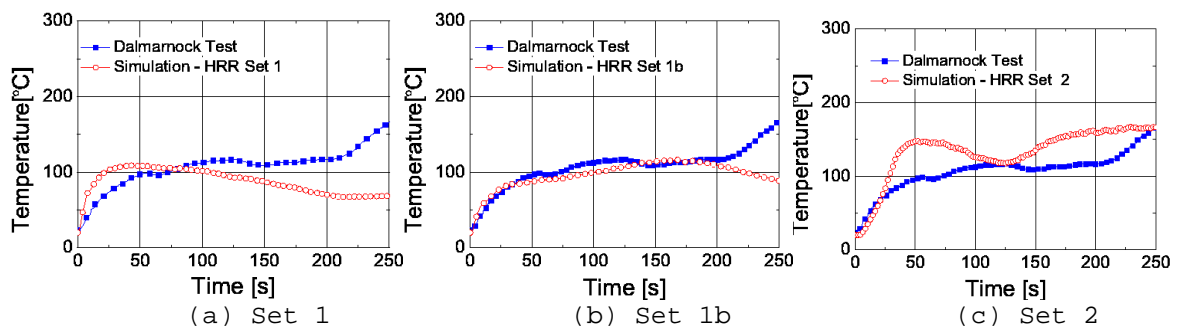


Fig. 11.7 Predicted average hot layer temperatures; a) Set 1; b) Set 1b and c) Set 2.

11.6 COMPARISON OF LOCAL MEASUREMENTS

The density of measurements in Test One presents an opportunity to assess field level simulations. Fig. 11.8 shows the temperature vs. height distributions at different locations (three vertical thermocouple racks) in the experimental compartment using the two bounding HRR curves Set 1b and Set 2. Two different times, 150 s (HRR plateau) and 200 s (rapid HRR rise), are chosen arbitrarily for illustration purposes. In general the simulations are in reasonable agreement with the measurements, although it can be seen that the further away from the burning sofa the better the agreement between measurements and simulations.

As expected the lower and upper HRR bounds result in upper and lower bounds for the smoke temperatures. It is observed that the thickness of the hot layer is not significantly affected by the HRR within the bounds, but the upper HRR leads to higher temperatures in smoke. Within the cold layer, the simulations underpredict the temperature even for the upper HRR bound. This indicates that the Dalmarnock Fire Test had a less well defined hot layer than predicted.

At thermocouple rack 7, roughly 1.5 m from the fire, the temperatures are underpredicted by 20-200% at 150 s (Fig. 11.8a) for both lower HRR bound (Set 1b) and the upper HRR bound (Set 2). At

rack 11, near the centre of the compartment, and 150 s into the fire (Fig. 11.8b) the simulations with both input HRR curves are in good agreement with the measured data lying within the experimental error in the hot layer, and underpredicting the temperatures in the cold layer by about 40%. At rack 19, near the window, and 150 s (Fig. 11.8c), the lower HRR bound produces temperatures that lie within the experimental error in the hot layer, while the upper HRR bound results in overprediction by about 30%.

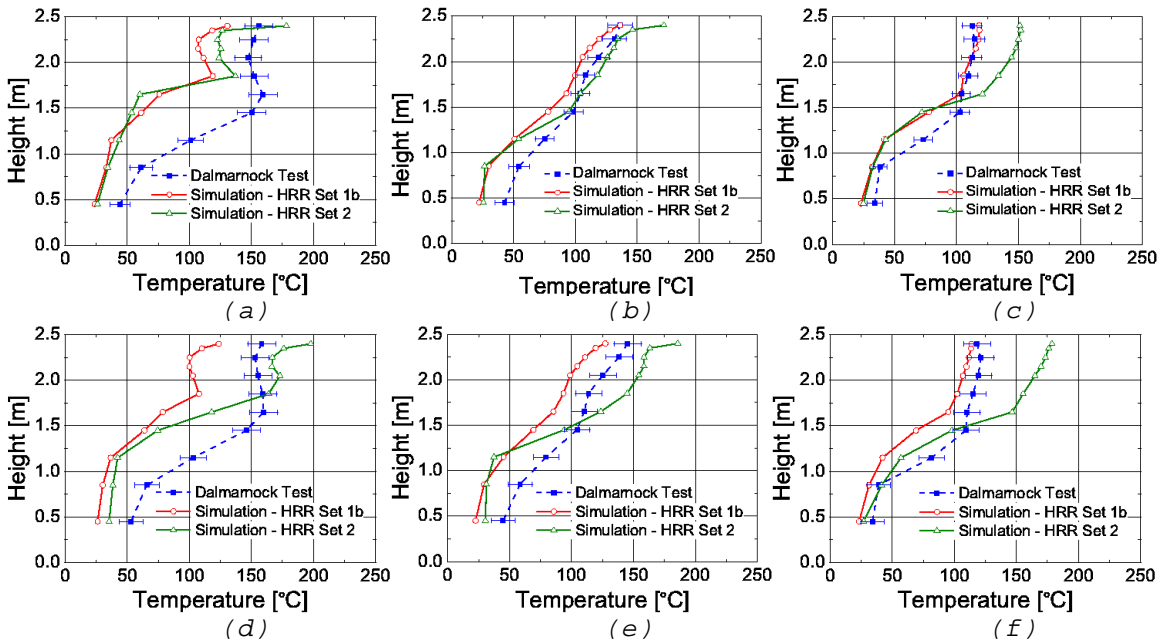


Fig. 11.8 Temperature vs. height distribution at different locations in the compartment at 150 s (a,b and c) and 200 s (d, e and f). Thermocouple rack 7 (a,d) is located near the fire, rack 11 (b,e) is located near the centre of the compartment, and rack 19 (c,f) is located near the window. See Fig. 1 for rack location.

Data are averaged over 10 s.

At 200 s the hot layer temperatures at rack 7 are slightly overestimated (although close to the experimental error, Fig. 11.8d) when using the upper HRR bound, and underestimated by around 35% when using the lower HRR bound. The cold layer temperatures are underestimated by 50-100% for both input HRR curves. At rack 11 temperatures simulated with the lower HRR bound are underpredicted by less than 20% in the hot layer (Fig. 11.8e), having similar shape to the measured distribution. With the upper HRR bound as input, the temperatures at rack 11 are overpredicted by about 25% in the hot layer, but underpredicted by about 35% in the cold layer, thus indicating higher temperature differences between hot and cold layer. Near the window, at rack 19 (Fig. 11.8f), the temperatures are in good agreement with the lower HRR bound as input, although the predicted hot layer height is around 0.5 m higher than that observed. But the upper HRR bound overpredicts the hot layer temperature by 40%,

which is in accordance to the overprediction by around 40% of the hot layer average temperature resulting from the upper HRR bound at 200 s (Fig 11.7c).

11.7 CONCLUSIONS

This work presents a detailed account of the modelling of Dalmarnock Test One. A priori and a posteriori simulations of the growth phase were compared against detailed measurements.

A priori simulations overpredicted the hot layer temperature by 20-500%, whereas a posteriori simulations were able to reduce the error to 10-50%. For the field values, a priori simulations overpredicted the local temperatures by 20-800%, and a posteriori simulation reduced it to 20-200%.

Comparison of the field temperatures in the experimental compartment show that far away from the fire, the simulations are capable of capturing the temperature vs. height distribution of the gas phase (provided an acceptable HRR is input), while close to the fire important differences between simulations and measurements were consistently observed, both qualitatively and quantitatively.

Three main conclusions are reached:

- Even in a posteriori simulations (with full access to the measurements), it is not easy to satisfactorily reproduce the fire.
- The incapability of predicting fire growth is shown to be a fundamental constraint to fire modelling.
- When the HRR is unknown as it is in most practical cases, the use of lower and upper HRR bounds should be included as to reflect in the predictions the effect of uncertainty in the HRR. This is an important issue for the application of fire modelling to real scenarios when the HRR is unknown (ie, forensic investigations and assumed design scenarios).

References

- Emmons, 1985: Emmons H., The Further History of Fire Science, *Combustion Science and Technology*, 40(1):167–174, 1984 (reprinted in *Fire Technology* 21 (3), pp. 230-238, 1985, doi: 10.1007/BF01039976).
- McGrattan, 2005: McGrattan K., Fire Modelling: Where Are We? Where Are We Going?, *Fire Safety Science*, 8:53–68, 2005, doi:10.3801/IAFSS.FSS.8-53.
- Ma, 2003: Ma T., Quintiere J., Numerical simulation of axi-symmetric fire plumes: accuracy and limitations, *Fire Safety Journal*, 38(5):467–492, 2003.
- Hasib, 2007: Hasib R., Kumar R., Shashi, Kumar S., Simulation of an Experimental Compartment Fire by CFD, *Building and Environment*, 42(9):3149–3160, 2007.
- Lattimer, 2003: Lattimer B., Hunt S., Wright M, Sorathia U., Modeling fire growth in a combustible corner, *Fire Safety Journal*, 38(8):771–796, 2003.
- McGrattan, Bouldin, 2005: McGrattan K., Bouldin C., Forney G., Computer Simulation of the Fires in the World Trade Center Towers (Draft), Technical report, NIST, 2005.
- Grosshandler, 2005: Grosshandler W., Bryner N., Madrzykowski D., Report of the Technical Investigation of The Station Nightclub Fire, Technical report, NIST, 2005.

- Hofmann: Hofmann A., Muehlnikel R., Experimental and numerical investigation of fire development in a real fire in a five-storey apartment building. *Fire and Materials*, n/a. doi: 10.1002/fam.1065.
- Rein, 2009: Rein G., Torero J.L., Jahn W., Stern-Gottfried J., Ryder N.L., Desanghere S., Lazaro M., Mowrer F., Coles A., Joyeux D., Alvear D., Capote J., Jowsey A., Abecassis-Empis C., Reszka P., Round-Robin Study of a priori Modelling Predictions of the Dalmarnock Fire Test One, *Fire Safety Journal*, 44 (4):590–602, 2009. doi:10.1016/j.firesaf.2008.12.008.
- Kwon, 2007: Kwon J.W., Dembsey N., Lautenberger C., Evaluation of FDS v.4: Upward Flame Spread, *Fire Technology*, 43 (4):255–284, 2007, doi:10.1007/s10694-007-0020-x.
- Reneke, 2001: Reneke P., Peatross M., Jones W., Beyler C., Richards R., A Comparison of CFAST Predictions to USCG Real-Scale Fire Tests, *Journal of Fire Protection Engineering*, 11:43–68, 2001. doi:10.1106/HH4D-0CKMJ53X-FQK1.
- Miles, 2002: Miles S., Kumar S., Cox G., Comparisons of Blind Predictions of a CFD Model with Experimental Data, *Fire Safety Science*, 6:543–554, 2002, doi:10.3801/IAFSS.FSS.6-543.
- Rinne, 2007: Rinne T., Hietaniemi J., Hostikka S., Experimental Validation of the FDS Simulations of Smoke and Toxic Gas Concentrations, VTT Working Papers 66, 2007. <<http://www.vtt.fi/inf/pdf/workingpapers/2007/W66.pdf>>
- Jahn, 2010: Jahn W., Rein G., Torero J.L., A posteriori modelling of the growth phase of Dalmarnock Fire Test One, *Building and Environment* (2010), doi:10.1016/j.buildenv.2010.11.001.
- Rein, 2007: Rein G., Abecassis-Empis C., Carvel C., editors. The Dalmarnock Fire Tests: Experiments and Modelling. ISBN 978-0-9557497-0-4. The University of Edinburgh, 2007 <www.era.lib.ed.ac.uk/handle/1842/2037>.
- Abecassis-Empis, 2007: Abecassis-Empis C., Reszka P., Steinhaus T., Cowlard A., Biteau H., Welch S., Rein G., Characterisation of Dalmarnock Fire Test One, *Experimental Thermal and Fluid Science*, 32(7):1334–1343, 2008. doi:10.1016/j.expthermflusci.2007.11.006
- Steinhaus, 2007: Steinhaus T., Jahn W., Full-Scale Furniture Tests, Internal Publication BRE Centre for Fire Safety Engineering, University of Edinburgh, 2007.
- Drysdale, 1998: Drysdale D., An Introduction to Fire Dynamics, ISBN 0-471-97290-8. Wiley & Sons, New York, 2nd edition, 1998.
- McGrattan, 2003a: McGrattan K., Fire Dynamics Simulator (Version 4) – Technical Reference Guide. NISTIR 6783, 2003.
- McGrattan, 2003b: McGrattan K., Fire Dynamics Simulator (Version 4) – User’s Manual. NISTIR 6784, 2003.
- Smagorinsky, 1963: Smagorinsky J., General Circulation Experiments with the Primitive Equations, the Basic Experiment, *Monthly Weather Review*, 91(3):99–164, 1963. doi:10.1175/1520-0493(1963)091<0099:GCEWTP>2.3.CO;2
- Jahn, 2008: Jahn W., Rein G., Torero J.L., The Effect of Model Parameters on the Simulation of Fire Dynamics, *Fire Safety Science*, 9:1341–1352, 2008. doi:10.3801/IAFSS.FSS.9-1341. <<http://hdl.handle.net/1842/2696>>
- Dreisbach, 2006: Dreisbach J., McGrattan K., Verification and Validation of Selected Fire Models for Nuclear Power Plant Applications, Volume 6: FDS. Technical report, U.S. Nuclear Regulatory Commission, Office of Nuclear Regulatory Research, 2006.
- McGrattan, 1998: McGrattan K., Rehm R., Baum H., Large Eddy Simulations of Smoke Movement, *Fire Safety Journal*, 30(2):161–178, 1998.

Kalliopi Zografopoulou, kazograf@gmail.com

WG3 - Mistakidis E., emistaki@gmail.com

12 FDS – CFD ANALYSIS OF TEMPERATURE DEVELOPMENT IN AN ENCLOSURE FROM A FIRE WITH A DEFINED HEAT RELEASE RATE

Summary

In this benchmark study, a fire experiment in a small enclosure is simulated with the use of Computational Fluid Dynamics (CFD). The geometry and material properties of the enclosure along with the recorded Heat Release Rate of the fire of the actual experiment are used as input to create the model. The temperatures that are predicted by the CFD analysis at specific points inside the compartment are compared with the experimental values that were recorded during the test. The predicted temperature values are in close agreement with the experimental results, and the described model could be used as a benchmark test for CFD software.

12.1 DESCRIPTION OF THE EXPERIMENT

12.1.1 Geometry

In a series of experiments by Lonnermark and Ingason (BRANFORSK project) that were performed to study the fire spread in large industrial premises and warehouses, one of the tests was a set up to study the influence of the enclosure in the fire spread. Three tests with different enclosure dimensions were performed. Among them, the test with the smallest enclosure dimensions, which consisted of a compartment of 1.00 x 1.00 x 0.925 m, is used here for the benchmark study. In the specific test, one of the walls had an opening of 0.30 x 0.30 m. The setup of the enclosure test is given in Fig. 12.1.

Five thermocouples were placed in the enclosure, one in the opening and four on a thermocouple tree in one of the corners. The thermocouple in the opening was placed 5cm below the soffit of the opening, on the vertical centerline. The thermocouple tree was placed in a distance of 10cm from each wall, in one of the front corners. The thermocouples on the tree were positioned at a distance of 5cm, 10cm, 20cm and 50cm below the ceiling. The recorded Heat Release Rate (HRR) and temperature-time histories of the test are given in Fig. 12.2 and Fig. 12.3 respectively.

12.1.2 Thermal properties

The fuel used in the experiment was a wood crib occupying approximately a floor area of 0.30x0.30m. The Heat Release Rate of the burning wood crib was recorded during the test (Fig. 12.2). The material of the compartment walls was not given in the test report.

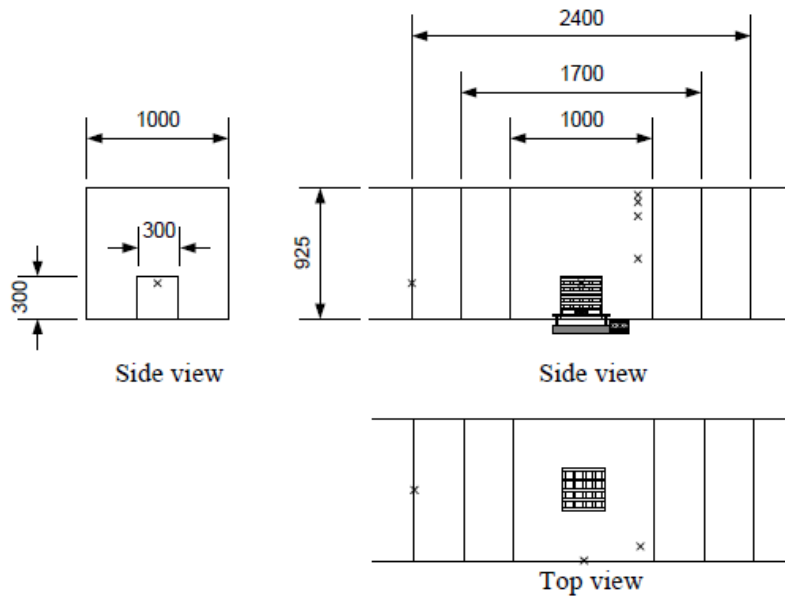


Fig. 12.1 Side view and top view of the experiment's setup. The mark (x) indicates the position of the thermocouples. Dimensions in mm (Lonnermark and Ingason)

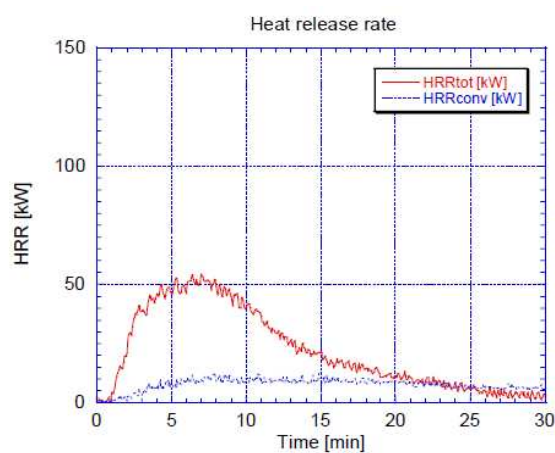


Fig. 12.2 Recorded Heat Release Rate of the burning wood crib during the test. (Lonnermark and Ingason)

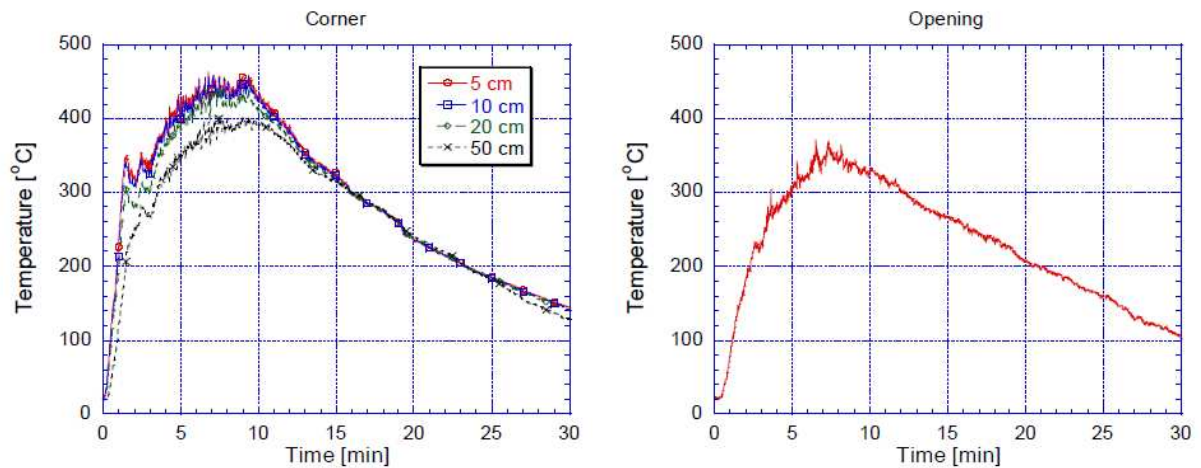


Fig. 12.3 Recorded temperature-time histories of the thermocouples during the test. (Lonnermark and Ingason)

12.2 MODEL DESCRIPTION

12.2.1 Software

The simulation is performed with Fire Dynamics Simulator (FDS), a Computational Fluid Dynamics code for the simulation of thermally driven flows with an emphasis on smoke and heat transport from fires. The partial derivatives of the conservation equations of mass, momentum and energy are approximated as finite differences, and the solution is updated in time on a three-dimensional, rectilinear grid. Thermal radiation is computed using a finite volume technique on the same grid as the flow solver. Lagrangian particles are used to simulate smoke movement, sprinkler discharge, and fuel sprays.

FDS is capable of performing either a Direct Numerical Simulation (DNS) for the solution of the partial differential equations, or implementing a Large Eddy Simulation (LES) code, which models separately the effect of the small scale structures thus, simplifying the overall computational domain. In the proposed problem, the LES solver option is used.

12.2.2 Geometry

Due to the symmetry of the geometry of the enclosure and the opening placement, only half of the compartment is simulated. In the numerical model the internal sides of the enclosure are placed at the distances provided in the experiment description, and an arbitrary width of 0.05m is used for the wall width, as this information was not given in the test report. The model dimensions are given in Fig. 12.4 and a 3-d view of the model in Fig. 12.5.

The whole compartment is presented but only half of it is used for the numerical simulation (dimensions in cm).

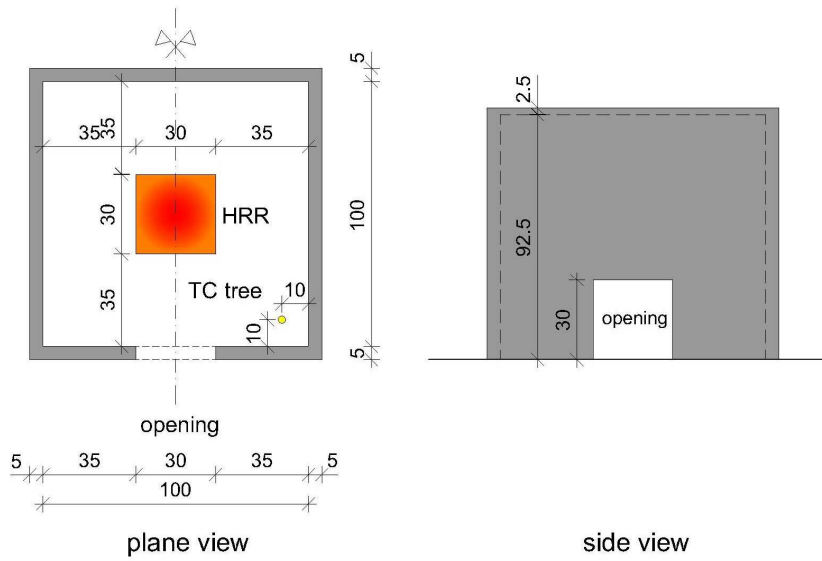


Fig. 12.4 Geometry of the model.

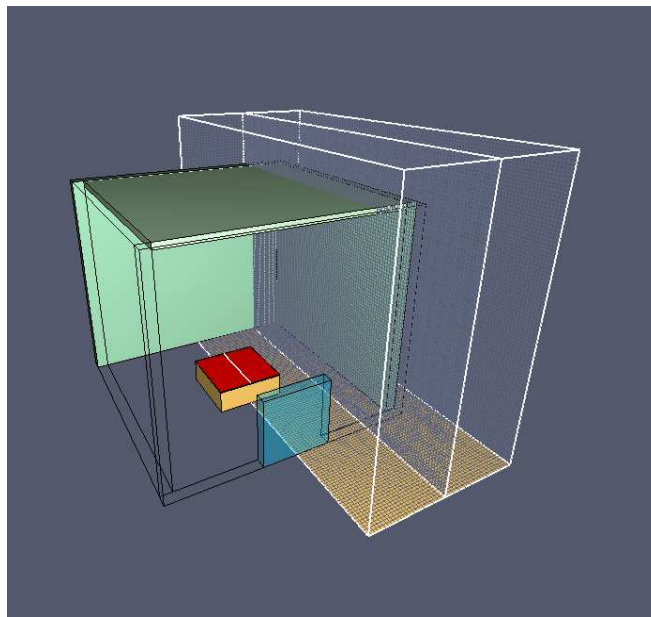


Fig. 12.5 3-d view of the model and computational meshes.

12.2.3 Material properties

The actual materials of the enclosure walls were not given in the experiment report. However, considering the type of the experiment and the fact that the walls were adjustable, the properties of gypsum plaster were used in the simulation. The thermal properties of gypsum plaster that are used in the model are given in Tab. 12.1.

Tab. 12.1 Thermal properties of gypsum plaster

| Gypsum Plaster | |
|----------------------------|--------|
| Specific Heat [kJ/(kg. K)] | 0.84 |
| Conductivity [W/(m.K)] | 0.48 |
| Emissivity | 0.9 |
| Absorption Coeff. [1/m] | 0.0005 |

12.2.4 Fire properties

A key factor of the present benchmark test is the prediction of compartment temperature time histories, by providing as main input the Heat Release Rate – time curve of the fire. In fire development simulations, the HRR is the major indicator of the intensity of the fire and is widely used as the sole input that describes the compartment fire in the analysis. In the present simulation, the recorded HRR – time curve of the experiment is used as input for the fire description. The experimental and the simplified for the model input HRR curves are given in Fig. 12.6. Since the HRR in FDS is described per m^2 , the model HRR values were adjusted so that the HRR of the experiment would correspond to the $0.30 \times 0.30 \text{ m}^2$ area of the HRR section in the model. The HRR section is positioned 10 cm above the floor. In Tab. 12.2 the mathematical description of the model’s input HRR fire curve is given.

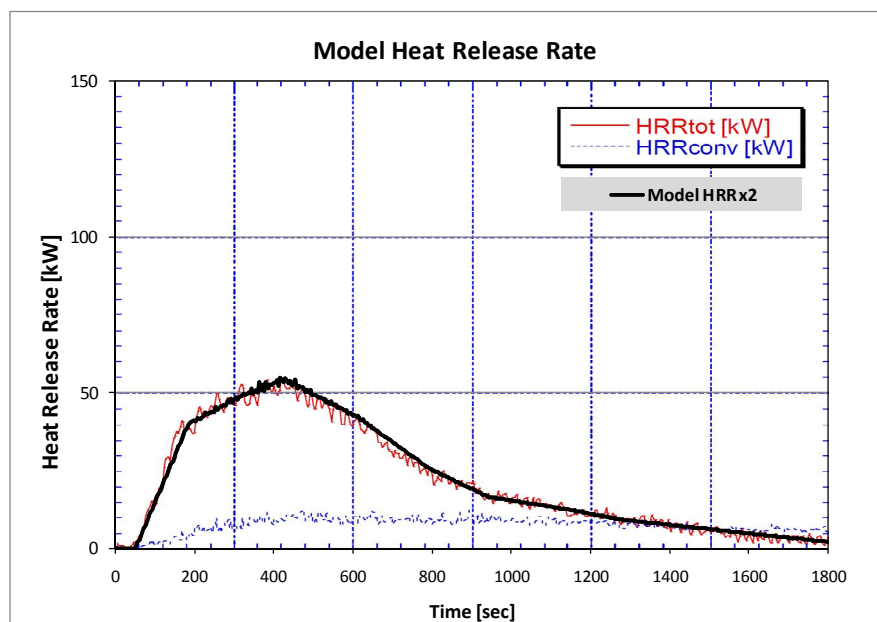


Fig. 12.6 Experiment and model calculated Heat Release Rate curves.

12.2.5 Computational mesh

The half of the model that was simulated was divided in two meshes for parallel calculation (Fig. 12.7). Each mesh was divided in 259.200 uniform cells of dimensions $0.01 \times 0.01 \times 0.01 \text{ m}$. In total, the

computational domain consisted of 518.400 cells. The above mentioned mesh division resulted in the best agreement between the numerically obtained and experimentally recorded temperature time histories in the thermocouple tree, and especially in the thermocouples that were placed close together near the ceiling of the enclosure. The mesh is extended by 50 cm in front of the opening, to allow for better simulation of the flow in front and outside of the opening. The mesh height is 1.20m and the time step was set not to exceed 0.1 sec. The simulation time was 1800 sec.

Tab. 12.2 FDS model custom HRR curve data

| Model Heat Release Rate curve | |
|----------------------------------------------------|-----------------|
| Heat Release Rate per Unit Area = 604.44 kW | |
| Time [s] | fraction |
| 0.0 | 0.000 |
| 48.0 | 0.000 |
| 181.0 | 0.736 |
| 314.0 | 0.906 |
| 419.0 | 1.000 |
| 610.0 | 0.774 |
| 790.0 | 0.472 |
| 943.0 | 0.302 |
| 1105.0 | 0.245 |
| 1276.0 | 0.170 |
| 1800.0 | 0.038 |
| 1860.0 | 0.000 |

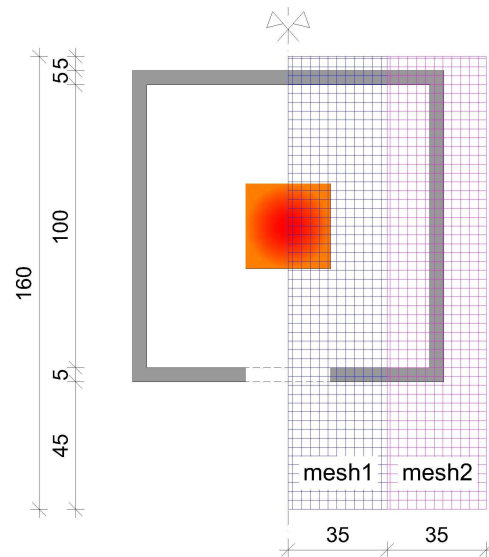


Fig. 12.7 Mesh division and dimensions (cm)

12.2.6 Other model parameters

The Large Eddy Simulation method was used for the analysis, with its parameters set at the FDS default values. Any parameters that are not described are set to the default values used by the software. The complete FDS input file is given in Appendix A.

12.3 RESULTS

The temperature-time histories obtained from the simulation are compared with the temperatures recorded by the thermocouples in the experiment. In figures (Fig.12.8, 12.9, 12.10, 12.11) each numerically obtained time history is plotted separately against the test results. In Fig. 12.12 all the predicted temperature time histories of the model are given and the variation in the temperatures between the different heights can be observed.

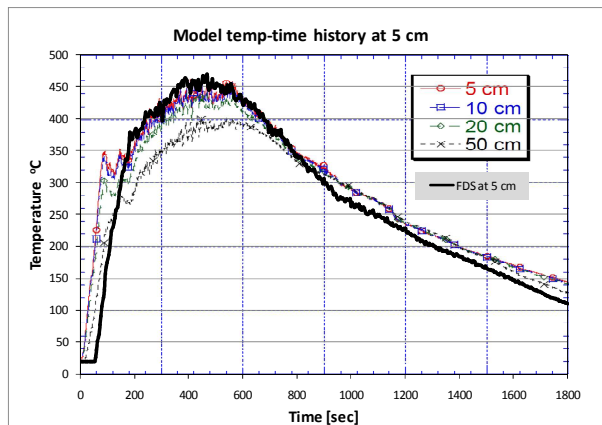


Fig. 12.8

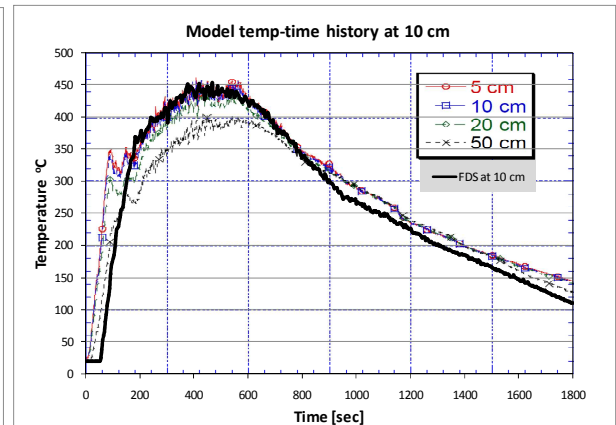


Fig. 12.9

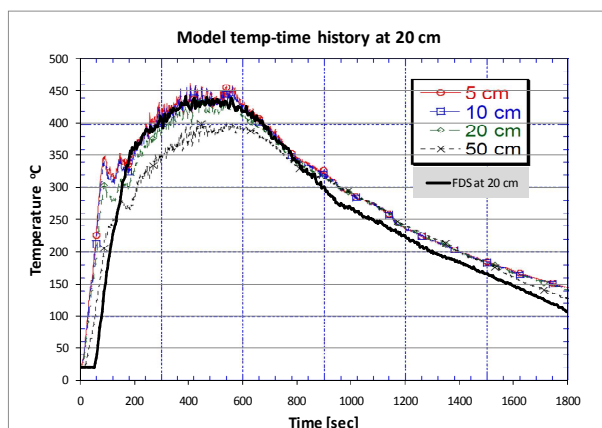


Fig. 12.10

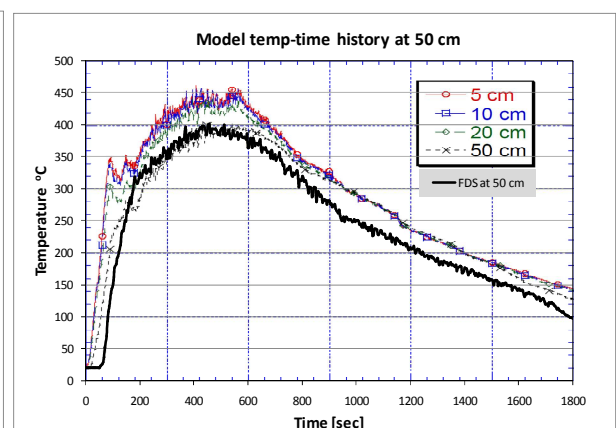


Fig. 12.11

Figs. 12.8, 9, 10, 11 Numerically obtained and experimentally recorded temperature-time histories for the four different points in the model (the background in the plot area is taken from the experiment report).

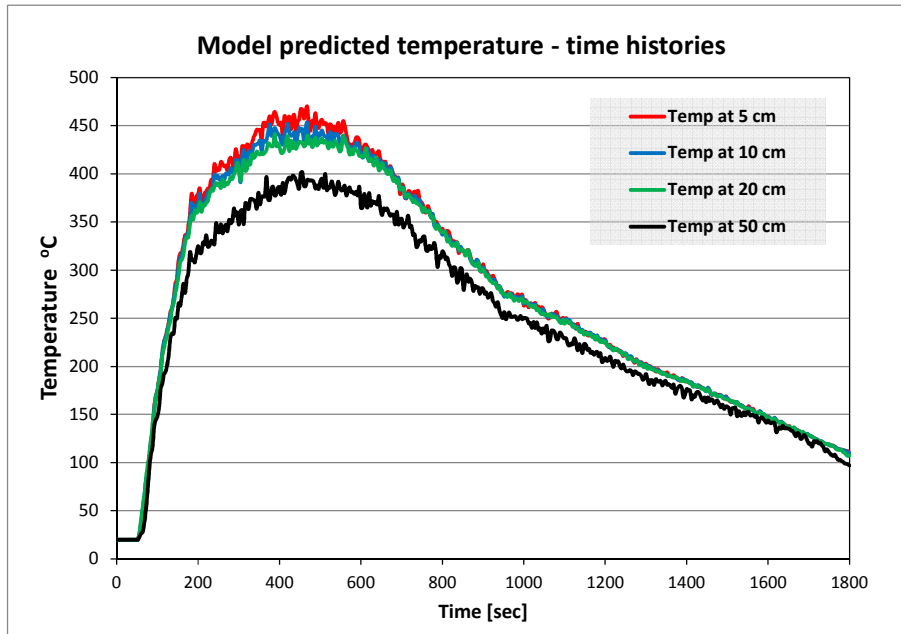


Fig. 12.12 Numerically obtained temperature-time histories for the four different points in the model.

In the present study a direct comparison between the temperature time histories of one experiment, and the corresponding temperatures obtained at specific points by the model is performed. The results of the FDS model are compared with the experimental ones in order to display that the model is a valid representation of the experiment.

In figures 12.8 – 12.11 it is shown that the calculated maximum temperatures are very close to the experimental recordings, in all four points. There is a delay of about 50 sec in the temperature rise at the beginning of the simulation, which is clearly caused by the denoted delay in the HRR of the input fire curve (Fig. 12.6) which starts to escalate after exactly 48 sec. Also there is a small difference between the experiment and the calculated temperature at the decay phase, of approximately 20-30 °C. However the slope of the calculated and experimental results is almost the same.

12.4 SUMMARY

A Computational Fluid Dynamics – Large Eddy Simulation analysis of an enclosure fire with a defined Heat Release Rate curve is presented, which can be considered as a simple benchmark case for CFD software. It consists of a small cubical compartment with an opening at one of the walls and a fire breaking inside. The fire is specified by its Heat Release Rate (HRR) curve which is the most indicative and widely used parameter of fire intensity. With the specified HRR curve as input, gas temperatures are calculated at different heights at one of the corners of the compartment and temperature-time histories are obtained. The calculated temperatures are in close agreement to the experimental results. Most of the FDS analysis parameters are set to default values and the results are produced without any extra calibration of the model, thus it is suggested as a simple, yet very useful benchmark case for fire

simulations, which includes the basic case of temperature prediction through combustion calculation, given an explicitly (through the HRR) described fire.

References

Fire Dynamics Simulator and Smokeview, FDS-release5.5.3 SMV-release5.6,
website:<http://code.google.com/p/fds-smv/>, 2012.

Lönnermark, 2005, Lönnermark A, Ingason H., Fire Spread in Large Industrial Premises and Warehouses,
SP Swedish National Testing and Research Institute, 2005.

Appendix A

benchmark_enclosure.fds

Oct 4, 2013 12:38:11 PM

&HEAD CHID='benchmark_enclosure', TITLE='benchmark_enclosure'/

&TIME T_END=1800.0, DT=0.1/

&DUMP RENDER_FILE='benchmark_enclosure.ge1', COLUMN_DUMP_LIMIT=.FALSE., NFRAMES=450/

&MESH ID='MESH01', IJK=24,120,90, XB=0.5,0.85,-0.5,1.1,0.0,1.2/

&MESH ID='MESH02', IJK=24,120,90, XB=0.85,1.2,-0.5,1.1,0.0,1.2/

&DEVC ID='A-05', QUANTITY='TEMPERATURE', XYZ=0.9,0.1,0.875, ORIENTATION=-1.0,1.0,0.0/

&DEVC ID='A-10', QUANTITY='TEMPERATURE', XYZ=0.9,0.1,0.825, ORIENTATION=-1.0,1.0,0.0/

*&DEVC ID='A-20', QUANTITY='TEMPERATURE', XYZ=0.9,0.1,0.725, ORIENTATION=-1.0,1.0,0.0/&DEVC ID='A-50',
QUANTITY='TEMPERATURE', XYZ=0.9,0.1,0.45, ORIENTATION=-1.0,1.0,0.0/*

&MATL ID='GYPSUM PLASTER',

FYI='Quintiere, Fire Behavior - NIST NRC Validation',

SPECIFIC_HEAT=0.84,

CONDUCTIVITY=0.48,

DENSITY=1440.0/

&SURF ID='gypsum_plaster',

RGB=146,202,166,

MATL_ID(1,1)='GYPSUM PLASTER',

MATL_MASS_FRACTION(1,1)=1.0,

THICKNESS(1)=0.05/

&SURF ID='burner-604',

COLOR='RED',

HRRPUA=604.44,

RAMP_Q='burner-604_RAMP_Q'/

&RAMP ID='burner-604_RAMP_Q', T=0.0, F=0.0/

&RAMP ID='burner-604_RAMP_Q', T=48.0, F=0.0/

&RAMP ID='burner-604_RAMP_Q', T=181.0, F=0.736/

&RAMP ID='burner-604_RAMP_Q', T=314.0, F=0.906/

&RAMP ID='burner-604_RAMP_Q', T=419.0, F=1.0/

&RAMP ID='burner-604_RAMP_Q', T=610.0, F=0.774/

&RAMP ID='burner-604_RAMP_Q', T=790.0, F=0.472/

&RAMP ID='burner-604_RAMP_Q', T=943.0, F=0.302/

&RAMP ID='burner-604_RAMP_Q', T=1105.0, F=0.245/

&RAMP ID='burner-604_RAMP_Q', T=1276.0, F=0.17/

&RAMP ID='burner-604_RAMP_Q', T=1800.0, F=0.038/

&RAMP ID='burner-604_RAMP_Q', T=1860.0, F=0.0/

&OBST XB=-0.05,0.0,0.0,1.0,0.0,0.95, SURF_ID='gypsum_plaster'/ WALL1

&OBST XB=1.0,1.05,0.0,1.0,0.0,0.95, SURF_ID='gypsum_plaster'/ WALL1[1]

&OBST XB=-0.05,1.05,-0.05,0.0,0.0,0.95, SURF_ID='gypsum_plaster'/ Obstruction

&OBST XB=-0.05,1.05,1.0,1.05,0.0,0.95, SURF_ID='gypsum_plaster'/ Obstruction[1]
&OBST XB=0.35,0.65,0.35,0.65,0.0,0.1, SURF_ID='INERT'/ Obstruction
&OBST XB=0.85,0.995833,-0.00666667,0.993333,0.92,0.946667, COLOR='INVISIBLE', SURF_ID='gypsum_plaster'/
Slab
&OBST XB=0.5,0.85,-0.00666667,0.993333,0.92,0.946667, COLOR='INVISIBLE', SURF_ID='gypsum_plaster'/ Slab
&HOLE XB=0.35,0.65,-0.05,0.0,0.0,0.3/ Hole
&VENT SURF_ID='MIRROR', XB=0.5,0.5,-0.5,1.1,0.0,1.2, COLOR='INVISIBLE'/ Vent Min X for MESH03
&VENT SURF_ID='OPEN', XB=0.85,0.85,-0.5,1.1,0.0,1.2, COLOR='INVISIBLE'/ Vent Max X for MESH03
&VENT SURF_ID='OPEN', XB=0.5,0.85,-0.5,-0.5,0.0,1.2, COLOR='INVISIBLE'/ Vent Min Y for MESH03
&VENT SURF_ID='OPEN', XB=0.5,0.85,1.1,1.1,0.0,1.2, COLOR='INVISIBLE'/ Vent Max Y for MESH03
&VENT SURF_ID='OPEN', XB=0.5,0.85,-0.5,1.1,1.2,1.2, COLOR='INVISIBLE'/ Vent Max Z for MESH03
&VENT SURF_ID='OPEN', XB=0.85,0.85,-0.5,1.1,0.0,1.2, COLOR='INVISIBLE'/ Vent Min X for MESH04
&VENT SURF_ID='OPEN', XB=1.2,1.2,-0.5,1.1,0.0,1.2, COLOR='INVISIBLE'/ Vent Max X for MESH04
&VENT SURF_ID='OPEN', XB=0.85,1.2,-0.5,-0.5,0.0,1.2, COLOR='INVISIBLE'/ Vent Min Y for MESH04
&VENT SURF_ID='OPEN', XB=0.85,1.2,1.1,1.1,0.0,1.2, COLOR='INVISIBLE'/ Vent Max Y for MESH04
&VENT SURF_ID='OPEN', XB=0.85,1.2,-0.5,1.1,1.2,1.2, COLOR='INVISIBLE'/ Vent Max Z for MESH04
&VENT SURF_ID='burner-604', XB=0.35,0.65,0.35,0.65,0.105,0.105/ Vent
&TAIL /

13 THE COMPARISON OF THE RESULTS OF A FULL SCALE EVACUATION TEST TO THE CALCULATION METHOD OF HUNGARIAN REGULATIONS AND TO THE PATHFINDER SOFTWARE

Summary

Action of people in different building has large scale of uncertainty and there is poor availability of experimental data describing it. Evacuation software might be a solution of the problem, but their validation is a key issue. To analyze these key questions, a full scale test was conducted with more than 200 persons participating in it. The test was divided to two phases, first the comparison to Hungarian regulations with a numerical method taking the speed, the width of doors and stairs into consideration and then the comparison to three calculation methods of Pathfinder software. The criteria of calculation defined by the AHJ resulted two different egress scenarios. There were interesting differences between the results of the full scale test, the calculation and the three simulation methods, and also the reasons of the differences were interesting. We show the calculation method of the door- and path selection procedure according to the Hungarian regulations and to the Pathfinder software, and a method of utilising them.

13.1 INTRODUCTION

The evacuation of buildings and open air event areas in Hungary is controlled by the 28/2011. (IX. 6.) BM regulation, concerning the National Fire Safety Codes & Standards (NFSCS). This regulation is a law, therefore obeying it is obligatory. Designers and authorities began to doubt the evacuation proceedings due to the development of architecture and the needs of the modern age. As a result of architectural development, bigger and bigger buildings are constructed and in such buildings the number of escape routes may rise dramatically. Due to the needs of the modern age, such technological devices are installed into the buildings some of which have a favourable effect and some of which have an unfavourable effect on the evacuation proceedings.

Evacuation aims to provide people a way to leave the building in safety. The method of analysis provided by the law is not detailed enough to reach a safe enough solution. Since the number of variants is high during the evacuation process and also, the effect of these variants on each other is rather high, the analysis without computer simulation is extremely difficult. However, using softwares may generate doubts. The question is whether we can accept these results or not.

Validations can help to answer these questions. Validation is a process during which we analyse a real scale experiment with the help of a software as well, and then the data of the analyses are compared to each other. After the assessment of the comparison we can decide how trustworthy the given software is to be considered. Today in Hungary Pathfinder is one of the most widespread evacuation simulator softwares. This program offers several calculation methods that can be used during a simulation.

There are validation documents available to the software that we all know but we wanted to gather our own experiences concerning the credibility of the program. Thus, the aim of the analysis is to find out how reliable the program is and to decide which of the three calculation methods reflects reality in its fullest, indicating the level of safety as well at the same time.

13.2 REAL EXPERIMENT

13.2.1 Describing the location

According to the evacuation calculation carried out based on the regulation, Dance Club would provide room for too few people, and this way, the club wouldn't be profitable (the owners say). Larger parties have already been organised in the club and authorities did not find the evacuation of the place problematic (only on-sight evaluation was conducted). The owners decided to start an analysis, in order to find real possible solutions that are safe. Evacuation simulations were run with Pathfinder's three simulation modes and one of the results would have been acceptable by the owners but since the results were different, it was necessary to make further calculations. After the discussions with the National Directorate General for Disaster Management, Ministry of the Interior (NDGDM) the next analysis took place on the location.

The NDGDM defined the Dance Club as a disco that can be found on the 3-4-5-6th levels of a six-storey building. Its only entrance is on the 3rd level at the meeting point of the hanging corridor surrounding the building and the overhead pedestrian crossing that leads to the railway station. Before and after the evacuation, the participants were to be found on the hanging corridor or on the overhead crossing.

The floor area of the various levels can be seen on Table 13.1. Net floor area doesn't include areas where built-in furniture and equipment can be found.

Tab 13.1 Dance Club

| Dance Club | | |
|------------|----------------------|---------------------|
| Level | Gross floor area | Net floor area |
| 3. | 19,76 m ² | 8,35 m ² |
| 4. | 78,25 m ² | 49,4 m ² |
| 5. | 98,64 m ² | 50,3 m ² |
| 6. | 58,75 m ² | 35 m ² |

13.2.2 Variations

Hungarian regulations stipulate that each m² of built-in furniture equals (provides room for) 4 people. Therefore, the distribution of the people who is in the club is to be calculated using the most unfavourable scenario, that is, starting with the furthest point from the entrance and using 4 people / m² units. Owners said that if the distribution of the people would be like above described, then the club wouldn't be able to work so they set a number limit for the maximum people to be let in. This way, they ensure a comfortable atmosphere on all the levels and the club cannot be overcrowded. To solve this, partly access control systems and partly security service are used. Since there are two different ways of control, it was necessary to run the simulation with two different distributions.

Thus, the analysis was carried out using two different methods. Both of these cases were run twice, therefore a total of four evacuation simulations were run. The following were noted down in both cases: the number of people who left the building within 90 seconds after the fire alarm went off, and the time required for the last person to leave the building. The people who left the building were counted after exiting as well. The numbers of the tables were verified using the video recordings.

13.2.2.1 NFSCS (OTSZ) variation

According to table 1, appendix 22 of NFSCS the building has to be evacuated in 90 seconds. When defining the number of people to be allowed in, we have taken net floorspace and the number of people allowed/m² into account (table 3, appendix 22 in NFSCS). In the case of discos, pop concerts and programs that take place in the open (and no seats are provided) this value is 4 people/m² (the number of employees wasn't taken into account). We couldn't fill all the levels of the club because only 243 students participated in the analysis. 1022 participants would have been required to fill the whole place (if we count with 4 people/m²) so we could only fill the upmost floor (see Table 13.2).



Fig. 13.1 The Dance floor

Tab. 13.2 2nd part of the analysis

| Level | Gross floorspace | Visitors | Employees |
|-------------------------------|----------------------|----------|-----------------------------|
| 3. | 19,76 m ² | 0 | Were not taken into account |
| 4. | 78,25 m ² | 0 | Were not taken into account |
| 5. | 98,64 m ² | 103 | Were not taken into account |
| 6. | 58,75 m ² | 140 | Were not taken into account |
| Total: | | 243 | Were not taken into account |
| Total number of participants: | | 243 | |

13.2.2.2 Pre-arranged variation (Owner's distribution)

During the analysis we calculated with those numbers (on the three top levels) that were set by the owners (see table 2). We assumed that there are 14 employees and 206 guests can be found in the

building (220 total). Participants that were employees had pre-defined points of location. Participants could only begin to leave the building after everyone else has left the level they were on.

Tab. 13.3. 1st part of the analysis

| Level | Gross floorspace | Visitors | Employees |
|-------------------------------|----------------------|----------|---------------------------------------------------|
| 3. | 19,76 m ² | 0 | 1 (cloakroom attendant) |
| 4. | 78,25 m ² | 47 | 1 barman + 2 security guards |
| 5. | 98,64 m ² | 94 | 1 DJ + 2 barmen + 2 security guards |
| 6. | 58,75 m ² | 65 | 2 barmen + 2 security guards + 1 business manager |
| Total: | | 206 | 14 |
| Total number of participants: | | 220 | |

13.2.3 Results of the variations

Tab. 13.4 Results of the variations

| Simulation | Number of simulation | People in the club | Simulation | | Number of people exiting in 90 second | Total time required for evacuation |
|------------|----------------------|--------------------|------------|-------|---------------------------------------|------------------------------------|
| | | | Beginning | End | | |
| I. Owner's | 1. | 220 | 10:48 | 10:50 | 164 | 137 |
| | 2. | 220 | 11:02 | 11:04 | 170 | 120 |
| II. NFSCS | 1. | 243 | 11:15 | 1:17 | 158 | 136 |
| | 2. | 239 | 11:25 | 11:27 | 176 | 120 |

13.3 CALCULATIONS OF THE NFSCS (analysis of the 1st and 2nd part)

In Hungary, NFSCS is responsible for regulating the evacuation procedures of buildings. Evacuation analyses have two parts: first, they examine the process of leaving the room, and then the exiting of the building is analysed. In the current scenario, only the first section is regulated because the different levels have one airspace (people are outdoors after exiting it).

The analysis of the 1st section consists of two parts. First, the length of the escape paths is examined, and then they determine how many people can exit the doors in a given period of time. The width of the entrance door is 1.6 m.

Table 1, appendix 22 of NFCS stipulates that rooms with “C”-“E” flammability class in a building with III fire resistance rating it is required that people are evacuated within one and a half minutes.

NFSCS calculations are as follows:

$$t_{1b} = \frac{N_1}{kx_l}$$

where t_{1b} is the evacuation time of the first section (given in minute, considering how many people can exit the doors), N_1 is the number of people in the room, k is the permeability coefficient (value set to determine how many people leave the exit in a given time period) of the exit that has a constant value of 41,7 people/m/m², x_1 is the width of exit N_1 , given in meter.

On the basis of this, a maximum of 100 people (who can reach the exit in one and a half minutes) may exit the narrowest cross-section.

According to the NFSCS:

Time required to evacuate 220 people: 3.29 minutes (198 s)

Time required to evacuate 239 people: 3.59 minutes (216 s)

Time required to evacuate 243 people: 3.64 minutes (219 s)

13.4 SOFTWARE

13.4.1 Introducing the software

The introduction of the software is based on the user's guide and technical reference documents of Pathfinder. Several parts are quote from them. Pathfinder is a simulator program (simulating evacuations and human motion) developed by Thunderhead Engineering. It has a graphical interface used for both 2D and 3D simulations. Thus, the program is capable of analysing an evacuation as time and place changes. The simulation is basically modelled with the help of a 3D triangular mesh that is set up on the dimension of a given building. This mesh can be imported manually or automatically. Objects are not displayed in the mesh directly but they do have a real important role, since participants may only move within this simulation area. Doors are displayed on the verges of the navigation meshes. Doors control the direction people move (although special simulation settings are very important). Stairways can be found on the verges of the meshes as well and they are visualised as triangles. One factor hinders the advancement on stairways, namely the ascent of the stairway. Two doors have to be inserted to create a stairway. These doors function just like the other ones but they are required to "create" a stairway in the user's interface (ensuring the errorless geometric linkage between the stairway and the doors). People are represented as vertical, cylinder-shaped objects, when using single person mode (called inverse control or steering). A given participant may have a uniquely set pathing and special parameters can be also added (maximum velocity, choice of exit, 3D model, etc).

Pathfinder supports two pathing simulation modes. In "steering" mode doors have no effect on the pathing of the participants; this simulation mode uses a steer-control based system instead. This can ensure an optimal distance between the participants present in a simulation. In SFPE mode participants do not attempt to avoid each other (the small circles, representing participants may overlap) but doors do have an effect on their pathing and velocity is affected by the size of the group of exiting participants.

One may change freely between the different simulation modes in the user's interface, so the results can be compared this way.

In steering simulation mode Pathfinder combines path design, navigation and the collision of participants to coordinate the movement of the participants. Participants remain on their path (from their current position, heading to a given point or room), according to the orders given to them. This calculation of paths and participants last throughout the whole simulation. Other factors, such as colliding with other participants may lead to alteration of the original path but normally, the pathing of the participants remains the same. If the distance between the participant and the next point exceeds the threshold limit, then the path is redesigned, adapting to the new scenario.

In SFPE mode Pathfinder uses a flux-based evacuation model, which was published in SFPE Handbook of Fire Protection Engineering (Nelson and Mowrer, 2002) and the SFPE Engineering Guide: Human Behaviour in Fire (SFPE, 2003). As the book says, SFPE calculation is a flux model where the doors and the permeability coefficient of the corridors are given. Navigation geometry consists of three groups in SFPE mode (doors, rooms and stairways). Rooms are open places where participants can move around. Stairways can be considered special rooms where the ascent of the stairway limits velocity. Doors can be considered points that limit participants' movement at the connecting points of rooms and stairways.

There are no corridors in SFPE mode; these are defined as rooms with a door on one side. Thus, corridors are treated just like rooms. Doors control the flow of participants. When the settings are default, participants can be at the same location. Pathfinder allows for the adding of incremental option when using SFPE mode. For instance, the hindrance factor of the doors can be kept and one may add an option so that the program considers collision factor. This way, participants line up at a door.

13.4.2 Comparing the results of the three methods of analysis

The mathematic model, run by the computer models evacuation scenarios, which is basically the computerised analysis of a given case. Several difficulties may arise during traditional analysis methods. When carrying out an analogous analysis, it is not possible to examine the joint effects of geometry, mass or waiting in a line (taking all the details into consideration). This way, all the factors can be analysed that haven't been taken into consideration before.

The simulation was made with Pathfinder, which was developed by Thunderhead Engineering.
Version number: 2011. 1. 1104

Two distribution scenarios were analysed. One of these was the one defined by the NFSCS (4 people/m²) and the other was the one defined by the owners. The simulation aimed to examine what kind of results are produced by the software compared to reality.

13.4.2.1 Default data of the model

There can be given more parameter for the behave of the occupants in the software. The shoulder width and the maximum speed of occupants. The default values at shoulder width and maximum speed are 45,58 cm and 1,19 m/s respectively. The other variable parameters at the simulation parameters are follows:

Max Agent Radius Trim Error: this parameter affects how accurately occupants can navigate through tight spaces when the occupants in the simulation have varying sizes. The default value is: 2,54cm.

Constrain Edge Length is not checked.

In SFPE Mode:

Max Room Density: controls the density at which doors will no longer admit occupants into a room. Default value is 1,88 person/m²

Door Boundary Layer: is a global setting for boundary layer used only by the SFPE, Flow based simulation mode at doors. Default value is 150 mm.

Door Flow Rate is a global setting for algorithm used to calculate door flow rate. Default value is use max flow

In Steering mode:

Collision handling behaves just like in SFPE mode except this is on by default for Reactive Steering.

Inertia forces occupants to ramp up to their maximum speed and down to a stop. Default value is checked.

Steering update interval specifies how often (in simulation time) to update the steering calculation. Default value is 0,1 sec.

13.4.2.2 Geometry

The levels of the club were considered rooms in the simulation (as it is given in Pathfinder's user's guide). Thus, we've examined 4 levels as rooms and additional 4 rooms were required as flight of stairs. The rooms were connected by 10 stairs. The size of these stairs was 17.78 cm – 27.94 cm. An entrance door was also modelled on the entry level. The model was built based on the drawings of the building. This model had 4 levels (entry level and three other), The exit was also to be found on the entry level.

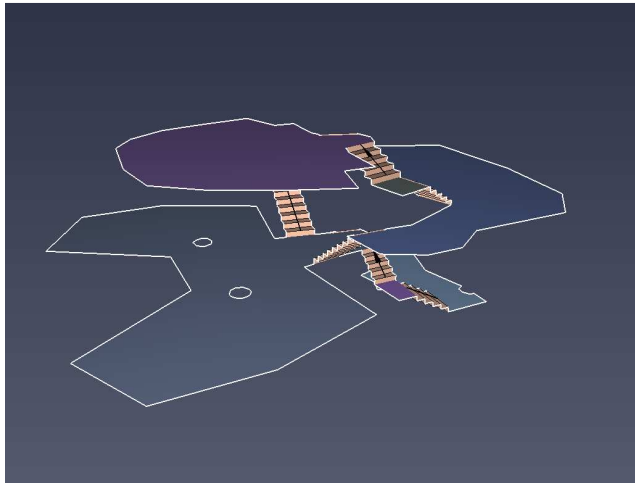


Fig. 13.2. Simulation picture of the club

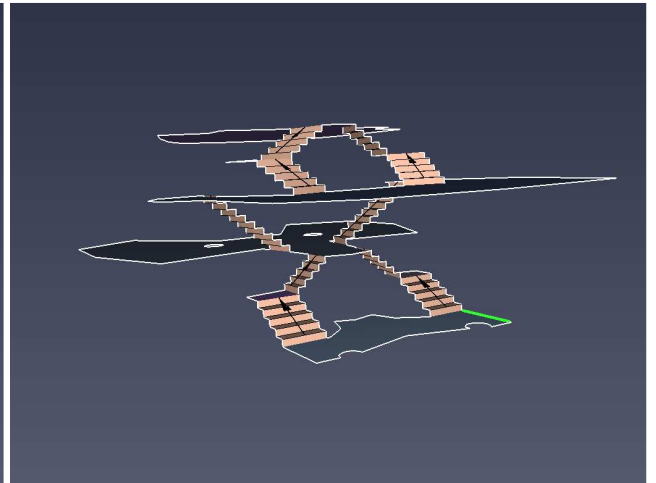


Fig. 13.3. Simulation picture of the club

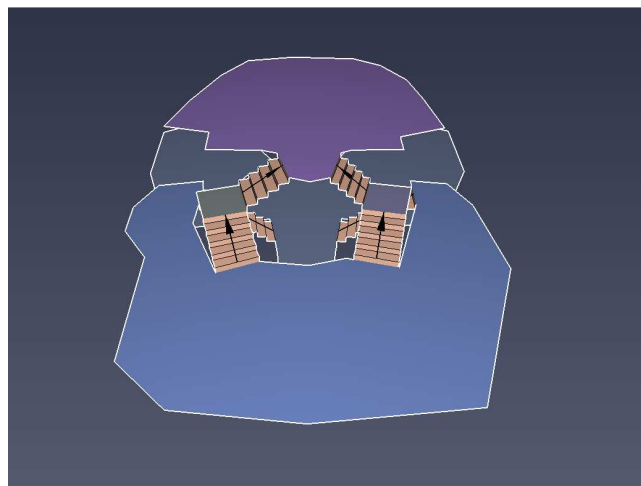


Fig. 13.4. Simulation picture of the club

13.4.2.3 Properties of the participants, calculation mode

Width of shoulders: 45.58 cm

Maximum velocity: 1.19 m/s

Calculation mode: steering, SFPE

Evacuation begins at 0.0 s

Number of people to be evacuated:

220 (owner's distribution)

243 (NFSCS scenario)

Tab 13.5 1st simulation (owner's distribution)

| Level | Gross floor space | Visitors | Employees |
|-------|----------------------|----------|-----------------------|
| 3. | 19.76 m ² | 0 | 1 cloakroom attendant |

| | | | |
|-------|----------------------|-----|---------------------------------------------------------|
| 4. | 78.25 m ² | 47 | 1 barman + 2 security guards |
| 5. | 98.64 m ² | 94 | 1 DJ + 2 barmen + 2 security guards |
| 6. | 58.75 m ² | 65 | 2 barmen + 2 security guards + 1 chief business manager |
| Total | | 206 | 14 |
| Total | | 220 | |

Tab. 13.6 2nd simulation (NFSCS scenario)

| Level | Gross floor space | Visitors | Employees |
|-------|----------------------|----------|-----------------------------|
| 3. | 19.76 m ² | 0 | were not taken into account |
| 4. | 78.25 m ² | 0 | were not taken into account |
| 5. | 98.64 m ² | 103 | were not taken into account |
| 6. | 58.75 m ² | 140 | were not taken into account |
| Total | | 243 | were not taken into account |
| Total | | 243 | |

In the owner's scenario the staff (14 people) began to leave the building with a 60 seconds delay. The reason behind this is the fact that they helped other people during the evacuation.

13.4.2.4 Path-critical points, varying parameters

Table 13.7. Width of the doors on figures

| Sign on the Figure | Width of openings in the model [cm] | Number [pc] |
|--------------------|-------------------------------------|-------------|
| 0 | 160 | 1 |
| 1 | 100 | 1 |
| 2 | 107 | 1 |
| 3 | 90 | 1 |
| 4 | 72 | 1 |
| 5 | 91 | 1 |
| 6 | 91 | 1 |
| 7 | 115 | 1 |
| 8 | 113 | 1 |
| 9 | 106 | 1 |
| 10 | 107 | 1 |

Defining where the critical points greatly affect the results of the simulation. The sizes of the critical points (Figures 2, 3, 4) are the following:

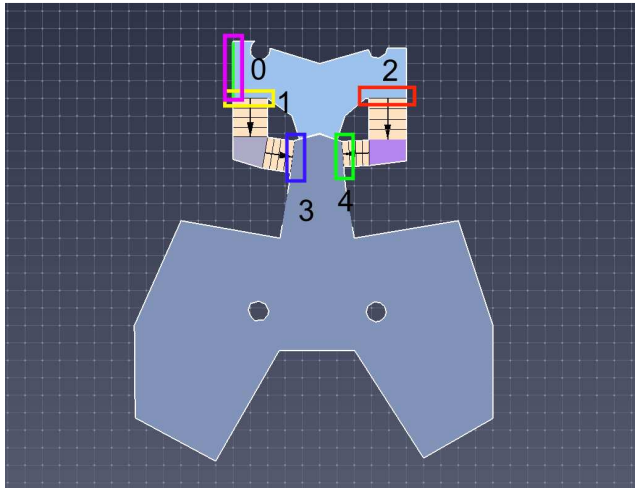


Fig 13.5 Critical cross-sections (on the entry level and on the level above)

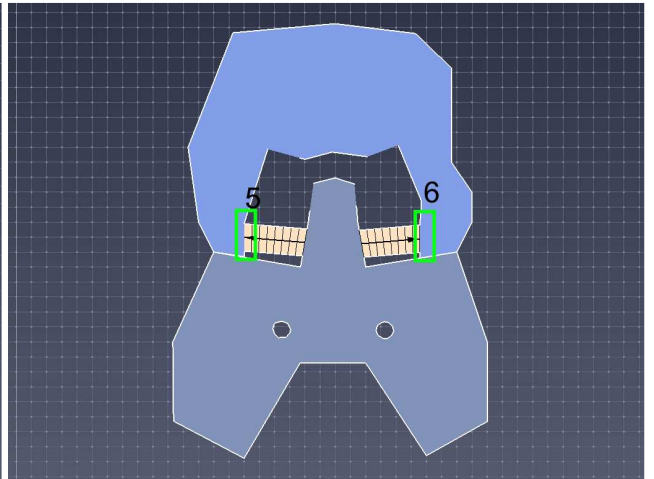


Fig 13.6 Critical cross-sections on the first level and on the second level

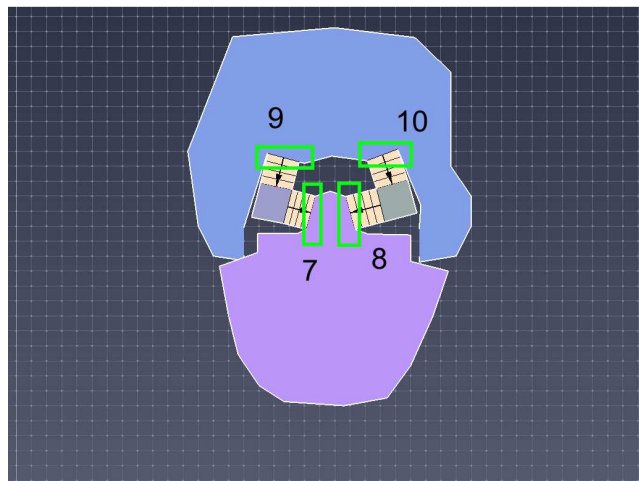


Fig 13.7 Critical cross-sections on the second and on the third level

13.4.3 Results

Steering:

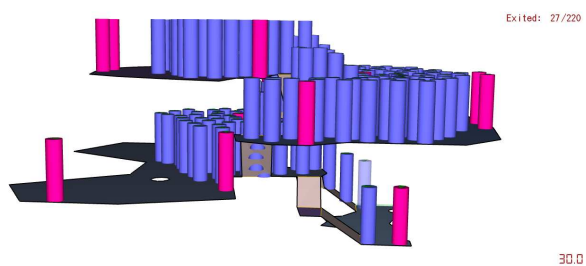


Fig. 13.8 Evacuation in the 30th second

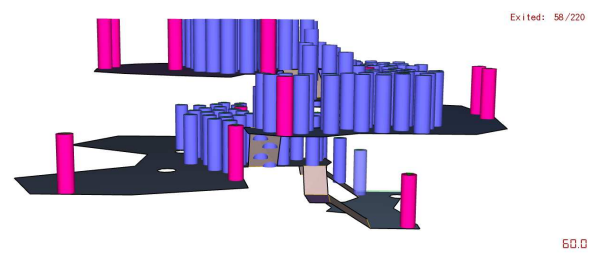


Fig 13.9 Evacuation in the 60th second

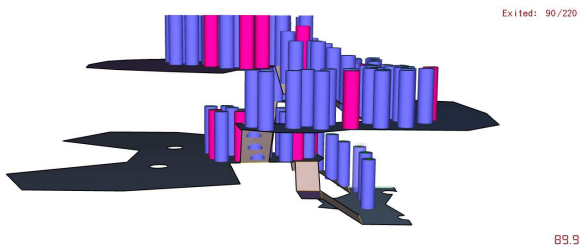


Fig. 13.10 Evacuation in the 90th second

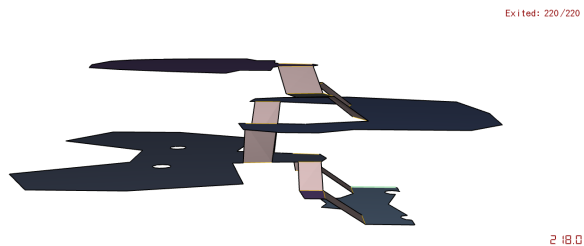


Fig 13.11 Evacuation in the 218th second

SFPE:

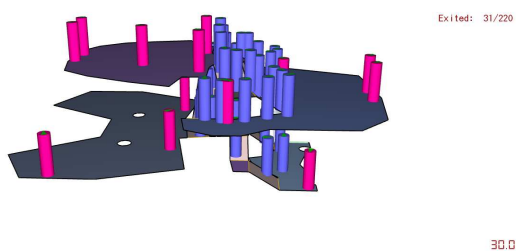


Fig 13.12 Evacuation in the 30th second

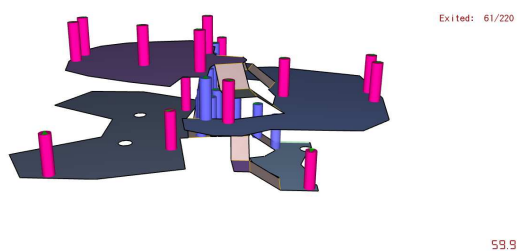


Fig 13.13 Evacuation in the 60th second

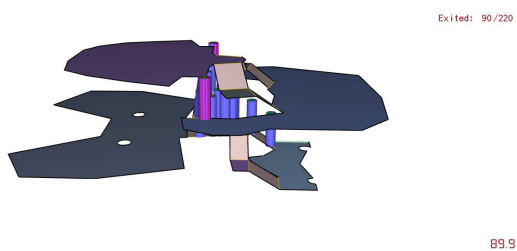


Fig 13.14 Evacuation in the 90th second

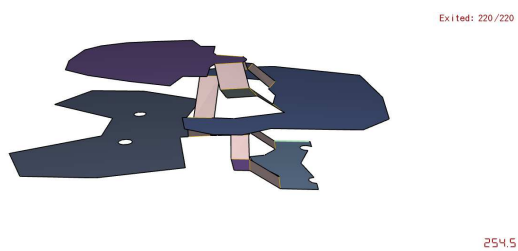


Fig 13.15 Evacuation in the 254th second

SFPE⁺ (with collision management):

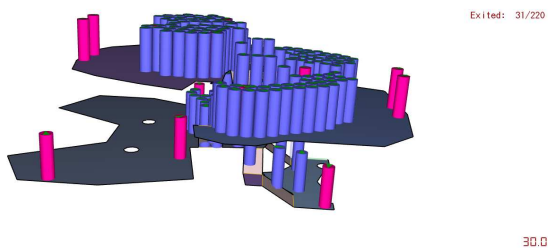


Fig 13.16 Evacuation in the 30th second

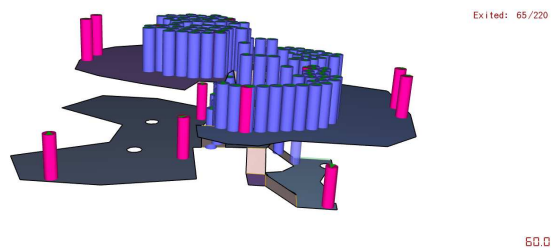


Fig 13.17 Evacuation in the 60th second

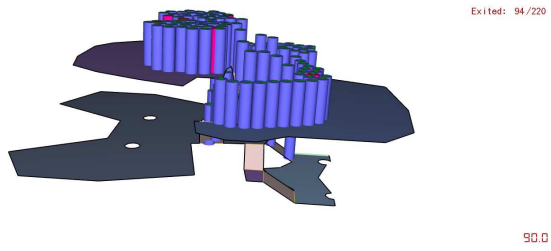


Fig. 13.18 Evacuation in the 90th second

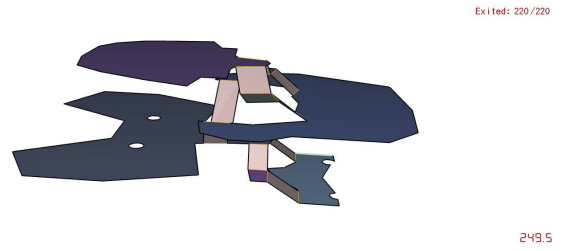


Fig. 13.19 Evacuation in the 250th second

NFSCS scenario:

Steering:

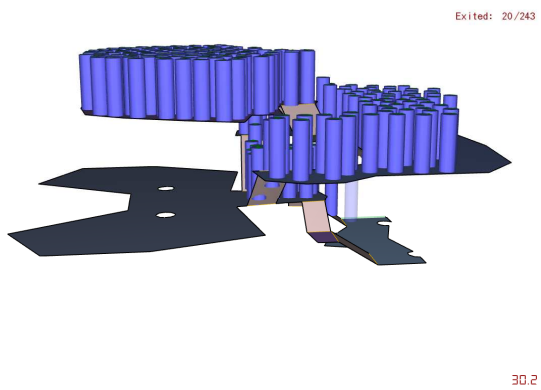


Fig. 13.20 Evacuation in the 30th second

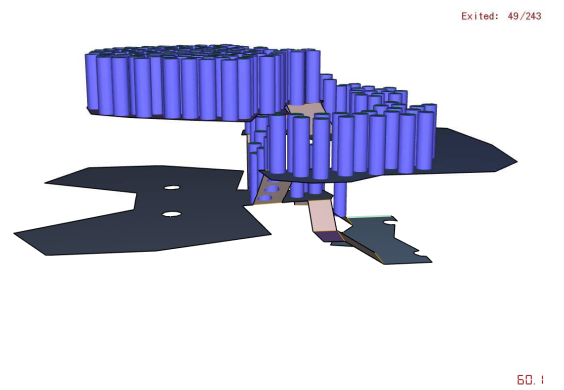


Fig. 13.21 Evacuation in the 60th second

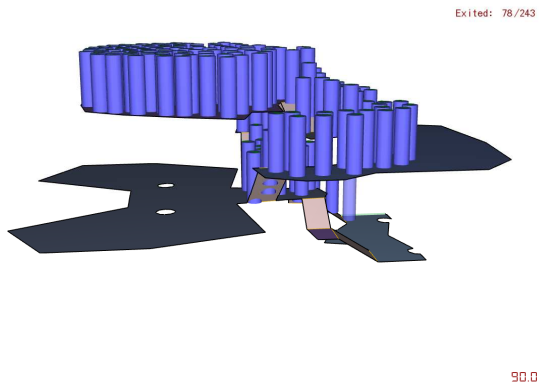


Fig. 13.22 Evacuation in the 90th second

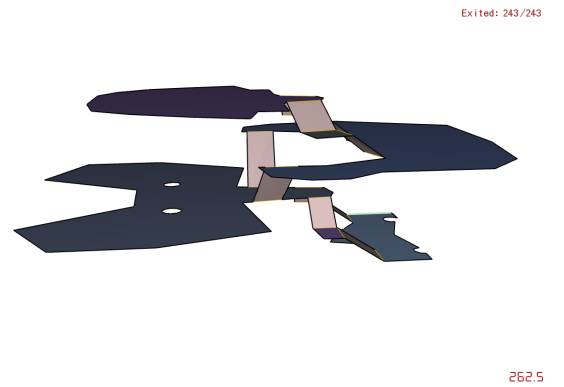
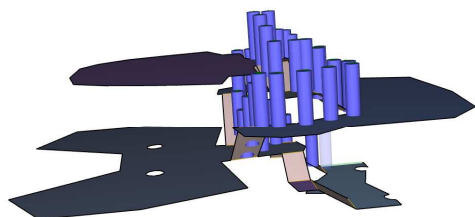


Fig. 13.23 Evacuation in the 263rd second

SFPE:

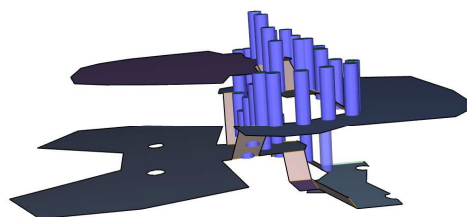
Exited: 16/243



30.0

Fig. 13.24 Evacuation in the 30th second

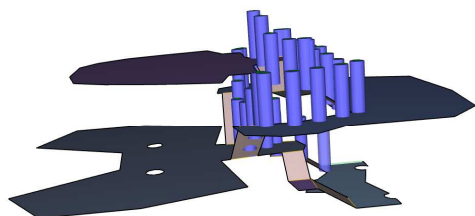
Exited: 40/243



60.0

Fig. 13.25 Evacuation in the 60th second

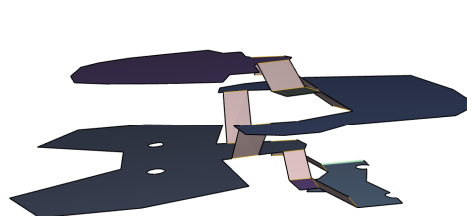
Exited: 64/243



90.2

Fig. 13.26 Evacuation in the 90th second

Exited: 243/243

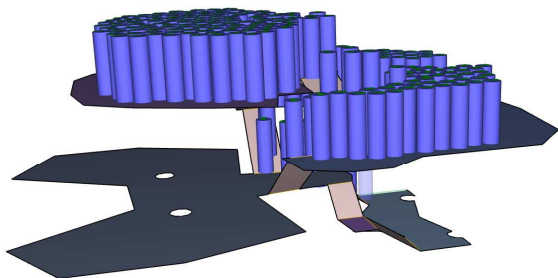


316.3

Fig. 13.27 Evacuation in the 316th second

SFPE⁺ (with collision management):

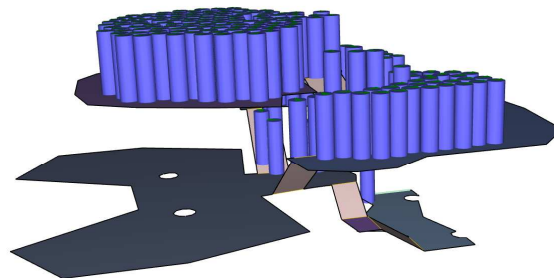
Exited: 16/243



30.1

Fig. 13.28 Evacuation in the 30th second

Exited: 40/243



60.0

Fig. 13.29 Evacuation in the 60th second

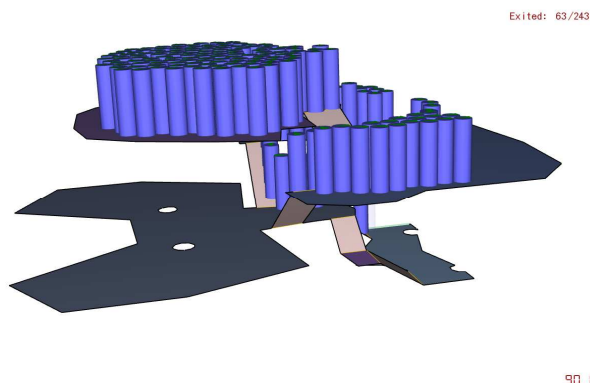


Fig. 13.30 Evacuation in the 90th second

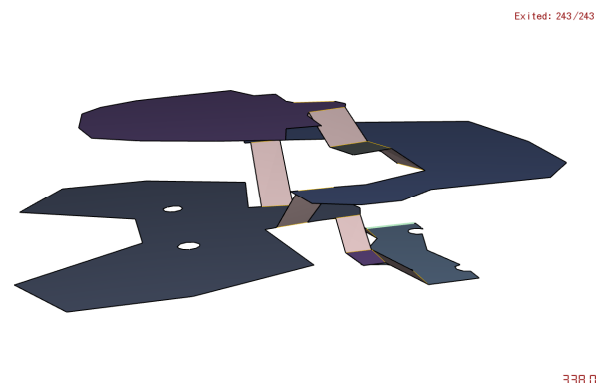


Fig. 13.31 Evacuation in the 338th second

13.5 CONCLUSION

Tab. 13.8 Number of people evacuated in 90 s

| | Owner's distribution | | According to NFSCS | | Minimum Safety Ratios Between Real experiment and calculation or model. to Owner's/ to NFSCS |
|-----------------------|----------------------|------------|--------------------|----------------|--------------------------------------------------------------------------------------------------------------|
| | Reps I. | Reps II. | Reps I.* | Reps II.* | |
| Real experiment | 164 people | 170 people | 158 people* | 176 people* | - |
| | Calculation | | Calculation | | |
| Calculations by NFSCS | 100 people | | 100 people* | 100 people* | 1.64x / 1.58x |
| | Simulation | | Simulation I. | Simulation II. | |
| Pathfinder steering | 90 people | | 78 people* | 78 people* | 1.82x / 2.02x |
| Pathfinder SFPE | 90 people | | 64 people* | 64 people* | 1.82x / 2.46x |

Tab. 13.9 Total evacuation time

| | Owner's distribution | | According to NFSCS | | Minimum Safety Ratios Between Real experiment and calculation or model. to Owner's/ to NFSCS |
|------------------------------|----------------------|----------|--------------------|----------------|--------------------------------------------------------------------------------------------------------------|
| | Reps I. | Reps II. | Reps I.* | Reps II.* | |
| Real experiment | 137 sec | 120 sec | 136 sec* | 120 sec* | - |
| | Calculation | | Calculation | | |
| Calculations by NFSCS | 198 sec | | 219 sec* | 216 sec* | 1.44x / 1.58x |
| | Simulation | | Simulation I. | Simulation II. | |
| Pathfinder steering | 218 sec | | 263 sec* | 261 sec* | 1.59x / 1.91x |
| Pathfinder SFPE | 255 sec | | 316 sec* | 313 sec* | 1.86x / 2.32x |
| Pathfinder SFPE ⁺ | 250 sec | | 338 sec* | 318 sec* | 1.82x / 2.33x |

*243 people was in the first reps, and 239 in the second reps

It is observable that the 60 seconds latency of the staff in the owner's scenario results in different behaviour on the various levels. There aren't any people on the lower levels but the staff is still

at its original spot. On the upper levels, however, the staff begins to exit the building when the area is still crowded. It would be a lot better if they started to exit a given level when it's empty, but this was the Authority's initial input parameter. On the basis of the results, we can safely claim that the evacuation simulations with Pathfinder take more time than the evacuations themselves (in all 3 modes). Calculations take place with 1.82 x safety level in steering and SFPE modes and 1.74 x SFPE⁺ mode during the 90 s simulation. When the whole evacuation process is analysed, calculations have a safety level of 1.59 x in steering mode, 1.86 x in SFPE mode and 1.82 x in SFPE⁺ mode. The deviation of the simulation modes isn't high but somewhat greater differences are observable between steering mode and the other two modes. This is the result of the two different mathematic models. SFPE modes are flux-based models, where cross-sections of the doors and the level of crowdedness (affecting the pace of advancement) play a major role. Steering mode on the other hand provides a more detailed way of analysis. This is provided by the evasive model, which is a lot more sensitive to a decrease in crowdedness. Due to this sensitivity, an evacuation simulation can speed up to a greater extent (than in SFPE mode) when a decrease takes place. NFSCS calculation results fell between real experiment values and simulation values. This leads to the conclusion that the three modes can be considered stricter than the NFSCS requirements, thus resulting in more representative results.

Acknowledgement

The authors would like to thanks Bryan Klein Thunderhead Engineering, the participants on experiments, the owners of the club and to the authorized people who attended to the experiment.

References

- Thunderhead Engineering Pathfinder 2011 User Manual.
- Thunderhead Engineering Pathfinder 2011 Technical Reference.
- Thunderhead Engineering Pathfinder 2009.1.0417 Verification and Validation.
- Tadahisa Jin Visibility and Human Behavior in Fire Smoke The SFPE Handbook Of Fire Protection Engineering, National Fire Protection Association, Quincy, Massachusetts, 3rd edition, 2002. 2-42 – 2-53.

WG2- Eva Caldova, eva.caldova@fsv.cvut.cz

WG2-František Wald, wald@fsv.cvut.cz

WG2-Abdelhamid Bouchair, Abdelhamid.bouchair@univ-bpclermont.fr

Vymlatil Petr, vymlatil.p@designtec.cz

14 CHARRING OF TIMBER

Summary

This work was carried out to test the validity of currently accepted charring rates of glue laminated timber and describes the experimental and numerical investigation into parameters that influence charring rate. The effect of the charring is founding out by experiment of timber-fibre concrete slab under nominal fire conditions and 3D FE model developed to predict the mechanical behaviour of timber-fibre concrete composite floors, in order to derive more simple models for representing the partially protected composite floors in fire. The numerical analysis of the structure is non-linear and considers orthotropic behaviour for timber and isotropic behaviour for concrete. The description of the model used general parameters and values are given in this paper. All this modelling was done using a commercial programme ANSYS 14. The numerical models are calibrated using the results of full scale furnace test. This report is intended for researchers, designers and manufacturers of laminated timber products.

14.1 INTRODUCTION

One of the most important requirements of timber structures is fire resistance, because timber is highly combustible material and as such it differs from all the other commonly used construction materials. For the design and verification of the reliability of timber structures exposed to fire by EN 1995-1-1 and EN 1995-1-2 can be used alternatively three methods. It is the reduced cross-section method, the reduced properties method and general method. These methods are sorted in ascending order according to the complexity of calculation and subsequently according to the resulting fire resistance of the structure. The principle of all these methods is to calculate the depth of charring cross-section or change of physico-mechanical properties and residual cross-section capacity at the required time of fire resistance. The charring depth is based on a design charring rate of the material and time fire resistance. The design charring rate (ranging between 0.5 and 1.0 mm/min.) is mainly dependent on the density and moisture content of wood or wood based materials (generally inversely) and is presented tabulate by characteristic value in EN 1995-1-2.

High temperatures cause thermal degradation (pyrolysis) followed by decrease of mass and cross-section. A surface char layer is then formed, which, because of its low thermal conductivity, protects the interior of the timber cross-section against heat. The temperature inside the timber member depends particularly on the cross-sectional dimensions and shape, on the density and moisture content of wood and on the fire load and temperature development during the fire. Thermal degradation process starts when the wooden surface reaches sufficient temperature which depends on the type of wood, fire duration time and on whether there is source of ignition or not. In case the source of ignition is present, this value varies around 300 °C, without the source the surface temperature has to exceed 400 °C in short and medium time period. The surface of timber construction elements ignites quickly and burns rather strongly, but only till the surface develops charred layer of wooden material. Charred layer is good thermo insulation and prevents access of air into the inner parts of cross-section and inhibits burning. A part of this layer with temperature between 200 °C and 300 °C is a pyrolysis layer. An accurate calculation is considered to be a transient conduct of heat and moisture over timber beam exposed to standard fire conditions. The time-dependent thermal degradation of wood is quantified by the charring rate, which is defined as the ratio between the distance of the char-line from the original wood surface and the fire duration time. The charring rate of wood, which is the main parameter to describe the fire behaviour of timber structures, is mainly determined by the type of wood, (Frangi, 2003). For fire resistance calculations is commonly assumed a constant charring rate, (Konig, 1995).

Because of the good insulation behaviour of the charred wood, typical temperature profiles through wood members exposed to fire exhibit a steep temperature gradient. The thermal penetration depth is defined as the distance from the char-line to the part of wood at room temperature and is of about 25 mm, (Lache, 1992). It is an important parameter to describe the temperature profile in wood members exposed to fire.

14.2 EXPERIMENT WITH TIMBER-FIBRE CONCRETE SLAB

14.2.1 Specimen details

The slab was tested in the furnace at elevated temperature in fire testing laboratory PAVUS in Veselí nad Lužnicí. The full scale floor specimen was designed to span 3.5 m by 4 m according to the furnace interior dimensions. The composite timber-concrete floors were composed of timber frame, two secondary beams and concrete slab connected to floor joists. The cross section of the secondary beams was 120/160 mm with the timber class GL24h. A 4.57 m by 3.96 m concrete slabs with a thickness of 60 mm were reinforced by steel fibre only without added steel bars. The fibre content was 70 kg/m³ with type of fibres HE 75/50 Arcelor. As connectors were used TCC 7.3 x 150 mm screws inclined 45 degrees to the beam axis in two rows, distance of screws in one row is 0.1 m. The timber frame was fire

protected by timber desks and the secondary beams in the centre of the floor slab were left unprotected. The mechanical load during fire was created by concrete blocks uniformly distributed over the floor. The arrangement of the test specimen is shown in Fig. 14.1 and Fig. 14.2.



Fig. 14.1 Fire test set-up



Fig. 14.2 Fire test set-up from bottom

14.2.2 Experimental results

During the heating phase of the test, the standard fire curve was followed which lasted for 150 mins. After that, burners were turned off and the furnace was cooled down naturally. In this phase the floor slab specimen fell down.

The behaviour of the composite slabs in the furnace was recorded by 27 thermocouples. Thirteen thermocouples were concreted in the composite slab at three separate points across the slab, four thermocouples were located in the centre of timber beams in depth 40 mm from the lower surface and ten thermocouples recorded the gas temperature in the furnace and were located just below the floor, see Fig. 14.3. The unprotected timber beams located at the middle of the floor were heated up to 250 °C, see Fig. 14.3 and Fig. 14. 4.

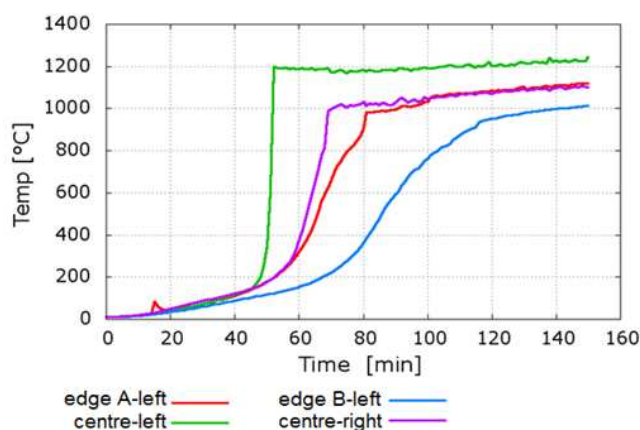


Fig. 14.3 Measured temperatures in timber beams at four separate points

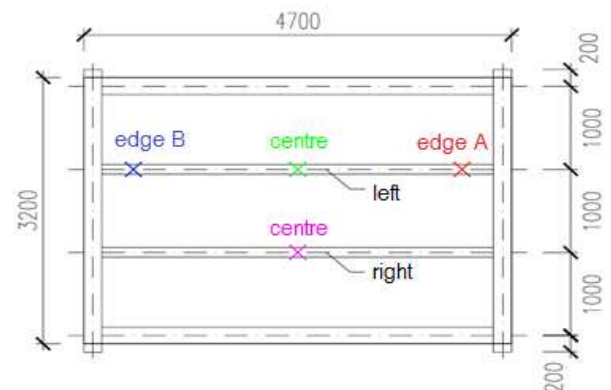


Fig. 14.4 Location of the thermocouples by the test set up

In the test, the glue laminated timber beams were exposed to fire on three sides in the furnace, Fig. 14.5. The temperature development of four beams was very similar. The maximum recorded temperature occurred after 45 mins at the centre span of left beam. Then the secondary beams failed, see Fig. 14.6. This phenomenon was evaluated by analytical calculation according to EN 1995-1-2 and EN 1992-1-2. To measure the charcoal width after the test was not possible due to burning of the whole secondary beams.



Fig. 14.5 Charring of timber at 15 mins



Fig. 14.6 Charring of timber at 45 mins

14.3 NUMERICAL MODELLING

14.3.1 Details

Mechanical behaviour of the timber-concrete composites in fire is very complex transient thermo-mechanical problem. This problem can be solved as one-way coupling between thermal analysis and mechanical analysis. Nonlinear transient heat flow consists of thermal load (fire) as radiation and convection, thermal material properties depend on time (nonlinear analysis) and timber charring effects.

The tests were numerically simulated using two-dimensional finite element model. Finite element model was implemented in ANSYS 14 software package to simulate the experimental tests and to analyse the thermal performance unprotected timber sections. The load, boundary and initial conditions of the numerical model are below, see Fig. 7. The fire temperature was applied according to the standard fire.

The temperature-dependent relationships for timber properties proposed by the European code for fire design of timber structures were adopted in the modelling, see Figs. 14.8, 14.9, 14.10. Timber was assumed as a non-linear orthotropic material, with temperature depended Young's modulus, see Fig. 14. 11.

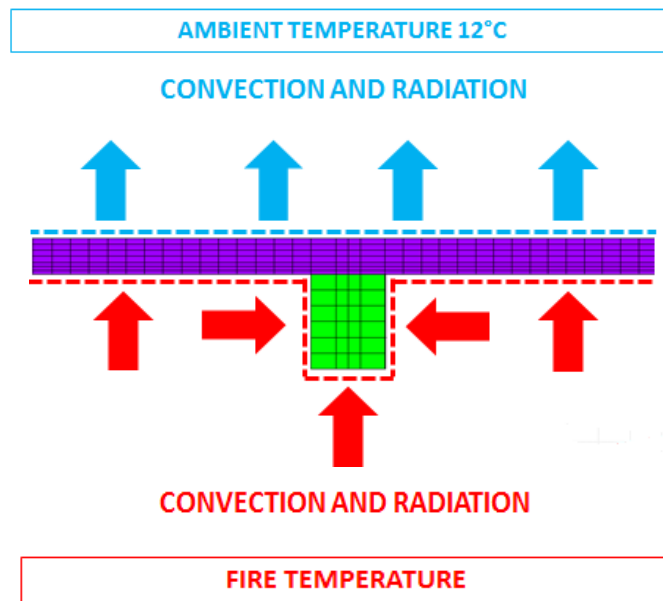


Fig. 14.7 Boundary and initial conditions of the numerical model

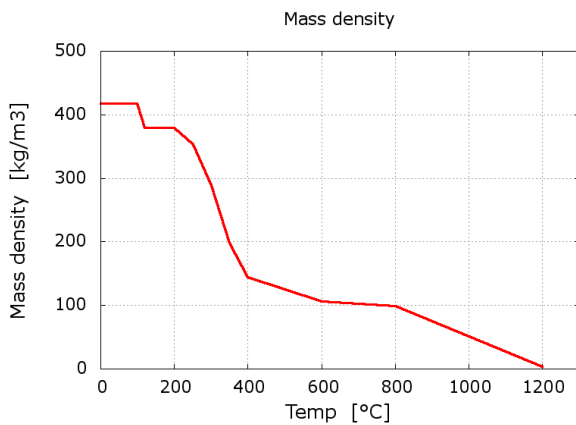


Fig. 14.8 Mass density

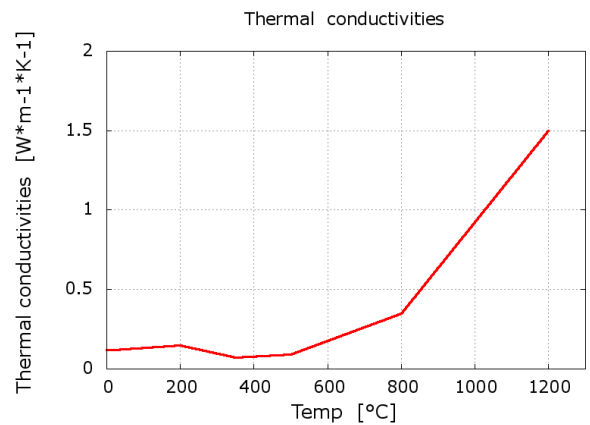


Fig. 14.9 Thermal conductivities

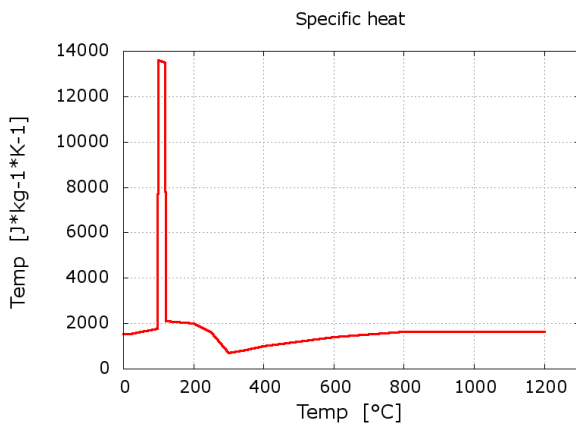


Fig. 14.10 Specofoc heat according to the Eurocode

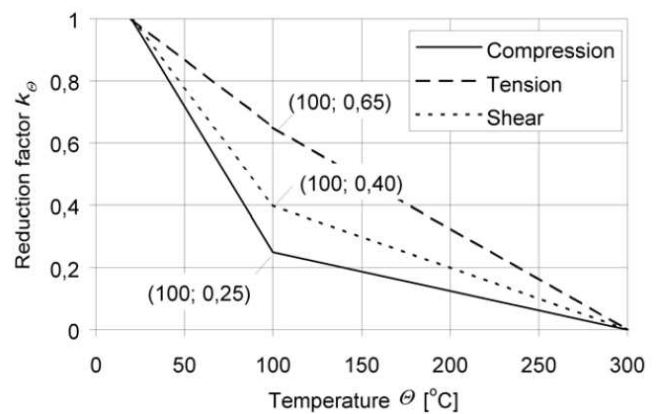


Fig. 14.11 Thermal conductivities

14.3.2 Results

Numerical results in terms of temperature development are presented in the Figs. 14.12, 14.13.

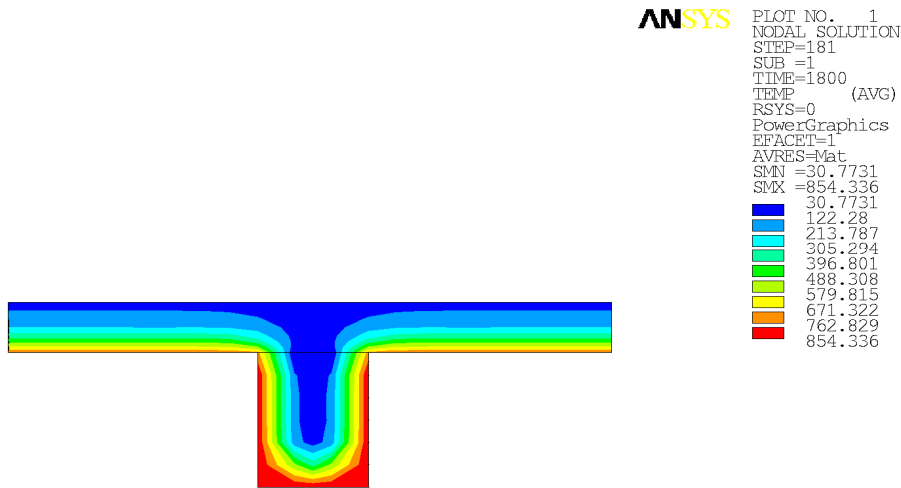


Fig. 14.12 Temperature development at 30 mins

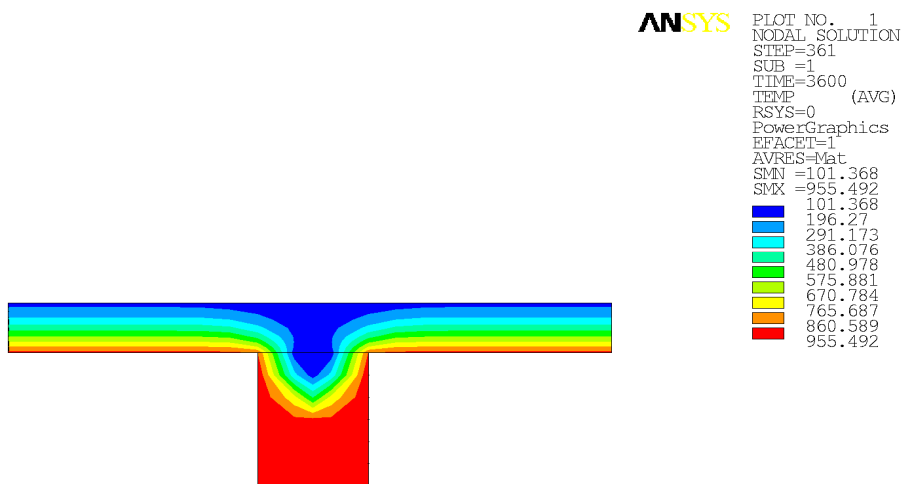


Fig. 14.13 Temperature development at 60 mins

The results of thermal analysis have showed similar temperatures development of timber specimen in experiment and in the numerical simulations. Thermal decomposition begins at 200°C and the highest mass loss rate occurred at approx. 430°C after 45 minutes.

14.5 SUMMARY

The chapter summarises the thermal analysis of timber specimen in fire conditions. This thermal analysis is prepared based on the fire experiment and the numerical modelling of the tested floor slab. The numerical analysis of timber structure behaviour under fire was composed of two mutually coupled physical phenomena such the determination of fire scenario, which means determination of temperature and moisture of surrounding air during fire and the determination of temperature and

moisture distribution in structural elements as a function of time. The problem of simultaneous heat and moisture transfer in glued laminated timber elements during the standard fire in which the charring of wood is taken into accounts has been solved with the use of finite element method. For calculation was used ANSYS 14 programme. Results obtained and numerical model used have been verified by comparison to the analytical solutions in the literature.

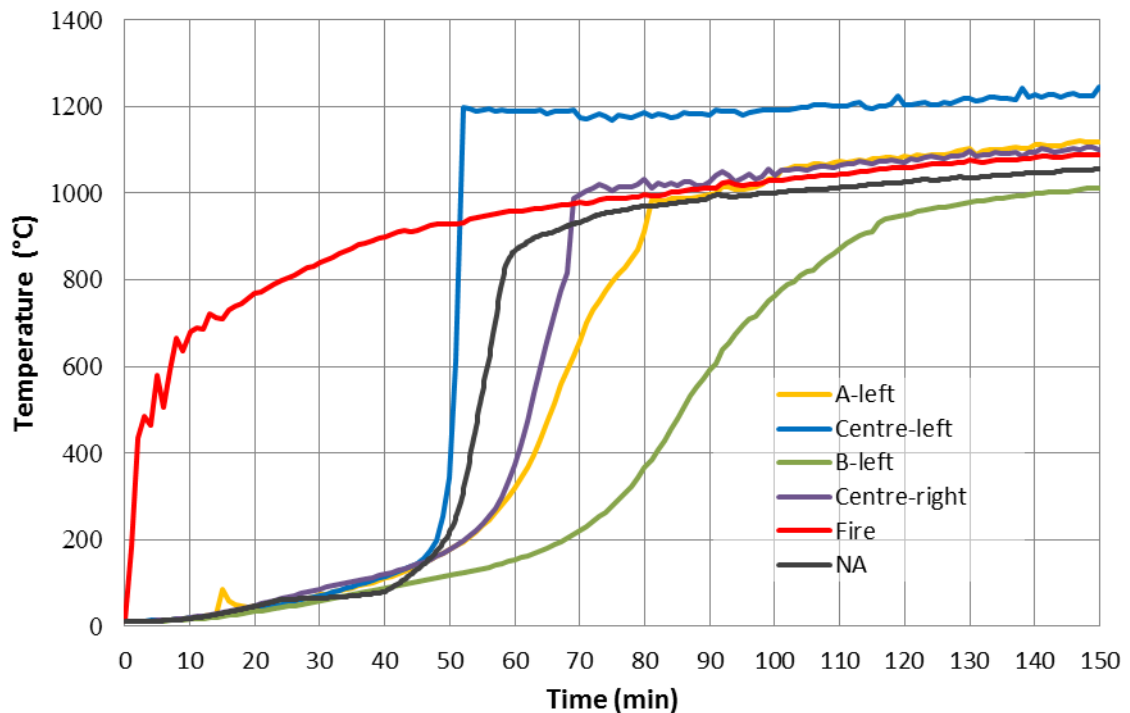


Fig. 14.14 Comparison of the measured and calculated temperature

Acknowledgement

The authors would like to thank COST action network number TU0904 and to the research project of the Grant Agency of Czech Republic No. P105/10/2159.

References

- Frangi, 2003: Frangi A., Fontana M., Charring rates and temperature profiles of wood sections, in: *Fire and materials*, John Wiley & Sons, Ltd., 2003, vol. 27, pp. 91-102.
- König, 1995: König J., Die Bemessung von Holzbauten für den Brandfall nach ENV 1995-1-1. Informationsdienst Holz, in: *Holzbauwerke nach Eurocode 5. STEP 3 Fachverlag Holz: Dusseldorf*, 1995.
- Lache, 1992: Lache M., Untersuchungen zur Abbrandgeschwindigkeit von Vollholz und zur Feuerwiderstandsdauer biegebeanspruchter BSH-Träger, in: *Institut für Holzforschung der Universität München*, 1992.

WG3 - Federico Massimo Mazzolani, fm@unina.it

Luke Bisby, luke.bisby@ed.ac.uk

Antonio Formisano, antoform@unina.it

Roberta Fonti, roberta.fonti@unina.it

15 OLD MASONRY VULNERABILITY AGAINST FIRE ACTION

Summary

The main issue analysed is related to old masonry upgrade against combined fire and earthquake actions. In order to development, this topic the examination of a real case study is proposed.

During the 2009 year, an Old Palace placed in the heart of Naples' historical centre; it was devastated by fire action. Degradation effects were directly observed on tuff block elements; no fire scenario data and no mechanical parameters are well known. Nerveless, this condition is quite common for ancient constructions by considering oldness' effects on material decay and catastrophic occurrences like seismic one, during building lifetime. Therefore, with particularly reference to public edifices, subjected to Cultural Heritage protective restrictions, it is possible try to evaluate the robustness in front of no ordinary actions by performing a lessening of the original wall thickness, by supposing fixed range of old masonry mechanical features reduction and by corresponding partial safety coefficients, as basic idea. The following paper will show this basic concept by code and standards critical aspects recognition and simple examples demonstration.

15.1 FOREWORD

Currently, masonry behaviour under fire action have to be performed according to the in force European standards with the main purpose in pointing out some critic aspects related to no codified rules for old masonry typologies. In particular, the case study proposed is placed in Italy; therefore, The Italian Code (NTC '08) and the Eurocode 6 (Part 1-2) will be take into account as starting know-how platform.

15.2 OLD MASONRY UPGRADE AGAINST COMBINED FIRE AND EARTHQUAKE ACTIONS: CODE AND STANDARDS SUGGESTIONS

15.2.1 The Italian Code

The Italian Code is based on the European code and standards; therefore, it essentially takes into account structure safety as fundamental principle by considering the Italian Country placement in very

high seismic zone. Therefore, correlate building analyses to different levels of damage is basic. These different limit states can be performed in accordance to definite range of reference life (VR) and assumed as bourn conditions related to the typology considered. This approach join together usable life and the use idea, respectively considered as the building time in which the structure can be considered safe by assuring structural health monitoring and maintenance; and exploitation degrees: occasional, frequent or frequent with crowding (see Table 15.1).

Tab. 15.1 Parameter for reference life VR definition

| Parameter | values |
|---------------------|-------------|
| Usage life (VN) | ≥ 50 |
| Use (Cu) | (II) Cu=1,0 |
| Reference Life (VR) | ≥ 50 |

Therefore, the limit states is a borderline condition; when it exceeded, the structure cannot satisfy the design requirements. In particular, structures have to match the following requests:

- Safety in front of damage limitation (ultimate limit states [ULS])
- Safety in front of operational performance (serviceability limit state [SLS])
- Robustness in front of no ordinary actions by considering it the capacity to avoid disproportionate damages (effects) under catastrophic actions (fire, explosion and hurt).

When the ULS is over, the structure collapse cannot be avoided. With regard to existing structures, the ultimate damage level cannot be achieved with exploitation of the capacity design criteria, which do not characterise old masonry buildings. In fact, it is important point out that the Italian building code adopt for masonry existing building the SLV condition (Life Safety level) as maximum Limit State possible. Consequently, will be possible considered equal to 10% the possibility of the reference life (VR) exceedance for this specific level of damage, as showed in Table 15.2.

Tab. 15.2 Parameter for local seismic action definition

| | |
|-------------|------|
| Limit State | SLV |
| Pvr (%) | 0.10 |
| TR (year) | 475 |

Regarding the SLS level, the durability concept can be defined as the capacity in preserving structure physical and mechanical features during its Service Life. Therefore, the materials mechanical

features, the dimension of structural elements and the protection system and maintenances eventually applied have to be accurately chosen.

With regarding to the material mechanical parameters, they have to be clearly identified in order to assess structure safety (section §11 NTC 08). This can be accomplished by comparing material resistance to the effects of applied actions through the semi-probabilistic approach with the use of Partial Safety Coefficients foreseen in the Italian technical code NTC08.

The mentioned check can be expressed by means of the following formulation:

$$R_d \geq E_d \quad (1)$$

where R_d is the design resistance of the material and E_d is the design action value defined into the § 2.5.3 of NTC08.

For masonry constructions, it is commonly considered material resistance reduced and/or developed by both the structure knowledge levels CF (confidence factor) and the safety factor γ_M (see Table 15.3), in order to work out unknown degradation effect due to:

- Oldness;
- Past fire action occurrence;
- Past seismic action occurrence;
- No use of the structure – lack in maintenances;
- Local problems due to mortal joints failure and rough setting of the single components.

The Confidential Factor can be calculated by partial coefficients based on the information previously obtained on the building life (see eq. 2), with the final outcome of establishing the most largely “confidence” level for the structure analyzed.

$$F_c = 1 + \sum_{k=1}^4 F_{ck} \quad (2)$$

Instead, following Table (15.3) can choose the γ_M factor.

Tab. 15.3 Table 4.5.II of NTC 08: coefficients γ_M listed in accordance to the masonry execution classes (1 or 2) related to the resistance category of structural elements and mortar type.

| Material | Manufacture classes | |
|-----------------------------------------------------------------------------------|---------------------|-----|
| | 1 | 2 |
| Masonry with I category resistant elements and mortar with certified composition | 2,0 | 2,5 |
| Masonry with I category resistant elements and mortar with restricted composition | 2,2 | 2,7 |
| Masonry with II category resistant elements and every kind of mortar | 2,5 | 3,0 |

Moreover, with particular reference to the masonry section §4.5.9. “Check for no ordinary actions”, it is possible to point out the *Robustness* concept by supposing different damage levels where the partial factors γ_M can be assumed equal to $\frac{1}{2}$ of the ordinary values reported in Table 15.3. Nevertheless, the assumptions reported into §4.5.9 section are related to UNI EN 1996-1-2 Eurocode 6.

15.2.2 The UNI EN 1996-1-2.

Eurocode 6 – Design of masonry structures – Part 1-2: General rules - Structural fire design

Regarding to the Eurocode 6, at the first, it is fundamental to define different categories in which old masonry types can be filled, by distinguish one each other for original materials source and settings. In particular, as stated in UNI EN 1996-1-2 “General rules - Structural fire design”, a basic classification of masonry types, namely clay, calcium silicate, autoclaved aerated concrete or dense/lightweight aggregate concrete and manufactured stone, is reported. It is possible notice that this classification does not take into account directly old masonry typologies, which could be framed within manufactured stone group.



Fig. 15.1 Old masonry type selection

By analyzing the Annexes A and B of the UNI EN 1996-1-2 (“Guidance on selection of fire resistance periods” and “Tabulated fire resistance of masonry walls”, respectively), data and suggestions are strictly related to each stonework category by considering masonry single components checked and codified into UNI certification track, with ordinary setting, standard reference fire and related resistance classes. Obviously, they are concerned to design aspects and no to refurbishment issues. The minimum thicknesses reported do not take into account the additional resistance reduction due to materials oldness and local problems related to vertical interlock failures; only manufacture problems related to horizontal interlocks (double leaf wall failure) are considered. Instead, many difficulties can be recognized like unknown parameters:

- Large variety of mechanical limits into the same category, by considering manufacture setting and single components placement no ordinary (see Figure 15.1);

- Indefinite reducing of the material robustness against no ordinary actions due to boundary conditions connected to unknown starting degradation factors;
- The recognition of single degradation factors influence on the thickness falling and the partial amount of one each other by considering the mechanical parameters lessening.

Therefore, old masonry cannot be filled into any category reported into the Eurocode 6; nevertheless, the code final outcome is to point out the minimum requirements of thickness for each masonry class and category, by considering data filled into Tables from B.1 to B.6 (Eurocode 6, Annex B) the minimum wall thicknesses (t_r) assumable for fire resistance classification (EI) and time of exposure ($t_{fi,d}$).

All above means that in order to forecast old masonry t_r it is possible to adopt, as basic idea, geometrical wall thickness lessening in relation to fire degradation occurrences (post- fire action in-situ detected) and loading conditions applied; without neglect seismic hazard requirements.

Therefore, in-situ testing campaign becomes the only way for recognize real material mechanical parameters by performing them as decreasing in compression resistance and weight.

15.2.3 Fire effects performing as degradation issue

Degradation issues for old masonry is quite codified into the Italian Code; in fact, in §2.5.4 it is possible point out the Use class (CU) and Nominal life (VN) as concepts able to take into account degradation effect due to lack in maintenance into a reference life period. Moreover, the FC and γ_M factors are able to get the theoretical mechanical parameters more close by the real ones, as showed into the previous section.

Therefore, in order to correlate fire and seismic actions, the first occurrence is considered able to produce permanent degradation effects, strictly related to masonry type and the time of fire exposure; instead the second one is concerned to old masonry local behavior (out-of-plane mechanisms) under seismic load and the assessment of the residual resistance against horizontal actions after fire exposure.

Consequently, Fire effects can be evaluated as material resistance reduction by assuming an additional partial factor into FC formulation (see ii). Instead, masonry structural elements residual resistance against horizontal actions and seismic occurrence can be assessed as suggested into the Guidelines for the assessment of Cultural Heritage Seismic hazard and Vulnerabilities in conformity with the NTC' 08 Code (MiBAC, 2010).

Therefore, with reference to the limit state approach, at the first, it is possible to recognize the α_0 (see eq. 3) assessment, in order to perform the horizontal force necessary for local mechanism activation.

$$\alpha_0 M_S + M_{EST} = M_{RC} + M_{RA} + M_{RF} \quad (3)$$

α_0 calculation is strictly related to the geometrical dimensions of the masonry elements considered and the local failure supposed. In fact, by apply EQU procedure, α_0 formulation is basically equal to the following ratio (4), by comparing the moment resistance, due to vertical loads applied (principally compound to masonry weight) and the overturning moment, owing to the corresponding horizontal forces by supposing them equal to a share of the vertical ones multiply for α_0 (see Figure 15.2). Therefore, α_0 can be considered the collapse multiplier.

$$\alpha_0 * M_S = M_R \quad (4)$$

where: M_S is equal to Overturning moment and the M_R value is corresponding to the Resisting moment.

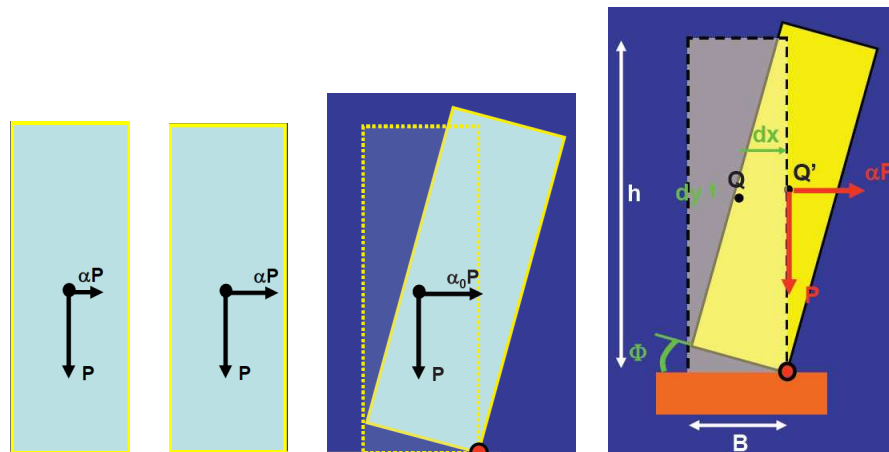


Fig 15.2 Out-of-plane mechanism: α_0 steps (De Maria, 2010)

The corresponding a_0^* (see eq. 5) value have to be assumed by comparing the anchor acceleration (a_g), due to the building site position and the limit condition performed (SLV), to the acceleration (a_0^*) necessary for panel overturning (see eq. 6).

$$a_0^* = \frac{\alpha_0 g}{e^* F_c} \quad (5)$$

where:

$$\alpha_0 \text{ is equal to } M_S/M_R; \quad e^* \text{ is equal to } e^* = \frac{gM^*}{\sum_{i=1}^{n+m} P_i} \quad \text{and } M^* \text{ is equal to } M^* = \frac{\left(\sum_{i=1}^{n+m} P_i \delta_{X,j} \right)^2}{g \sum_{i=1}^{n+m} P_i \delta_{X,j}^2}$$

The CF factor was introduced since anchor acceleration reduction achievement, by assuming a_0^* more close to the real possibility of the structure analyzed, during a seismic event. Consequently, the strengthening methods will result strictly related to the “confidence” achieved and the specific structural engineering characteristics detected.

$$\frac{a_g (P_{vr}) S}{q} \leq a_0^* \qquad a_0^* \geq \frac{S_e(\tau_1) \psi(Z) \gamma}{q} \qquad (6)$$

a) b)

In order to get in correlation the minimum thickness required for fire action and seismic hazard with local failures occurrences, masonry panels as single rigid blocks (EQU approach) can be assumed. According to Giuffrè proposals (Giuffrè, 1991) to every cause of degradation, it is possible point out a lessening of the real wall thickness, by considering the moving of the hinges position from the external panel surface to the inner part (see Figure 15.2 “t” position), during panel overturning (see Figure 15.3a). This means that part of it is not able to oppose resistance against horizontal forces and a reduction of the corresponding force necessary to the mechanism activation (see eq. 3 and 4) can be noticed. Consequent the crashing of the bottom part of the panel will be detected (see Figure 15.3b).

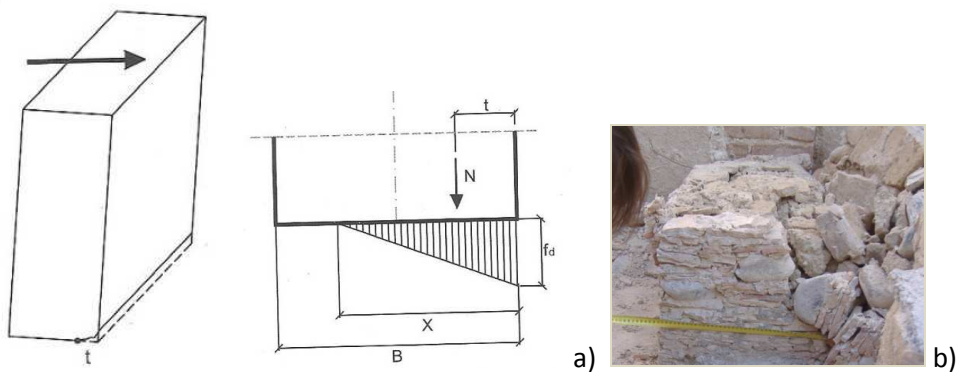


Fig 15.3 the hinge position changing during panel overturned due to degradation effects: theoretical sketches (Cangi et al, 2010) and experimental activity photo (Fonti, 2013).

The equilibrium condition for overturning state imposes the application of the total amount of the vertical load in barycenter position respect the strains triangles, as showed in figure 15.3a. Therefore, t will be equal to 1/3 of x. Assuming N equal to $\sum P_i$, it is possible obtain the following formulation (8):

$$t = 2 \sum P_i / 3 f_d L \qquad (8)$$

where: t : is the moving of the hinges position; $\sum P_i$: is the vertical load total amount applied to the section analyzed; L : is the largeness of the wall; f_d : is the design masonry compression resistance.

Therefore, material resistance becomes the joint point, and degradation effects due to fire action can be performed starting from the seismic combination sequence (9) by introducing a partial factor related to exceptional occurrence into a_0^* calculation or by supposing different f_d in situ experimental obtained (related to fire classes and materials) for altered and unaltered specimens and consequently t values.

Seismic Load Combination related to the seismic action (E) (§ 3.2 NTC08):

$$E + G1 + G2 + P + \psi_{2i} \cdot Q_{k1} + \psi_{22} \cdot Q_{k2} + \dots \quad (9)$$

15.3 THE CASE STUDY

15.3.1 The Tuff stonework

The study case proposed shows tuff stonework as reference masonry type. This typology is wide spread in Italian country, especially in the Centre-south area, where many monumental structures are made about it, from the ancient time to the first part of the last siècle. Rome, Naples, Pozzuoli, Pompei, Ercolano and so on are the most important hosting sites; therefore, their safety against no ordinary actions is important and significant. In order to codify and filled Tuff stonework into categories it is possible work out two main difficulties:

- Large variety in mechanical parameters values recognition related to tuff origin and workmanship.
- Unknown reducing of the real resistance to compression stress for material decay.

15.3.2 The Marquees Vernasse of Akaia Palace, in Naples (Italy)

The Vernasse Palace is placed in the heart of Naples historical centre. It shows irregular shape in plane (see Figure 15.4) principally impressed by the roads distribution. The structure was settled into one of the most ancient urban multi-unit building in headers position. The early edifice façade was regular in elevation with five stories from the bottom to the top; nowadays, it shows one level more and one level in basement position (see Figure 15.5). All the Palace plane is mainly developed around a courtyard with the presence of Palazziata staircase.



Fig 15.4 Naples urban plane.

During November 5th, 2009, the building was hit by a strong no ordinary occurrence. The fire action involved many levels and the main effects are shown into the Figure sequence 15.6a and b.

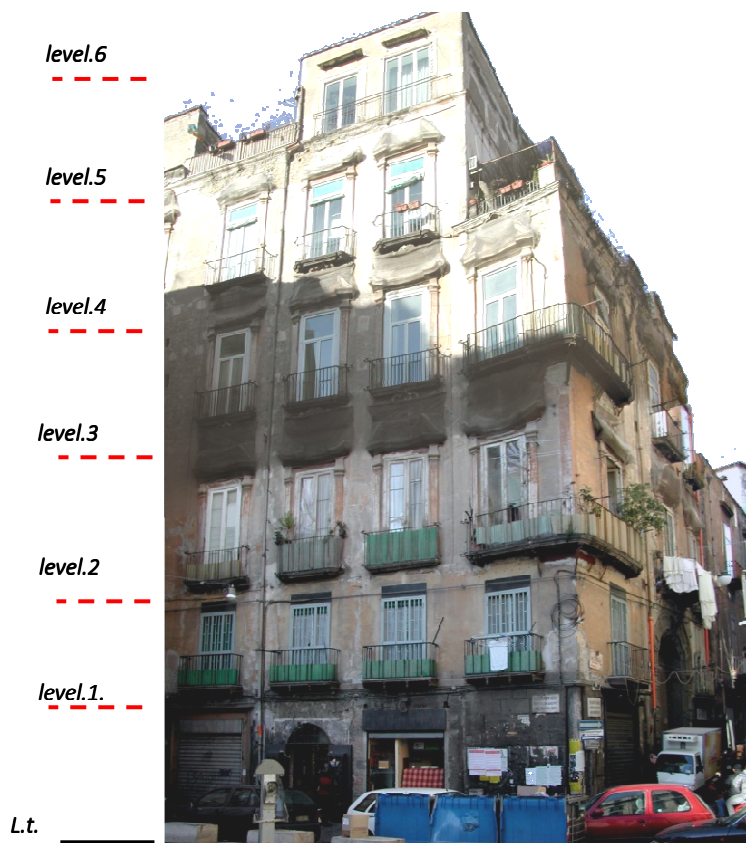


Fig 15.5 Marqueses Vernasse of Akaia Palace

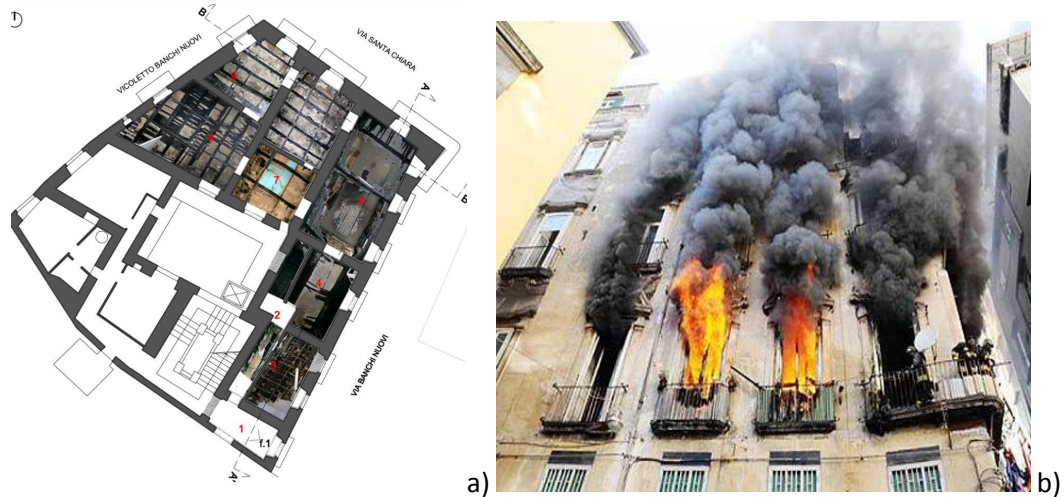


Fig 15.6 Marqueses Vernasse of Akaia Palace: a) plane; b) photo during fire exposure.

15.3.3 The experimental activity

With reference to old masonry types, data can be only experimentally detected and they should be correlated to fire exposure in time, by choosing a reference period (for example 10, 15, 20, 30, 40, 45,...minutes) and corresponding range of thickness reductions (t_r), due to oldness, headers absence, mortal joint failure and fire action.

In order to take apart fire action value in resistance reduction from the others thickness reduction factors (just listed in the previous section), two identical specimens, burned and unburned, have to be tested in compression and data results must be compared each to other. The experimental test set up takes into account the possibility in apply vertical force only orthogonally to the burned specimen' face (see Figure 15.7), in order to reproduce real fire conditions. Each specimen must be previously weighed and according to the starting state (burned or not) two parameters will get in correlation: weight variation and compression strength. According to the above main purposes 21 specimens affected by fire action and corresponding unaltered ones were tested (see Figure 15.7).

The main results for burned specimens are reported into the Table 15.4.

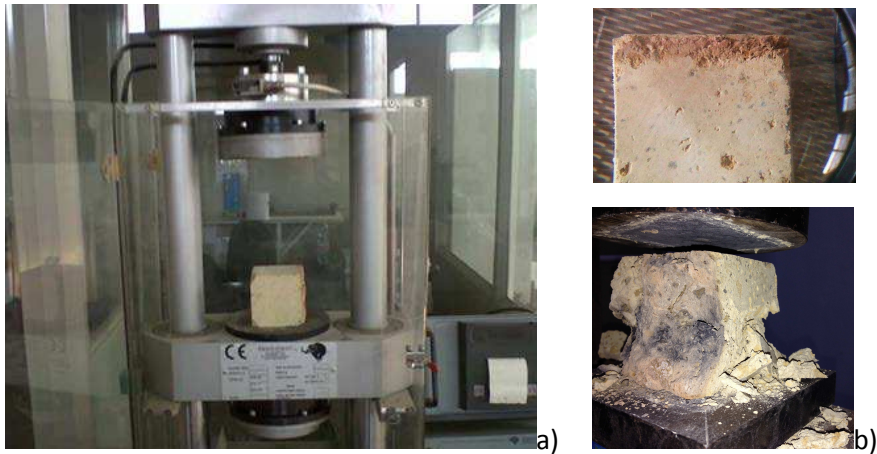


Fig 15.7 Marquees Vernasse of Akaia Palace: a) plane; b) photo during fire exposure.

Tab. 15.4 Burned specimens

| BURNED SPECIMENS | | a | a'' | a''' | a'''' | b | h | MASS | RESISTENCE |
|------------------|----------|-------|-------|-------|-------|-------|-------|-------|-----------------------|
| | | (mm) | (mm) | (mm) | (mm) | (mm) | (mm) | (kg) | (kg/cm ²) |
| 1 | BURN | 75,20 | 76,00 | 81,70 | 82,00 | 71,50 | 74,50 | 0,581 | 39,17 |
| 2 | BURN | 70,40 | 79,00 | 81,40 | 73,80 | 74,40 | 71,00 | 0,569 | 49,784 |
| 3 | BURN | 74,40 | 70,40 | 83,80 | 78,30 | 68,00 | 72,90 | 0,498 | 46,091 |
| 4 | BURN | 59,80 | 77,80 | 71,00 | 73,30 | 72,40 | 65,00 | 0,487 | 32,145 |
| 5 | BURN | 70,80 | 74,20 | 82,00 | 81,20 | 73,10 | 73,60 | 0,569 | 34,764 |
| 6 | BURN | 71,90 | 73,60 | 70,00 | 69,80 | 66,90 | 72,30 | 0,527 | 36,069 |
| 7 | BURN | 76,60 | 77,70 | 70,00 | 72,20 | 78,20 | 73,30 | 0,512 | 21,889 |
| 8 | BURN | 74,00 | 69,90 | 74,20 | 68,60 | 68,00 | 74,10 | 0,522 | 28,317 |
| 9 | BURN | 70,50 | 63,00 | 93,00 | 81,50 | 72,70 | 70,70 | 0,573 | 38,543 |
| 9 | BURN (1) | 63,00 | 81,40 | 84,40 | 59,70 | 77,00 | 70,70 | 0,574 | 21,350 |
| 10 | BURN | 66,00 | 87,20 | 88,00 | 69,60 | 74,30 | 69,80 | 0,571 | 39,813 |
| 10 | BURN (1) | 65,70 | 89,70 | 88,00 | 64,00 | 75,80 | 70,50 | 0,576 | 34,842 |
| 11 | BURN | 74,50 | 87,60 | 84,00 | 76,00 | 78,50 | 74,00 | 0,547 | 18,793 |
| 11 | BURN (1) | 69,70 | 66,00 | 61,10 | 66,00 | 69,10 | 71,80 | 0,432 | 18,542 |
| 12 | BURN | 63,30 | 69,40 | 72,50 | 62,20 | 66,00 | 67,70 | 0,375 | 23,920 |
| 13 | BURN | 67,20 | 76,80 | 71,30 | 70,50 | 67,00 | 72,40 | 0,486 | 27,995 |
| 14 | BURN | 62,50 | 64,80 | 71,90 | 66,70 | 62,20 | 68,20 | 0,351 | 24,532 |
| 14 | BURN (1) | 63,50 | 61,00 | 72,10 | 67,30 | 71,40 | 70,00 | 0,400 | 25,836 |
| 15 | BURN | 62,30 | 70,60 | 70,20 | 71,00 | 77,90 | 66,10 | 0,434 | 23,766 |
| 16 | BURN | 62,90 | 59,20 | 64,40 | 72,90 | 72,30 | 73,70 | 0,514 | 23,142 |
| 17 | BURN | 69,00 | 69,50 | 66,20 | 64,90 | 68,60 | 57,00 | 0,380 | 21,064 |
| 18 | BURN | 66,00 | 68,60 | 72,50 | 56,00 | 69,70 | 74,20 | 0,493 | 24,274 |

Finally, by considering a reference area of 50cm, the compression resistance can be assessed near 219 N/cm² for burned specimens and equal to 263,3 N/cm² for unburned ones, as medium values.

15.4 THE OUT-OF-PLAIN RESPONSE FOR COMBINATED SEISMIC AND FIRE ACTIONS: THE EXSAMPLE AND MAIN RESULTS

Building Input data (see Table 15.5 – 15.7):

Tab. 15.5 Tuff stonework data

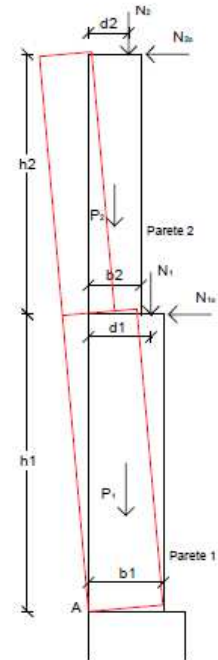
| | |
|--------------------|------|
| F_m (t/mq) | 219 |
| f_d (t/mq) | 81 |
| τ_0 (t/mq) | 4,00 |
| τ_{0d} (t/mq) | 1,5 |
| f (-) | 0,4 |

Tab. 15.6 Safety factor assumed

| | |
|----------------|------|
| FC (-) | 1,12 |
| γ_M (-) | 2 |

Tab. 15.7 Building data

| | |
|----------|-------|
| q (-) | 2 |
| Z (ml) | 21,70 |
| H (ml) | 30 |
| N (-) | 6 |



Data for horizontal elastic spectrum in acceleration definition: see Table 15.8 and 15.9.

Tab. 15.8 Parameters for local seismic action definition: Naples a_g , F_0 e T_c^* values for SLV limit state

| | |
|------------------------|-------|
| Limit State | SLV |
| P_{vr} (%) | 0.10 |
| T_R (year) | 475 |
| a_g acceleration (g) | 0,168 |
| F_0 amplification | 2,368 |
| T^*c period (sec) | 0,34 |
| Soil Class | B |
| Topographic category | T1 |
| S_s (-) | 1,20 |
| C_c (-) | 1,36 |

| | |
|-----------|------|
| $S_T (-)$ | 1 |
| $S (-)$ | 1,20 |

Tab. 15.9 Periods assumed for spectral ordinate calculation (see figure 15.8)

| | |
|--------------------|-------|
| Period T_B (sec) | 0,15 |
| Period T_C (sec) | 0,46 |
| Period T_D (sec) | 2,272 |

| | | |
|---|-----------------------------------------------------------------|------------------------------|
| A | 1,00 | 1,00 |
| B | $1,00 \leq 1,40 - 0,40 \cdot F_0 \cdot \frac{a_g}{g} \leq 1,20$ | $1,10 \cdot (T_C^*)^{-0,20}$ |
| C | $1,00 \leq 1,70 - 0,60 \cdot F_0 \cdot \frac{a_g}{g} \leq 1,50$ | $1,05 \cdot (T_C^*)^{-0,33}$ |
| D | $0,90 \leq 2,40 - 1,50 \cdot F_0 \cdot \frac{a_g}{g} \leq 1,80$ | $1,25 \cdot (T_C^*)^{-0,50}$ |
| E | $1,00 \leq 2,00 - 1,10 \cdot F_0 \cdot \frac{a_g}{g} \leq 1,60$ | $1,15 \cdot (T_C^*)^{-0,40}$ |

a)

$$0 \leq T < T_B \quad S_e(T) = a_g \cdot S \cdot \eta \cdot F_0 \cdot \left[\frac{T}{T_B} + \frac{1}{\eta \cdot F_0} \left(1 - \frac{T}{T_B} \right) \right]$$

$$T_B \leq T < T_C \quad S_e(T) = a_g \cdot S \cdot \eta \cdot F_0$$

$$T_C \leq T < T_D \quad S_e(T) = a_g \cdot S \cdot \eta \cdot F_0 \cdot \left(\frac{T_C}{T} \right)$$

$$T_D \leq T \quad S_e(T) = a_g \cdot S \cdot \eta \cdot F_0 \cdot \left(\frac{T_C T_D}{T^2} \right)$$

b)

Fig 15.8 a) Soil classes S_s and C_c values; b) Periods formulations scheme assumed by the Italian Code.

As a result, it is possible to define the horizontal elastic spectrum in acceleration $[S_e(T)]$.

The spectral ordinate must be calculated according to the probabilities of exceedance respect the reference life V_R and the Limit State selected (SLV). Instead, the natural period T_1 have to be calculated by the following simplified formulation (10):

$$T_1 = 0,05 H^{3/4} = S_e(T_1) = 0,346 g = 3,391 \text{ m/sec}^2 \quad (10)$$

Once calculated the site seismic action expected, and the reduced spectrum ordinate related to the case study analysed [$S_e(T_1)$]; it is possible proceed to local failure response assessment by DEI Software (Analisi Strutturale Per Il Recupero Antisismico) in linear and nonlinear range. The simple case takes into account a single masonry panel (dimensions: $h = 8,7\text{m}$; $b = \text{variable}$ see Table 15.10; $w = 6\text{m}$), by supposing the elements placement in top level (see Table 15.7), with vertical loads applied, no constrain effects and reduced f_m values application, experimental detected.

Tab. 15.10 Panel data

| | |
|---------------------------|--------|
| b_1 (ml) | 0,60 |
| b_2 (ml) | 0,45 |
| h_1 (ml) | 2,6 |
| h_2 (ml) | 1,75 |
| d_1 (ml) floor position | 0,45 |
| d_2 (ml) roof position | 0,3 |
| N_1 (kg) | 1064* |
| N_1 (kg) | 1881** |

Note: the $\psi_{2i} \cdot Q_{k1}$ were respectively assumed equal to * 0.3 and 200 Kg/m^2 for roof structure and equal to** 0 and 50 Kg/m^2 for floor structures.

By considering equation (3) it is possible calculate α_0 value. It is equal to 0,184; with a corresponding t value close to 6cm (by apply eq. viii) by assuming f_m input data, equal to 219 t/mq (see section 3.2.1). a_0^* results equal to $2,012 \text{ m/sec}^2$. By assuming f_m equal to 363,3 t/mq, a_0^* will result equal to $2,113 \text{ m/sec}^2$; for $\alpha_0 = 0,193$ and $t = 3,7\text{cm}$. As a result, by applying the (6 a,b) formulations, it is possible evaluate the verifications pointed out satisfied. For any additional information see both Input and Output spreadsheets.

Acknowledgement

The authors would like to thanks the TecnoLab Testing laboratory.

References

- Borri, 2013: Borri, A., Candela M. and Fonti R., Full-scale testing of old masonry structural elements: The out-of-plane response, in: *the Fifth International Conference on Structural Engineering, Mechanics and Computation (SEMC 2013)*, Cape Town, 2-4 September 2013, South Africa.
- Cangi, 2010: Cangi G., Carboni M. and De Maria A. Analisi strutturale per il recupero antisismico. Calcolo dei cinematismi per edifici in muratura secondo le NTC. Con CD-ROM. Roma. Dei srl Tipografia del Genio Civile.
- Ceradini, 1992: Ceradini V. Modellazione e Sperimentazione per lo studio della muratura storica. Roma: Tesi di Dottorato.
- Circolare 2 Febbraio 2009, n°617 (C.M.), 2009. Istruzioni per l'applicazione delle Norme tecniche per le costruzioni di cui al D.M. 14 Gennaio 2008, G.U. n. 47 del 26/02/2009 – Suppl. Ordinario n. 27.
- Fonti, 2013: La statica della muratura in pietra grezza. Napoli: tesi di Dottorato.
- Giuffrè, 1991: Giuffrè A. Letture sulla Meccanica delle Murature Storiche. Roma: Edizioni Kappa.
- Ministero per i Beni e le Attività Culturali (MiBAC), 2010. Circolare 2 Dicembre 2010 n°26 "Linee Guida per la valutazione e riduzione del rischio sismico del patrimonio culturale allineate alle nuove Norme tecniche per le costruzioni (D.M. 14/01/08)".
- Munari, 2010: Munari M., Bettiol G., da Porto F., Milano L. and Modena C. Esempio di calcolo su rafforzamento locale di edifici in muratura con tiranti, in: Allegato alle Linee Guida per la Riparazione e il Rafforzamento di Elementi Strutturali, Tamponature e Partizioni. <http://www.reluis.it/>.

INDEX OF AUTHORS

| | | | |
|---------------|--------------------------|----------------------------------------------------------------------------------------------------|-------------|
| Bisby | Luke | luke.bisby@ed.ac.uk | 180 |
| Bouchair | Abdelhamid | Abdelhamid.bouchair@univ-bpclermont.fr | 173 |
| Burgess | Ian | ian.burgess@sheffield.ac.uk | 9 |
| Caldová | Eva | eva.caldova@fsv.cvut.cz | 173 |
| Couto | Carlos | ccouto@ua.pt | 21 |
| Craveiro | Hélder D.S. | heldercraveiro.eng@gmail.com | 73 |
| Cvetkovska | Meri | cvetkovska@gf.ukim.edu.mk | 48, 98 |
| Fonti | Roberta | roberta.fonti@unina.it | 180 |
| Formisano | Antonio | antoform@unina.it | 180 |
| Franssen | Jean-Marc | jm.franssen@ulg.ac.be | 60 |
| Haremza | Cécile | haremza@dec.uc.pt | 60 |
| Hricák | Jan | jan.hricak@fsv.cvut.cz | 34 |
| Jahn | Wolfram | w.jahnva@gmail.com | 134 |
| Jandera | Michal | michal.jandera@fsv.cvut.cz | 21, 34 |
| Jovanoska | Milica | m.jovanoska@hotmail.com | 98 |
| Kowalski | Robert | r.kowalski@il.pw.edu.pl | 107 |
| Laím | Luís | luislaim@hotmail.com | 73 |
| Lazarov | Ljupcho | lazarov@gf.ukim.edu.mk | 48, 98 |
| Lopes | Nuno | nuno.lopes@ua.pt | 21, 60 |
| Mazzolani | Federico Massimo | fmm@unina.it | 180 |
| Milanovic | Milivoje | pbarhisnp@gmail.com | 48, 98 |
| Mistakidis | Euripidis | emistaki@gmail.com | 147 |
| Prachař | Martin | martin.prachar@fsv.cvut.cz | 21 |
| Rein | Guillermo | g.rein@imperial.ac.uk | 134 |
| Ribeiro | João | joao.ribeiro@uc.pt | 123 |
| Rigueiro | M ^a Constança | constanca@ipcb.pt | 123 |
| Rodrigues | João Paulo C. | jpaulocr@dec.uc.pt | 73 |
| Rush | David | d.rush@ed.ac.uk | 86 |
| Santiago | Aldina | aldina@dec.uc.pt | 60, 123 |
| Szilagyí | Csaba | sz.csaba@optomm.hu | 157 |
| Todorov | Koce | todorov@gf.ukim.edu.mk | 48 |
| Torič | Neno | neno.toric@gradst.hr | 9 |
| Vila Real | Paulo | pvreal@ua.pt | 21 |
| Vymlátil | Petr | vymlatil.p@designotec.cz | 173 |
| Wald | František | wald@fsv.cvut.cz | 21, 34, 173 |
| Zografopoulou | Kalliopi | kazograf@gmail.com | 147 |

MANAGEMENT COMMITTEE

BJEGOVIĆ Dubravka, *Croatia*
BLOCK Florian, *United Kingdom*
BORG Ruben, *Malta*
BOUCHAIR Abdelhamid, *France*
BURGESS Ian, *United Kingdom*
Vice-Chair
CADONI Ezio, *Switzerland*
CVETKOVSKA Meri, *Macedonia*
DE NAEYER André, *Belgium*
DUBINA Dan, *Romania*
FAGGIANO Beatrice, *Italy*
FERRER Miquel, *Spain*
FRANGI Andrea, *Switzerland*
FRANSSEN Jean-Marc, *Belgium*
GABER Metod, *Slovenia*
GILLIE Martin, *United Kingdom*
GORANSSON Ulf, *Sweden*
HAJPÁL Monika, *Hungary*
HEINISUO Markku, *Finland*
HICKS Stephen, *New Zealand*
HOZJAN Tomaz, *Slovenia*
KAKLAUSKAS Gintaris, *Lithuania*
DC Rapporteur
KIRSCH Thomas, *Germany*
KOLSEK Jerneja, *Slovenia*
KWASNIEWSKI Leslaw, *Poland*
LACASTA Ana Maria, *Spain*
LAZAROV Ljupcho, *Macedonia*
MARIMON Frederic, *Spain*
MARTIN GOMEZ César, *Spain*
MASLAK Mariusz, *Poland*
MAZZOLANI Federico, *Italy*
MISTAKIDIS Euripidis, *Greece*
OSWALD Monika, *Austria*
OUTINEN Jyri, *Finland*
SANTIAGO Aldina, *Portugal*
SELAMET Serdar, *Turkey*
SCHAUMANN Peter, *Germany*
STAVROULAKIS Georgios, *Greece*
ŠTUJBEROVÁ Magdaléna, *Slovakia*
TAKÁCS Lajos Gábor, *Hungary*
TOMASSON Bodvár, *Iceland*
TURK Goran, *Slovenia*
VELJKOVIC Milan, *Sweden*
VILA REAL Paulo, *Portugal*
WALD František, *Czech Republic*
Chairman
WANG Yong, *United Kingdom*
ZAHARIA Raul, *Romania*
ZHAO Bin, *France*

WORKING GROUP 1

Fire Behaviour and Life Safety

BISKUP Krzysztof, *Poland*
BLOCK Florian, *United Kingdom*
Co-Chairman
CADORIN Jean-Francois, *Belgium*
CASCIATI Fabio, *Italy*
COUTO Carlos, *Portugal*
DE MATTEIS Gianfranco, *Italy*
DRABOWICZ Zenon, *Poland*
DRAKULIC Miodrag, *Croatia*
FRANSSEN Jean-Marc, *Belgium*
GORANSSON Ulf, *Sweden*
HEINISUO Markku, *Finland*
HOROVÁ Kamila, *Czech Republic*
KLINZMANN Christoph, *Germany*
LACASTA Ana Maria, *Spain*
MASLAK Mariusz, *Poland*
NIGRO Emidio, *Italy*
PINTEA Dan, *Romania*
REIN Guillermo, *United Kingdom*
Chairman
RODRIGUES Joao Paulo, *Portugal*
SETTE Bart, *Belgium*
SOKOL Zdeněk, *Czech Republic*
TAKÁCS Lajos Gábor, *Hungary*
TOMASSON Bodvár, *Iceland*
TSATSOULAS Dimitrios, *Greece*
TURK Goran, *Slovenia*
ZHAO Bin, *France*
ZOGRAFOPOULOU Kalliopi, *Greece*

WORKING GROUP 2

Structural Safety

BEDNÁŘ Jan, *Czech Republic*
BJEGOVIĆ Dubravka, *Croatia*
BOUCHAIR Abdelhamid, *France*
CADONI Ezio, *Switzerland*
CALDOVA Eva, *Czech Republic*
CEFARELLI Giuseppe, *Italy*
CVETSKOVSKA Meri, *Macedonia*
DAVISON Buick, *United Kingdom*
DELLA CORTE Gaetano, *Italy*
DUMITRESCU Dan, *Romania*
FERRER Miquel, *Spain*
FILIPOVA-CHIFLIGANEC Cvetanka, *Macedonia*
GILLIE Martin, *United Kingdom*
HAJPÁL Monika, *Hungary*
HAREMZA Cécile, *Portugal*
HICKS Stephen, *Switzerland*
HOZJAN Tomaž, *Slovenia*
JÁNA Tomáš, *Czech Republic*
JIMENÉZ Albert, *Spain*
JOVANOSKA Milica, *Macedonia*

KIRSCH Thomas, *Germany*
KOLSEK Jerneja, *Slovenia*
KNOBLOCH Markus, *Switzerland*
KRÓL Pawel, *Poland*
KVASNIEWSKI Leslaw, *Poland*
Chairman
LAIM Luís, *Portugal*
LANDOLFO Raffaello, *Italy*
LAZAROV Ljupcho, *Macedonia*
MARIMON Frederic, *Spain*
MENSINGER Martin, *Germany*
OSWALD Monika, *Austria*
PANTOUSA Daphne, *Greece*
PECENKO Robert, *Slovenia*
PEROS Bernardin, *Croatia*
RUKAVINA JELCIC Maria, *Croatia*
SANTIAGO Aldina, *Portugal*
SCHAUMANN Peter, *Germany*
ŠTUJBEROVÁ Magdalena, *Slovakia*
TODOROV Koce, *Macedonia*
TSALIKIS Chris, *Greece*
VARGOVSKÝ Kamil, *Slovakia*
VELJKOVIC Milan, *Sweden*
WALD František, *Czech Republic*
WANG Yong, *United Kingdom*
ZAHARIA Raul, *Romania*
Co-chairman
ZEHFUSS Jochen, *Germany*

SZILÁGYI Csaba, *Hungary*
UPMEYER Jens, *Germany*
VILA REAL Paulo, *Portugal*
Chairman

WORKING GROUP 3

Integrated Design

BAHR Olivier, *Germany*
BILOTTA Antonio, *Italy*
BURGESS Ian, *United Kingdom*
DE NAEYER André, *Belgium*
DE SANCTIS Gianluca, *Switzerland*
DHIMA Dhionis, *France*
DUBINA Dan, *Romania*
FAGGIANO Beatrice, *Italy*
GOLGOJAN Ionel-Puiu, *Romania*
HOJ Niels Peter, *Switzerland*
JENKINS Paul, *United Kingdom*
KAISER Rudolf, *Czech Republic*
KOWALSKI Robert, *Poland*
KUČERA Petr, *Czech Republic*
LOPES Fernanda, *Portugal*
LOPES Nuno, *Portugal*
MARSDEN Jim, *United Kingdom*
MAZZOLANI Federico, *Italy*
MISTAKIDIS Euripidis, *Greece*
NADOR András, *Hungary*
OUTINEN Jyri, *Finland*
Co-chairman
SOUTO Carlos, *Portugal*
STAVROULAKIS George, *Greece*

